ADOPTION NOTICE

SAE-AIR1419, "Gas Turbine Engines, Inlet Total-Pressure-Distortion Considerations for," was adopted on October 3, 1994, for use by the Department of Defense (DoD). Proposed changes by DoD activities must be submitted to the DoD Adopting Activity: ASC/ENOS, 2664 Skyline Drive., Wright-Patterson AFB, OH 45433-7800. DoD activities may obtain copies of this standard from the Standardization Document Order Desk, 700 Robbins Avenue, Building 4D, Philadelphia, PA 19111-5094. The private sector and other Government agencies may purchase copies from the Society of Automotive Engineers, Inc., 400 Commonwealth Drive, Warrendale, PA 15096.

Custodians:
Army - AV
Navy - AS
Air Force - 11

Adopting Activity
Air Force - 11

FSC 2840

DISTRIBUTION STATEMENT A. Approved for public release; distribution is unlimited.

K-33-09

SAE The Engineering Resource For Advancing Mobility

400 COMMONWEALTH DRIVE, WARRENDALE, PA 15096

AEROSPACE INFORMATION REPORT

AIR 1419

Issued May 1983
Revised

INLET TOTAL-PRESSURE-DISTORTION CONSIDERATIONS FOR GAS-TURBINE ENGINES

PREPARED BY
SOCIETY OF AUTOMOTIVE ENGINEERS
AEROSPACE COUNCIL DIVISION
TECHNICAL COMMITTEE S-16

Printed and Bound by Publishers Choice Book Mfg. Co.
Erie, Pennsylvania 16046

Printed in U.S.A.

AIR 1419

TABLE OF CONTENTS

TABLE OF CONTENTS (Cont'd)

TABLE OF CONTENTS (Cont'd)

TABLE OF CONTENTS (Cont'd)

LIST OF FIGURES

LIST OF FIGURES (Cont'd)

LIST OF FIGURES (Cont'd)

LIST OF FIGURES (Cont'd)

LIST OF FIGURES (Cont'd)

LIST OF FIGURES (Cont'd)

LIST OF TABLES

PREFACE

Industry and government agencies concerned with aircraft design and operation recognize a need to improve methodology and communication on spatial total-pressure distortion aspects of the inlet/engine compatibility problem. The appearance of modern turbofan engines in the late 1960's focused attention on this need, and there followed a period of intense activity to develop engineering techniques for assuring adequate stability. These techniques were identified, formulated and exercised independently in various parts of industry to solve flow distortion problems on specific systems. The aircraft and engine companies form a matrix of cooperative engineering activity in the international military and civil aircraft market, and a third dimension is added by the group of customers. The three groups needed to consolidate individual experience, establish common ground, and gain a perspective concerning the applicability and accuracy of these techniques. Adequate resolution of the aircraft/engine stability problem would depend upon generating generally usable guidelines addressing analysis, test, data processing, and information transfer which would be applied in a manner consistent with the expected severity of the problem.

The Society of Automotive Engineers (SAE) Aerospace Council Divisional Technical Committee S-16 was formed in 1972 to examine the aircraft gas turbine inlet/engine compatibility development process, as affected by flow distortion, to assess what experience was common throughout industry, or what could be agreed as desireable to make common. The Committee formulated a number of guidelines to improve communications and minimize repetitive workloads among program participants. It recognized that practices employed to cope with flow distortion effects were young and changing and that in several critical areas, practice was not sufficiently common or defined to warrant establishing guidelines. For these reasons the guidelines were purposely limited, and were organized and published in March 1978 as Aerospace Recommended Practice (ARP) 1420, "Gas Turbine Engine Inlet Flow Distortion Guidelines." ARP 1420 was circulated widely in the U.S. and European aeronautical industries. Significant comments and opinions were expressed, and were carefully considered by the Committee prior to submitting the ARP to the SAE Aerospace Council for publication.

The S-16, in its proceedings, produced a wealth of information which, in its entirety, contained a significant part of the flow-distortion- related corporate knowledge of the industry as it existed in the mid-1970's time period. The Committee decided that this information, organized into a generally available document, would provide a source of knowledge for engineers new to the problems of inlet-engine compatibility. The Committee, therefore, compiled Aerospace Information Report (AIR) 1419 "Inlet-Total-Pressure Distortion Considerations for Gas-Turbine Engines" to amplify the information contained in ARP 1420 and to provide a "corporate memory."

SAE Technical Committee S-16, through its members and liaison representatives, represents a cross section of the part of government and industry having the major share of the responsibility for assuring economical, safe, and surge-free propulsion systems. Table A lists the organizations that

sponsored S-16 and made possible, through its members and representatives, ARP 1420 and AIR 1419. These organizations should be commended. These documents exist today because of their active concern for the distortion problem and their willingness to provide resources to obtain solutions. The members and representatives, listed in Table A, collectively contributed hundreds of hours of work between Committee meetings to assure worthwhile results and productive meetings.

H. I. BUSH
Chairman, S-16

TABLE A

SPONSORING ORGANIZATIONS AND PARTICIPATING PERSONNEL
SAE AEROSPACE COUNCIL TECHNICAL COMMITTEE S-16

INDUSTRY ORGANIZATIONS

Boeing
W. J. Hastings
G. W. N. Lampard

Detroit Diesel Allison Dev., General Motors Corporation
S. Baghdadi
J. A. Korn

Garrett Turbine Engine Company
G. W. Burley

General Dynamics, Fort Worth Division
P. P. Truax

General Electric, Aircraft Engine Business Group
P. H. Kutschenreuter, Jr.
W. G. Steenken

Lockheed California Company
T. Sedgwick

McDonnell Aircraft Company
A. P. Farr, III

Northrop Corporation, Aircraft Division
R. D. Sutton

Pratt & Whitney Aircraft, United Technologies, Inc.
Commercial Products Division
D. Kenison
D. L. Motycka
J. M. Tringali
Government Products Division
S. H. Ellis

Rockwell International, North American Aircraft
C. J. MacMiller

Rolls-Royce, Ltd.
D. D. Williams

Sverdrup Technology, Inc.
R. E. Smith, Jr.
J. T. Tate

GOVERNMENT ORGANIZATIONS

Department of Defense, Air Force Wright Aeronautical Laboratories,
Aero Propulsion Laboratory
H. I. Bush
J. E. Lueke
R. J. Martin
H. E. Schumacher
Flight Dynamics Laboratory
D. Sedlock

Department of Defense, Naval Air Propulsion Center
J. F. Boytos

Department of Transportation, Federal Aviation Agency
R. F. Nugent

National Aeronautics and Space Administration
Ames Research Center
D. P. Bencze
Lewis Research Center
E. J. Graber
J. H. Povolny

INTRODUCTION

Aerospace Information Report (AIR) 1419 "Inlet Total Pressure Distortion Considerations for Gas Turbine Engines" documents engineering information for use as reference material and for guidance. Inlet total-pressure distortion and other forms of flow distortion that can influence inlet/engine compatibility require examination to establish their effect on engine stability and performance. This report centers on inlet-generated total-pressure distortion measured at the Aerodynamic Interface Plane (AIP), not because this is necessarily the sole concern, but because it has been given sufficient attention in the aircraft and engine communities to produce generally accepted engineering practices for dealing with it. The report does not address procedures for dealing with performance destabilizing influences other than those due to total-pressure distortion, or with the effects of any distortion on aeroelastic stability. The propulsion system designer must be careful to assure that, throughout the development process, other forms of inlet flow distortion, which can have just as serious effects on system stability and performance, have been effectively addressed.

The report deals with spatial total-pressure distortion, as defined by an array of high-response total-pressure probes. Time-variant total-pressure distortion, synthesized from statistical data, can provide useful information. However, the consensus of SAE S-16 is that such techniques are not developed sufficiently to permit general guidelines to be formulated.

Concepts which are fundamental to this report are:

a. Inlet flow quality can be characterized, in a form relevant to engine distortion response, with numerical descriptors derived from an array of high-response total-pressure probes;

b. Propulsion system stability can be controlled by the aircraft and engine designers;

c. Engine stability can be demonstrated by tests using equivalent levels of steady state distortion.

The report is organized into seven sections, expanding upon the ideas and recommended practice set forth in ARP 1420. The first two sections deal with surge margin, loss of surge pressure ratio, and procedures for correlating the loss of surge pressure ratio with total-pressure distortion. Through use of the terms and procedures discussed earlier, Sections 3 and 4 develop engine stability and performance assessment techniques for handling total-pressure distortion by putting them into context with other destabilizing influences and performance detriments. Section 5 describes various test procedures, equipment, and methods currently available for generating the information needed to apply distortion assessment techniques. Section 6 discusses interface instrumentation, data-

acquisition system accuracy, frequency response, record length, recording systems, and the data management procedures necessary to minimize communication errors among participating organizations. Section 7 provides a short overview of "state-of-the-art", a brief discussion of other forms of distortion at the inlet/engine Aerodynamic Interface Plane, a summary of other considerations involved in assessments of inlet/engine compatibility, and brief summaries of probable future activity in each of these areas.

The distortion descriptor is the vehicle by which engine reaction to inlet distortion is forecast and assessed, from program outset well into field use of the system. ARP 1420 defines the distortion descriptor as a non-dimensional, numerical representation of the measured inlet pressure distribution, and provides a means for identifying critical inlet flow distortions and for communicating during propulsion system development. Central issues are the distortion descriptors, methods of correlating them with performance and stability changes and test and information acquisition techniques. Use and accuracy of the descriptors vary, depending upon the stage of the engine development, but their definitions and purpose remain constant - to assess status, forecast stability and identify required engineering activity.

The activities associated with distortion descriptor use can be categorized for convenience in phases (Table B), recognizing that there is little consensus concerning the definitions of these phases and that no clear lines of demarcation exist between them.

Conceptual Studies Phase: This phase, the initial step in the life cycle for an aircraft system, is characterized by analytical evaluations of candidate aircraft/propulsion system configurations. Generally, no new testing is planned for this phase and information for the evaluations is based on historical sources. Recognition of and planning for stability assessment during concept evaluation serves to assure that 1) distortion effects are a prime consideration in the selection of the candidate propulsion system, 2) those conditions that are considered areas of risk are given particular attention during the subsequent design and development phases, and 3) distortion patterns, inherent to the type of aircraft inlet, are defined to enable the engine to be designed with consideration for predominant patterns.

The distortion descriptor is used to determine the relative standing of several candidate inlet configurations. Specific items to be evaluated include: design concept and location, inlet performance, aircraft maneuverability—as affected by distortion, armament location, approximate inlet/engine matching characteristics, overall distortion trends with inlet geometry and primary and secondary airflow requirements. The descriptor is used to evaluate the stability characteristics of candidate compressor and engine configurations, their sensitivity to distortion, the surge margin available for distortion, and potential problems peculiar to the various thermodynamic cycles and engine control modes.

This phase should end when the general aircraft and the propulsion system configurations that can best meet generalized mission requirements are defined. Limiting operating conditions within the anticipated flight envelope should have been identified, including those due to inlet total-pressure distortion, unstart, buzz, temperature distortion, water ingestion, armament-exhaust-gas ingestion, and unusual amounts of engine bleed or power extraction. The consequence of surge associated with these conditions should have been assessed and a procedure established for continuously tracking compatibility throughout the development program.

Preliminary Design Phase: This phase is the second step in the development cycle during which mission requirements are defined in more detail and a baseline vehicle has been selected. Airframe-inlet integration and inlet component testing have begun with small scale models to update compatibility estimates and to define the extent of required development work. Preliminary indications of the extent of the distortion problems to be expected are identified using data obtained from steady state and dynamic probes located at the inlet/engine aerodynamic interface plane. Fan and compressor performance maps, flow path geometry and blade sizes are estimated. Where appropriate, applicable engine components are tested with distortion patterns characteristic of the inlets being considered by the airframe contractor.

The distortion descriptor is used to aid in selecting those inlet/airframe components that result in a favorable flow field. Preliminary distortion characteristics are determined for critical aircraft operating conditions. The distortion descriptors are used to assess the effects of distortion on the engine and its components. Engine simulations, with transient capability and control logic, are initiated and used to perform preliminary engine stability audits, to define engine surge margin utilization and to aid in establishing distortion goals for the inlet.

Engine distortion tolerance estimates are used to establish the allowable airflow range for inlet/engine matching, supercritical or subcritical limits, start/unstart procedure, control criteria, bleed configuration, boundary layer diverter design, noise requirements, maneuver capability, lip shape and radius, low-speed flow augmentation, and low-speed crosswind capability.

At the end of this phase, initial stability audit coordination has occurred between engine and airframe companies. The basic inlet and engine configurations have been defined but require further refinement. The vehicle mission has become well-defined. Provisions for coordinating any mission changes will have been made. Agreement should exist between airframe and engine contractors on:

a. The distortion goals for the inlet and the engine at specific points within the flight envelope. These represent the maximum level of distortion the inlet will generate and the level the engine will tolerate.

b. The type, severity and number of equivalent classical patterns to be used during initial development testing.

c. The distortion patterns from subscale inlet testing to be used for engine development tests.

d. A well-defined compatibility program including the definition of the data transmission formats, test sequence, criteria for decision making, the scope of dynamic distortion tests, demonstration points, type of instrumentation and location of aerodynamic interface plane.

Development Phase: This phase starts when system mechanical configurations are defined and terminates when the propulsion system is ready for field use. The airframe, inlet and engine configurations are refined through extensive test programs. The performance and compatibility of the airframe/inlet system are developed through wind-tunnel tests of large-scale models, and of the engine, through engine and component tests using suitable distortion generators. A full complement of dynamic instrumentation, located at the agreed AIP, is utilized during testing. Prior inlet distortion and engine tolerance committments are updated based on realistic test data and changing requirements.

Updated surge margin and surge pressure ratio changes due to distortion are obtained from compressor rig and engine tests with inlet distortion. Distortion stability coefficients are adjusted correspondingly, and the process is repeated as engine design changes occur. The descriptor is used to verify inlet distortion levels, and design variables such as throat height, ramp position, cowl shape, bleed and bypass are examined for their effects on distortion. Updated distortion patterns, obtained from wind tunnel and flight tests, are used to refine stability and performance assessments. Descriptors and engine simulations are used to focus attention on components requiring further development. At the end of this phase, the airframe and engine have demonstrated compatibility throughout the required flight envelope.

Engine Qualification Or Certification Phase: This phase represents the period during which tests are performed to clear the engine for initial flight testing, for limited production, and eventually, for full production. Qualification or certification requires quantitative assessments of engine performance and stability at a number of selected conditions. Distortion patterns are used during this phase to define the inlet/engine interface test conditions. The test conditions are defined in terms that include:

Inlet/Engine Interface Conditions
- Airflow
- Total-Pressure (local point-by-point values)
- Total-Temperature
- Altitude Ambient Pressure

Installation Interface Conditions (aircraft service requirements)
- Customer Bleed
- Power Extraction

Engine Operating Conditions
- Engine Power Setting
- Engine Service Bleeds (intercompressor, anti-ice)
- Control Trim Status

At the conclusion of this phase, the engine configuration will have demonstrated acceptable performance and stability for the specified sets of operating conditions.

Flight Test Phase: Distortion testing through the early part of the development phase defines necessary design changes and provides an assessment of system performance and stability well in advance of flight. Flight testing may identify design changes and may uncover problems requiring further development because ground test facilities are limited in their ability to simulate the full flight and maneuver envelopes.

The primary engine uses of the descriptor are to correlate flight and ground test data, and to identify sources of flight-revealed performance and stability problems. Comparisons are made with previous engine stability predictions at specific steady-state and transient operating conditions. Stability assessment procedures may be updated and improved. Flight stability limits are identified and tracked in terms of descriptor level, aircraft Mach number, altitude, attitude, and inlet and engine control parameters.

The flight test phase is complete when adequate aircraft propulsion system performance and stability have been demonstrated over the flight and maneuver envelopes and there are no further requirements for flight-generated compatibility information prior to certification for full production.

Operational Phase: During this phase, system engineering changes, alterations in aircraft usage, maintenance effects, and aging effects are assessed for their impact upon inlet/engine compatibility. If additional testing and instrumentation are required, use of the distortion descriptor would be identical to that previously described in the flight test phase.

The complexity and expense of a compatibility program to execute the multi-phased process described will depend on system requirements. The program for a re-engining of an existing aircraft, or development of a podded installation for which significant background data exist based on similar designs and similar applications, may be uncomplicated and inexpensive to execute. More stringent mission requirements may force severe departures from experience, thus incurring added risk and therefore added program complexity and expense. The information in this report can be used as necessary to create a development method to minimize the risk of inlet/engine compatibility problems. The degree to which information regarding descriptor formulation and use, assessment techniques, and testing outlined in this document is applied to a specific program should be consistent with the expected severity of the compatibility problem.

TABLE B

DISTORTION ASSESSMENT USES DURING THE PROPULSION SYSTEM LIFE CYCLE

PHASE	ACTIVITY	AIRFRAME	ENGINE	STATUS AT END OF PHASE
1. Conceptual Studies	1. Analytical evaluation of candidate aircraft and propulsion system configurations 2. Mission evaluation	1. Establish inlet distortion trends. 2. Evaluate alternative inlet designs and locations 3. Estimate maneuver limitations 4. Evaluate armament location 5. Evaluate airframe/propulsion system integration	1. Include distortion effects in selection of engine configurations based on past experience	1. Candidates that can potentially meet requirements 2. Preliminary definition of stability requirements
2. Preliminary Design	1. Design, analysis and test of inlet and engine components 2. System design selection 3. Establish flight maneuver envelope goals	1. Determine preliminary distortion characteristics 2. Evaluate airframe/propulsion system integration 3. Determine preliminary airflow matching 4. Establish distortion level goals for inlet 5. Perform periodic stability assessments jointly with engine manufacturers	1. Define surge margin requirements and select compression system design 2. Define engine distortion tolerance goals	1. Distortion goals defined 2. Mission defined 3. Inlet/engine compatibility approach defined 4. Propulsion system defined
3. Development	1. Development of required quality through continuing analysis and test of airframe and engine components and systems	1. Verify airflow matching 2. Define inlet design effects on distortion 3. Identify critical distortion patterns/levels 4. Establish distortion level commitments 5. Perform periodic stability assessment jointly with engine manufacturer	1. Establish distortion level commitments. 2. Define patterns for qualification tests 3. Correlate surge margin and performance changes due to distortion	1. Distortion commitments agreed 2. Data bank established 3. Full scale engine/inlet compatibility tests performed 4. Propulsion system ready for production
4. Engine Qualification or Certification	1. Demonstration of required levels of propulsion system stability/compatibility	1. Perform joint stability assessments 2. Perform wind tunnel tests of production changes 3. Perform installed performance calculation of "status" configuration	1. Demonstrate engine operation with distortion	1. Propulsion System with acceptable performance and stability at specified conditions
5. Flight Test	1. Demonstration of propulsion system operation 2. Inlet and engine improvements flight tested to produce best combination of performance and stability	1. Establish flight/maneuver envelopes 2. Determine distortion levels at propulsion system limits 3. Resolve deficiencies 4. Compare flight test and wind tunnel data	1. Correlate flight and development data 2. Identify sources of flight-revealed stability problems	1. Propulsion system performance and stability demonstrated over flight and maneuver envelopes
6. Operational	1. Collection of operational data 2. Propulsion system modified as necessary	1. Evaluate propulsion system modifications 2. Evaluate operational anomalies	1. Service, overhaul and modification evaluation 2. Operational trouble shooting	1. Operational capability monitored

AIR 1419

SECTION 1

SURGE MARGIN AND LOSS OF SURGE PRESSURE RATIO

Compressor surge margin definitions fall into two general classes: surge margin defined at constant corrected airflow, usually at the compressor inlet, and surge margin defined at constant corrected rotor speed.

Surge margin defined at constant airflow has advantages for engine-inlet airflow matching and stability assessment. With this definition both inlet distortion and engine distortion tolerance can be expressed as functions of airflow. Consequently, the corrected airflow passing through the interface plane can be used as the common denominator for both inlet distortion and engine distortion tolerance.

Surge margin defined at constant rotor speed has advantages for the engine manufacturer; most compressor design procedures and testing are carried out at constant rotor speed. Also, surge margin at limiting rotor speed can be defined without extrapolation.

The inlet/engine compatibility guidelines of ARP 1420, Reference 1, recommend a total-pressure-distortion methodology which utilizes one definition of surge margin as a basis. This section discusses that definition and the rationale for its choice against a background of some alternative definitions currently used in industry.

1.1 ARP 1420 DEFINITIONS AND RATIONALE

ARP 1420 surge margin is defined at constant corrected airflow at the inlet of the compression component, with variable geometry, if any, in the scheduled position. ARP 1420 surge margin is the difference between the surge pressure ratio and the operating pressure ratio, normalized by the operating pressure ratio. Referring to Figure 1.1, the ARP 1420 undistorted surge margin is defined as:

$$SM = \frac{(PR1-PRO)}{PRO} \times 100$$

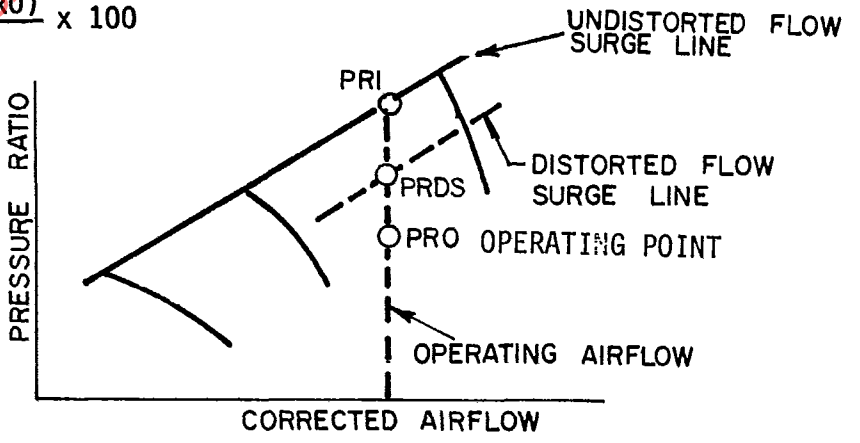

FIGURE 1.1 ARP 1420 Surge Margin Definition

The ARP 1420 loss in surge pressure ratio due to inlet total pressure distortion (ΔPRS) also is measured at constant inlet corrected airflow with the variable geometry, if any, in the scheduled position. ΔPRS is the loss in surge pressure ratio due to inlet distortion normalized by the undistorted surge pressure ratio. With reference to Figure 1.1:

$$\Delta PRS = \frac{(PR1-PRDS)}{PR1} \times 100$$

The loss in surge pressure ratio is normalized by the undistorted surge pressure ratio rather than by the operating pressure ratio because the operating pressure ratio may not have been defined when compressor rig tests are made to determine the effect of distortion on compressor stability. Also, a better comparison among compressors from different engines can be made using a distortion sensitivity that is independent of the operating point.

Figure 1.2 shows fan data, both with and without inlet distortion, that illustrate the definitions of surge margin and loss of surge pressure ratio due to inlet distortion. Using the nomenclature of Figure 1.2, ARP 1420 surge margin, with no inlet distortion, at 96.4 percent airflow is:

$$SM = \frac{PR(3) - PR(8)}{PR(8)} \times 100 = 15\,\%$$

In the example shown in Figure 1.2, the dashed lines represents a shift in performance due to circumferential inlet distortion. The loss in surge pressure ratio due to distortion is calculated at the surge airflow with inlet distortion. At 89.3 percent corrected inlet airflow

$$\Delta PRS = \frac{PR(1) - PR(4)}{PR(1)} \times 100 = 1.2\,\%$$

At this airflow, the clean flow surge margin is:

$$SM = \frac{PR(1) - PR(6)}{PR(6)} \times 100 = 20.29\,\%$$

With reference to Figures 1.1 and 1.2, the surge margin with distorted flow is:

$$SM\ dist = \frac{(PRDS-PRO)}{PRO} \times 100 = \frac{PR(4) - PR(6)}{PR(6)} \times 100 = 18.84\,\%$$

The change in surge margin for a fixed operating pressure ratio is related to the loss of surge pressure ratio, ΔPRS, by

$$\Delta SM = \frac{PR1}{PRO}\,\Delta PRS = \left(1 + \frac{SM}{100}\right)\Delta PRS$$

For example, at 89.3 percent airflow:

$$\Delta SM = 1.203 \times 1.2 = 1.44\,\%$$

AIR 1419

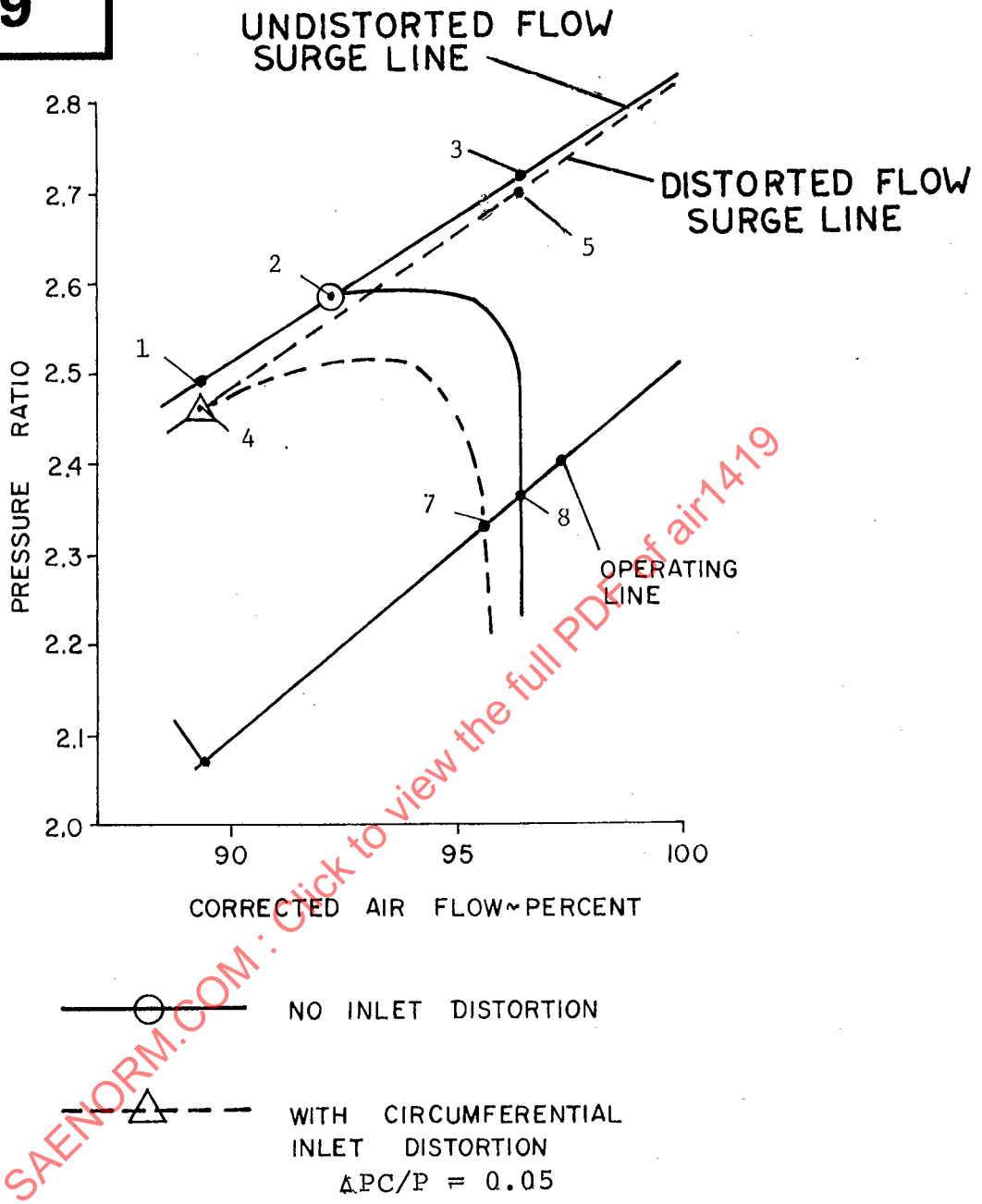

POINT NO.	PRESSURE RATIO	AIRFLOW
(1)	2.49	89.3
(2)	2.58	92.2
(3)	2.72	96.4
(4)	2.46	89.3
(5)	2.70	96.4
(6)	2.07	89.3
(7)	2.33	95.6
(8)	2.36	96.4

FIGURE 1.2 Fan Map to Illustrate Surge Margin Definition

1.2 OTHER DEFINITIONS OF SURGE MARGIN

Many definitions of surge margin have been used. Some of these are used in compressor design and development. Some of the more common definitions are given in Table 1.1, in terms of the nomenclature and numerical values of the undistorted flow lines in Figure 1.2 to illustrate that the numerical value of surge margin is dependent on surge margin definition.

TABLE 1.1

Alternative Surge Margin Definitions

NUMBER	DEFINITION	PERCENT SURGE MARGIN	
1	$\frac{PR(3) - PR(8)}{PR(8)} \times 100$	15.2 (ARP 1420)	CONSTANT AIRFLOW
2	$\frac{PR(3) - PR(8)}{PR(3)} \times 100$	13.2	
3	$\frac{PR(3) - PR(8)}{PR(8)-1} \times 100$	26.5	
4 +	$\frac{(PR/WA)_2 - (PR/WA)_8}{(PR/WA)_8} \times 100$	14.3	CONSTANT SPEED
5 +	$\frac{(PR/WA\sqrt{TR})_2 - (PR/WA\sqrt{TR})_8}{(PR/WA\sqrt{TR})_2} \times 100$	11.2 *	
6 +	$\frac{(PR/WA)_2 - (PR/WA)_8}{(PR/WA)_2} \times 100$	12.5	
7	$\frac{PR(2) - PR(8)}{PR(8)} \times 100$	9.3	
8	$\frac{PR(2) - PR(8)}{PR(2)} \times 100$	8.5	
9	$\frac{PR(2) - PR(8)}{PR(8)-1} \times 100$	16.2	

+ WA denotes compressor inlet corrected airflow.
TR denotes compressor total temperature ratio.

*Assuming 80 percent adiabatic efficiency

The above list of surge margin definitions is not comprehensive; other definitions exist, utilizing for example, compressor exit static pressure.

The above definitions fall into two general classes: (1) surge margin evaluated at constant airflow (definitions 1-3) which may require an increase in rotor speed between the operating point and the surge point and (2) surge margin evaluated at constant rotor speed (definitions 4-9) which may have a reduction in airflow between the operating point and the surge point. For a vertical compressor rotor speed line, when constant rotor speed and constant corrected inlet airflow are achieved simultaneously (compressor choke), the constant rotor speed definitions will calculate the same surge margin as the corresponding constant airflow definitions. For example, definitions 1, 4 and 7 will calculate the same surge margin with a vertical speed line, while definitions 2, 6 and 8 are another such set of corresponding definitions.

Every surge margin definition that is normalized by the operating point has a corresponding definition normalized by the surge point. Table 1.1 shows three of these corresponding pairs, namely: 1 and 2, 4 and 6, 7 and 8. Definitions 3 and 9 are normalized by compressor total pressure rise rather than total pressure ratio. Definition 5 is proportional to compressor exit throttle closure; it is the percentage reduction in compressor exit corrected airflow from the operating point to the surge point at constant corrected rotor speed. Definition 6 is derived from 5 by neglecting temperature ratio differences between surge and operating points.

Surge margin values vary between 8.5 percent and 26.5 percent for the examples shown in Table 1.1. This wide variation for the same compressor, at the same operating condition, illustrates the need for a preferred surge margin definition.

1.3 SURGE MARGIN WITH INLET DISTORTION

Table 1.2 compares clean flow surge margin, distorted flow surge margin and the loss in surge margin due to inlet distortion calculated for the nine definitions of surge margin presented in Table 1.1. Surge margins in Table 1.2 range from 8.5 percent to 26.5 percent, while the corresponding loss in surge margin due to the test level of circumferential distortion ranges from 0.5 percent to 6.4 percent.

The effects of inlet total-pressure distortion on engine stability can be accounted for consistently using any of the above compressor surge margin definitions. Definitions which give higher values of surge margin usually have greater sensitivity to distortion so that all definitions reproduce the test surge point for the test level of inlet distortion. However, each method may estimate a different surge point for distortions different from the test level.

Rotor speed and airflow relationships are required, both with and without inlet distortion, to match inlet operating airflow for constant speed surge margin definitions. Constant airflow surge margin definitions, on the other hand, enable rapid assessments of distortion effects on surge margin to be made at the matched inlet and engine airflow. Stability assessments made at constant

TABLE 1.2

Different Surge Margin Definitions Result in Different Distortion Accounting

Definition No.	Data Points		Clean Flow Surge Margin Percent	Distorted Flow Surge Margin Percent	Loss In Surge Margin Due to Distortion Percent
	Clean Flow	Distorted Flow			
1	3, 8	5, 8	15.2	14.4	0.8 (ARP 1420)
2	3, 8	5, 8	13.2	12.6	0.6
3	3, 8	5, 8	26.5	25.0	1.5
4	2, 8	4, 7	14.3	13.0	1.3
5	2, 8	4, 7	11.2	10.7	0.5
6	2, 8	4, 7	12.5	11.5	1.0
7	2, 8	4, 7	9.3	5.6	3.7
8	2, 8	4, 7	8.5	5.3	3.2
9	2, 8	4, 7	16.2	9.8	6.4

inlet corrected airflow, defined at the interface plane, simplify communication across the interface plane since inlet performance, inlet stability, inlet distortion, engine performance and engine stability are all functions of the corrected airflow at the interface plane.

Different definitions of surge margin give different numerical values for surge margin and loss in surge margin, as illustrated by Table 1.2. This can cause appreciable confusion in inlet/engine compatibility studies because each definition provides a different numerical description of stability. Consequently, an engineer trying to compare the stability of propulsion systems that utilize different definitions of surge margin and different accounting procedures has to understand different methodologies and then translate surge margins into a common base. This translation may require data that are not readily available, such as compressor maps with and without distortion. Translation will certainly require a significant amount of additional work.

The ARP 1420 surge margin definition and the associated ΔPRS definition were recommended by the SAE S-16 committee to meet the need for a consistent approach to quantifying inlet/engine stability assessment with inlet total-pressure distortion. Stability accounting systems based on these definitions are widely used and have been successful on all applications to date.

The use of the ARP 1420 definition of surge margin for inlet total pressure distortion assessment does not preclude the use of alternative surge margin definitions for compressor design and development purposes. As stated in ARP 1420, a particular engine configuration may require an alternative surge margin definition. In this case, the surge margin definition, surge margin loss and stability assessment procedure need to be specified.

1.4 SURGE LINE EXTRAPOLATION IN THE COMPRESSOR OVERSPEED REGION

In the example of Figure 1.2, the surge line was defined up to the operating airflow by testing at higher rotor speeds on the compressor rig. In some test rig situations, the achievement of high corrected rotor speeds and corresponding airflows may not be possible, for example, rig power supply constraints may make it impossible to determine experimentally a surge line at high airflows in the compressor overspeed regime. If the operational limit rotor speed is achievable, extrapolation of the surge line still may be required to extend the surge line to the highest operating airflow.

It is common practice to test compression components without distortion and at one level of distortion. Linear interpolation is used to estimate the loss of surge pressure ratio due to differing inlet distortion intensities. The following example shows how different surge line extrapolations can affect this estimation procedure. Figure 1.3 has the same undistorted speed line as in Figure 1.2, but in Figure 1.3 it is assumed that the speed line shown is a limiting speed line. Figure 1.3 also includes a speed line with radial distortion intensity of 0.10. Surge line extrapolation 1 is the same surge line as shown in Figure 1.2 for undistorted operation. Surge line extrapolation 2 is a higher surge line extrapolation. The matched inlet-engine airflow has been selected as the test airflow with inlet distortion, 94.9 percent airflow, so that stability accounting can reproduce the test conditions.

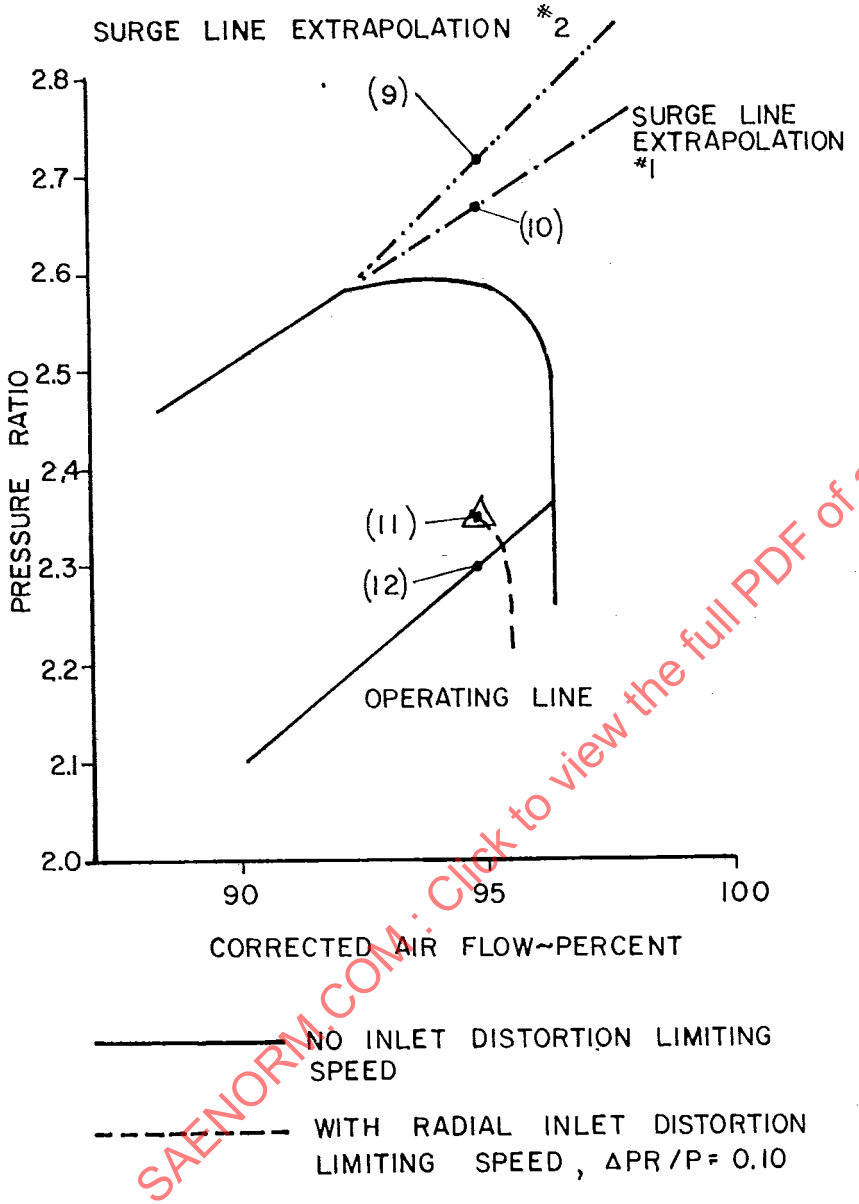

POINT NO.	PRESSURE RATIO	AIRFLOW
(9)	2.71	94.9
(10)	2.67	94.9
(11)	2.35	94.9
(12)	2.30	94.9

FIGURE 1.3 Fan Map to Illustrate Effect of Surge Line Extrapolation

Table 1.3 shows the effect of these different surge line extrapolations on estimates of the ARP 1420 surge margin for various levels of distortion.

TABLE 1.3

Effect of Surge Line Extrapolation on Stability Accounting

Inlet Distortion Level (ΔPR/P)	SM - Surge Margin With Inlet Distortion		ΔPRS - Loss In Surge Pressure Ratio Due To Inlet Distortion	
	Surge Line 1	Surge Line 2	Surge Line 1	Surge Line 2
0	16.1	17.8	0	0
0.05	9.1	10.0	6.0	6.6
0.10	2.2	2.2	12.0	13.3
0.11	0.8	0.6	13.2	14.6

Table 1.3 shows:

- o A higher undistorted surge line is compensated by an increased loss in surge pressure ratio with inlet distortion, so that both surge line extrapolations produce the same distorted surge margin for the test conditions of ΔPR/P = 0.10.
- o A high surge line extrapolation (2) gives higher surge margin estimates for distortion levels that are lower than tested and lower surge margin estimates for distortions higher than tested.

Distortion tests should be conducted at or above maximum anticipated distortion levels because interpolation is safer than extrapolation.

1.5 INDEPENDENT CONTROL OF VARIABLE GEOMETRY

When compressor variable geometry is scheduled as a function of a defined engine operating parameter such as corrected rotor speed, surge margin can be defined by the ARP 1420 method using compressor maps representing variable geometry in the scheduled position. Errors from the scheduled geometry setting can be accounted for by utilizing terms describing the effects of these errors on

the surge line and operating airflow. Engines with fan geometry under the direct control of the pilot have been proposed for some applications. In such cases, the variable geometry setting is an independent variable adding a new dimension to compressor maps, surge margin definition, and stability accounting.

SECTION 2

SURGE PRESSURE RATIO CORRELATION

Estimation of the loss of surge pressure ratio (ΔPRS) due to inlet total-pressure distortion is fundamental to accomplishing a stability assessment (Section 3.0). ΔPRS defined in Section 1.0, can be correlated using the distortion descriptor elements described in this section. This section also discusses the rationale underlying the selection of these distortion descriptor elements.

Sample probe readings based upon screen test data are given for a variety of patterns useful for constructing a surge pressure-ratio correlation system and for checking out a distortion descriptor element computation program. To aid this process, the data are given in terms of probe-by-probe total-pressure readings and the associated contour plot; the results are presented as descriptor element values and illustrated with bar charts.

Three correlation systems are described to familiarize the reader with the type of data required for constructing a surge pressure ratio distortion correlation system and to illustrate achievable accuracies. Section 2 ends with discussions of methods for, and problems of, screening inlet data and formulating a universal screening procedure.

2.1 DISTORTION DESCRIPTOR ELEMENT DEFINITIONS

Aerodynamic Interface Plane total-pressure probe data are used to describe inlet distortion directly in terms of the probe readings (pattern) and numerically in terms of distortion descriptors that are related to the severity of the distortion. Distortion descriptors provide a means of identifying critical distorted inlet-flow conditions and of communicating during propulsion system development. A universal distortion descriptor is beyond the state-of-the-art; however, distortion descriptor elements have been identified (Reference 1) for use in structuring a distortion descriptor for a particular engine. These elements are used to define each distortion descriptor system and its associated computation procedure. The distortion descriptor elements are used to quantify the distortion at the AIP. Fundamental to the distortion-descriptor elements is the set of pressure-probe readings that are used to describe the total-pressure distribution. The pressure probes usually are arranged in rake and probe arrays, as described in Section 6. Circumferential and radial distortion elements, which are calculated using the pressure-probe readings, are defined on a ring-by-ring basis. Inlet spatial distortion is described in terms of circumferential and radial elements and is discussed in detail in the following paragraphs.

Circumferential distortion is described for each instrumentation ring in terms of intensity, extent and multiple-per-revolution elements.

Intensity: The circumferential distortion intensity element ($\Delta PC/P$) is a numerical indication of the magnitude of the pressure defect for each ring.

Extent: The circumferential distortion extent element (θ^-) is the angular region, in degrees, in which the pressure is below ring average pressure.

Multiple-per-Revolution: The circumferential distortion multiple-per-revolution element (MPR) is a numerical indication of the "effective" number of low-pressure regions for each ring.

The radial distortion intensity element ($\Delta PR/P$) describes the difference between the ring-average pressure and the face-average pressure for each ring. Both positive and negative values of radial intensity are possible. Positive values reflect a ring-average pressure that is below the face-average pressure.

2.1.1 CIRCUMFERENTIAL DISTORTION ELEMENTS - ONE-PER-REV PATTERNS

The "intensity" and "extent" elements of circumferential distortion are obtained by linear interpolation of the pressures in a given instrumentation ring. Figure 2.1 shows typical pressures for the probes in the i-th ring for one-per-revolution pattern (one pressure defect in 360 degrees). Theta minus, θ_i^-, is the circumferential extent of the low-pressure region measured in degrees. It is defined by the intersection between the ring average pressure and the linear interpolation which subtends the low-pressure region.

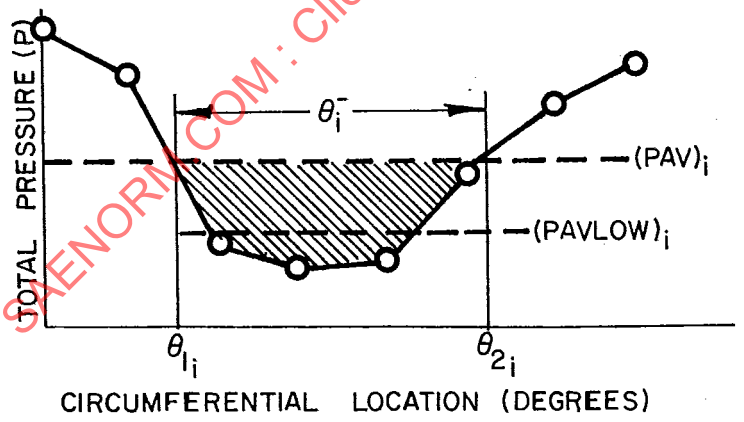

FIGURE 2.1 Ring Circumferential Distortion for a One-Per-Rev Pattern

$$\text{Extent} = (\theta^-)_i = \theta_{2_i} - \theta_{1_i} \qquad (2.1)$$

$$\text{Intensity} \left(\frac{\Delta PC}{P}\right)_i = \frac{(PAV)_i - (PAVLOW)_i}{(PAV)_i} \qquad (2.2)$$

where: $(PAV)_i = \frac{1}{360} \int_0^{360} P(\theta)_i \, d\theta$ = ring average pressure

$P(\theta)_i$ is a function resulting from a linear fit between the data points.

$$(PAVLOW)_i = \frac{1}{\theta_i^-} \int_{\theta_i^-} P(\theta)_i \, d\theta \qquad (2.3)$$

The intensity element is equal to the shaded area of Figure 2.1 divided by the product of θ_i^- times $(PAV)_i$.

$$\text{Multiple-Per-Rev} = (MPR)_i = 1 \qquad (2.4)$$

2.1.2 CIRCUMFERENTIAL DISTORTION ELEMENTS - MULTIPLE-PER-REV PATTERNS

The circumferential distortion intensity and extent elements for multi-lobe distortion patterns also are determined by a linear interpolation procedure. Figure 2.2 shows a pattern with two low-pressure regions separated by two high-pressure regions of extents θ_{i1}^+ and θ_{i2}^+. In all that follows, the analytical expressions are written for the k-th low-pressure region for Q low-pressure regions for each ring. The extent and intensity elements of each low pressure region are calculated by Equations 2.1 and 2.2.

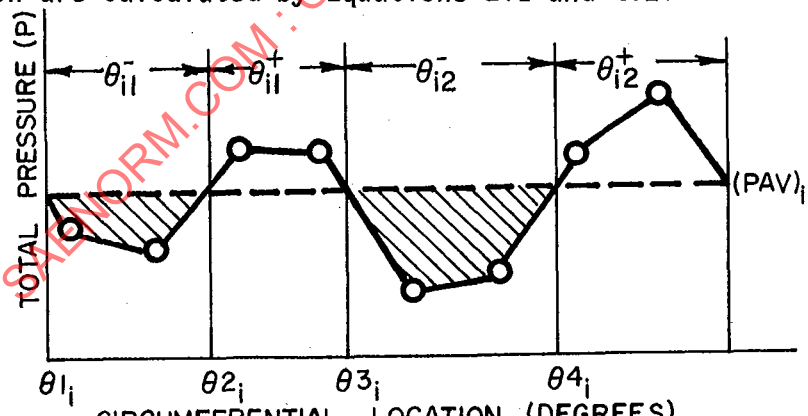

FIGURE 2.2 Ring Circumferential Distortion for a Multiple-Per-Rev Pattern

Patterns with $\theta_{ik}^+ \leq \theta^+$ min

If the pattern has low-pressure regions circumferentially separated by high-pressure regions with extents less than or equal to θ^+ min, it is considered as an equivalent one-per-revolution low-pressure region. θ^+ min is

specified by the descriptor developer and is a function of the predicted or measured engine response to distortion. A value of θ^+ min of approximately 25 degrees is suggested in the absence of other information.

$$\text{Extent} = \theta_i^- = \sum_{k=i}^{Q} \theta_{ik}^- \qquad (2.5)$$

$$= (\theta 2 - \theta 1)_i + (\theta 4 - \theta 3)_i \text{ for Figure 2.2}$$

$$\text{Intensity } \left(\frac{\Delta PC}{P}\right)_i = \frac{(PAV)_i - (PAVLOW)_i}{(PAV)_i} \qquad (2.6)$$

$$\text{where: } (PAVLOW)_i = \frac{1}{\theta_{\cdot i}^-} \sum_{k=1}^{Q} \int_{\theta_{ik}^-} P(\theta)_i \, d\theta \qquad (2.7)$$

$$\text{Hence } \left(\frac{\Delta PC}{P}\right)_i = \frac{\sum_{k=1}^{Q} \left(\frac{\Delta PC}{P}\right)_{ik} \theta^-_{ik}}{\sum_{k=1}^{Q} \theta^-_{ik}} \qquad (2.8)$$

Multiple-Per-Rev = MPR = 1 for this case.

Patterns with $\theta^+_{ik} > \theta^+$ min

If the pattern has low-pressure regions circumferentially separated by high-pressure regions with extents greater than θ^+ min, then the multiple-per-revolution element is greater than one.

Intensity $\left(\frac{\Delta PC}{P}\right)_i$ is the $\left(\frac{\Delta PC}{P}\right)_{ik}$ corresponding to the maximum value of $\left[\left(\frac{\Delta PC}{P}\right)_{ik} \theta^-_{ik}\right]$

Extent θ_i^- is the θ_{ik}^- corresponding to the maximum value of $\left[\left(\frac{\Delta PC}{P}\right)_{ik} \theta^-_{ik}\right]$

The multiple-per-revolution term is defined as the number of equivalent low-pressure regions, the equivalence being based on the ratio of the total integrated area beneath $(PAV)_i$ in Figure 2.2 to the largest single area beneath $(PAV)_i$. This is given by the equation:

$$\text{Multiple-per-revolution} = (MPR)_i = \frac{\sum_{k=1}^{Q}\left[\left(\frac{\Delta PC}{P}\right)_{ik} e^{-ik}\right]}{\max\left[\left(\frac{\Delta PC}{P}\right)_{ik} e^{-ik}\right]} \qquad (2.9)$$

2.1.3 RADIAL DISTORTION ELEMENTS

The radial distortion intensity of a ring is defined as the difference between the face-average pressure and the ring-average pressure divided by the face-average pressure. Both positive and negative values of radial intensity therefore occur; positive values reflect a ring-average pressure that is below the face-average. A typical tip-radial distortion pattern is shown in Figure 2.3. The arrows indicate the difference in radial pressure for Ring 5. For the general ring, i, the radial intensity is given as:

$$\left(\frac{\Delta PR}{P}\right)_i = \frac{(PFAV) - (PAV)_i}{(PFAV)} \qquad (2.10)$$

where (PFAV) is the area-weighted face-average pressure. For N rings at centers of equal areas:

$$(PFAV) = \frac{1}{N}\sum_{i=1}^{N}(PAV)_i \qquad (2.11)$$

It should be noted that the definition of the radial intensity implies that

$$\frac{1}{N}\sum_{i=1}^{N}\left(\frac{\Delta PR}{P}\right)_i = 0.$$

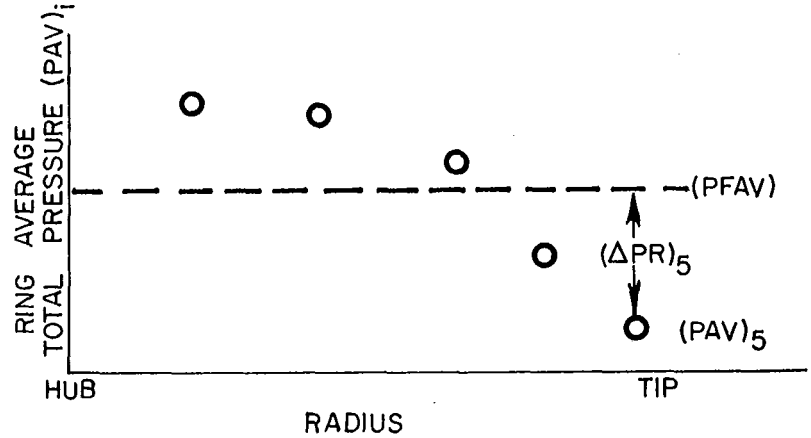

FIGURE 2.3 Radial Distortion Pattern

2.2 RATIONALE FOR ELEMENT DEFINITIONS

The definitions of the distortion-descriptor elements given in Paragraph 2.1 were chosen for a number of reasons. The most important requirement was that the elements should describe well-established facts, that is, the stability of an engine compression component is sensitive to the magnitude of a circumferentially varying total-pressure defect (circumferential intensity), the time a blade spends in the defect region (extent), the number of defects encountered by a blade in one revolution (multiple-per-rev), the magnitude of a radially-varying total-pressure defect (radial intensity) and whether the circumferential and/or radial defects occur in the hub, mid-span or tip regions of the compression-component inlet (Reference 2).

The particular form of the circumferential distortion intensity element was chosen to aid in making hand calculations by avoiding complicated mathematical expansions and to avoid sensitivity to a single-probe low total-pressure reading. The latter was accomplished by averaging the pressures in the low total-pressure region, thus avoiding an expression such as $(P_{MAX} - P_{MIN})/P_{AVG}$ which is descriptive of the flow, but does not take the response of the turbomachinery into account. The circumferential intensity element was nondimensionalized by the ring-average total pressure rather than face-average total pressure in an attempt to reduce the apparent "double bookkeeping" that occurs when analyzing complex aircraft patterns. This "double bookkeeping" occurs when the low total-pressure region may contribute to both the circumferential and radial intensity elements so as to effectively make the defect appear more severe than it actually is.

To reduce the computation time for the time-variant distortion descriptor elements, linear interpolation is considered adequate for determining the angular extent (θ^-) of a low pressure region thus avoiding differing results due to the type of interpolation used (Fourier curve fit, polynominal, spline). This pragmatic approach to handling large amounts of data produces results that correlate to an acceptable degree of accuracy.

A continuous functional representation, indicating the presence of multiple-per-rev regions, rather than an integer jump function, was chosen because the stability response of compression components varies in a continuous manner, depending on the relationship between the intensity-extent products for each of the low-pressure regions.

2.3 SAMPLE ELEMENT CALCULATIONS

As an aid to interpreting and calculating the distortion-descriptor elements, an example inlet pattern, illustrated in Figure 2.4, is examined in detail. The corresponding probe readings, normalized by face-average total pressure, are given in Figure 2.9. The pattern has two low pressure regions separated by more than 25 degrees in the outer rings and is termed a "two-per-rev pattern". The ARP 1420 recommended probe array is superposed. Figure 2.5 illustrates the calculation of the circumferential distortion elements for the

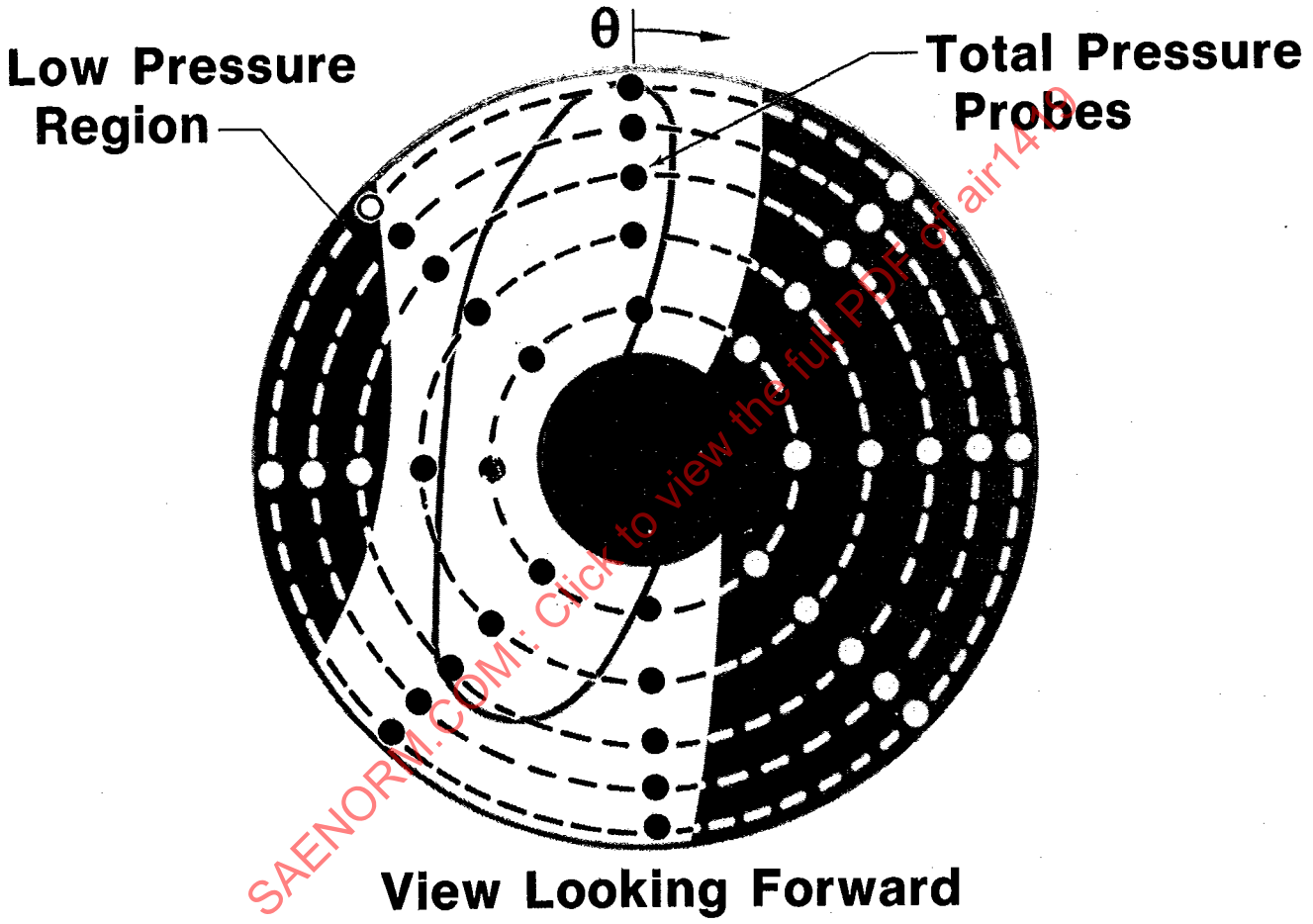

FIGURE 2.4 Example of Inlet Pattern

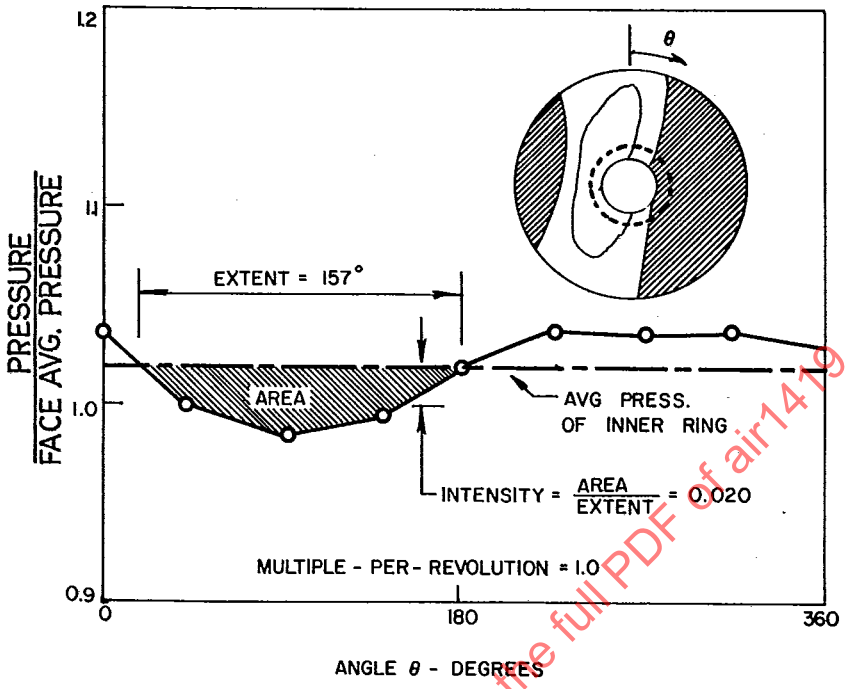

FIGURE 2.5 Circumferential Distortion Elements for Inner Ring

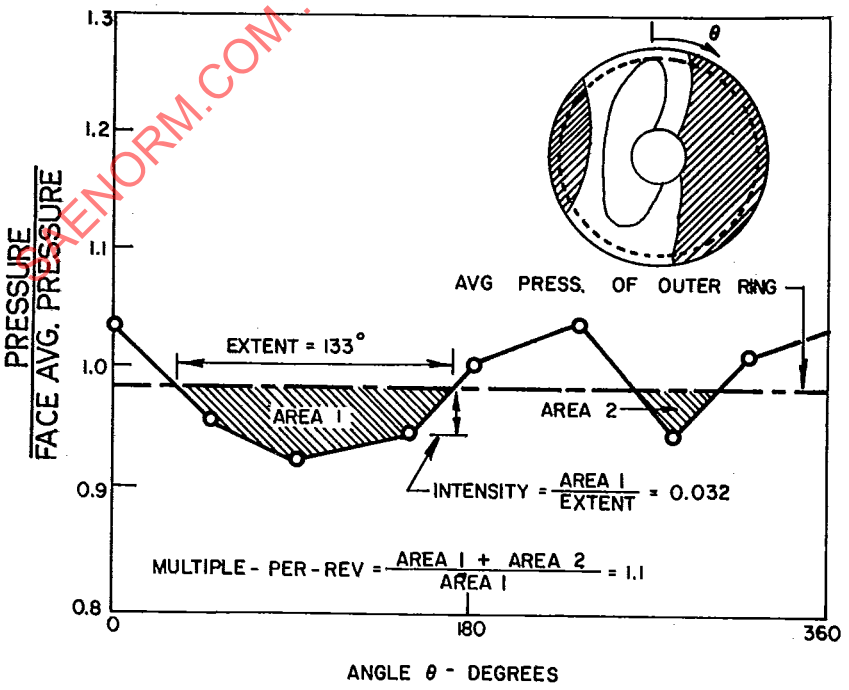

FIGURE 2.6 Circumferential Distortion Elements for Outer Ring

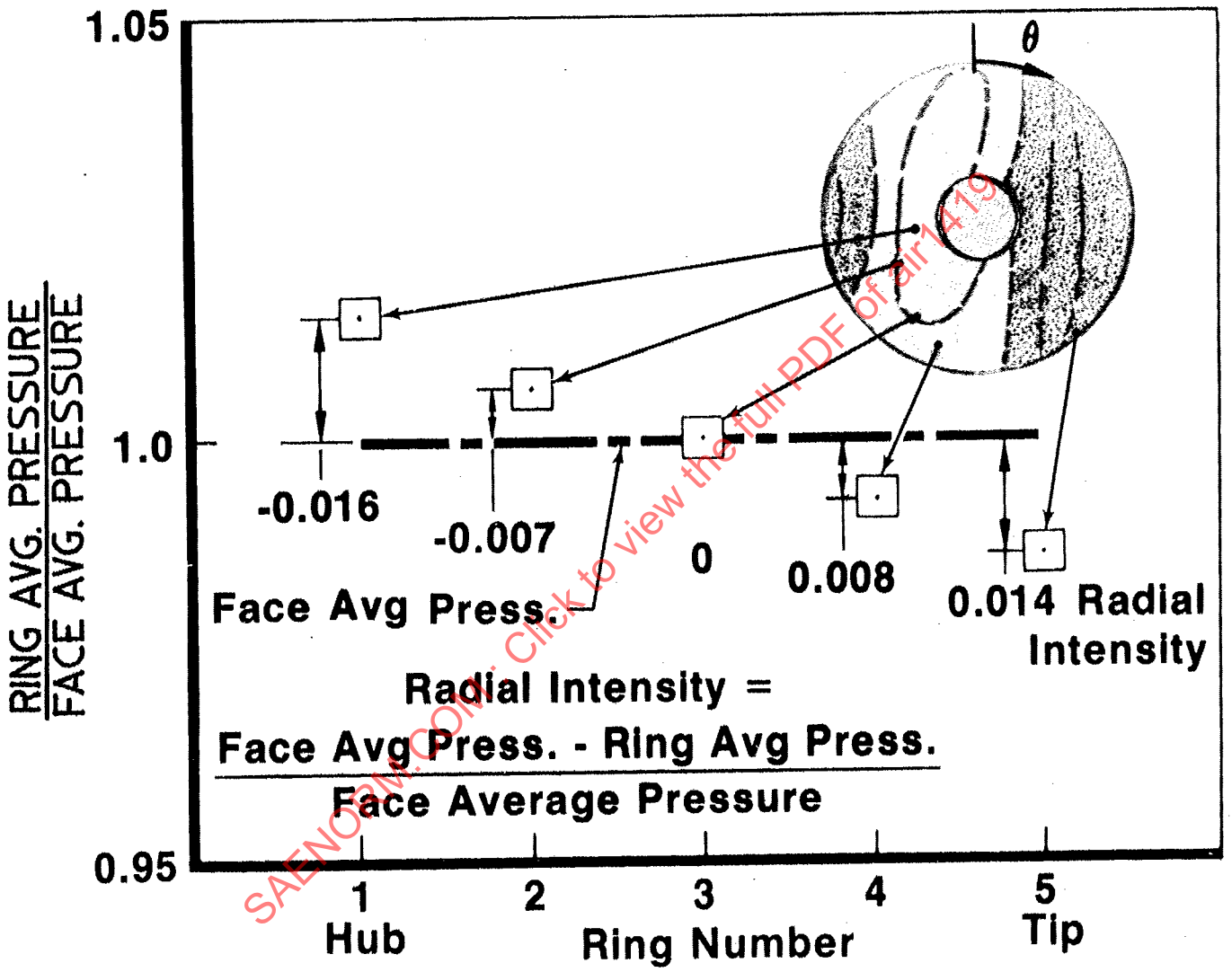

FIGURE 2.7 Radial Distortion Elements

inner ring where the circumferential profile is only a one-per-rev profile. The intensity element ($\Delta PC/P$) is 0.02 per Equations 2.2 and 2.3. The extent element ($\bar{\theta}$) is 157 degrees and the multiple-per-rev element (MPR) is 1.0 per Equation 2.4. The calculation of the circumferential distortion elements for the outer ring is illustrated in Figure 2.6. This ring has two low-pressure regions separated by more than θ^{+}_{min}. In this case, the intensity is equal to the value associated with the largest area under the ring-average total pressure. The multiple-per-rev factor is equal to 1.1 per Equation 2.9. The values of the radial distortion elements, as calculated according to Equation 2.10, are illustrated in Figure 2.7.

All distortion elements for each ring of this pattern can be illustrated using a bar graph display as shown in Figure 2.8. This type of display makes it possible to obtain quickly the following characteristics of the pattern:

1) The circumferential intensity is greatest at the tip.

2) The circumferential extent is greatest at the hub.

3) The only multiple-per-rev content exists at the tip.

4) The radial intensity is greatest at the tip.

This format gives the data and the results in both tabular and pictorial form and will be used to summarize the data and the results for the sample distortion patterns of the next subsection. The data for this example as well as the results are given in Figure 2.9.

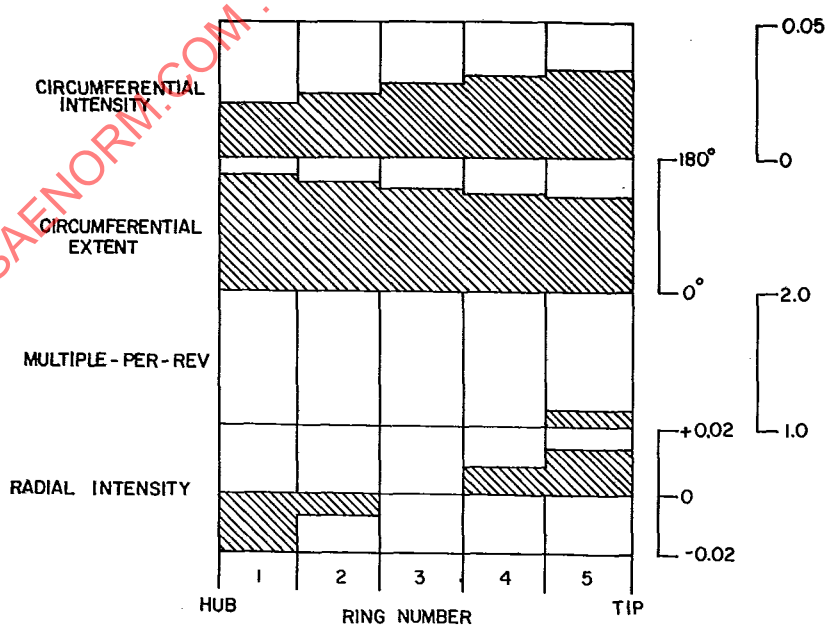

FIGURE 2.8 Distortion-Descriptor Elements for the Example Inlet Pattern

A pattern with two low-pressure regions separated by less than θ^{+}_{min} is illustrated in Figure 2.10. The circumferential distortion intensity element for the outer ring was calculated according to Equation 2.6 and has a value of 0.026.

2.4 EXAMPLE DISTORTION PATTERNS

Example distortion patterns are given in this paragraph for use in checking computer program results and to illustrate the results obtained when calculating the distortion descriptor elements for each of the patterns. The elements of the probe-by-probe data arrays are the probe readings normalized by the area-weighted face-average total pressure.

Each of these patterns is taken from screen test data. Although the patterns of Paragraphs 2.4.1 through 2.4.6 were intended to be classical patterns (180 degree one-per-rev square wave, hub radial, and tip radial), and/or stylized combined patterns (180 degree one-per-rev + hub radial, 180 degree one-per-rev + tip radial, and 90 degree one-per-rev + tip radial), the actual patterns often had significant differences from the intended patterns. It should be noted that screen design is in itself an art and careful attention to detail is required if the desired pattern shapes and distortion element values are to be achieved for all test conditions.

Probe by Probe
(Clockwise From TDC)

RAKE / RING	1	2	3	4	5	6	7	8
1 (HUB)	1.021	.987	.976	.985	1.010	1.028	1.024	1.028
2	1.024	.980	.960	.970	1.005	1.020	1.008	1.018
3	1.027	.972	.948	.960	1.001	1.017	.995	1.010
4	1.025	.963	.938	.950	1.000	1.006	.985	1.004
5 (TIP)	1.026	.957	.930	.942	1.000	1.024	.952	.998

Distortion Descriptor Elements

ELEMENT / RING	$\left(\frac{\Delta PC}{P}\right)_i$	$(\theta^-)_i$	$(MPR)_i$	$\left(\frac{\Delta PR}{P}\right)_i$
1	.0196	157.2	1.00	-.0158
2	.0238	144.7	1.00	-.0065
3	.0272	140.1	1.00	.0005
4	.0298	135.6	1.00	.0079
5	.0315	132.7	1.13	.0139

Contour Plot Pattern

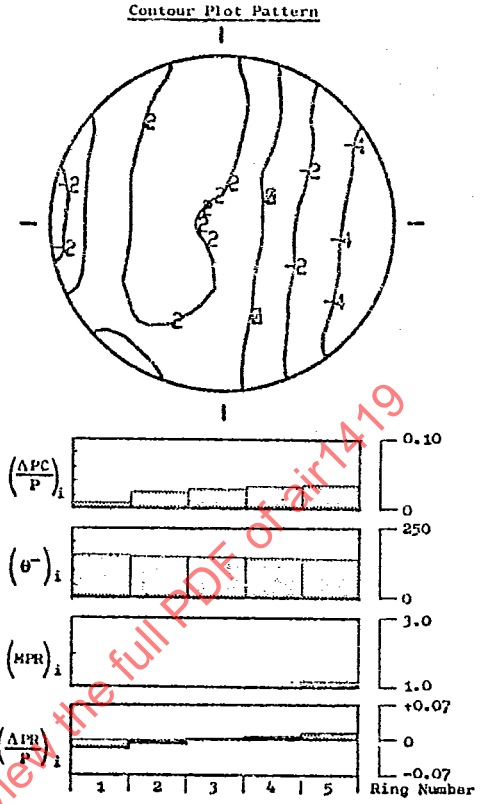

FIGURE 2.9 Sample Pattern Definition and Results

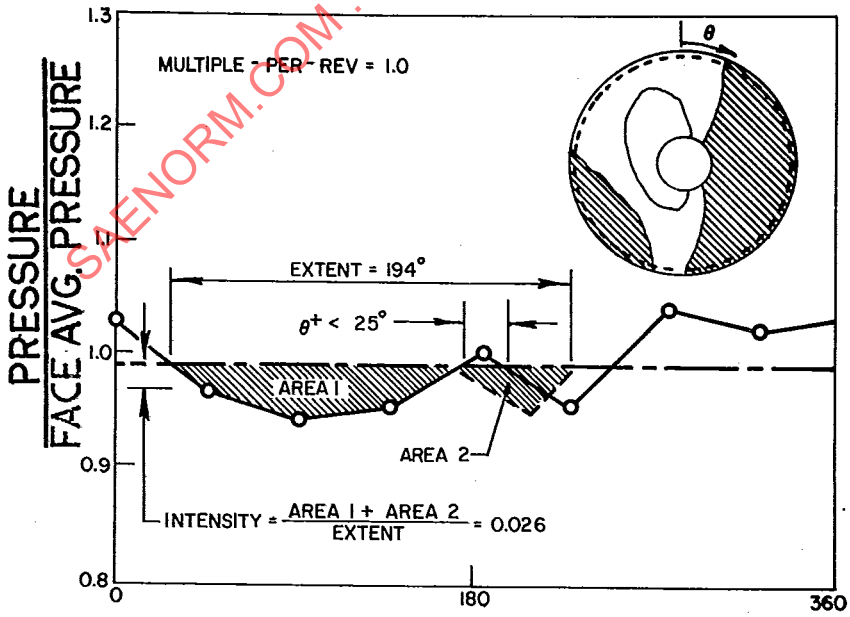

FIGURE 2.10 Equivalent One-Per-Rev Pattern

2.4.1 180 DEGREE ONE-PER-REV CIRCUMFERENTIAL DISTORTION PATTERN

The information relevant to this pattern is given in Figure 2.11. The ring circumferential intensity values are nearly constant and the angular extent of the circumferential distortion is uniform from ring-to ring. There is no multiple-per-rev content and very little radial distortion content.

2.4.2 HUB RADIAL DISTORTION PATTERN

The information relevant to this pattern is given in Figure 2.12. This hub radial pattern has almost no circumferential distortion. The angular extent and multiple-per-rev elements have little physical significance.

2.4.3 TIP RADIAL DISTORTION PATTERN

The information relevant to this pattern is given in Figure 2.13. This tip radial pattern has essentially no circumferential distortion. The angular extent and multiple-per-rev elements have little physical significance.

2.4.4 180 DEGREE ONE-PER-REV + HUB RADIAL COMBINED DISTORTION PATTERN

The information relevant to this pattern is given in Figure 2.14. This 180 degrees one-per-rev + hub radial combined distortion pattern has fairly uniform circumferential angular extent, and tip radial distortion intensity elements. There is minor multiple-per-rev content in the tip.

2.4.5 180 DEGREE ONE-PER-REV + TIP RADIAL COMBINED DISTORTION PATTERN

The information relevant to this pattern is given in Figure 2.15. This 180 degree one-per-rev + tip radial combined distortion pattern has fairly uniform circumferential and angular extent distortion elements. There is no multiple-per-rev content. The tip-radial-distortion content is not as uniform as might be desired.

2.4.6 90 DEGREE ONE-PER-REV + TIP RADIAL COMBINED DISTORTION PATTERN

The information relevant to this pattern is given in Figure 2.16. This 90 degree one-per-rev + tip radial combined distortion pattern has essentially uniform circumferential and angular extent distortion elements. There is no multiple-per-rev content in this pattern. The nonuniformity of the tip radial content is similar to that of the 180 degree one-per-rev + tip radial combined distortion pattern.

2.4.7 TWO-PER-REV WITH LOWS CLOSER THAN 25 DEGREES AND WITH TIP RADIAL DISTORTION PATTERN

The information relevant to this pattern is given in Figure 2.17. This pattern is treated as a one-per-rev pattern which has a nearly uniform circumferential extent of approximately 140 degrees. The circumferential distortion level is nearly uniform ring-to-ring with a value of approximately 0.07, and the radial distortion is located at the tip with a value of approximately 0.02.

2.4.8 TWO-PER-REV WITH LOWS FURTHER APART THAN 25 DEGREES AND WITH TIP RADIAL DISTORTION PATTERN

The information relative to this pattern is given in Figure 2.18. The multiple-per-rev descriptor element for this pattern has a value of almost two, making it a "bona fide" two-per-rev pattern. The extent of the largest low pressure region is approximately 71 degrees. The circumferential distortion is essentially uniform from hub to tip with a value of approximately 0.07 and a tip-radial-distortion value of approximately 0.02.

2.4.9 AIRCRAFT PATTERN

The information relevant to this pattern is given in Figure 2.19. This pattern has strong mid-span circumferential distortion and strong tip radial content. The circumferential distortion is essentially 180 degrees in extent, and no multiple-per-rev content is present.

2.5 CORRELATION METHODS

The loss of compressor surge pressure ratio is related to the distortion-descriptor elements given in Paragraph 2.1. There does not appear to be any simple or unique form for combining the elements to correlate the loss in surge pressure ratio that will meet the accuracy requirements for every compressor. However, the equation given below and in Figure 2.20 is general in nature and can be expanded to include nearly any distortion descriptor used to date:

$$\Delta PRS = \sum_{i=1}^{N} \left[KC_i \left(\frac{\Delta PC}{P} \right)_i + KR_i \left(\frac{\Delta PR}{P} \right)_i + C_i \right] \times 100 \qquad (2.12)$$

where ΔPRS is the loss of surge pressure ratio due to distortion, expressed as a percent of the undistorted surge pressure ratio.

N is the number of instrumentation rings

KC is the circumferential distortion sensitivity

KR is the radial distortion sensitivity

$\frac{\Delta PC}{P}$ is the circumferential distortion intensity defined in 2.1.1

$\frac{\Delta PR}{P}$ is the radial distortion intensity defined in 2.1.2

C is an offset term

The sensitivity and offset coefficients are generalized coefficients and will vary with distortion content (extent, multiple-per-rev), compression system design, and operating conditions. They are derived from test data and should be

AIR 1419

Probe by Probe
(Clockwise from TDC)

RING \ RAKE	1	2	3	4	5	6	7	8
1 (HUB)	.906	.912	.962	1.101	1.116	1.079	.924	.915
2	.903	.897	1.075	1.119	1.103	1.139	.946	.902
3	.905	.904	1.048	1.076	1.096	1.107	.935	.907
4	.906	.899	1.058	1.090	1.107	1.115	.943	.905
5 (TIP)	.908	.914	1.028	1.069	1.071	1.090	.949	.925

Distortion Descriptor Elements

RING \ ELEMENT	$\left(\frac{\Delta PC}{P}\right)_i$	$(\theta^-)_i$	$(MPR)_i$	$\left(\frac{\Delta PR}{P}\right)_i$
1	0.0652	207.8	1.00	0.0095
2	0.0877	178.7	1.00	-0.0117
3	0.0755	180.4	1.00	0.0016
4	0.0800	180.1	1.00	-0.0040
5	0.0634	181.1	1.00	0.0046

Contour Plot Pattern

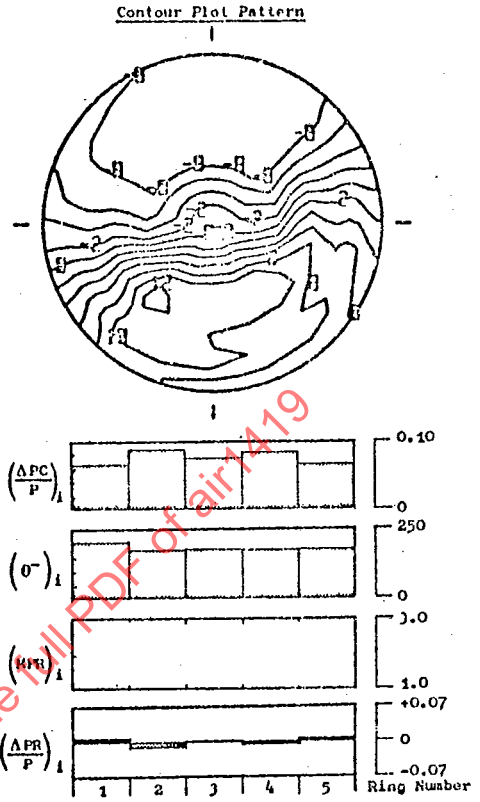

FIGURE 2.11 180 Degree 1/Rev Circumferential Distortion Pattern

Probe by Probe
(Clockwise from TDC)

RING \ RAKE	1	2	3	4	5	6	7	8
1 (HUB)	.943	.944	.938	.942	.945	.946	.947	.938
2	.972	.955	.982	.967	.957	.968	.959	.941
3	1.023	1.013	1.017	1.011	1.021	1.003	1.020	1.007
4	1.038	1.038	1.053	1.045	1.048	1.050	1.063	1.051
5 (TIP)	1.031	1.026	1.030	1.020	1.019	1.043	1.032	1.035

Distortion Descriptor Elements

RING \ ELEMENT	$\left(\frac{\Delta PC}{P}\right)_i$	$(\theta^-)_i$	$(MPR)_i$	$\left(\frac{\Delta PR}{P}\right)_i$
1	0.0025	94.7	1.7419	0.0571
2	0.0103	94.5	1.2779	0.0374
3	0.0056	58.5	1.7627	-0.0143
4	0.0039	191.9	1.0000	-0.0507
5	0.0048	178.32	1.0000	-0.0395

Contour Plot Pattern

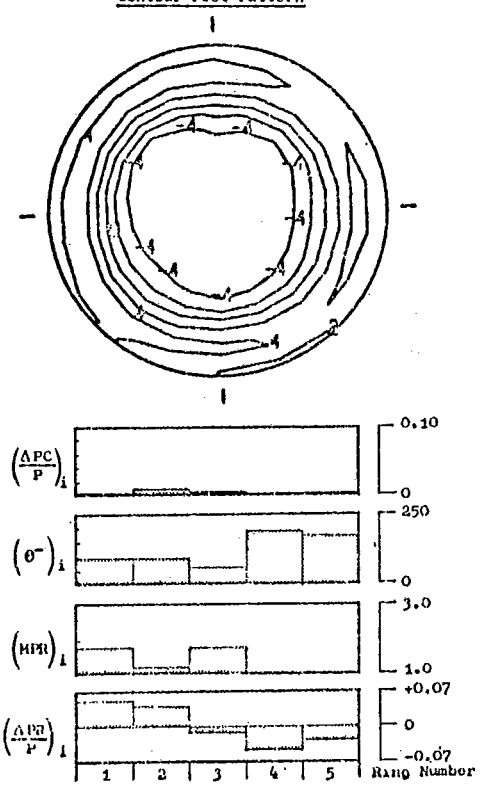

FIGURE 2.12 Hub-Radial Distortion Pattern

Probe by Probe
(Clockwise from TDC)

RING \ RAKE	1	2	3	4	5	6	7	8
1 (HUB)	1.044	1.037	1.028	1.030	1.038	1.032	1.043	1.032
2	1.054	1.033	1.051	1.040	1.035	1.048	1.045	1.034
3	1.000	1.010	.997	1.029	1.002	1.022	1.008	1.021
4	.970	.960	.961	.960	.954	.976	.960	.975
5 (TIP)	.948	.943	.943	.943	.945	.954	.952	.945

Contour Plot Pattern

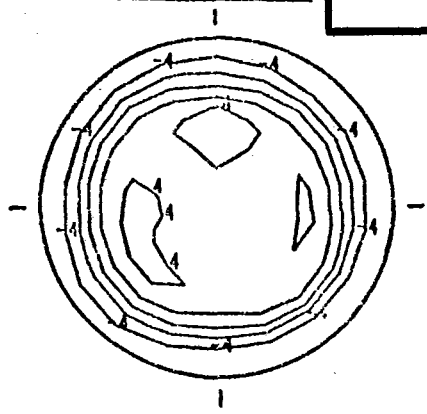

Distortion Descriptor Elements

RING \ ELEMENT	$\left(\frac{\Delta PC}{P}\right)_i$	$(\theta^-)_i$	$(HPR)_i$	$\left(\frac{\Delta PR}{P}\right)_i$
1	0.0044	113.4	1.2297	-0.0354
2	0.0040	81.2	2.3086	-0.0424
3	0.0066	133.7	1.2195	-0.0111
4	0.0050	176.7	1.0687	0.0356
5	0.0031	175.7	1.0555	0.0534

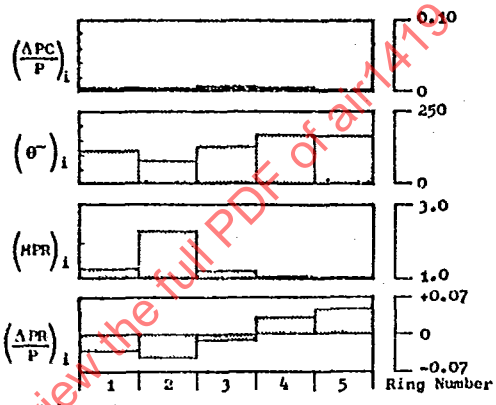

FIGURE 2.13 Tip-Radial Distortion Pattern

Probe by Probe
(Clockwise from TDC)

RING \ RAKE	1	2	3	4	5	6	7	8
1 (HUB)	.874	.874	.941	1.035	1.050	1.037	.910	.877
2	.884	.898	.996	.988	1.009	1.013	.965	.889
3	.925	.930	1.067	1.086	1.077	1.090	.961	.920
4	.940	.938	1.124	1.151	1.143	1.140	.986	.942
5 (TIP)	.938	.930	1.104	1.010	1.086	1.120	1.007	.949

Contour Plot Pattern

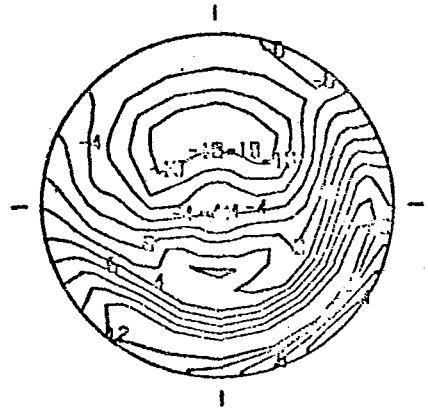

Distortion Descriptor Elements

RING \ ELEMENT	$\left(\frac{\Delta PC}{P}\right)_i$	$(\theta^-)_i$	$(HPR)_i$	$\left(\frac{\Delta PR}{P}\right)_i$
1	0.0610	198.3	1.00	0.0456
2	0.0541	155.5	1.00	0.0400
3	0.0660	176.3	1.00	-0.0120
4	0.0808	178.4	1.00	-0.0566
5	0.0403	162.1	1.0034	-0.0230

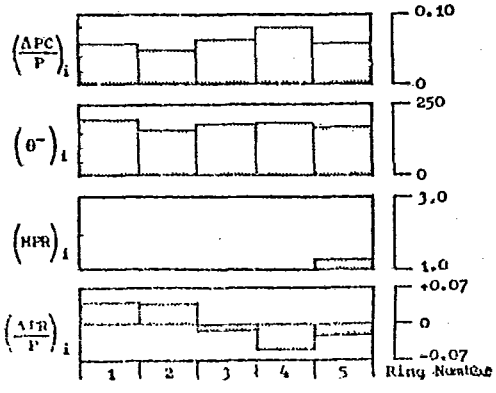

FIGURE 2.14 180 Degree 1/Rev + Hub-Radial Combined Distortion Pattern

AIR 1419

Probe by Probe
(Clockwise from TDC)

RAKE / RING	1	2	3	4	5	6	7	8
1 (HUB)	.961	.936	1.024	1.144	1.175	1.120	.988	.947
2	.939	.943	1.128	1.131	1.143	1.166	1.000	.930
3	.927	.910	1.102	1.131	1.104	1.082	.958	.924
4	.876	.885	1.062	1.041	1.050	1.057	.931	.889
5 (TIP)	.873	.871	1.002	1.006	1.032	1.006	.921	.868

Distortion Descriptor Elements

ELEMENT / RING	$\left(\frac{\Delta PC}{P}\right)_i$	$\left(\theta^-\right)_i$	$\left(MPR\right)_i$	$\left(\frac{\Delta PR}{P}\right)_i$
1	0.0662	201.5	1.00	-0.0322
2	0.0839	173.3	1.00	-0.0427
3	0.0757	181.6	1.00	-0.0126
4	0.0744	172.9	1.00	0.0306
5	0.0628	175.2	1.00	0.0569

Contour Plot Pattern

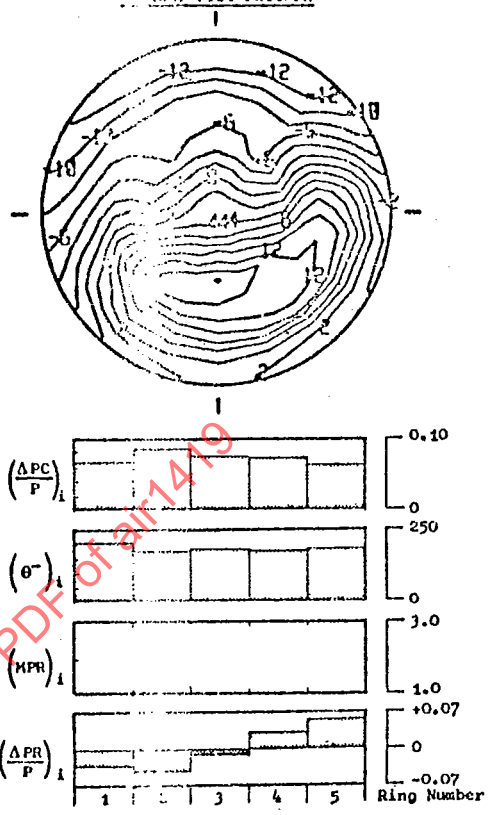

FIGURE 2.15 180 Degree 1/Rev + Tip-Radial Combined Distortion Pattern

Probe by Probe
(Clockwise from TDC)

RAKE / RING	1	2	3	4	5	6	7	8
1 (HUB)	.987	.962	.982	1.068	1.086	1.061	1.076	1.069
2	.961	.939	1.091	1.072	1.086	1.064	1.080	1.064
3	.911	.913	1.020	1.034	1.010	1.046	1.012	1.026
4	.878	.873	.989	1.002	.984	.987	.985	.997
5 (TIP)	.872	.858	.970	.983	.981	.985	.972	.961

Distortion Descriptor Elements

ELEMENT / RING	$\left(\frac{\Delta PC}{P}\right)_i$	$\left(\theta^-\right)_i$	$\left(MPR\right)_i$	$\left(\frac{\Delta PR}{P}\right)_i$
1	0.0472	145.5	1.00	-0.0390
2	0.0631	112.8	1.00	-0.0473
3	0.0592	113.6	1.00	0.0009
4	0.0631	111.2	1.00	0.0356
5	0.0600	113.4	1.00	0.0498

Contour Plot Pattern

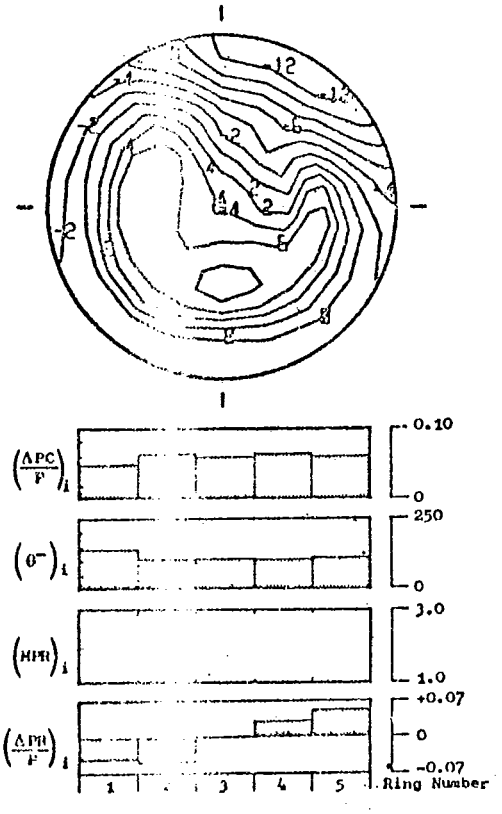

FIGURE 2.16 90 Degree 1/Rev + Tip-Radial Combined Distortion Pattern

Probe by Probe

RING \ RAKE	1	2	3	4	5	6	7	8	9	10	11	12
1 (HUB)	1.060	0.911	0.911	1.056	0.905	0.905	1.055	1.055	1.056	1.056	1.057	1.060
2	1.073	0.900	0.900	1.062	0.903	0.903	1.056	1.056	1.062	1.062	1.058	1.073
3	1.060	0.911	0.911	1.057	0.907	0.907	1.059	1.059	1.057	1.057	1.054	1.060
4	1.058	0.908	0.902	1.049	0.899	0.899	1.052	1.052	1.049	1.049	1.029	1.058
5 (TIP)	1.010	0.895	0.895	1.026	0.889	0.889	1.021	1.021	1.026	1.026	0.998	1.010

Contour Plot Pattern

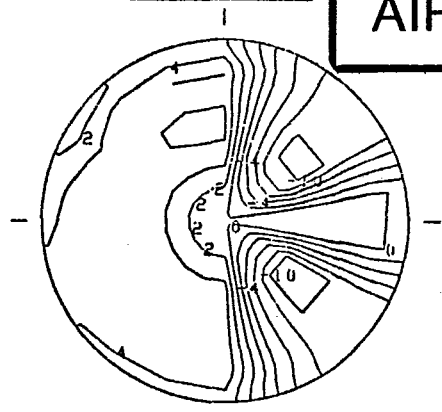

Distortion Descriptor Elements

ELEMENT / RING	$\left(\frac{\Delta PC}{P}\right)_i$	$(\theta^-)_i$	$(MPR)_i$	$\left(\frac{\Delta PR}{P}\right)_i$
1	0.0704	140.0	1.00	-0.0072
2	0.0761	139.8	1.00	-0.0091
3	0.0704	139.8	1.00	-0.0082
4	0.0710	138.7	1.00	0.0001
5	0.0613	138.0	1.00	0.0244

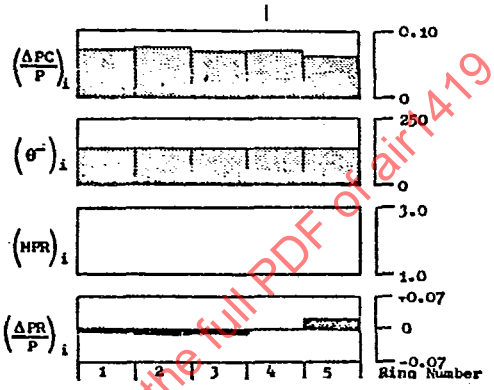

FIGURE 2.17 2/Rev With Lows Closer Than 25 Degrees and With Tip-Radial Distortion Pattern

Probe by Probe

RING \ RAKE	1	2	3	4	5	6	7	8	9	10	11	12
1 (HUB)	1.060	0.911	0.911	1.056	1.056	1.056	1.057	0.905	0.905	1.055	1.055	1.060
2	1.073	0.900	0.900	1.062	1.062	1.062	1.056	0.903	0.903	1.056	1.056	1.073
3	1.060	0.911	0.911	1.057	1.057	1.057	1.054	0.907	0.907	1.059	1.059	1.060
4	1.058	0.908	0.902	1.049	1.049	1.049	1.029	0.899	0.899	1.052	1.052	1.058
5 (TIP)	1.010	0.895	0.895	1.026	1.026	1.026	0.998	0.889	0.889	1.021	1.021	1.010

Contour Plot Pattern

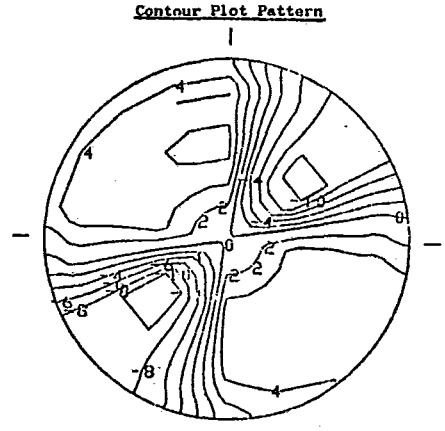

Distortion Descriptor Elements

ELEMENT / RING	$\left(\frac{\Delta PC}{P}\right)_i$	$(\theta^-)_i$	$(MPR)_i$	$\left(\frac{\Delta PR}{P}\right)_i$
1	0.0724	70.7	1.93	-0.0072
2	0.0749	71.4	2.00	-0.0091
3	0.0717	70.7	1.94	-0.0082
4	0.0710	73.0	1.93	0.0001
5	0.0626	73.5	1.89	0.0244

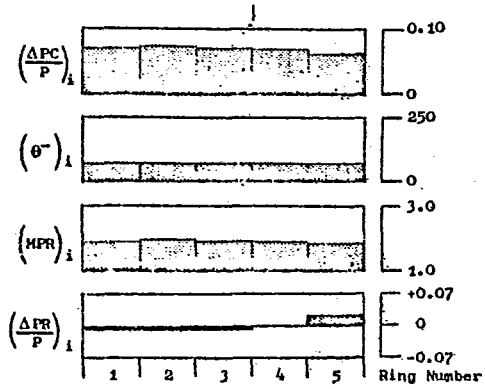

FIGURE 2.18 2/Rev With Lows Further Apart Than 25 Degrees and With Tip-Radial Distortion Pattern

AIR 1419

Probe by Probe
(Clockwise from TDC)

RAKE / RING	1	2	3	4	5	6	7	8
1 (HUB)	1.124	1.089	1.010	.947	1.017	1.037	1.039	1.082
2	1.109	1.100	1.024	.888	.937	1.020	1.025	1.092
3	1.088	1.075	1.030	.891	.896	.972	.980	1.088
4	1.050	1.027	1.008	.938	.893	.989	.948	1.029
5 (TIP)	.949	.945	.953	.897	.902	.913	.904	.972

Contour Plot Pattern

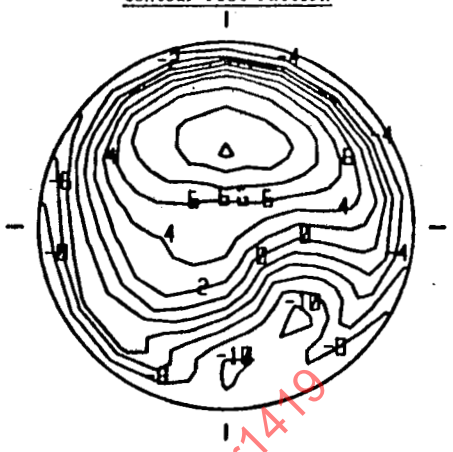

Distortion Descriptor Elements

ELEMENT / RING	$\left(\frac{\Delta PC}{P}\right)_i$	$(\theta^-)_i$	$(MPR)_i$	$\left(\frac{\Delta PR}{P}\right)_i$
1	0.0327	203.2	1.00	-0.0463
2	0.0574	174.6	1.00	-0.0275
3	0.0624	180.5	1.00	-0.0056
4	0.0394	180.2	1.00	0.0117
5	0.0236	177.8	1.00	0.0678

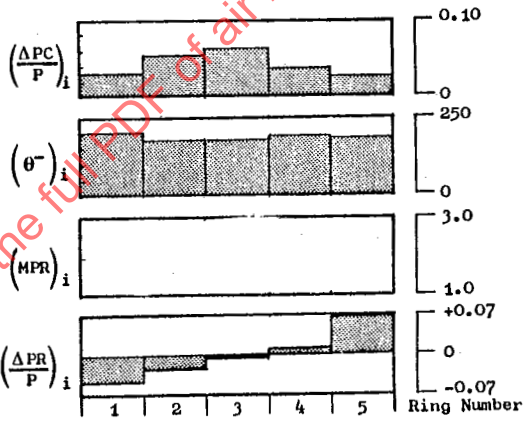

FIGURE 2.19 Aircraft Pattern

$$\Delta PRS = [\text{Circ Term} + \text{Radial Term} + \text{Constant Term}]$$

$$\Delta PRS = \sum_{I=1}^{N} \left[KC_I \left(\frac{\Delta PC}{P}\right)_I + KR_I \left(\frac{\Delta PR}{P}\right)_I + C_I \right] \times 100$$

Circ Sensitivity

Circ Intensity

Radial Sensitivity

Radial Intensity

Constant Term

FIGURE 2.20 Basic Equation for Calculating Surge Pressure Ratio Loss (ΔPRS)

of sufficient accuracy to correlate the effect of critical distortion patterns within ±2 percent surge pressure ratio. For practical purposes, the generalized coefficients are often expanded. An example of the expanded circumferential sensitivity is given in Figure 2.21. This expanded sensitivity is a function of the defect location (hub, mid-span, or tip), the extent and multiple-per-rev circumferential distortion descriptor elements, as well as the reference sensitivity. The reference sensitivity, usually based on a 180 degrees one-per-rev circumferential distortion pattern, is generally represented by a constant at a given corrected speed. If significant nonlinearities occur in the loss of surge pressure ratio with the level of intensity relationship for the reference pattern, especially at high levels, the relationship can be treated as being piecewise linear. This then leads to reference sensitivities which vary with level of intensity and contribute to the offset term, C_i.

$$\Delta PRS = \sum_{i=1}^{N} \left[KC_i \left(\frac{\Delta PC}{P} \right)_i + KR_i \left(\frac{\Delta PR}{P} \right)_i + C_i \right] \times 100$$

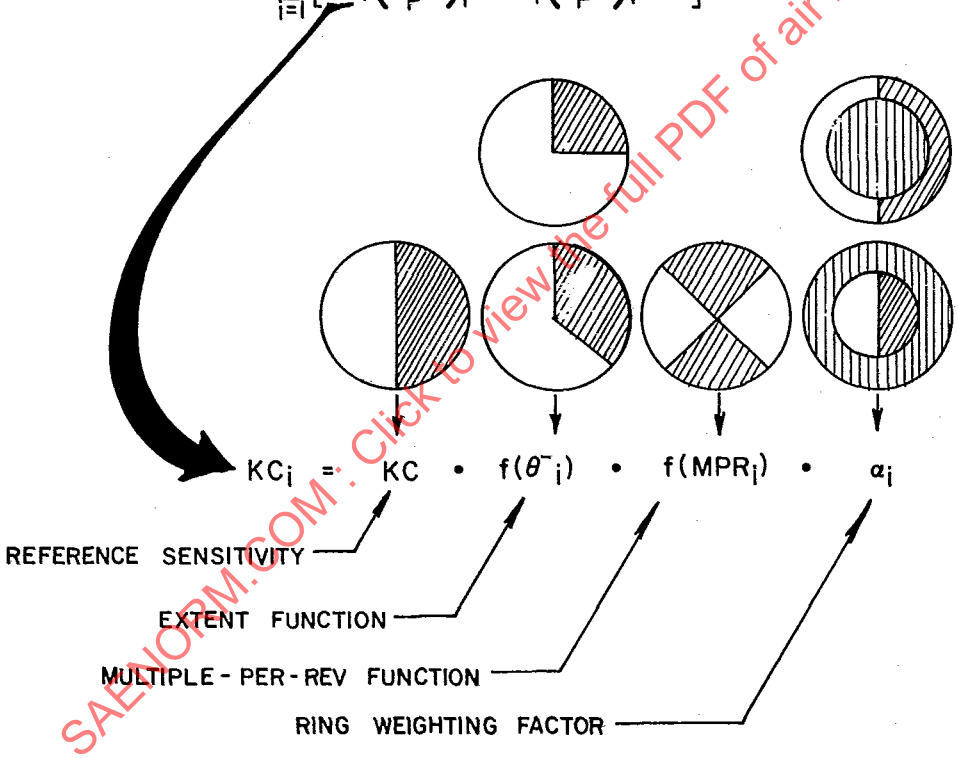

FIGURE 2.21 Example of Expanded Circumferential Sensitivity

The loss in surge pressure ratio for downstream compression components can be calculated according to Equation 2.12 through the introduction of distortion transfer and generation coefficients in the sensitivity parameters. Methods for accomplishing this are discussed in Paragraphs 2.5.2.4 and 2.5.3.4.

The following paragraphs provide examples of three methods that have been used to correlate the loss of surge pressure ratio for compression components. In two cases, the correlation makes full use of ARP 1420 distortion-descriptor elements, but are not in use in conjunction with an aircraft program, while the third is in use with an aircraft program, but the circumferential distortion intensity is not the ARP 1420 definition. Further, examples of correlations, based on distortion elements similar to those derived in ARP 1420, are given to show the broad range of components that can be treated using this correlation method.

2.5.1 METHOD A

Method A has been used to correlate data from a three-stage fan in terms of ARP 1420 distortion descriptor elements with the same accuracy as an existing distortion index that has been verified by distortion screen tests, propulsion system tests, and flight tests.

The example shows a data correlation in terms of four empirical correlation coefficients, namely: circumferential sensitivity, radial sensitivity, hub-radial offset, and tip radial offset. Fictional, but typical, values of these correlation coefficients are presented as functions of inlet corrected airflow.

The philosophy of Method A is:

- The circumferential sensitivity of Equation 2.12 is expanded to include ring-weighting factors, an extent factor, and a multiple-per-revolution factor.
- The loss in surge pressure ratio due to circumferential distortion is proportional to a weighted average of the distortion-descriptor elements over the entire interface plane.
- The loss in surge pressure ratio due to radial distortion is evaluated for two annular regions. For an interface plane defined by five instrumentation rings, the hub region consists of the inner two instrumentation rings and the tip region consists of the outer two instrumentation rings.
- The loss in surge pressure ratio due to radial distortion is the higher of the losses evaluated for the hub and tip regions.
- The loss in surge pressure ratio due to combined circumferential and radial distortions is obtained by algebraic superposition of circumferential and radial terms.
- Correlation coefficients are functions of corrected inlet airflow only, and are independent of the distortion pattern.
- Loss in surge pressure ratio due to inlet distortion is measured from an undistorted surge line with uniform inlet flow as defined in Section 1.2.

2.5.1.1 Definition of Terms

ΔPRS_C is the loss in surge pressure ratio due to circumferential distortion expressed as a percentage of the undistorted surge pressure ratio.

N is the number of instrumentation rings.

α_i is the weighting factor for ring i. To represent an existing distortion index, α_i was selected to be inversely proportional to the instrumentation ring diameter, subject to

$$\sum_{i=1}^{N} \alpha_i = 1.$$

K_C is the average circumferential sensitivity, determined empirically

$\left(\frac{\Delta PC}{P}\right)_i$ is the ARP 1420 circumferential distortion intensity of ring i.

$\bar{\theta}_i$ is the ARP 1420 circumferential extent of the distortion in ring i in degrees.

$(MPR)_i$ is the ARP 1420 multiple per revolution element for ring i.

ΔPRS_h is the loss in surge pressure ratio due to hub radial distortion expressed in percent of the undistorted surge pressure ratio.

ΔPRS_t is the loss in surge pressure ratio due to tip radial distortion expressed in percent of the undistorted surge pressure ratio.

ΔPRS is the loss in surge pressure ratio due to inlet distortion expressed in percent of the undistorted surge pressure ratio (ARP 1420 definition).

ΔPRS_r is the loss in surge pressure ratio due to radial distortion expressed in percent of the undistorted surge pressure ratio.

K_r is the average radial sensitivity, determined empirically.

$\left(\frac{\Delta PR}{P}\right)_i$ is the ARP 1420 radial distortion intensity of ring i. This intensity can be either positive or negative.

C_h, C_t are the radial offset terms for the hub and tip, respectively. Usually one is close to zero, denoting the region closest to surge, while the other is negative, reflecting the higher surge margin of the region furthest from surge.

2.5.1.2 Formulae for Loss of Surge Pressure Ratio

The loss in surge pressure ratio due to circumferential distortion is obtained from a weighted average of distortion-descriptor elements over the interface plane.

$$\Delta PRS_c = \left[\sum_{i=1}^{N} \alpha_i K_c \left(\frac{\Delta PC}{P}\right)_i \left(\frac{\bar{\theta}_i}{180}\right) \left(\frac{1}{MPR}\right)_i\right] \times 100 \qquad (2.14)$$

The ring weighting factor, extent function, and multiple-per-rev function of Equation 2.14 were based on experience with similar fans; consequently, the circumferential sensitivity, K_c, is the only empirically determined correlating parameter in Equation 2.14.

The loss in surge pressure ratio due to radial distortion is the higher of the loss of the hub or tip regions. Equation 2.15a describes the loss in surge pressure ratio in the hub region which consists of rings 1 and 2, weighted equally. Equation 2.15b describes the loss in surge pressure ratio in the tip region which consists of rings 4 and 5, weighted equally. Equation 2.15c determines whether the hub or tip region is critical for the stability of the particular radial inlet pattern and inlet airflow under investigation.

$$\Delta PRS_h = \left\{\left[\sum_{i=1}^{2} 1/2\, K_r \left(\frac{\Delta PR}{P}\right)_i\right] + C_h\right\} \times 100 \qquad (2.15a)$$

$$\Delta PRS_t = \left\{\left[\sum_{i=N-1}^{N} 1/2\, K_r \left(\frac{\Delta PR}{P}\right)_i\right] + C_t\right\} \times 100 \qquad (2.15b)$$

$$\Delta PRS_r = \text{larger of } \Delta PRS_h \text{ or } \Delta PRS_t \qquad (2.15c)$$

Circumferential and radial terms are added:

$$\Delta PRS = \Delta PRS_c + \Delta PRS_r \qquad (2.15d)$$

The set of Equations 2.14, 2.15a, 2.15b, 2.15c, and 2.15d are equivalent to general Equation 2.12. An example illustrating this equivalence is shown in Section 2.5.1.5.

2.5.1.3 Correlation Coefficients

Circumferential Distortion

The circumferential sensitivity is established from tests with 180 degrees classical inlet distortion screens. A typical variation of circumferential sensitivity with corrected airflow is shown in Figure 2.22.

Radial Distortion

Typical variations of radial sensitivity, hub-radial offset, and tip-radial offset are given in Figures 2.23, 2.24, and 2.25, respectively. The combination of radial sensitivity, hub-radial offset, and tip-radial offset is used to model the piecewise linear loss of surge pressure ratio with radial distortion, as discussed below. Under ideal conditions (no error), one radial offset should be zero while the other should be either zero or negative. From Figure 2.24 and 2.25, it can be seen that below 60 percent airflow the hub-radial offset is significantly negative while the tip-radial offset is not zero, but is between 0.0 and -0.02. This nonzero tip radial offset reflects error in the undistorted surge-pressure-ratio measurement. This correlation assumes that the undistorted surge pressure ratio was measured between 0 and 2 percent lower than the true value in this airflow range. Similarly, the nonzero hub-radial offset above 95 percent airflow describes an undistorted surge margin that is assumed to be measured a fraction of a percent lower than the true value.

Piecewise-linear Radial Distortion Correlation

The loss in surge pressure ratio due to hub-radial distortion usually has a significantly different characteristic than the loss in surge pressure ratio for a tip-radial distortion of the same magnitude as illustrated in Figure 2.26. The surge line of a fan can usually be increased by a small amount of either hub-radial or tip-radial distortion. Consequently, the piecewise-linear curve shown in Figure 2.27 is faired through the data of Figure 2.26. Figure 2.27 shows an increase in surge line (negative ΔPRS) over the undistorted surge line for hub distortions with an intensity less than 0.1. The slope of the line (radial sensitivity) is assumed equal for both hub and tip distortions. If there were more data points to justify different slopes, then different sensitivities could be used for hub-radial and tip-radial distortions.

Figure 2.28 illustrates the use of hub and tip radial offset terms to describe the intercepts of the linear correlation lines on the zero distortion axis. Figure 2.29 illustrates the equation used to correlate loss in surge pressure ratio due to radial distortion. In this example, the hub constant $C_h = -0.06$ while the tip constant $C_t = 0$. This can be interpreted as the hub having six percent more surge margin than the tip which can be used to offset the destabilizing effects of hub-radial and circumferential distortions. The loss in surge pressure ratio is the maximum value calculated from either the hub or tip correlation equations. For this example, the hub is critical for hub-distortion intensities greater than 0.05 while the tip is critical for hub-distortions less than 0.05 and for all tip distortions.

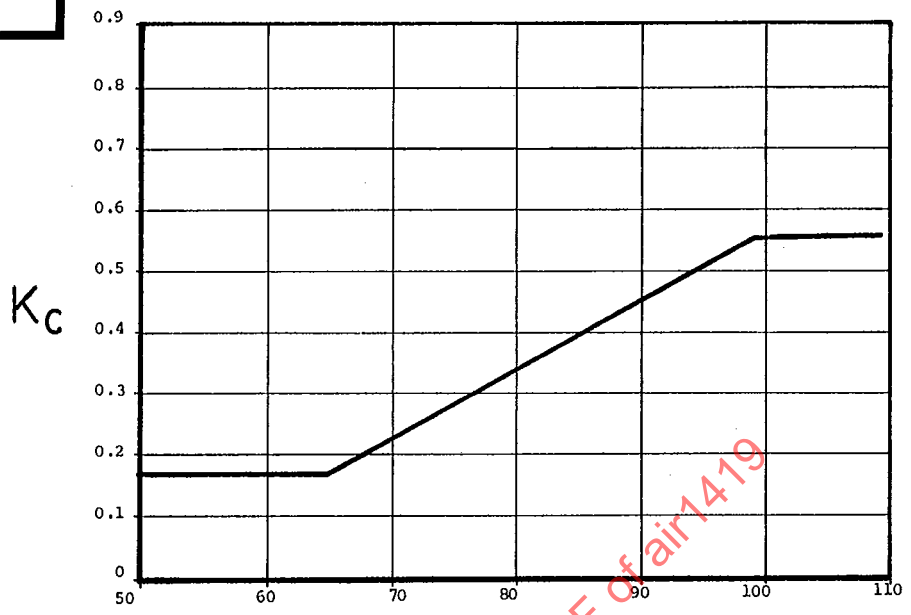

FIGURE 2.22 Circumferential Sensitivity

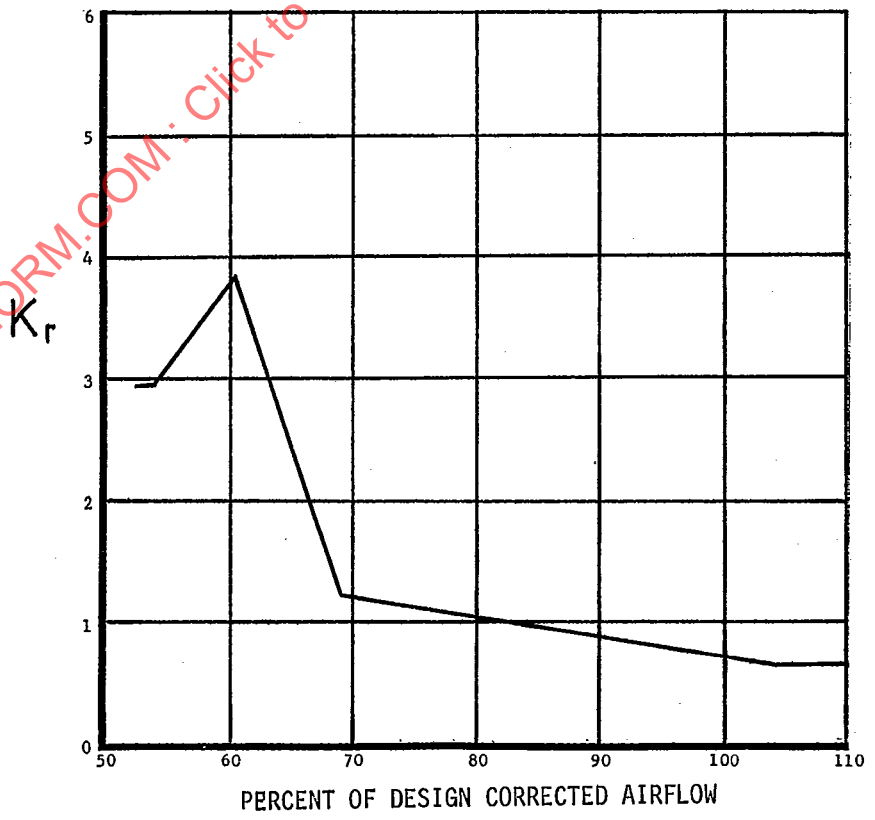

FIGURE 2.23 Radial Sensitivity

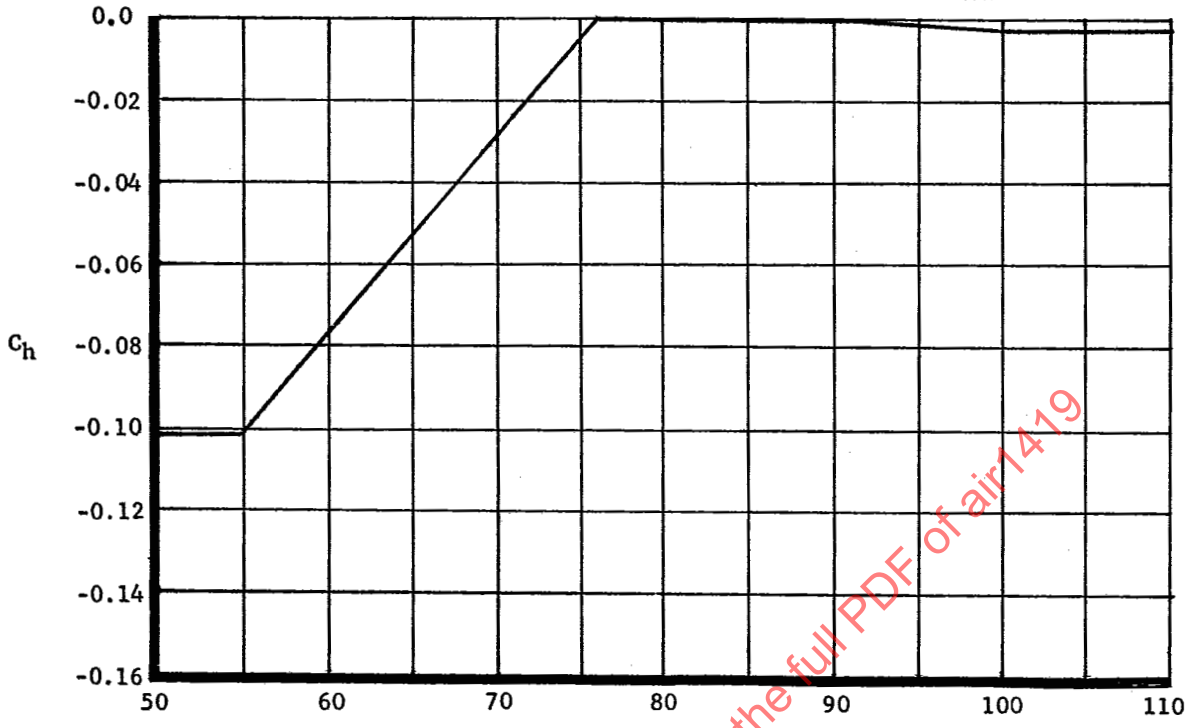

FIGURE 2.24 Hub-Radial Offset

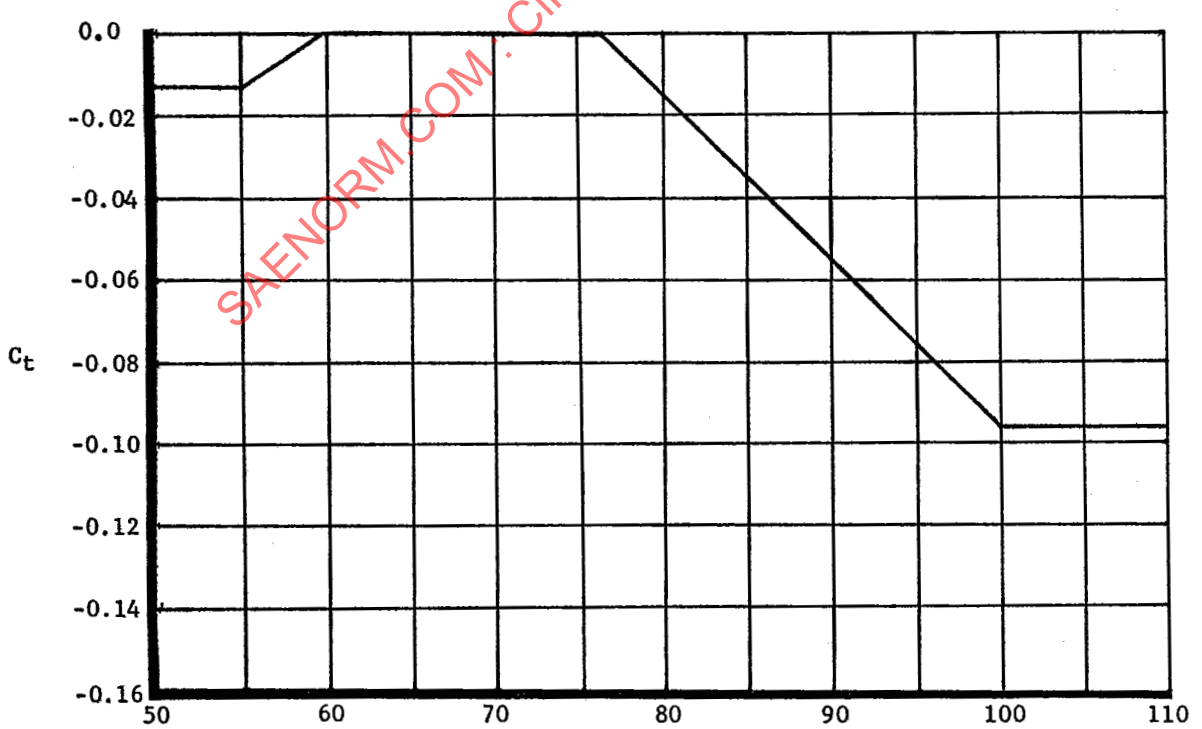

Figure 2.25 Tip-Radial Offset

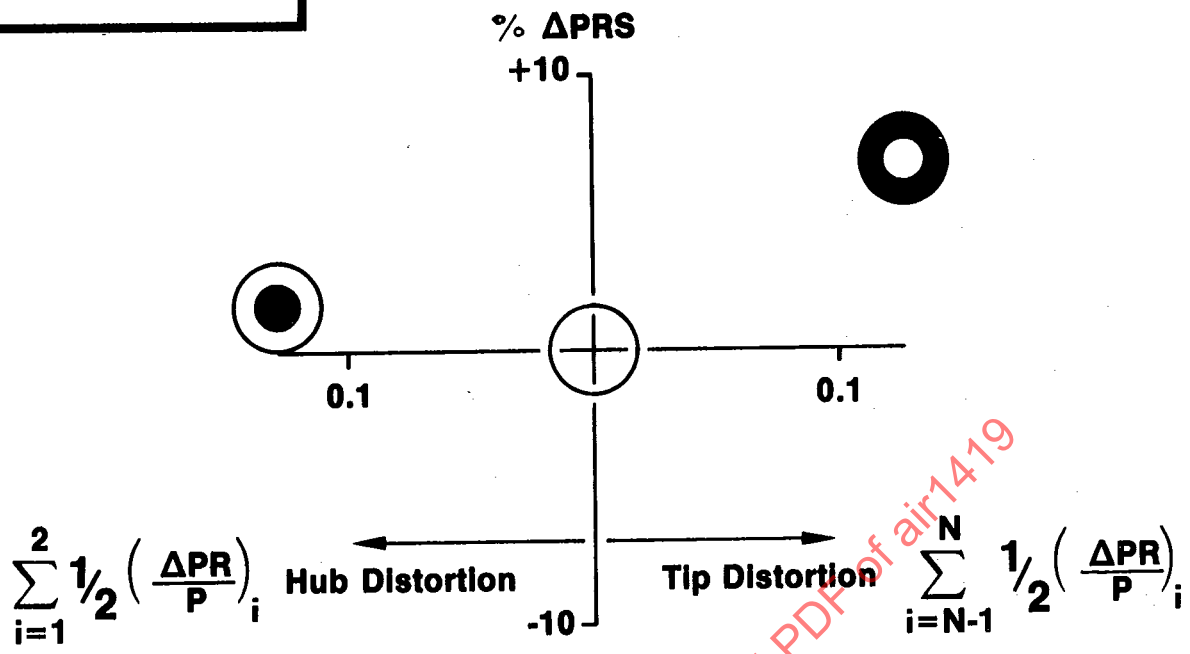

FIGURE 2.26 Example of Radial Distortion Data

$$KR = \frac{\text{Slope}}{100} = 0.6$$

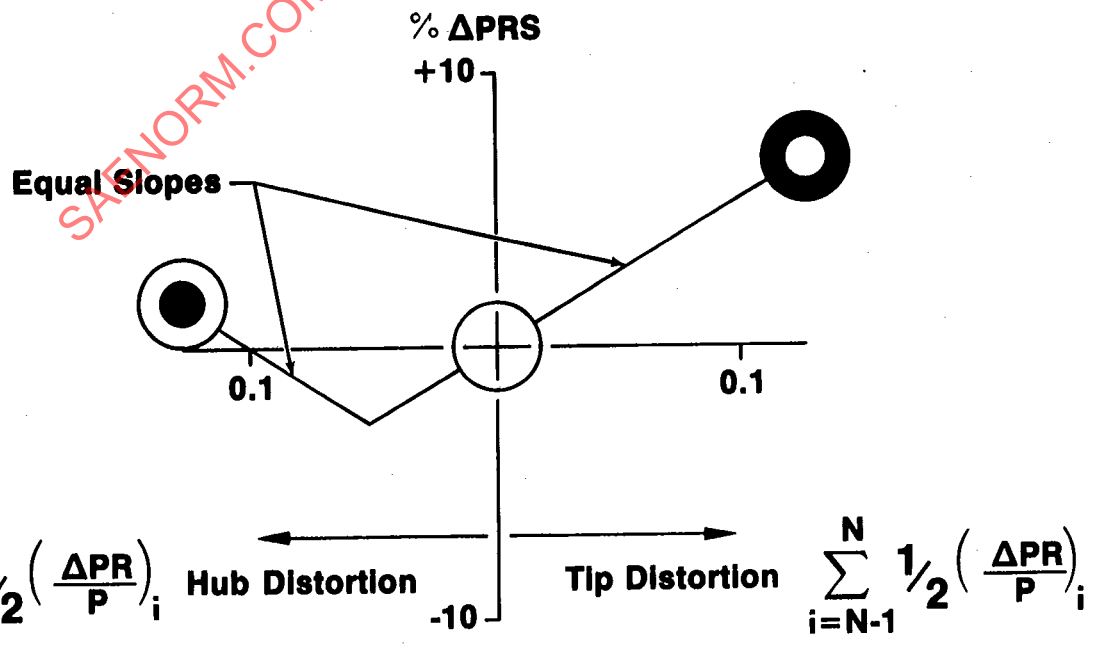

FIGURE 2.27 Radial Sensitivity Evaluation

$C_h = -0.06 \qquad C_t = 0$

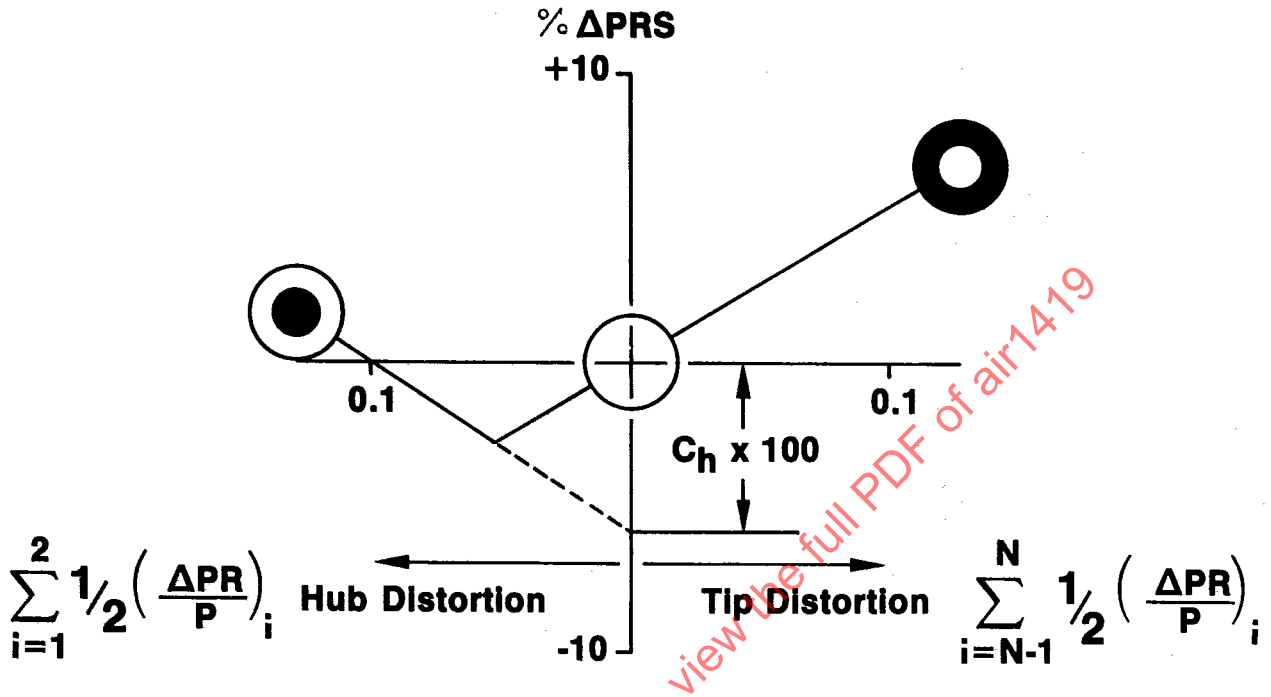

FIGURE 2.28 Constant Term

$$\Delta PRS = Max\left\{\left[\sum \frac{1}{2} KR \left(\frac{\Delta PR}{P}\right)_i\right] + C\right\} \times 100$$

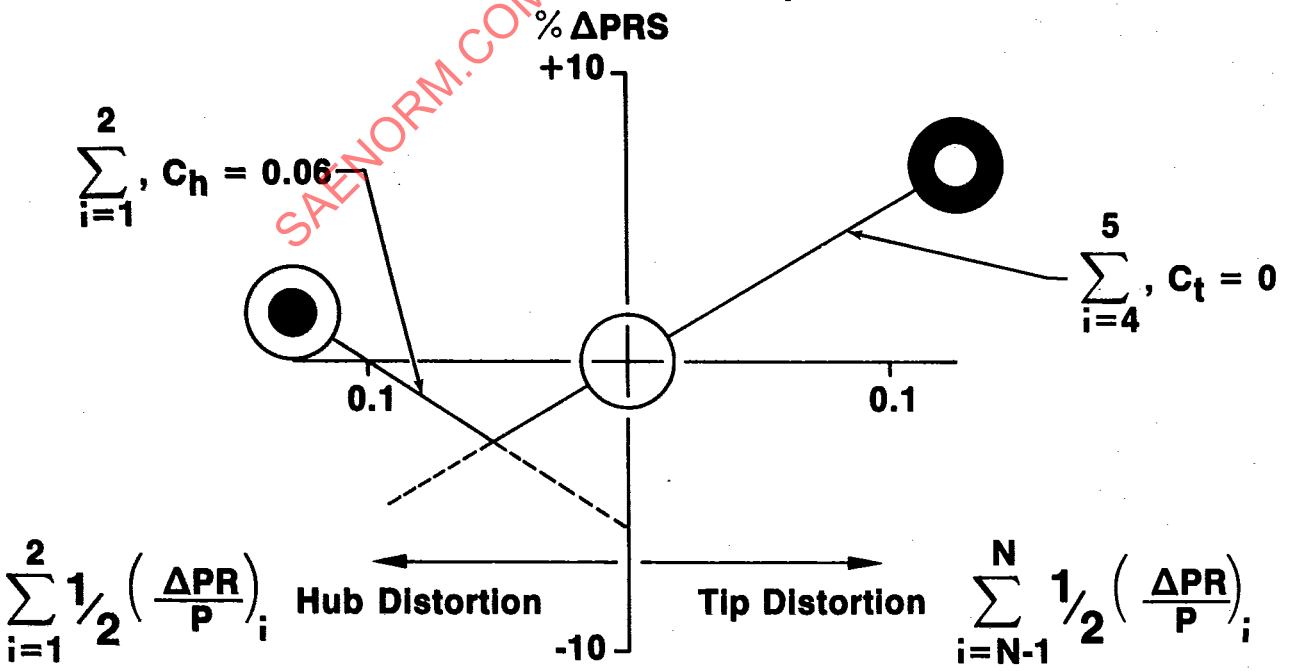

FIGURE 2.29 Modeling Radial Distortion

2.5.1.4 Example Calculations

Evaluate the loss in surge pressure ratio for the aircraft pattern shown in Figure 2.19 at 100 percent airflow.

From Figures 2.22, 2.23, 2.24 and 2.25 at 100 percent airflow, $K_c = 0.55$, $K_r = 0.7$, $C_h = -0.002$, and $C_t = -0.096$.

For an annular AIP with a hub-to-tip ratio of 0.33 and rings on centers of equal area, circumferential weighting factors are

$$\alpha_i = 0.303,\ 0.219,\ 0.180,\ 0.157 \text{ and } 0.141$$

Evaluating Equation 2.14 for the pattern defined by Figure 2.19 gives

$$\Delta PRS_c = (0.00615 + 0.00671 + 0.00619 + 0.00341 + 0.00181) \times 100 = 2.42$$

Evaluating Equation 2.15a gives

$$\Delta PRS_h = (-0.0162 - 0.0096 - 0.002) \times 100 = -2.78$$

Evaluating Equation 2.15b gives

$$\Delta PRS_t = (0.0041 + 0.0237 - 0.096) \times 100 = -6.82$$

From Equation 2.15c, the hub is critical, therefore:

$$\Delta PRS_r = -2.78$$

From Equation 2.15d $\Delta PRS = 2.42 - 2.78 = -0.36$

This particular pattern results in a small increase in surge pressure ratio at this operating condition because the gain in surge margin with tip-radial distortion more than offsets the loss in surge margin due to circumferential distortion.

2.5.1.5 Equivalence of Method A to the Basic Equation

Method A can be put into the form of the basic Equation 2.12, using Equation 2.15e which relates the ring sensitivity, KC_i, to the average sensitivity, KC, and by Equations 2.15f and 2.15g which set some of the terms to zero as a result of Equation 2.15c.

$$KC_i = \alpha_i K_c \left(\frac{\bar{\theta}_i}{180}\right)\left(\frac{1}{MPR_i}\right)^2 \qquad (2.15e)$$

If Equation 2.15c shows that the hub is critical, then

$$KR_1 = KR_2 = K_r/2$$
$$KR_3 = KR_4 = KR_5 = 0$$
$$C_1 = C_2 = C_h/2$$
$$C_3 = C_4 = C_5 = 0 \qquad (2.15f)$$

If Equation 2.15c shows that the tip is critical, then

$$KR_4 = KR_5 = K_r/2$$
$$KR_1 = KR_2 = KR_3 = 0$$
$$C_4 = C_5 = C_t/2$$
$$C_1 = C_2 = C_3 = 0 \qquad (2.15g)$$

The basic Equation 2.12 is shown below together with an array which shows each of the terms of the equation evaluated for the example of Paragraph 2.5.1.4. Each line of the array represents the terms of one ring of Equation 2.12 with the hub ring at the top.

For this example, Equation 2.15c shows that the hub is critical, therefore:

$$KR_1 = KR_2 = 0.35$$
$$KR_3 = KR_4 = KR_5 = 0$$
$$C_1 = C_2 = -.001$$
$$C_3 = C_4 = C_5 = 0$$

$$\Delta PRS = \sum_{i=}^{N} \left[KC_i \left(\frac{\Delta PC}{P} \right)_i + KR_i \left(\frac{\Delta PR}{P} \right)_i + C_i \right] \times 100$$

$$\begin{aligned}\Delta PRS = [&0.188\ (0.0327) + 0.35\ (-0.0463) - 0.001 \\ &+ 0.117\ (0.0574) + 0.35\ (-0.0257) - 0.001 \\ &+ 0.099\ (0.0624) + 0\ (-0.0056) + 0 \\ &+ 0.086\ (0.0394) + 0\ (0.0117) + 0 \\ &+ 0.0767\ (0.0236) + 0\ (0.0687) + 0] \times 100\end{aligned}$$

$$\Delta PRS = -0.36$$

The radial ring sensitivities and offset terms of Equation 2.12 can change with the inlet distortion pattern, whereas in the alternative, equivalent equations for calculating loss in surge pressure ratio (Equations 2.14, 2.15a, 2.15b, 2.15c and, 2.15d), the sensitivities and offset terms are functions of inlet corrected airflow only and are independent of the inlet distortion pattern.

2.5.2 METHOD B

In this paragraph, an expansion similar to an expansion of Equation 2.12 is developed to show how each term may be obtained. Although the following method has been used for a number of recent compression components, the information contained herein has been developed for a fictionalized fan compression component with two stages. This distortion sensitivity methodology is based on decomposing any aircraft pattern into its circumferential and radial elements and estimating the loss in surge pressure ratio due to each element. The loss in surge pressure ratio for each distortion element is based on sensitivities determined from classical and stylized pattern testing.

2.5.2.1 Definition of Terms

Correlation of the loss of surge pressure ratio for the fan component is accomplished using the empirical relationship:

$$\Delta PRS = b_p \cdot EX_p \left[KC_p \left(\frac{\Delta P}{PC} \right) + CC_p \right] + \left[KR_p \left(\frac{\Delta P}{PR} \right) + CR_p \right] \qquad (2.16a)$$

where ΔPRS is the loss in surge pressure ratio and:

b_p - Superposition function which accounts for coupling effects between the circumferential and radial components of total-pressure distortion.

EX_p - Extent function which accounts for change in loss of surge pressure ratio due to the extent of the total-pressure pattern differing from 180 degrees.

KC_p - Circumferential total-pressure distortion sensitivity.

$\Delta P/PC$ - Level of inlet circumferential total-pressure distortion.

CC_p - Circumferential total-pressure distortion offset coefficient for sensitivity or portion of sensitivity lines not passing through the origin.

KR_p - Radial total-pressure distortion sensitivity.

$\Delta P/PR$ - Level of inlet radial total-pressure distortion.

CR_p - Radial total-pressure distortion offset coefficient for sensitivity or portion of sensitivity lines not passing through the origin.

Equation 2.16a, when it is written in the form of Equation 2.12, is similar to an expansion of Equation 2.12.

$$\Delta PRS = KC\left(\frac{\Delta P}{PC}\right) + K_R\left(\frac{\Delta P}{PR}\right) + C \qquad (2.16b)$$

where:

$$KC = b_p \cdot EX_p \cdot KC_p \qquad (2.16c)$$

$$KR = KR_p \qquad (2.16d)$$

$$C = b_p \cdot EX_p \cdot CC_p + CR_p \qquad (2.16e)$$

The bracketed terms (Equation 2.16a) represent the loss in surge pressure ratio due to pure 180 degree one-per-rev circumferential and pure radial distortions, respectively. The circumferential total-pressure distortion term $\Delta P/PC$ was determined from the maximum value of the expression.

$$\Delta P/PC = 1/2 \sum_{i=1}^{2} \frac{(P\ RING\ AVG)_i - (P\ RING\ MIN)_i}{P\ FACE\ AVG} \qquad (2.17a)$$

or

$$1/2 \sum_{i=4}^{5} \frac{(P\ RING\ AVG)_i - (P\ RING\ MIN)_i}{P\ FACE\ AVG} \qquad (2.17b)$$

where i denotes a ring (hub ring is denoted by 1 and the tip ring by 5). Note that the definition differs from the ARP 1420 definition for the circumferential distortion level element, but is related to it for well-behaved patterns. The radial total-pressure distortion term $\Delta P/PR$ was determined from the maximum value of the expression

$$\Delta P/PR = \frac{(P\ FACE\ AVG) - (P\ RING\ AVG)_i}{P\ FACE\ AVG} \qquad (2.18)$$

Only positive values are considered. The maximum value usually is contributed by either i=5 (tip radial) or i=1 (hub radial). This definition is identical to the ARP 1420 radial distortion level element definition.

2.5.2.2 Coefficient Determination (Constant Corrected Speed)

This paragraph reviews the manner in which the coefficients of Equation 2.16a were determined. Prior to this discussion it is instructive to examine the coefficients in more detail to determine what they represent. Equation 2.16a can be arranged to give the following form:

$$\Delta PRS = \left[KC_p \left(\frac{\Delta P}{PC}\right) + CC_p\right] b_p \cdot EX_p + \left[KR_p \left(\frac{\Delta P}{PR}\right) + CR_p\right] \quad (2.19)$$

Equation 2.19 can be written in the following form:

$$\Delta PRS = \Delta PRS_{C,180} \left(\frac{\Delta PRS_{C,180,R}}{\Delta PRS_{C,180}}\right)\left(\frac{\Delta PRS_{C,\theta,R}}{\Delta PRS_{C,180,R}}\right) + \Delta PRS_R \quad (2.20)$$

where,

$\Delta PRS_{C,180}$ = $KC_p\ \Delta P/PC + CC_p$ and represents the loss of surge pressure ratio assuming the low pressure region has an extent of 180 degrees and that no radial distortion is present.

$\frac{\Delta PRS_{C,180,R}}{\Delta PRS_{C,180}}$ = b_p and represents the ratio of the loss of surge pressure ratio due to a 180 degree one-per-rev low pressure region with radial distortion to the loss of surge pressure ratio due to a pure circumferential 180 degree one-per-rev pattern.

$\frac{\Delta PRS_{C,\theta,R}}{\Delta PRS_{C,180,R}}$ = EX_p and represents the ratio of the loss in surge pressure ratio due to a circumferential low-pressure region of arbitrary angular extent with radial distortion to the loss in surge pressure ratio due to a 180 degree one-per-rev low-pressure region with radial distortion.

ΔPRS_R = Loss in surge pressure ratio due to radial distortion assuming no circumferential distortion is present.

The methodology screens defined in Table 2.2 were used to establish the loss in surge pressure ratio at the given corrected speeds. Further, this table indicates which screens were used in determining each coefficient.

TABLE 2.1

Methodology Screens and Coefficient Determination

TYPE	COEFFICIENTS
180° 1/rev	KC_p, CC_p
Hub Radial	$KR_{p_{Hub}}$, $CR_{p_{Hub}}$
Tip Radial	$KR_{p_{Tip}}$, $CR_{p_{Tip}}$
180° 1/rev + Tip Radial	b_p
135° 1/rev + Tip Radial 90° 1/rev + Tip Radial	EX_p

Circumferential Distortion Sensitivities

The circumferential distortion sensitivity coefficients were determined from test data which were obtained using 180 degree one-per-rev screens. The data are shown in Figure 2.30. Straight lines have been faired through the data and the origin. It was assumed that the radial distortion levels are sufficiently low (0.015 on the average) such that any loss of surge pressure ratio due to radial distortion could be assumed to be zero. In this case, Equation 2.16a can be written in the form:

$$KC_p = \frac{\Delta PRS - CC_p}{\Delta P/PC} \qquad (2.21)$$

since the coefficients b_p and EX_p are identically equal to one. Because straight lines can be drawn through the data and the origin, then the circumferential distortion offset coefficient is identically equal to zero. The manner in which the lines are faired is based upon experience and an examination of the degree of correlation at the completion of the first pass in this iteration process. The results of Figure 2.30 have been reduced to 180 degree one-per-rev circumferential distortion sensitivities using Equation 2.21 and are plotted as a function of corrected speed in Figure 2.31.

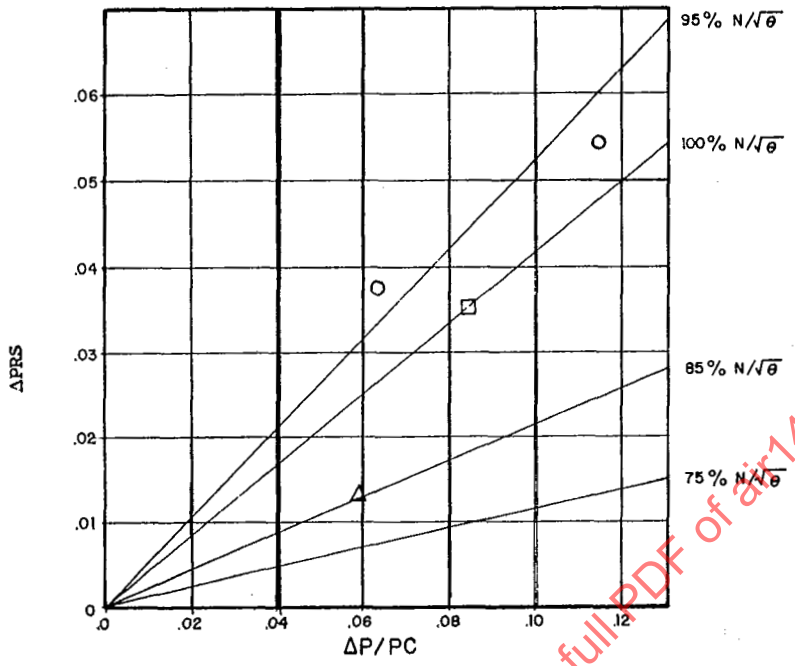

FIGURE 2.30 Loss of Surge Pressure Ratio Due to 180 Degree 1/Rev Total-Pressure Distortion

Radial Distortion Sensitivities

The radial distortion sensitivity coefficients were determined from test data that were obtained using graded* hub- or tip-radial screens. The data are shown in Figure 2.32. If the circumferential distortion is assumed to be negligible such that it produces no loss in surge pressure ratio, then Equation 2.16a can be written as

$$KR_p = \frac{\Delta PRS - CR_p}{\Delta P/PR} \qquad (2.22)$$

As in the case of circumferential distortion sensitivities, CR is zero for the line segments which pass through the origin. The hub-radial distortion sensitivity is given in Figure 2.33. To obtain the tip-radial distortion coefficients, it is necessary to determine whether the level of distortion is such that the line segments pass through the origin or whether the lines intercept the ordinate. This determination can be made by reference to Figure 2.34, and will permit entry to Figure 2.35 for the appropriate tip-radial distortion sensitivity coefficients, that is, $K_{R_{T1}}$ and $C_{R_{T1}}$ are associated with R_1 while $K_{R_{T2}}$ and $C_{R_{T2}}$ are associated with R_2.

*A graded pattern, as opposed to a uniform square pattern, is one in which the total-pressure losses are faired to a minimum to avoid creating significant levels of turbulence due to screen edge mixing of a shear layer.

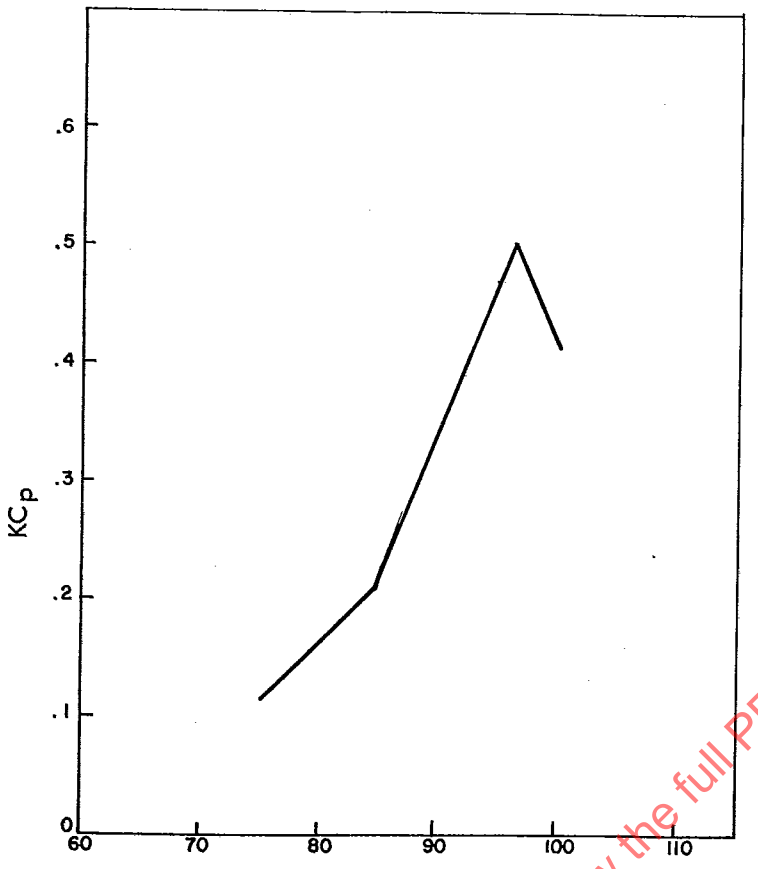

FIGURE 2.31 1/Rev Total-Pressure Distortion Sensitivity

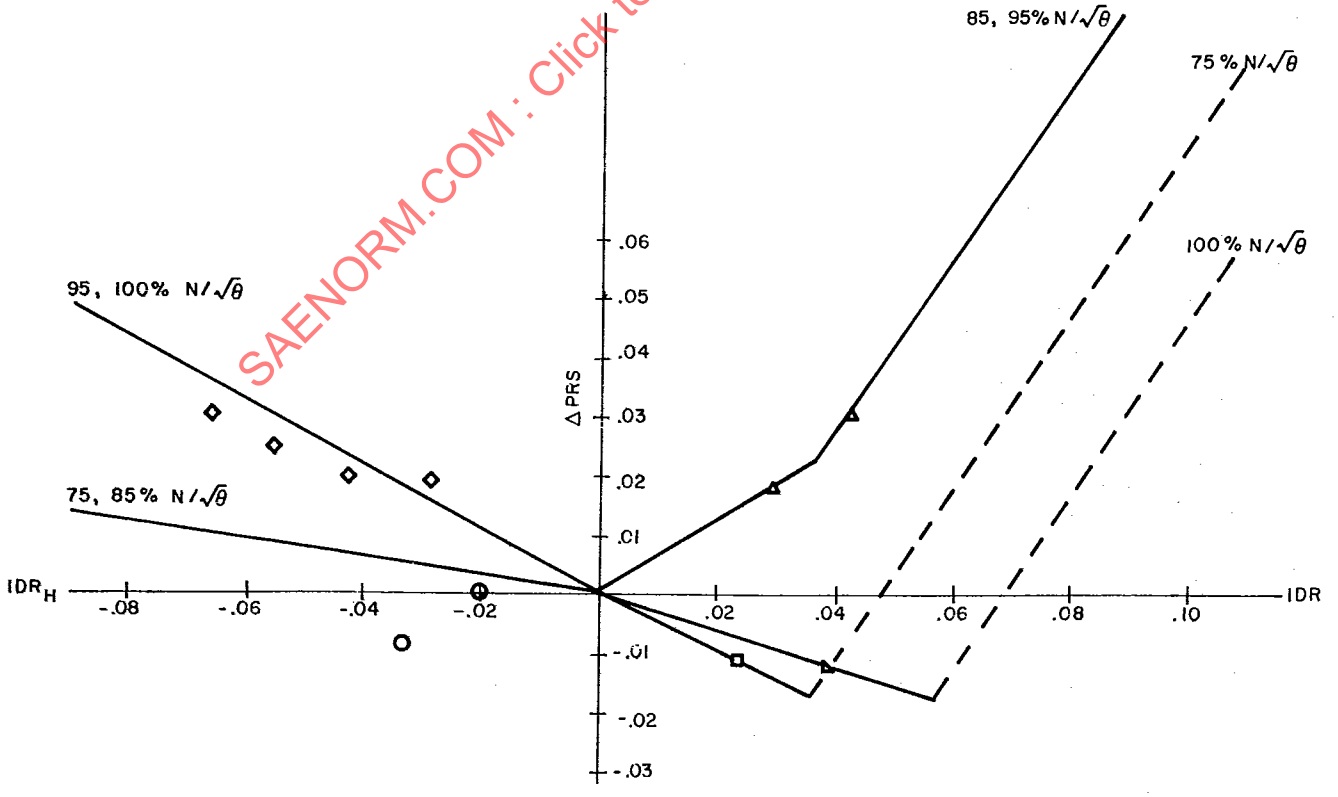

FIGURE 2.32 Loss of Surge Pressure Ratio Due to Hub-and Tip-Radial Total-Pressure Distortion

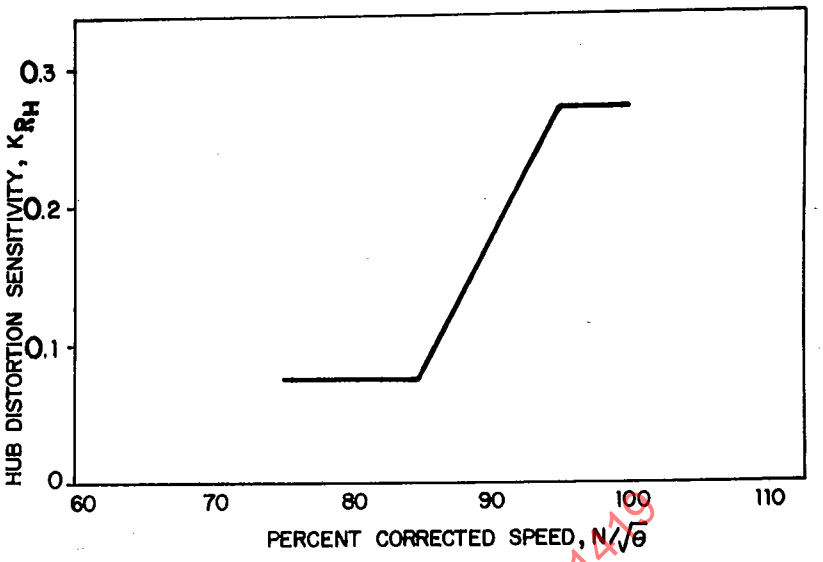

FIGURE 2.33 Hub-Radial Total-Pressure Distortion Sensitivity as a Function of Speed

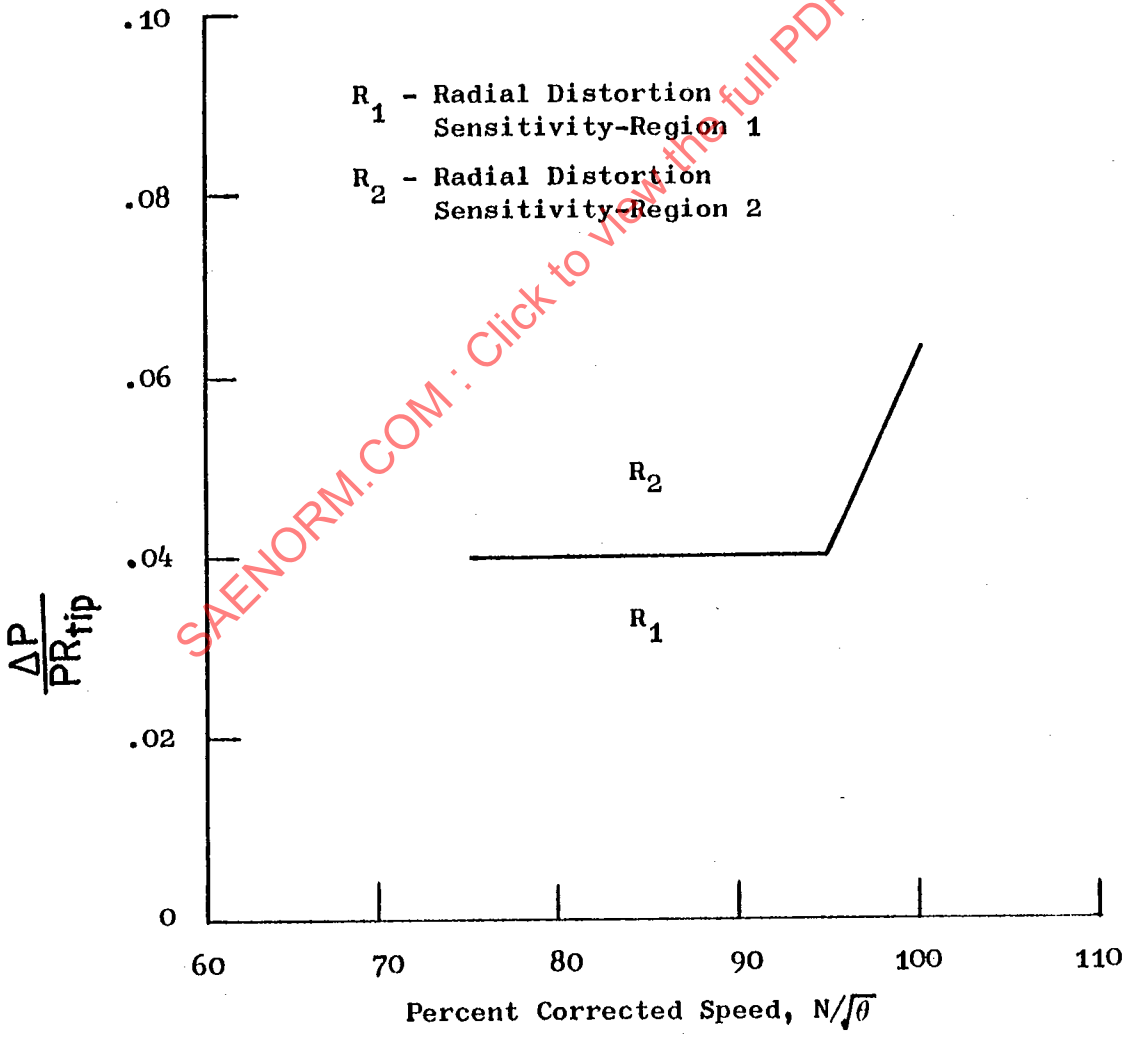

FIGURE 2.34 Tip-Radial-Distortion Logic Guide as a Function of Speed

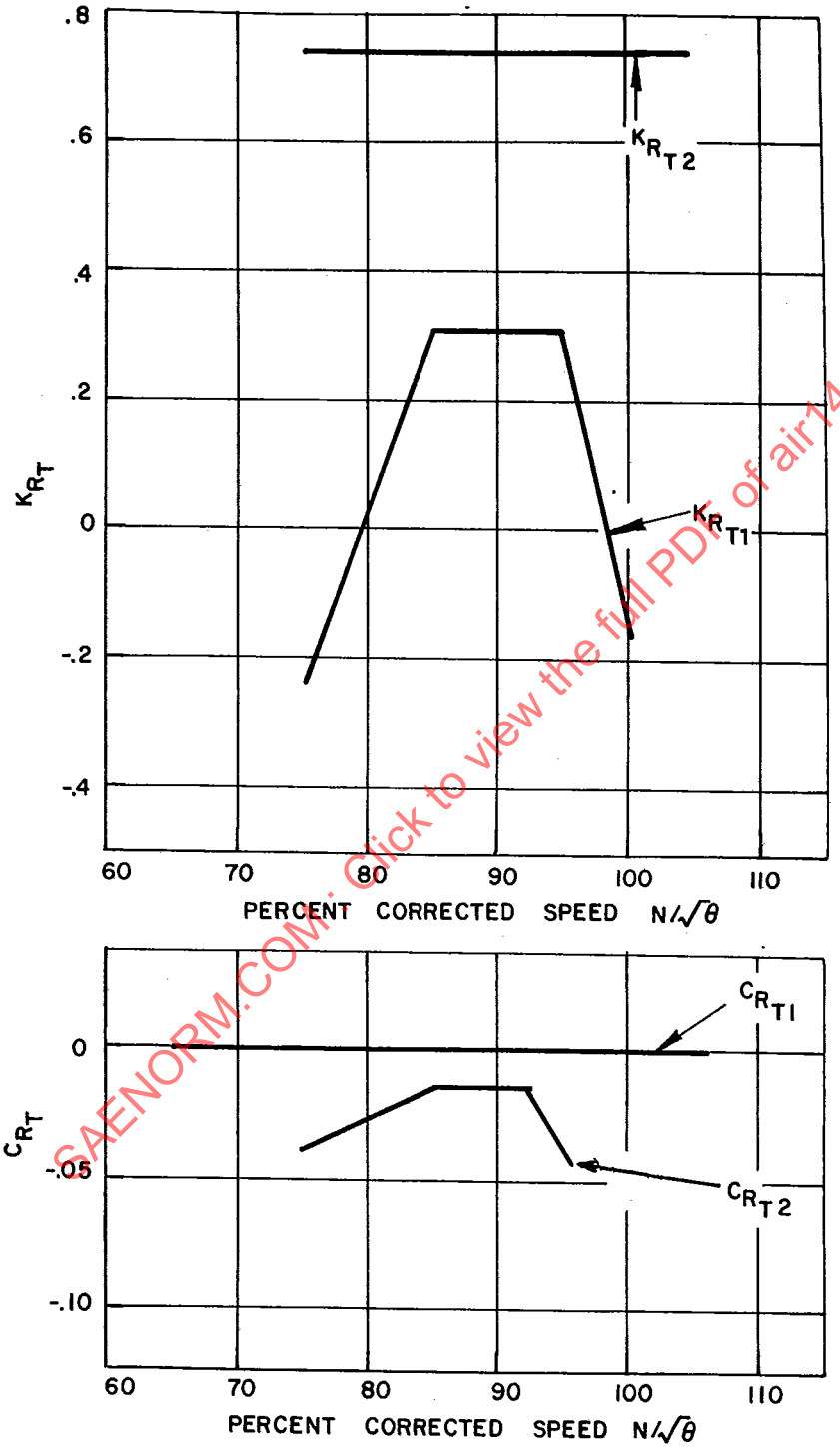

FIGURE 2.35 Tip Radial Distortion Sensitivity Coefficients, as a function of Speed

Superposition Factor

Once the circumferential and radial distortion sensitivity coefficients have been determined, it is possible to determine the superposition factor b_p from data obtained by testing 180 degree one-per-rev + tip radial combined distortion screens. This is accomplished through use of Equation 2.16a since the angular extent function EX_p is identically one. Hence, Equation 2.16a can be written in the form

$$b_p = \frac{\Delta PRS - KR_p \left(\frac{\Delta P}{PR}\right) + CR_p}{KC_p \left(\frac{\Delta P}{PC}\right) + CC_p} \qquad (2.23)$$

The results, expressed as a function of the ratio $(\Delta P/PR)/(\Delta P/PC)$, are given in Figure 2.36 with corrected speed as a parameter. Based on experience and by iteratively examining correlations of aircraft patterns, the superposition function is forced to be less than or equal to one.

Extent Function

The extent function can be determined from the data obtained from testing the 135 degree one-per-rev + tip radial and 90 degrees one-per-rev + tip radial screens and the previously determined circumferential and radial distortion sensitivities and the superposition factor. Equation 2.16a now can be written in a form to permit solution for the extent function, EX_p:

$$EX_p = \frac{\Delta PRS - \left[KR_p \left(\frac{\Delta P}{PR}\right) + CR_p\right]}{b_p \left[KC_p \left(\frac{\Delta P}{PC}\right) + CC_p\right]} \qquad (2.24)$$

The results of these computations are shown in Figure 2.37 as a function of distortion angular extent with corrected speed as a parameter. The angular extent, θ^-, is determined by averaging the angular extents of the two rings giving the maximum value of $\Delta P/PC$. By definition, the extent function has a value of one at 180 degrees. Further, based on experience and iterative examination of aircraft pattern correlations, the extent function is constrained from exceeding one.

This methodology permits Equation 2.16a to be used for estimating the loss of surge pressure ratio due to any pattern which falls within the range of the parameters tested.

2.5.2.3 Coefficient Determination (Constant Corrected Flow)

Because compression components normally are tested at constant speed, the first step in developing the loss in surge pressure ratio correlation as a function of corrected flow follows the method outlined in the previous paragraph. Translation of the corrected speed results to a corrected flow form is accomplished using a flow/speed correlation. Generally, this is based on results obtained from cycle deck predictions.

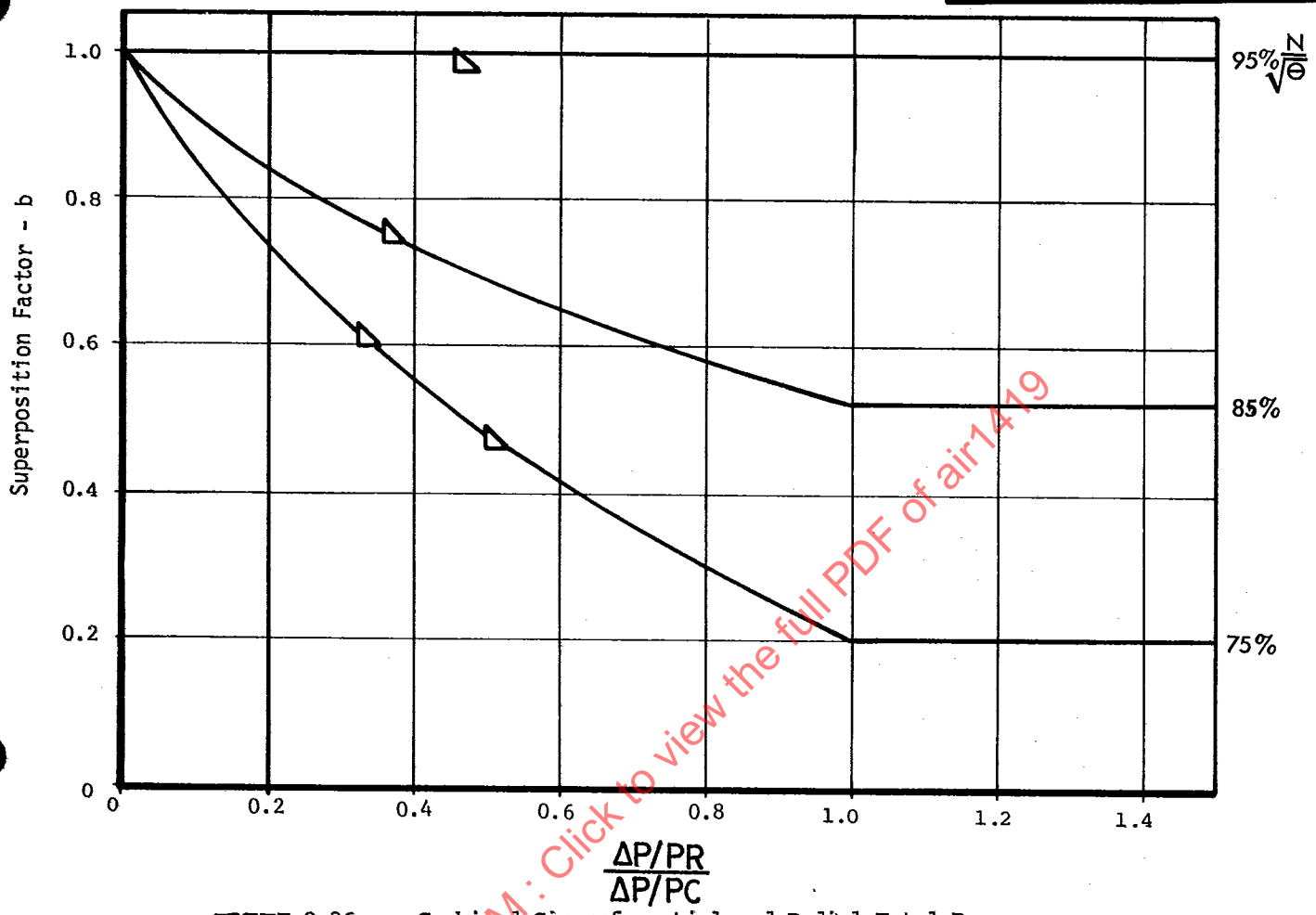

FIGURE 2.36 Combined Circumferential and Radial Total-Pressure Distortion Superposition Factors as a Function of Speed

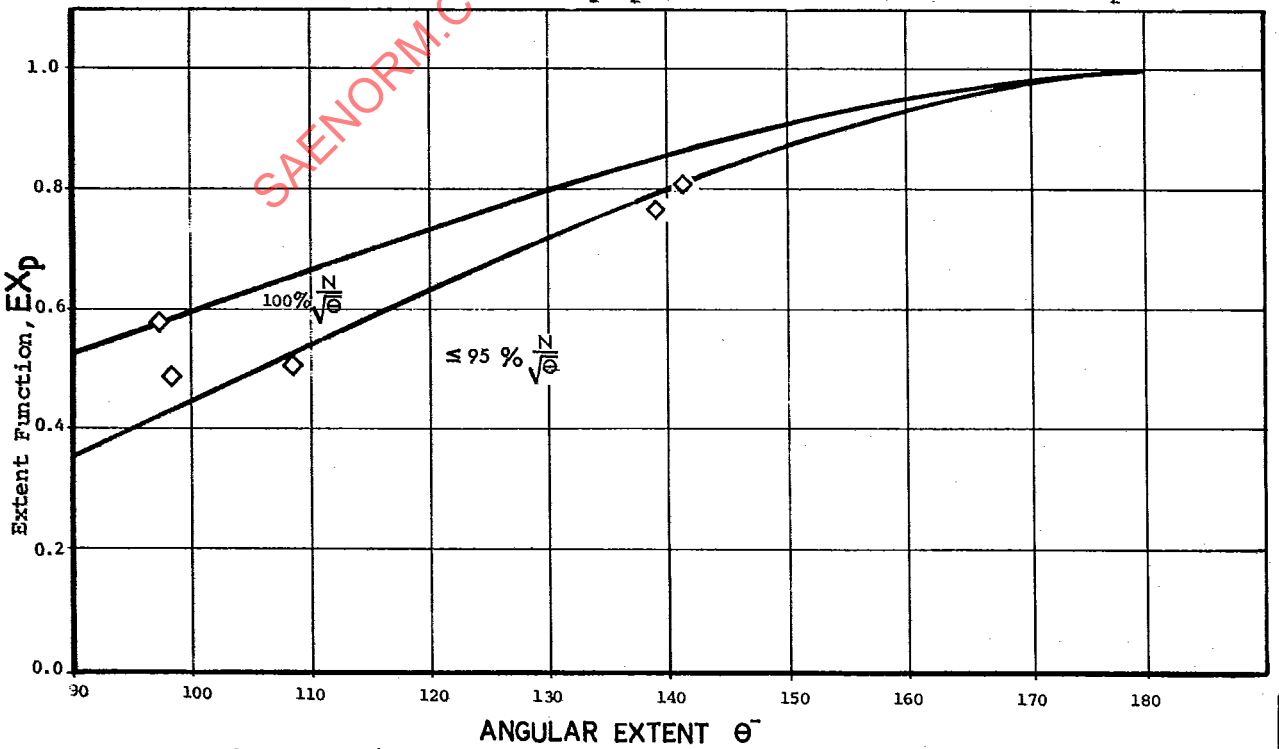

FIGURE 2.37 1/Rev Total-Pressure Distortion Angular Extent Function

2.5.2.4 Distortion Transfer and Generation Coefficients

The effect of inlet distortion on a compressor located downstream of the fictionalized fan can be estimated using Equation 2.16a. However, two additional facets of the stability estimation process are encountered for such cases: 1) the transfer of total-pressure distortion through a fan, and 2) the generation of total-temperature distortion due to the change in total-pressure distortion through the fan component.

Because total-temperature is handled in a manner similar to total-pressure distortion, Equation 2.16a can be extended in the following manner for estimating the loss of surge pressure ratio of a high-pressure compressor (HPC) (see Reference 3):

$$\Delta PRS_{HPC} = \left\{ b_P \, EX_P \left[KC_P \left(\frac{\Delta p}{PC} \right)_{25} + CC_P \right] + \left[KR_P \left(\frac{\Delta p}{PR} \right)_{25} + CR_P \right] \right\}_{HPC} +$$

$$S \left\{ b_T \, EX_T \left[KC_T \left(\Delta T/TC_{25} \right) + CC_T \right] + \left[KR_T \left(\Delta T/TR_{25} \right) + CR_T \right] \right\}_{HPC} \qquad (2.25)$$

where the terms in the first line of the equation are given in Paragraph 2.5.2.1, except that $\Delta P/PC_{25}$ and $\Delta P/PR_{25}$ are the circumferential and radial distortions measured at the HPC inlet. The remaining terms in the equation are defined as follows:

S - Superposition function which accounts for coupling effects between total-pressure distortion and total-temperature distortion.

b_T - Superposition function which accounts for coupling effects between the circumferential and radial components of total temperature distortion.

EX_T - Extent function which accounts for change in loss of surge pressure ratio due to the extent of the total-temperature pattern differing from 180 degrees.

KC_T - Circumferential total-temperature distortion sensitivity.

$\Delta T/TC_{25}$ - Level of HPC inlet circumferential total-temperature distortion.

CC_T - Circumferential total-temperature distortion offset coefficient for sensitivity or portion of sensitivity lines not passing through the origin.

KR_T - Radial total-temperature distortion sensitivity.

$\Delta T/TR_{25}$ - Level of HPC inlet radial total-temperature distortion.

CR_T - Radial total-temperature distortion offset coefficient for sensitivity or portion of sensitivity lines not passing through the origin.

Since it is the high-temperature regions which cause the loss of surge pressure ratio, then Equations 2.17a, 2.17b and 2.18 can be used to quantify the levels of temperature distortion through use of the following substitutions:

$\frac{\Delta T}{TC}$	for	$-\frac{\Delta P}{PC}$
T RING MAX$_i$	for	P RING MIN$_i$
T RING AVG$_i$	for	P RING AVG$_i$
T FACE AVG	for	P FACE AVG
$\frac{\Delta T}{TR}$	for	$-\frac{\Delta P}{PR}$

The loss of surge pressure for the high-pressure compressor can be estimated if the sensitivities and superposition functions are known and if the plane 25 distortion levels are known in terms of a plane 01 (engine inlet) distortion level. Hence, the following relationships can be written:

$$\frac{\Delta P}{PC}_{25} = f\left[\frac{\Delta P}{PC}_{01}\right] \tag{2.26}$$

$$\frac{\Delta P}{PR}_{25} = f\left[\frac{\Delta P}{PR}_{01}\right] \tag{2.27}$$

$$\frac{\Delta T}{TC}_{25} = f\left[\frac{\Delta P}{PC}_{01}\right] \tag{2.28}$$

$$\frac{\Delta T}{TR}_{25} = f\left[\frac{\Delta P}{PR}_{01}\right] \tag{2.29}$$

where Equations 2.26 and 2.27 represent total-pressure distortion transfer and Equations 2.28 and 2.29 represent total-temperature distortion generation. Both explicit and implicit distortion transfer and generation coefficients are illustrated in Figures 2.38 through 2.41. Equations 2.26 and 2.28 can be written in the following forms:

$$\frac{\Delta P}{PC}_{25} = CDTC_P\left[\frac{\Delta P}{PC}_{01}\right] \tag{2.30}$$

$$\frac{\Delta T}{TC_{25}} = CDGC_P \left[\frac{\Delta P}{PC_{01}}\right] \qquad (2.31)$$

where $CDTC_P$ and $CDGC_P$ are the distortion transfer and generation coefficients, respectively, for circumferential total-pressure distortion. These coefficients are examples of explicit coefficients which are illustrated by the examples of Figures 2.38 and 2.39. The radial distortion transfer and generation coefficients are implicit coefficients (Equations 2.27 and 2.29) and are illustrated by the examples of Figures 2.40 and 2.41.

Considerable effort is currently being exerted to determine temperature distortion effects on compression systems, temperature-and-pressure distortion superposition effects, and distortion transfer and generation coefficient definitions. Although the method discussed in these paragraphs represents the state-of-the-art, it has not yet been reduced to common practice.

2.5.3 METHOD C

In this method, Equation 2.12 is expanded to formulate regionally-averaged AIP total-pressure parameters e.g., for the fan inlet hub and tip regions, in terms of the ARP 1420 descriptor elements. Loss of compressor surge pressure ratio at a given inlet corrected mass flow is correlated with the distortion parameters utilizing radial and circumferential sensitivities which are independent of the AIP pattern. The regionally averaged parameters with appropriate low-pass filtering (Paragraph 2.6.4) are used to define screening parameters directly applicable to inlet time-variant distortion (Paragraph 2.6.3).

The form of combinatorial algebra needed to correlate loss of compressor surge pressure ratio to the desired accuracy in a particular case depends on the complexity of the AIP pattern, compressor type (e.g., single or dual stream), and compressor radial and circumferential sensitivities. Downstream (high pressure) compressor surge pressure ratio can be correlated explicity with numerical AIP distortion descriptors through the use of upstream (low pressure) compressor distortion transfer functions.

2.5.3.1 Definition of Terms

$\frac{\Delta PC}{P}$, $\frac{\Delta PR}{P}$, θ^-, MPR - Total pressure distortion elements defined in Paragraph 2.1

ΔPRS - Overall loss of surge pressure ratio at constant corrected inlet flow

ΔPRS_C - Surge pressure ratio loss due to circumferential total pressure distortion.

ΔPRS_R - Surge pressure ratio loss due to radial total pressure distortion.

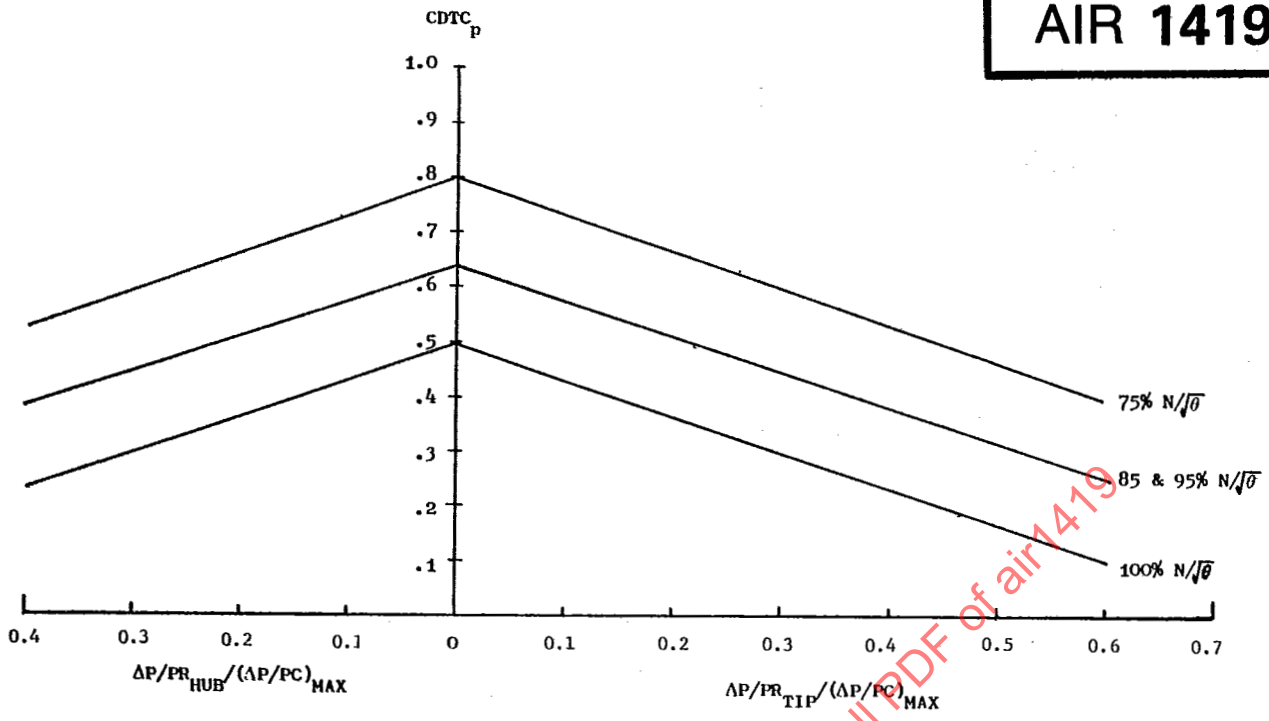

FIGURE 2.38 Circumferential Total-Pressure Distortion Transfer Coefficient

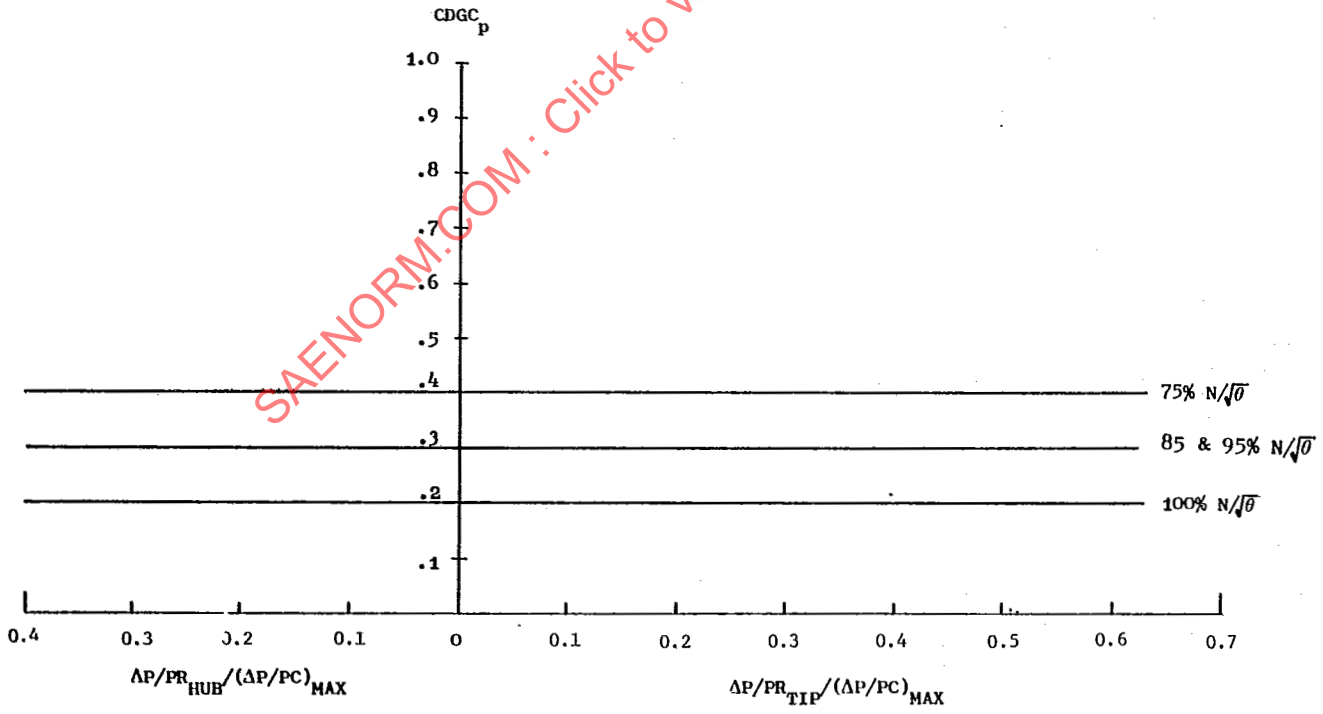

FIGURE 2.39 Circumferential Total-Temperature Distortion Generation Coefficient Due to Total-Pressure Distortion

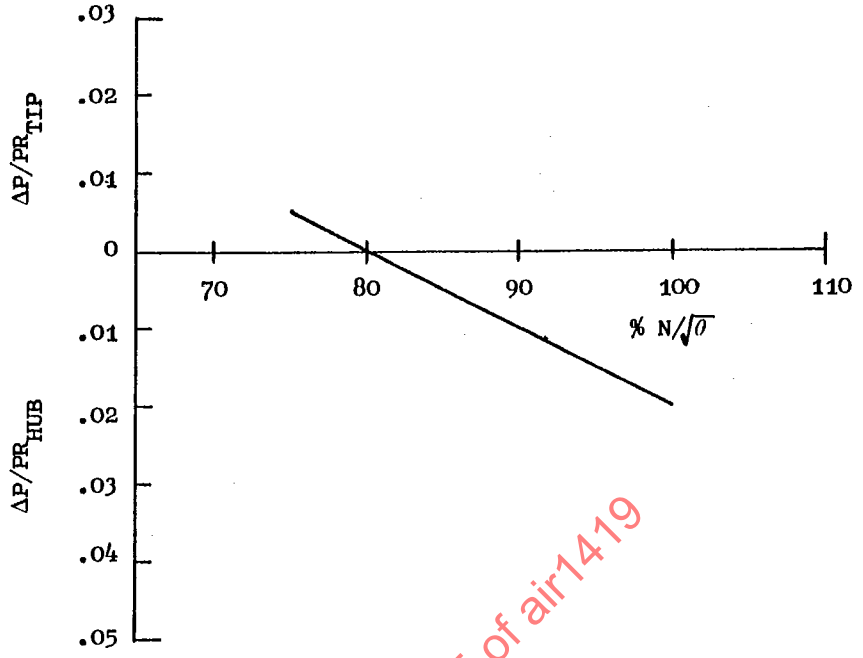

FIGURE 2.40 Radial Total-Pressure Distortion

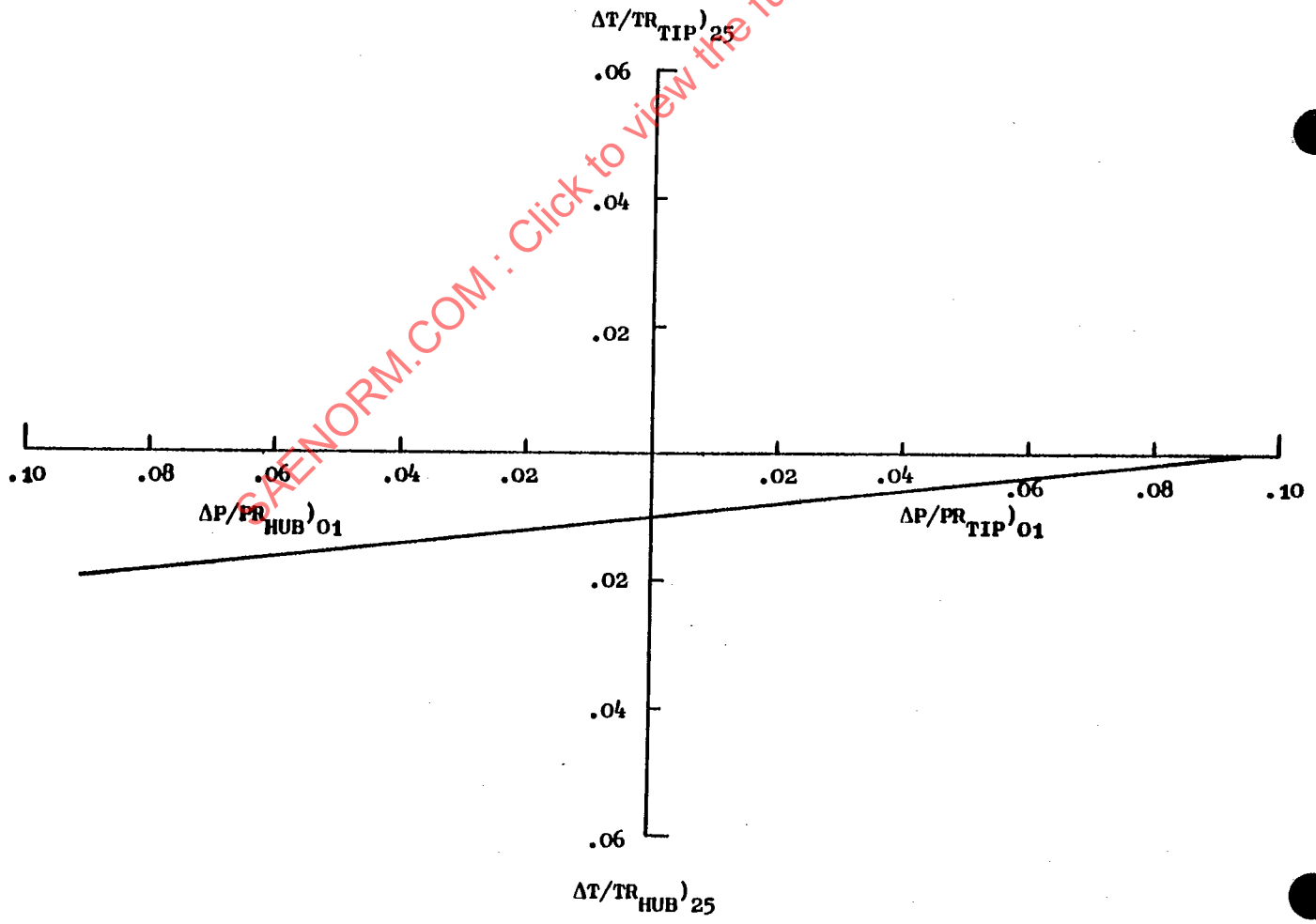

FIGURE 2.41 Radial Total-Temperature Distortion Due to Radial Total-Pressure Distortion

b	-	Surge line loss weighting or superposition factor.
K_C	-	Circumferential distortion sensitivity.
K_R	-	Radial distortion sensitivity.
B	-	AIP distortion parameter weighting or superposition factor.
DPC	-	Circumferential distortion parameter.
DPR	-	Radial distortion parameter.
DPS	-	AIP distortion screening parameter.
$\bar{e}_e$	-	Effective distortion extent factor.
α	-	A numerical exponent.
$f(\bar{e}_i)$	-	Extent function.
C_R	-	Radial offset term.
I_R	-	Radial intensity parameter.
ΔPRS_T	-	Loss of surge pressure ratio due to temperature distortion.
$f(\theta)$	-	Combined pressure and temperature distortion superposition and spatial orientation function.
K_T	-	Temperature distortion sensitivity.
DTC	-	Temperature distortion parameter.
A_p, A_T	-	Pressure and temperature distortion transfer functions.

2.5.3.2 Rationale

Equation 2.12 may be expressed for the full AIP or a tip or hub region at the AIP in the form:

$$\Delta PRS = \Delta PRS_C + b\ \Delta PRS_R \qquad (2.32)$$

Introducing circumferential and radial distortion parameters, DPC and DPR, for pure patterns

$$\Delta PRS_C = K_C\ (DPC) \tag{2.33}$$

$$\Delta PRS_R = K_R\ (DPR) \tag{2.34}$$

The terms K_C and K_R are empirically established circumferential and radial compressor sensitivities and are independent of the pattern. Then, for a combined distortion pattern

$$\Delta PRS = K_C\ (DPC) + bK_R\ (DPR) \tag{2.35}$$

which may be written

$$\Delta PRS = K_C \left[(DPC) + B(DPR)\right] \tag{2.36}$$

where

$$B = \frac{bK_R}{K_C}$$

The term B is a specified function of corrected flow and is independent of the pattern. Equation 2.36 may be used to define a screening parameter:

$$DPS = (DPC) + B(DPR) \tag{2.37}$$

For pure circumferential distortion DPR = 0

For pure radial distortion DPC = 0, b = 1.0

2.5.3.3 Correlating Parameters

A full discussion of all possible expansions of DPC and DPR is outside the scope of this discussion. Illustrative examples are provided below.

DPC

A general form of DPC, explicit in the ARP 1420 elements for a region comprising j rings at the AIP ($j \leq N$) is:

$$DPC = \frac{1}{j} \sum_j \left\{ \left[1 - \left(\frac{\Delta PR}{P}\right)_i \right] \left(\frac{\theta^-_i}{\theta^-_e}\right) f(\theta^-_i) \left(\frac{1}{MPR_i}\right)^{\alpha} \left(\frac{\Delta PC}{P}\right)_i \right\} \tag{2.38}$$

where $f(\bar{\theta}_i) = 1.0$ if $\left(\frac{\bar{\theta}_i}{\bar{\theta}_e}\right) \leq 1.0$

$$= \left(\frac{\bar{\theta}_e}{\bar{\theta}_i}\right) \quad \text{if} \left(\frac{\bar{\theta}_i}{\bar{\theta}_e}\right) > 1.0$$

depending on the shape of the circumferential pressure profile.

The effective distortion extent factor, $\bar{\theta}_e$, and multiple-per-rev exponent, α, depend on compressor dynamic response to circumferential extent and are specified functions of compressor inlet corrected flow. Descriptor elements are centered about the circumferential position surrounding the minimum total pressure in the region.

For classical one-per-rev circumferential patterns having $\bar{\theta}$ extent terms greater than $\bar{\theta}_e$, DPC is equal to the ARP 1420 circumferential distortion intensity descriptor element ($\Delta PC/P$).

For an important class of inlet distortion where radial and circumferential total-pressure defects occur in the same region, and for that region where either radial intensity elements, $\left(\frac{\Delta PR}{P}\right)_i$, are small compared with the circumferential intensity elements, $\left(\frac{\Delta PC}{P}\right)_i$, or compressor radial sensitivity, K_R, is low; ΔPRS may be correlated with DPC alone. If, for example, this holds for the AIP, then $(DPC)_j = (DPC)_N$. For dual stream low-pressure compressors (axial-flow fans), separate core flow (ID) and by-pass flow (OD) DPC parameters appropriate to core engine and fan OD stability may be utilized.

DPR

The general correlation of radial distortion presents difficulties as ΔPRS_R may not be monotonic with DPR, as illustrated by Figures 2.42 and 2.43. In such cases, a method logic, analogous to that embodied in $f(\bar{\theta})$ for circumferential distortion, needs to be incorporated into DPR to enable a unique radial sensitivity, K_R, defined positive, to be used for correlating ΔPRS_R. A typical form applicable to hub and tip sensitive compressors may be defined such that:

$$DPR = \left|I_R - C_R\right| - \left|C_R\right| \qquad (2.39)$$

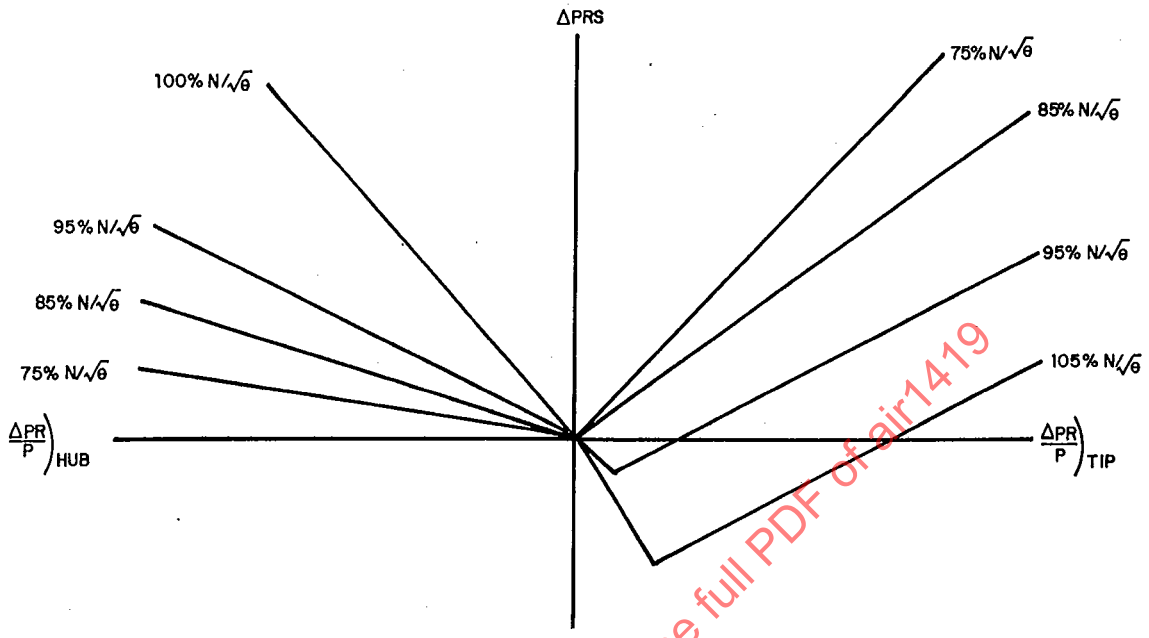

FIGURE 2.42 Effect of Radial Distortion on a Fan Designed for a Tip-Radial Profile

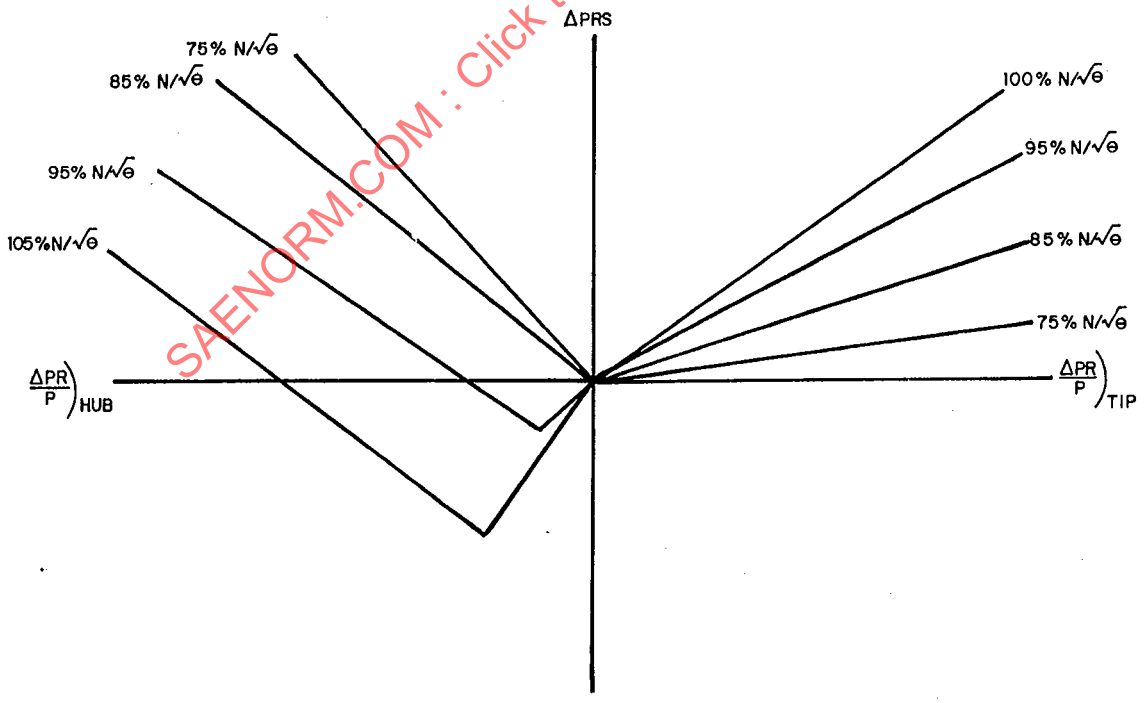

FIGURE 2.43 Effect of Radial Distortion on a Fan Designed for a Hub-Radial Profile

The term C_R is a radial offset term specified as a function of compressor-inlet corrected flow and represents a limiting value of the radial intensity parameter, I_R, and,

$$I_R = \frac{1}{2}\left[\sum_{i=4}^{5}\left(\frac{\Delta PR}{P}\right)_i - \sum_{i=i}^{2}\left(\frac{\Delta PR}{P}\right)_i\right]$$

For tip radial distortion, I_R is positive. For hub radial distortion, I_R is negative. The computational logic caters to the experimental observation that ΔPRS_R may be negative, i.e., a degree of radial distortion may have a favorable effect on surge line.

The application of Method C is conceptually similar to that of Method A (Section 2.5.1) for circumferential, radial, and mixed inlet distortion patterns. Circumferential and radial sensitivities, K_C and K_R, are similar to those of Figures 2.22 and 2.27.

2.5.3.4 Downstream (High Pressure) Compressors

Loss of surge pressure ratio due to total-pressure distortion may be correlated, as indicated above, utilizing distortion parameters defined at the high pressure compressor (HPC) entry. This is not sufficient for determining the effect of AIP pressure distortion on installed HPC stability, however, because total-temperature distortion, created by the low-pressure-compressor, can produce a significant loss of HPC surge line. Moreover, the spatial orientation between regions of high total-temperature and low total-pressure is also significant. Losses of surge pressure ratio due to pressure and temperature distortion may be additive or may cancel depending on their spatial orientation, their intensities, and extents, (Reference 4). These are all linked via the LPC distortion transfer characteristics to the AIP pressure distortion which, itself, may be time-variant.

A method for dealing with this complex problem is described below. For simplicity, it is assumed that only circumferential elements in the distortion are significant at the HPC entry - not an unreasonable assumption for engines having multistage low-pressure compressors. Otherwise, the method for DPS (Paragraph 2.5.3.2) may be utilized.

The total loss of HPC surge pressure ratio due to combined temperature and pressure distortion is:

$$\Delta PRS = \Delta PRS_P + f(\theta)\ \Delta PRS_T \qquad (2.41)$$

where, $f(\theta)$ is a combined superposition and spatial orientation function defined at the HPC entry.

ΔPRS_P and ΔPRS_T correspond to losses of surge pressure ratio due to

the total-pressure distortion and total-temperature distortion, respectively. Defining pressure and temperature distortion parameters DPC and DTC and corresponding sensitivities as K_P and K_T such that:

$$\Delta PRS_P = K_P\,(DPC)$$
$$\Delta PRS_T = K_T\,(DTC) \qquad (2.42)$$

and introducing LPC distortion transfer functions

$$A_P = \frac{(DPC)}{(DPC)_{AIP}} \qquad (2.43)$$

$$A_T = \frac{(DTC)}{(DPC)_{AIP}} \qquad (2.43)$$

then, it may readily be shown that

$$\Delta PRS = \left[A_P K_P + f(\theta)\, A_T\, K_T\right] (DPC)_{AIP} \qquad (2.44)$$

usually, $A_P < 1.0$ and $A_T > 0$.

The square-bracketed term in Equation 2.44 can be regarded as an overall or composite sensitivity factor for correlating HPC surge pressure ratio loss with AIP distortion, allowing $(DPC)_{AIP}$ to be used as a screening parameter applicable to time-variant distortion. Thus, for core engine stability assessment, $(DPC)_{AIP}$ may be defined in the hub region of the AIP and related to the ARP 1420 descriptor elements using, for example, a relation like Equation 2.38. It should be noted that the value of the composite sensitivity factor now depends on engine component matching.

2.5.4 SUBSTANTIATION OF CORRELATION METHODS

The wide range of applicability of Equation 2.12 when expanded for special applications, as illustrated by the discussion of Paragraphs 2.5.1, 2.5.2, and 2.5.3, is more dramatically illustrated by the results shown in Figures 2.44 through 2.51. These results are taken from rig component, and engine tests and cover a wide variety of compression components, including fans with one to three stages and compressors with eight to sixteen stages. Lines of ±0.02 ΔPRS (two standard deviations) have been superimposed about the line of perfect correlation. This tolerance value is generally accepted within the industry for inlet patterns that are critical for stability. It is clear that Equation 2.12 provides a framework around which the loss of surge pressure ratio for compression components can be correlated and represents the effects of inlet total-pressure distortion on surge line degradation.

2.6 INLET DATA SCREENING

The realities of establishing inlet/engine compatibility communication between the airframer and the engine manufacturer with their diverse needs and non-optimally time-aligned development programs cause inlet data screening to be

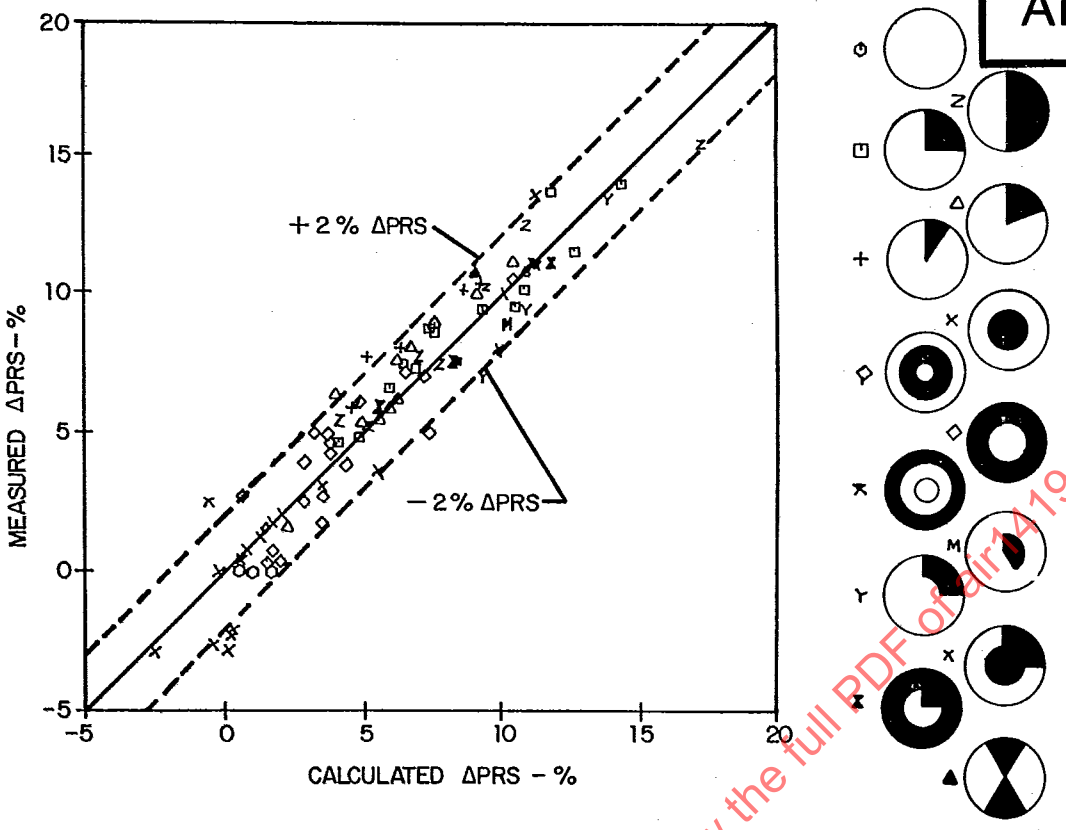

FIGURE 2.44 ΔPRS Correlation of J85 Data

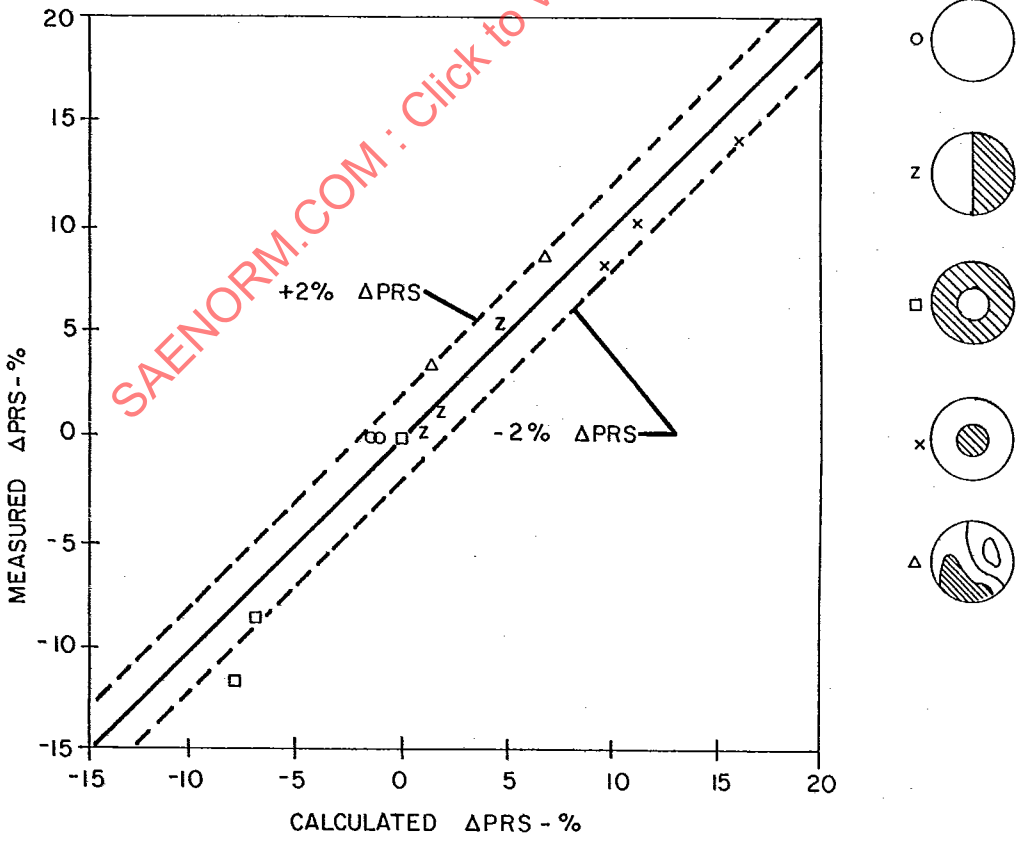

FIGURE 2.45 ΔPRS Correlation of a Research Fan

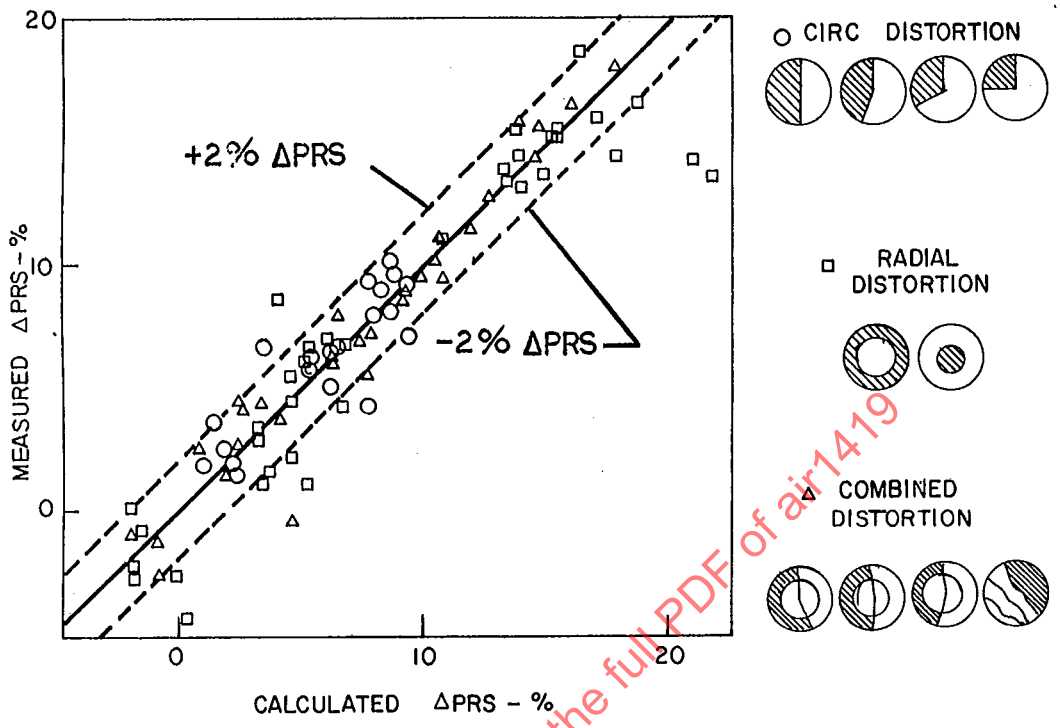

FIGURE 2.46 ΔPRS Correlation of F101 Fan

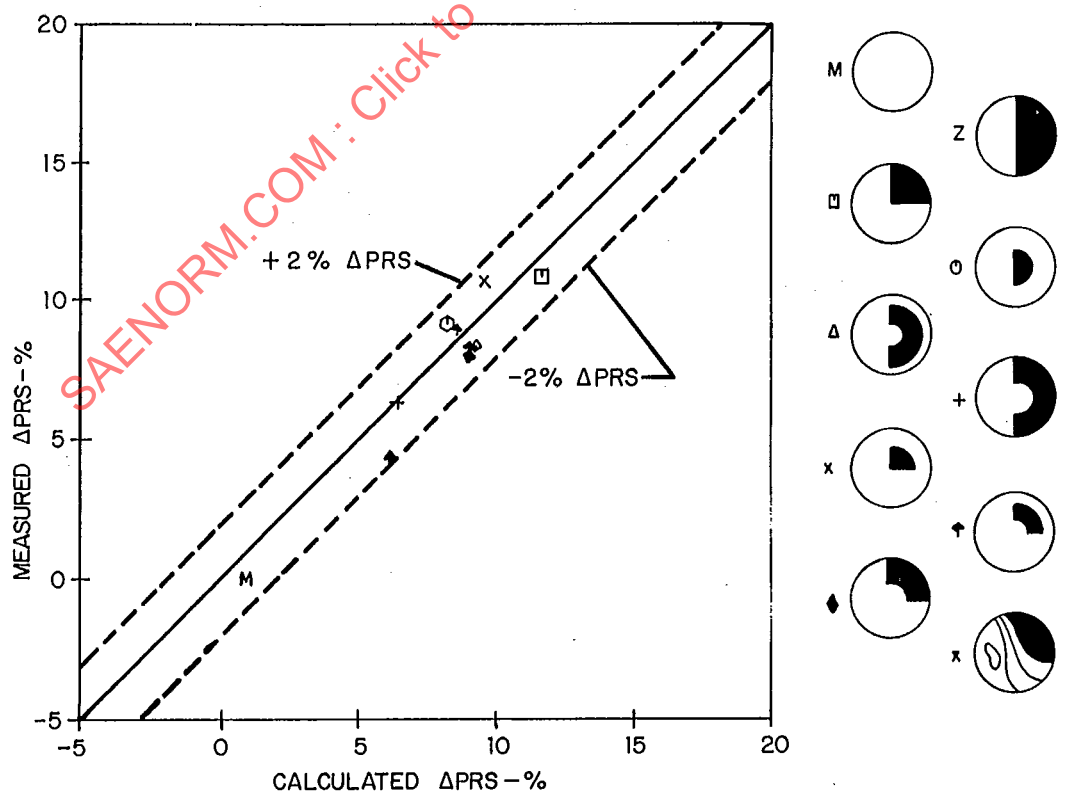

FIGURE 2.47 ΔPRS Correlation of J58 Compressor

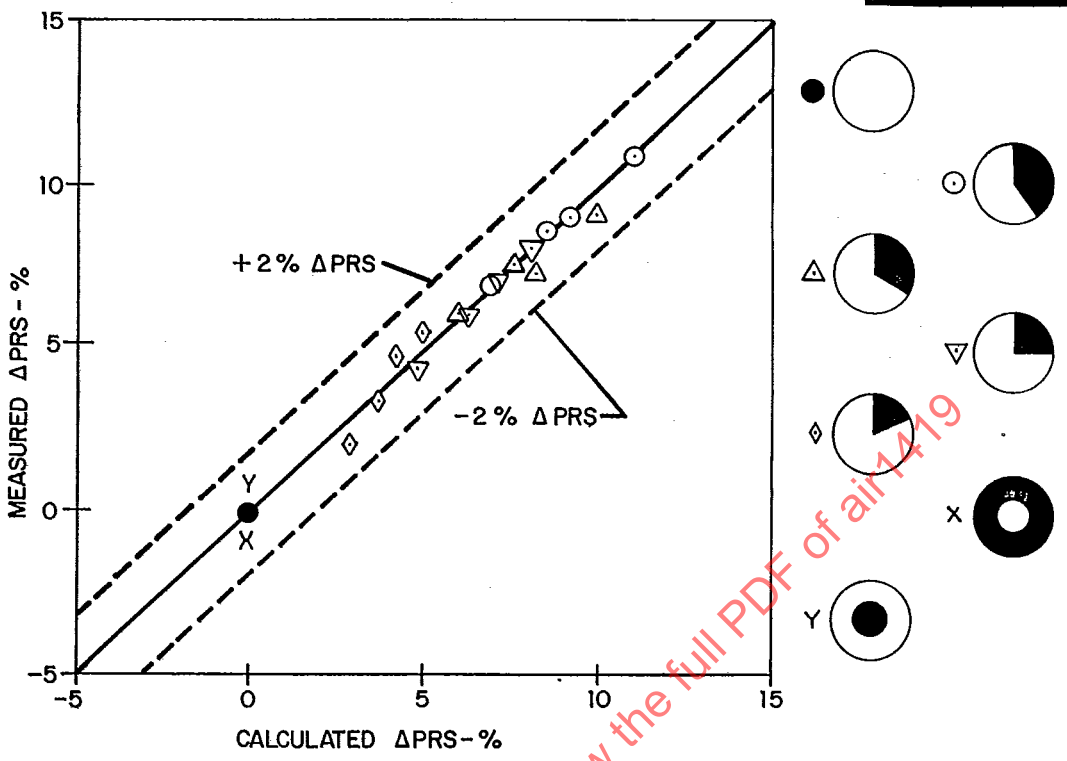

FIGURE 2.48 ΔPRS Correlation of a Turbofan Compressor

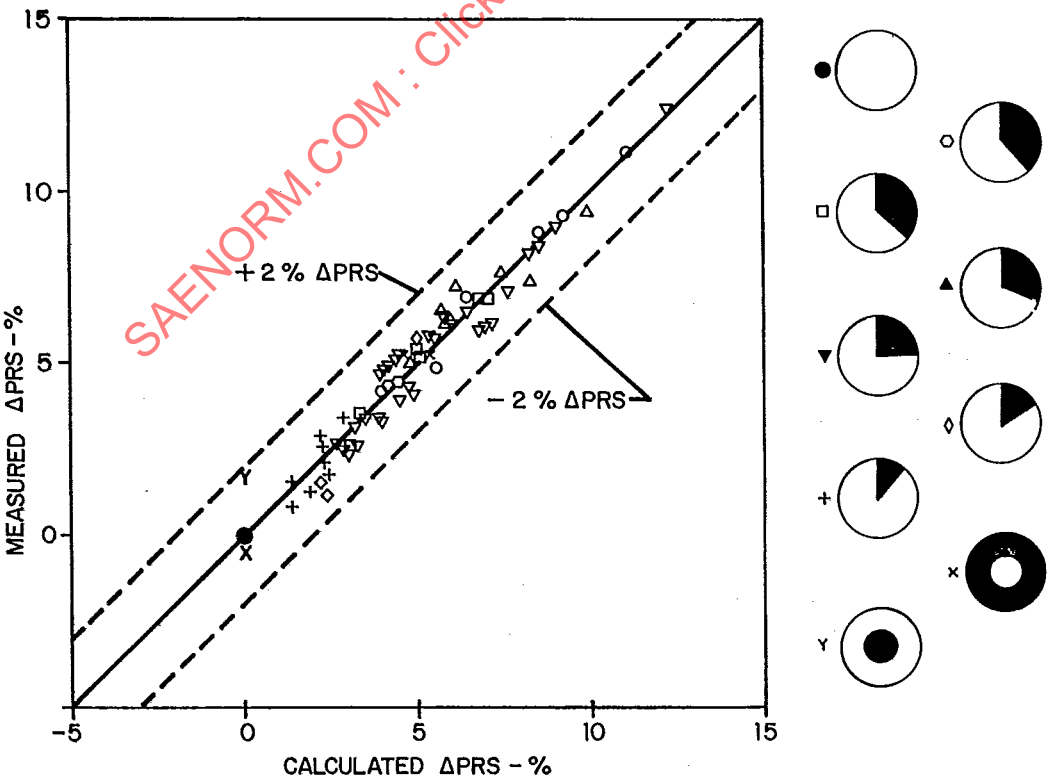

FIGURE 2.49 ΔPRS Correlation of a Turbofan Core

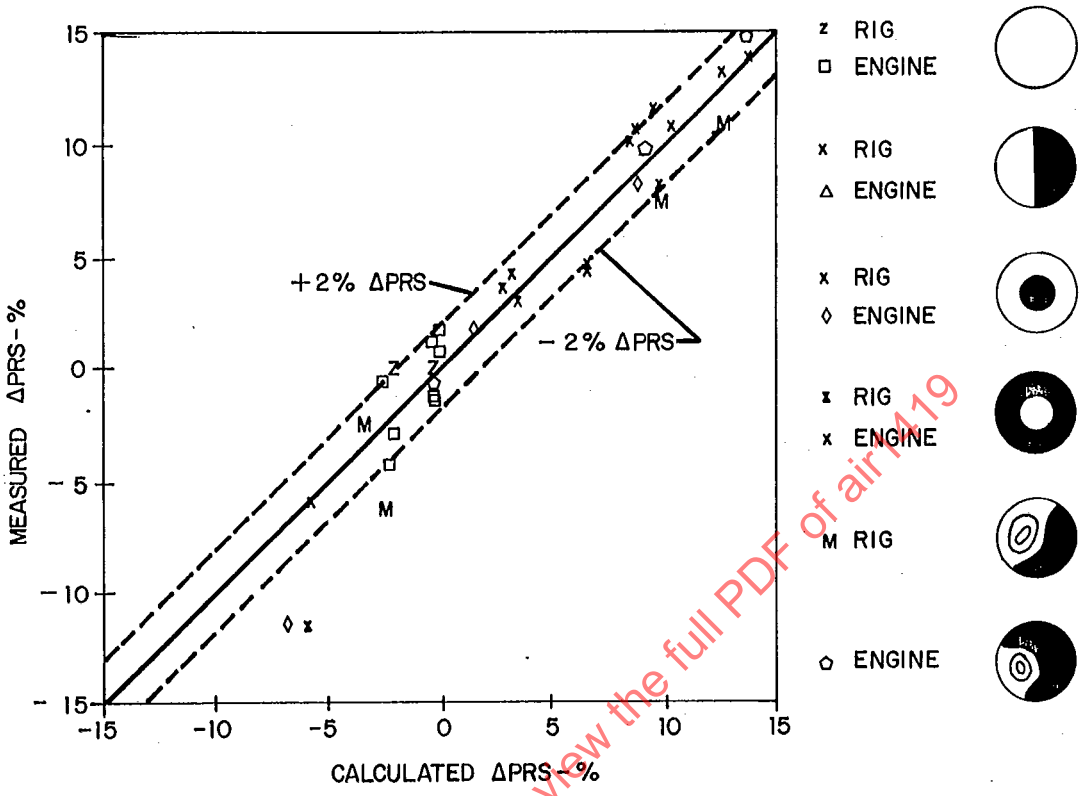

FIGURE 2.50 ΔPRS Correlation of F100 Fan

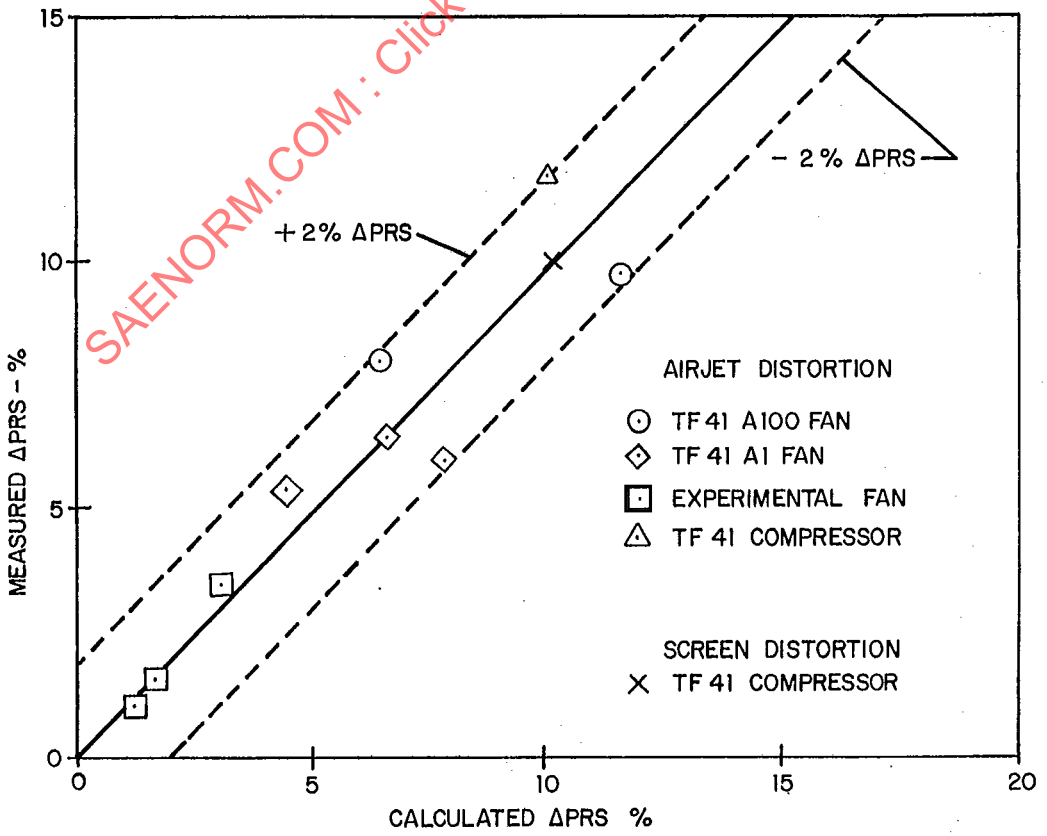

FIGURE 2.51 ΔPRS Correlation of TF41 Fan and Compressor

a sensitive issue. With proper recognition of each party's requirements and constraints, as discussed in the following paragraphs, a mutually beneficial dialogue can take place.

2.6.1 GENERAL CONSIDERATIONS

The requirement for a universal Aerodynamic Interface Plane flow distortion descriptor which will: 1) define the quality of the air supplied by the inlet and 2) describe the effect of the severity of the flow field upon engine stability, is in direct contrast to the requirement for engine-specific information to predict the effect of any distortion pattern upon engine stability. This dichotomy exists, especially when both the inlet and engine development programs start about the same time. Ideally, an inlet development program would be structured such that distortion sensitivity data would be available from engine component tests prior to the start of inlet development testing. The largest impediment to a "universal inlet distortion factor" is that, a priori, the engine manufacturer cannot predict how the radial distortion will couple with the circumferential distortion, nor whether a compression component will be hub-or tip-distortion sensitive.

2.6.2 EXAMPLES OF ENGINE DEPENDENCY

If an engine were designed for a specific application, such as an inlet which might have a significant amount of outer-wall boundary layer, then the fan might be designed for a tip-radial profile. In this case, the effect of radial distortion, relative to the clean-inlet surge line on which the loss in surge pressure ratio (ΔPRS) is based, might take the form shown in Figure 2.42. Low values of tip radial distortion may lead to negative values of ΔPRS and, hence, a "gain" in surge margin relative to the clean (uniform) inlet flow condition.

On the other hand, if the fan were designed for a hub-radial profile, as might be produced by a centerbody, then the effect of radial distortion on the fan might take the form shown in Figure 2.43. In this case, low values of hub radial distortion will lead to "gains" in loss of surge pressure ratio relative to a clean inlet flow.

Because of the choice of types of engine, be it turbojet, augmented turbofan, or non-augmented turbofan and because the fan designer has the choice of designing for a uniform inlet profile or for hub-or tip-radial profiles of varying intensity, it is essentially impossible at this time to develop an inlet flow distortion screening parameter which is universal and quite independent of engine sensitivity parameters. To a lesser extent, the multiple-per-rev (MPR) factor is also an impediment to establishing a universal distortion screening parameter. Multiple-per-rev patterns have a dominant effect upon stress levels, and hence, the pressure ratio at which the "effective" surge line may be set. For example, a compression system may have been designed for an application that produces essentially a one-per-rev pattern, but at a subsequent date, it is used

in a bifurcated-inlet-duct propulsion system with a two-per-rev pattern. The "effective" surge line may have to be reset so that stress limits are not exceeded or the compression component will have to be redesigned. In either case, the sensitivity to distortions of the same level will generally change.

By establishing communication between the airframer and the engine manufacturer sufficiently early in a program, it should be possible to develop meaningful inlet distortion screening parameters which will assure that the airframe manufacturer obtains optimal information from wind-tunnel testing efforts and will be able to provide the engine manufacturer with inlet patterns which can be used to influence compression system design.

The distortion-descriptor elements are independent of compression system characteristics. Since circumferential distortion always causes a loss of surge pressure ratio, minimization of the circumferential distortion intensity element will always be beneficial. Discussions with the engine manufacturer should indicate the most desirable radial profile for the given application, that is, whether a uniform profile or whether a hub, tip or a combination profile is desired and which component of distortion should be minimized.

2.6.3 INLET DATA SCREENING TECHNIQUES

Screening of time-variant inlet data identifies inlet patterns that cause the greatest loss of surge pressure ratio. It follows that screening parameters should be proportional to surge pressure ratio loss; and therefore, the screening parameters which use ARP 1420 distortion-descriptors will have a form similar to the basic equation used for calculating ΔPRS.

Screening techniques have been used successfully with many different distortion descriptors. A separate screening parameter is used for each component of the compression system that can initiate surge. Also, separate screening parameters may be used for the hub and tip regions of a fan. Each screening parameter usually will select a different inlet pattern from time-variant inlet data. A stability assessment, which includes all destabilizing influences, is used to select a set of critical patterns and associated operating conditions for use in engine stability verification testing.

If engine stability has been determined to the point where all terms have been defined in the equation used for estimating the loss of surge pressure ratio, then screening can be done on the basis of ΔPRS for each component. It is customary to provide guidelines representing the component distortion tolerance in the form of an allowable ΔPRS. These guidelines can be used to normalize the calculated values of ΔPRS to give the screening parameter shown in Equation 2.45. This screening parameter is similar to the current screening parameter ID. A value lower than 1.0 indicates that a level of inlet distortion is within the distortion allowance of the component, while a value higher than 1.0 indicates that the inlet distortion is greater than the distortion allowance of the component. In such cases, surge or stall would have a significant probability of occurence and the stability stack-ups at these conditions would warrant closer scrutiny.

$$\text{SCREENING PARAMETER} = \frac{\Delta\text{PRS}}{\text{Allowable } \Delta\text{PRS}} \qquad (2.45)$$

The radial distortion at the interface plane usually is completely attenuated by the first compressor. Consequently, screening parameters for downstream compressors usually contain only terms that include circumferential distortion. A family of such screening parameters is described by the general Equation 2.46. The terms for each ring are summed (although not always) over the portion of the interface plane that measures the quality of the air that passes through the downstream compressor. For example, on a particular fan engine with a bypass ratio of one, the screening parameter for the compressor will be summed over the inner two rings of interface instrumentation containing five rings. The extent and multiple-per-revolution functions may be different for each compressor. The engine manufacturer usually can define such functions, based on past experience with similar compressors for use in early screening of inlet data. This form of screening parameter is similar to the existing screening parameters K_θ, KC_2 and DC_θ, insofar as all these parameters include circumferential distortion only and the units are in terms of inlet distortion rather than surge pressure ratio, i.e, the screening parameter is independent of engine sensitivity to inlet distortion. Here again, it is customary to provide guidelines showing the estimated engine distortion tolerance in terms of maximum allowable values of the screening parameter.

$$\text{SCREENING PARAMETER} = \sum_{i=1}^{R} \left(\frac{\Delta PC}{P}\right)_i f(\bar{\theta}_i)\, f(MPR_i) \qquad (2.46)$$

For compressors that are sensitive to inlet radial distortion, as well as circumferential distortion, a screening parameter of the form shown in Equation 2.47 could be used. If such a screening parameter represents the stability of a fan hub, the terms are summed over rings 1 and 2. If the screening parameter is for the tip of the fan, the summation is over the outer two rings of the interface plane. The term describing circumferential distortion includes extent and multiple-per-revolution elements. The radial term has a superposition factor "b" which describes the ratio of radial distortion sensitivity to circumferential distortion sensitivity. This screening parameter is the equivalent of the existing screening parameter Ka_2. Here again, the engine distortion tolerance can be described in the same units as the screening parameter.

$$\text{SCREENING PARAMETER} = \sum_{i=R}^{S} \left\{ \left(\frac{\bar{\theta}_i}{MPR_i}\right)^2 \left(\frac{\Delta PC}{P}\right)_i + b\left[\left(\frac{\Delta PR}{P}\right)_i + C_i\right] \right\} \qquad (2.47)$$

The examples of screening parameters shown in Equations 2.45, 2.46, and 2.47 look different because they are tailored to different requirements. However:

- They all use ARP 1420 distortion-descriptor elements combined in the same manner as in the equation for calculating surge pressure ratio loss.
- They all can be used for comparing inlet distortion to engine distortion tolerance.

Current practice is to calculate distortion screening parameters in real time and identify the peak values. Short segments of data containing the observed peaks are then processed digitally to obtain greater accuracy than is available from the analog processor. This procedure for high speed screening of inlet data is described by Crites (Reference 5) and is discussed in Paragraph 6.4.1.

2.6.4 INLET DATA FILTERING (AVERAGING)

Central to the issue of selecting dynamic inlet patterns for replication by screens, and thereby validating adequate engine distortion allowance using steady-state distortion patterns, is the thesis that a low total-pressure region must last long enough to cause a loss of surge pressure ratio. Therefore, by low-pass filtering analog probe data (or performing the equivalent running average on digitized probe data) in conjunction with the use of the engine manufacturer's distortion computation algorithm, a distortion pattern may be selected for replication by a steady-flow distortion screen during engine testing.

The appropriate averaging time (Reference 6) can be selected by running an engine in a controlled dynamic-distortion environment such as that produced by a random-frequency generator or a turbulator. The loss of surge-pressure-ratio data are correlated versus averaging time using screen-determined distortion sensitivities to establish the filter cutoff frequency (averaging time) which produces the minimum difference between the measured and calculated (using the largest peak distortion just prior to surge) losses of surge pressure ratio.

It is important to note the relationship between "the steady-state inlet distortion level" associated with dynamic distortion levels and the steady screen-produced distortion which replicates the maximum dynamic distortion pattern. The steady screen-produced distortion will equal the maximum dynamic distortion level while the steady-state inlet distortion will be less, sometimes by as much as a factor of one-half. An example of the correlation between steady-state screen distortion and dynamic distortion (from three different sources) induced surges is shown in Figure 2.52, as taken from Reference 7. It shows that when total-pressure data are properly filtered to remove high frequency data that do not contribute to loss in surge pressure ratio, dynamic distortion will produce the same level of surge-pressure-ratio loss as steady-state distortion of an equivalent magnitude.

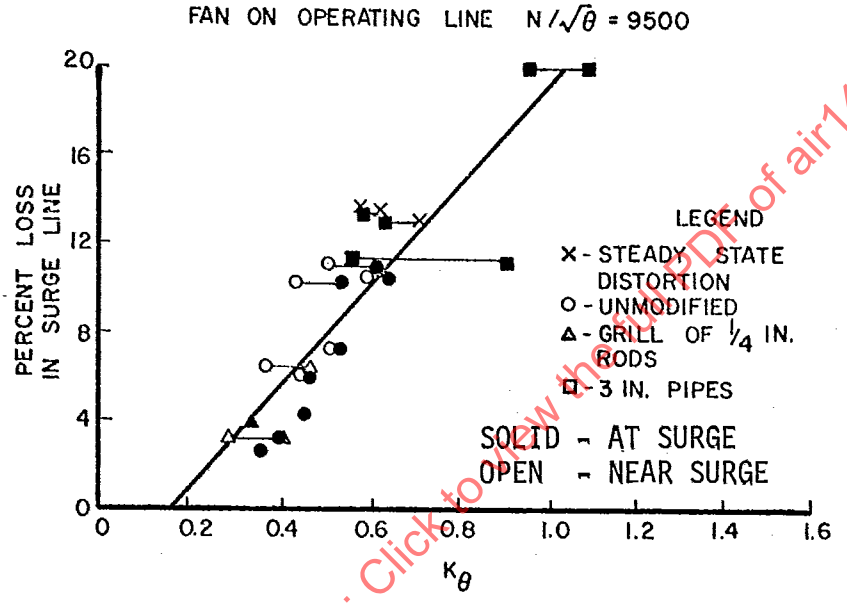

FIGURE 2.52 Surge Line Loss versus Instantaneous Spatial Distortion

SECTION 3

STABILITY ASSESSMENT

The overall purpose of a propulsion system stability assessment is to assure that the design meets the aircraft operational goals. It is a vital part of the propulsion system design and development process, providing the inlet and engine designers with data for defining operational capability and identifying any configuration changes needed, and the program manager with material for allocating development time and resources. To be effective, the stability assessment procedure must be timely, visible, and continuous from conceptual studies to operational service.

Stability assessment involves determining the inlet distortion, the baseline (essentially clean flow) engine stability, and accounting for the destabilizing influence of the AIP distortion as well as other engine operating and installation factors. AIP flow distortion may not be restricted solely to time-variant, spatial, total-pressure distortion. It is important at the outset of any stability assessment to identify when the AIP distortion can be accounted adequately in terms of total pressure alone.

The assessment of the influence of total-pressure distortion on engine stability forms part of a total procedure necessary to determine installed engine stability and stability margins. An assessment of all destabilizing effects must be made so that the contribution made by inlet distortion can be put in perspective. Stability assessments take various forms and are updated throughout the propulsion system design and development cycle. The methodology described in sections 1 and 2 addresses the "classic" turbomachinery aerodynamic instability whereby constituent compressors stall and reduce engine airflow, to produce rotating stall, engine surge (oscillating reverse flow), or combinations of these post-stall instabilities. Other important aspects of engine aerodynamic stability include control system effects and afterburner stability, both of which may be affected by AIP distortion. Engine distortion tolerance depends on the stability margin allocated and available when other destabilizing factors, operating on compression component operating lines and "surge" lines, are taken into account.

This section discusses the impact of AIP total-pressure distortion on engine stability in the broader context of an overall stability assessment.

3.1 STABILITY ASSESSMENT PHILOSOPHY

The assessment method depends upon the anticipated severity of the stability problem; for example, new engine/new installation, established engine/new application, the input information available, and the degree of complexity and expense of the assessment. Distortion stability assessments are unique in that they are complex and not amenable to standardized "cookbook" treatment. As stated previously, the scope of the assessment depends on the status of the

propulsion system development which dictates the quantity and accuracy of the component test data on which the assessment is based. Assessments will emphasize different facts: an assessment supporting the engine compression system designer's needs might emphasize surge margin sensitivity to blade shape, spool matching, and flow-path configurational changes for an anticipated distortion pattern. An assessment supporting the inlet designer's needs may stress the sensitivity of the engine to the various elements in the AIP distortion descriptor for various inlet configurations. The assessment may be largely empirical, i.e., engine tolerance to distortion may be derived through engine tests with suitable instrumentation, such as described in Sections 5 and 6, rather than being synthesized through the use of component test data and suitable engine computer simulations.

Although some features of distortion stability assessments make each assessment unique, assessments outputs are similar in that they provide estimates of surge margin utilization at critical points in the flight envelope, engine tolerance to distortion, and identify the margin required to achieve acceptable AIP distortion levels. All destabilizing effects must be considered to conduct a meaningful stability assessment. Destabilizing effects which influence both the component compressor operating lines and compressor surge lines have been compiled and are presented in Table 3.1. These factors may be random and/or non-random. Once numerical values for each significant factor have been determined, the stability assessment may proceed. Figure 3.1 illustrates some of these factors in schematic form.

TABLE 3.1

Stability Assessment Factors

FACTOR	OPERATING LINE	SURGE LINE
INLET DISTORTION		
a. STEADY-STATE TOTAL-PRESSURE DISTORTION	X	X
b. TEMPERATURE DISTORTION	X	X
c. SWIRL DISTORTION	X	X
d. MAX. INSTANTANEOUS TOTAL-PRESSURE DISTORTION		X
RAM RECOVERY	X	
HORSEPOWER EXTRACTION	X	
PLA TRANSIENT	X	
ENGINE DETERIORATION	X	X
FUEL CONTROL DETERIORATION	X	
DETERIORATION EFFECT ON TRANSIENT FUEL FLOW RATE	X	
FUEL CONTROL TOLERANCES	X	
VARIABLE GEOMETRY CONTROL TOLERANCES	X	X
ENGINE-TO-ENGINE VARIATION	X	X
ENGINE VARIATION EFFECT ON TRANSIENT FUEL FLOW RATE	X	
COMPRESSOR BLEED	X	X
REYNOLDS NUMBER EFFECTS	X	X
NOZZLE MATCHING EFFECTS	X	
HUMIDITY	X	X
CONTROL MODE	X	
BACK PRESSURE DISTORTION	X	X
COMPRESSOR INTERACTION EFFECTS	X	X
TRANSIENT VARIABLE GEOMETRY EFFECTS	X	X
PLA TRANSIENT HEAT TRANSFER	X	X

The more significant operating line assessment factors for a given engine build are:

- o Deterioration
- o Bleed
- o Horsepower extraction
- o Reynolds number effects
- o Steady-state inlet total-pressure distortion and temperature distortion
- o PLA transient (including augmentor operation)
- o Variable geometry control tolerance and transients
- o Gas-path control system sensor(s) in distorted regions

The more significant surge line assessment factors are:

- o Deterioration
- o Reynolds number effects
- o Time-variant inlet-total-pressure and temperature distortion
- o Variable geometry tolerances and transients

Steady-state effects of bleed, horsepower extraction and Reynolds number are contained within the engine digital simulations used to define the compression component's operating pressure ratio at the selected operating condition.

Early stability assessment procedures used a direct, algebraic summation of the worst possible combination of destabilizing factors to arrive at the required surge margin. As the list of identified destabilizing factors grew longer, the resulting demand on engine surge margin also grew, compromising performance and weight, and it became recognized that the probability of all worst cases occuring simultaneously was low. It has been established that some destabilizing factors should be summed statistically to establish more realistic stability-performance-weight trade-offs. This approach is justified in that the Root-Sum-Square (RSS) combination of the random effects retains the overall probability of the individual effects. The statistical approach to stability assessments has not been universally accepted. One approach to statistical assessment is shown in Appendix A.

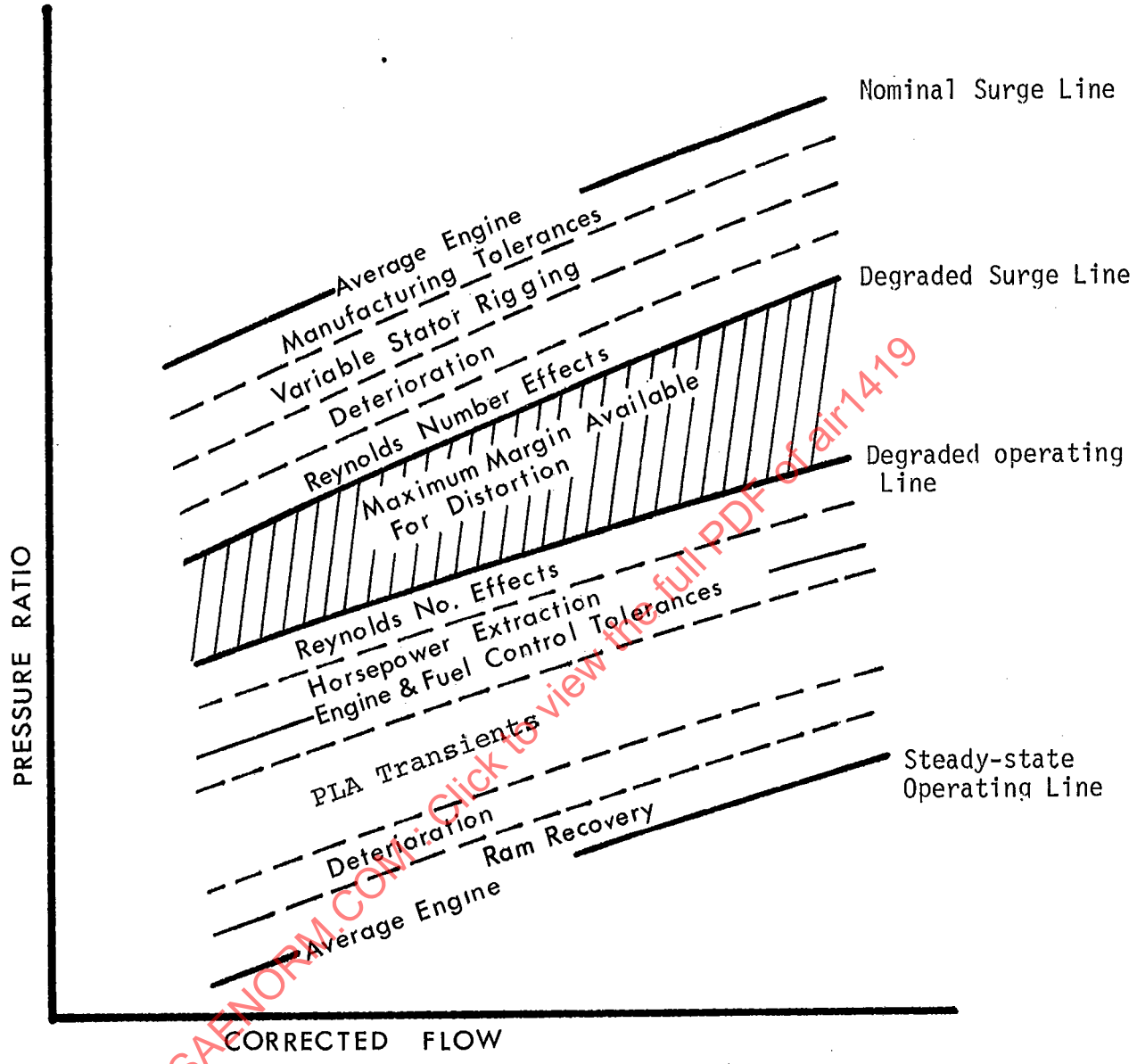

FIGURE 3.1 Typical Compressor Destabilizing Factors

For an individual compression component, the net surge margin is defined by the relation:

$$SM_{Net} = SM_{Baseline} - \left[(\Delta SM)_{NR} + (\Delta SM)_{R}\right]$$

where, $\Delta SM_{NR} = \sum_{i=1}^{n} (\Delta SM)_i$ = Total algebraic surge margin loss due to non-random factors

$$\Delta SM_{R} = \pm\sqrt{\sum_{j=1}^{m} (\Delta SM)_j^2}$$ = Total root-sum-square surge margin loss due to random factors (ΔSM_{RSS})

The loss in surge margin due to distortion is computed using the total-pressure distortion descriptors discussed in Section 2. Other destabilizing effects are evaluated from engine/control data obtained through testing and analysis. All destabilizing effects are combined to determine the net surge margin.

The limitations of current stability assessment procedures should be recognized in applying assessment results. Errors associated with total-pressure distortion assessment can occur because, (1) the value of the distortion descriptor varies with the amount and accuracy of test data, (2) other AIP flow distortions, such as in-phase oscillations, vortex ingestion and swirl may exist, and not be accounted for in the assessment, and (3) summations of individual effects may result in an oversimplification of the actual process.

3.2 STABILITY ASSESSMENT PROCEDURE

The stability assessment process, Figure 3.2, is independent of the complexity of a particular assessment. The results identify: the residual surge margins for the compression system components examined at the critical steady or transient operating points, the types and levels of distortion that are most likely to cause engine surge, and the need for additional engineering activity. The assessment procedure depicted in the figure is an integration of background experience, test-derived information, and synthesis techniques concerned with accounting inlet flow distortion effects and other destabilizing factors. The procedure produces information that is analyzed either to forecast or evaluate the stability status of a propulsion system at critical flight operating points.

Blocks A, B, and C in Figure 3.2 provide the input data necessary to conduct the distortion assessment. Synthesis refers to the process of developing estimates of the effects of destabilizing factors through analysis of component test data, and analytical predictions. In early development the synthesized items in Block B are usually based primarily on prior experience and analytical estimates. As development progresses, the synthesis activity relies more heavily on the expanding test data base, permitting the analysis activities to produce more accurate indications of stability margin. As development nears the qualification phase, testing objectives become more oriented toward stability evaluation, permitting the assessments to become, correspondingly, more oriented toward validating previous forecasts.

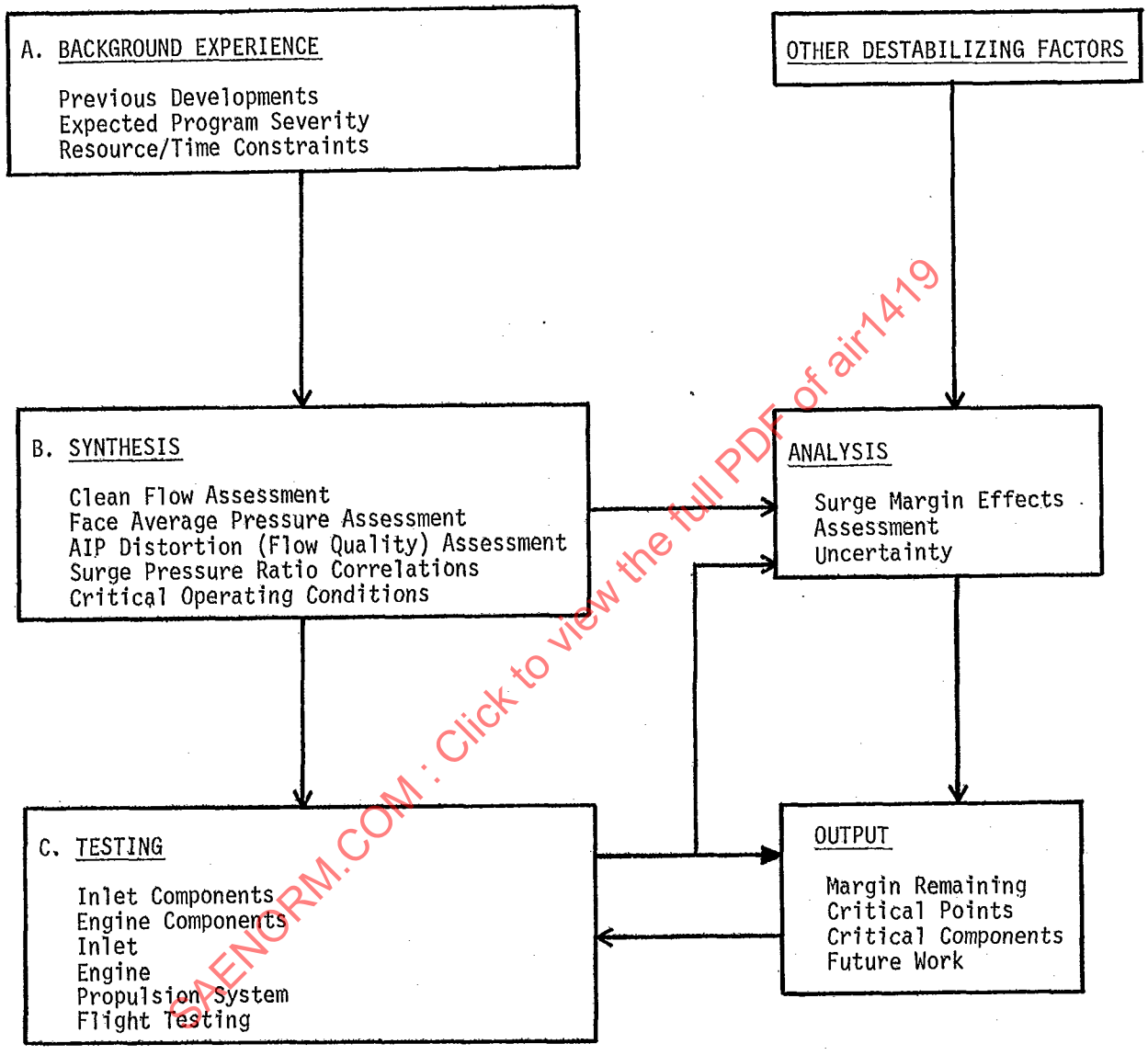

FIGURE 3.2 Stability Assessment Process

An example of the output section of the stability assessment process is presented for a fan/compressor propulsion system. In this example the propulsion system is assumed to be operating at an altitude flight condition where the inlet distortion is defined by the information contained in Figure 2.19.

Figure 3.3 presents an illustrative estimate for a fan operating at 98 percent inlet corrected airflow. The baseline operating pressure ratio, PRO, is 3.0 and the baseline surge pressure ratio PR1 is 3.75. The baseline SM is:

$$SM_{Baseline} = \frac{PR1-PRO}{PRO} \times 100 = \frac{3.75-3.0}{3.0} \times 100 = 25$$

The loss in fan surge pressure ratio due to inlet total-pressure distortion can be calculated using an expansion of Equation 2.12 in the following form:

$$\Delta PRS = b_p EX_p \left[KC \left(\frac{\Delta PC}{P} \right)_{max} + CC_P \right] + \left[KR_P \left(\frac{\Delta PR}{P} \right)_{max} + CR_P \right] \qquad (3.1)$$

This equation is similar to Equation 2.16a for a 1/rev pattern since MPR = 1.

The maximum circumferential distortion is the average of any two adjacent rings:

$$\left(\frac{\Delta PC}{P} \right)_{max} = 1/2 \left[\left(\frac{\Delta PC}{P} \right)_2 + \left(\frac{\Delta PC}{P} \right)_3 \right] = 0.0599$$

The circumferential extent is equal to the average of the extents of the two adjacent rings used to calculate the circumferential distortion and is equal to 177.6 degrees.

The maximum radial distortion occurs in the tip (ring 5):

$$\left(\frac{\Delta PR}{P} \right)_{max} = 0.0678$$

The value and source of the fan coefficients used in the calculation are given in Table 3.2. These coefficients apply at 95 percent corrected fan speed which corresponds to the matched-inlet corrected airflow of 98 percent.

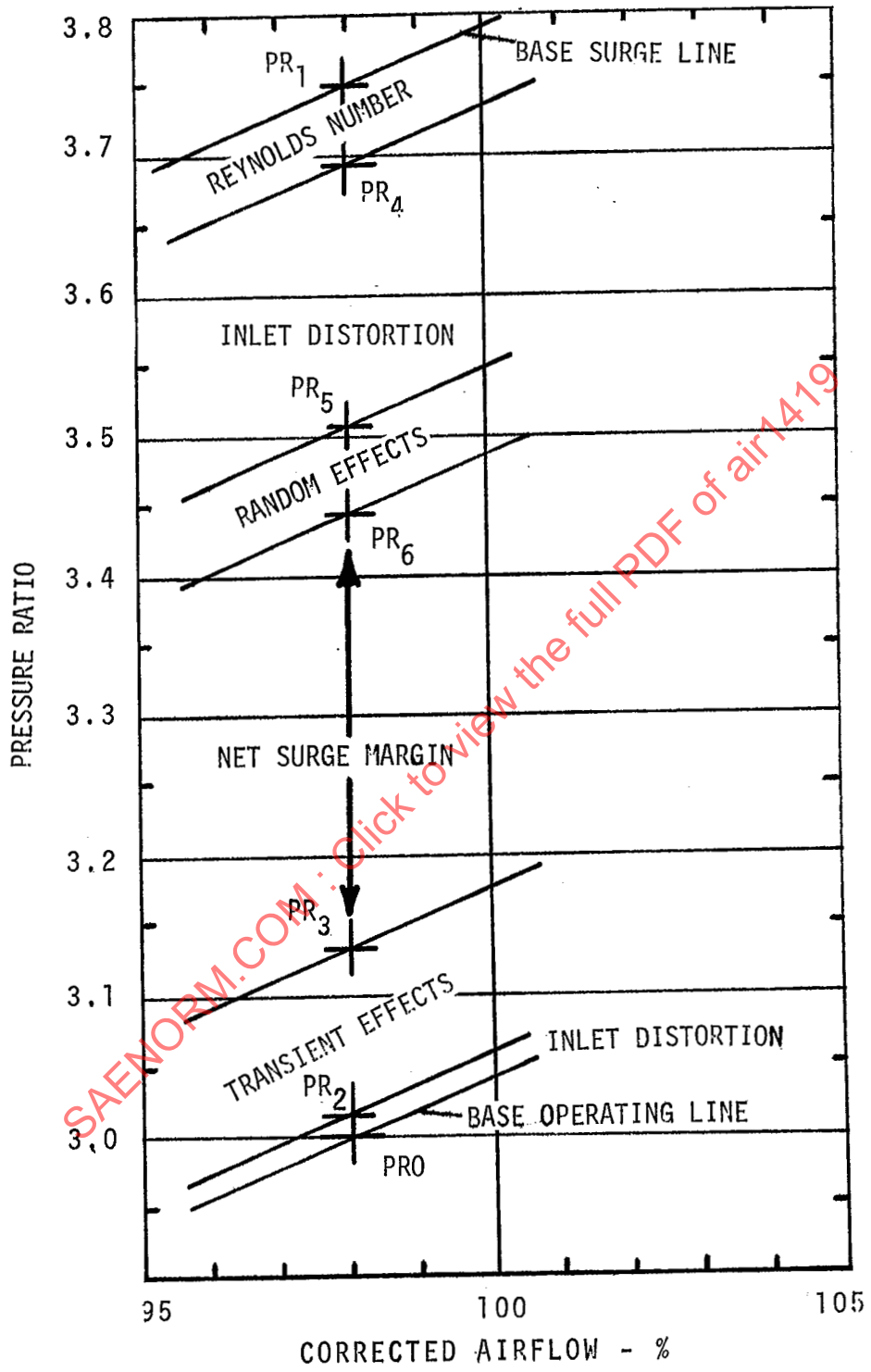

FIGURE 3.3 Fan Stability Assessment Example

TABLE 3.2

Fan Surge-Pressure-Ratio Loss Coefficients

Coefficient	Value	Source
KC_p	0.46	Figure 2.31
CC_p	0	Since ΔPRS curves pass through origin of Figure 2.30
KR_T	0.74	Figures 2.34 and 2.35
CR_T	-0.038	Figures 2.34 and 2.35
b_p	1.0	Figure 2.36
EX_p	0.995	Figure 2.37

$$\Delta PRS = (1)\ (0.995)\left[0.46\ (0.0599) + 0\right] + \left[0.74\ (0.0678 - 0.038)\right] \times (100) = 5.0\,\%$$

The loss in surge margin due to inlet total-pressure distortion and the other assumed surge margin utilizations for this example are presented in Table 3.3.

TABLE 3.3

Fan Surge Margin Assessment

Destabilizing Factor	Assumed Cause	Pressure Ratio (PR) and Surge Margin Loss (ΔSM)
Non-Random (NR)	Operating Line Shift due to AIP total pressure distortion	PR2 = 3.015 $\Delta SM = \frac{PR2-PR0}{PR0} \times 100 = 0.5$
	Operating Line Shift due to 4% ΔP/P Augmentor spike	ΔSM = 4.0 $PR3 = PR2 + (\frac{\Delta SM}{100}) \times PR0$ = 3.015 + 0.04 x 3.0 = 3.135
	Surge line loss due to Reynolds Number, ΔPRS = 1.5	$PR4 = PR1 - (\frac{\Delta PRS}{100}) \times PR1$ = 3.75 - 0.015 x 3.75 = 3.694 $\Delta SM = (\frac{PR1-PR4}{PR0}) \times 100 = 1.87$
	Surge line loss due to time-variant AIP Distortion, ΔPRS = 5.0	$PR5 = PR4 - (\frac{\Delta PRS}{100}) \times PR1$ = 3.694 - 0.05 x 3.75 = 3.507 $\Delta SM = (\frac{PR4-PR5}{PR0}) \times 100 = 6.25$
		TOTAL ΔSM_{NR} = 0.5+4.0+1.87+6.25 = 12.62
Random (R)	Operating Line Effects: - Variable Geometry Control Tolerances - Engine to Engine Variations	ΔSM = ± 1.1 ΔSM = ± 1.2
	Surge Line Effects of Engine to Engine Variations	ΔSM = ± 1.3
		TOTAL $\Delta SM_R = \Delta SM_{RSS} = \pm\sqrt{(1.1)^2 + (1.2)^2 + (1.3)^2}$ = ±2.08

For the purpose of determining net or residual surge margin, it is assumed that the total random effects may be used to lower the surge line or raise the operating line. For this example, it is assumed that the surge line is lowered so that:

$$PR6 = PR5 - \frac{\Delta SM}{100} \times PR0 = 3.507 - 0.0208 \times 3.0 = 3.44$$

The net or residual surge margin is then given by:

$$SM_{Net} = \frac{(PR6-PR3)}{PR0} \times 100 = 10.3 \text{ percent}$$

A similar example can be constructed for the compressor, where the effects of compressor inlet-total-pressure and total-temperature distortion need to be assessed taking into consideration the fan distortion transfer characteristics at fixed-throttle or transiently matched conditions. It is generally accepted that the data obtained from the two inner instrumentation rings, which are located in the core stream, are sufficient for developing core distortion sensitivities and distortion transfer correlations.

Table 3.4 presents the results of an example calculation, illustrating the assumptions made, in a format suitable for comparison with the fan stability assessment. In this example, the residual fan surge margin is 10.30 percent, the residual compressor surge margin is 3.27 percent. The critical component would appear to be the compressor. However, to proceed further, it may be necessary to calculate the probability of occurrence of an instability. This is discussed in Section 7.1.3 and Appendix A. At a given operating point, the critical component is that component having the highest probability of instability. It is important to note that the critical component at one flight, inlet, and engine operating condition need not be the critical component at other conditions. Because of this fact, stability assessments have to be conducted at several points throughout the operational flight envelope.

TABLE 3.4

Typical Surge Margin Stability Assessment

DESTABILIZING EFFECTS	COMPONENT			
	FAN		COMPRESSOR	
o OPERATING LINE	NON-RANDOM	RANDOM	NON-RANDOM	RANDOM
Inlet Distortion	0.5	-	0.7	-
PLA Transient	4.0	-	6.0	-
Variable Geometry Control Tolerances	-	+1.1	-	-
Fuel Control Tolerances	-	-	-	+1.15
Engine to Engine Variation	-	+1.2	-	+1.25
o SURGE LINE				
Reynolds Number	1.87	-	0.36	-
Inlet Distortion	6.25	-	7.50	-
Engine to Engine Variation	-	+1.3	-	+1.35
o TOTAL	12.62	±2.083	14.56	±2.169
o BASE SURGE MARGIN	25.0		20.0	
o NET SURGE MARGIN	10.30		3.27	

3.3 DISTORTION STABILITY ASSESSMENT

The above examples illustrate the impact of inlet-total-pressure distortion on the fan and compressor stability. The loss in fan surge margin due to AIP total-pressure distortion represented approximately 25 percent of the baseline fan surge margin, and the loss in compressor surge margin, due to the combined effects of total-pressure and total-temperature distortion at compressor entry, accounted for approximately 37.5 percent of the baseline compressor surge margin.

The distortion stability assessment procedure is shown graphically in Figure 3.4. As previously stated, the procedure is iterative and the level of confidence in the assessment increases through the propulsion system development process.

Section 2 describes the methodology involved in establishing ΔPRS and distortion sensitivities through correlations of compressor data. Figures 2.22 through 2.43 present typical data from which correlations are derived.

3.3.1 CIRCUMFERENTIAL DISTORTION

Figure 3.5 illustrates the effect on surge line of to one-per-rev circumferential distortions (MPR = 1.0) of varying extents from rig tests of a three-stage compressor with distortion screens. Similar examples, derived from engine tests, are shown in Figure 3.6 through Figure 3.9 for the J85-GE-13 engine. Figure 3.10 shows results for a two-per-rev circumferential distortion (Reference 8). Each test result provides distortion response data. Figure 3.11 shows an example for one-per-rev circumferential distortions. The experimentally established ΔPRS are plotted here in terms of a distortion descriptor. The descriptor is represented by the product of the ARP 1420 circumferential extent and intensity elements together with a correlation coefficient which varies with corrected airflow. The distortion descriptor is a special form of Equation 2.47, applicable to this compressor. The slopes of the correlation lines of Figure 3.11 represent the sensitivity of the compressor expressed in terms of the descriptor, i.e., screening parameter level as discussed in Section 2. Thus at 92 percent design airflow:

$$\frac{\Delta PRS}{100} = 1.54 \times \text{Screening Parameter}$$

3.3.2 RADIAL DISTORTION

Figure 3.12 illustrates the effect on surge line of a severe hub-radial distortion established from rig tests on a three-stage compressor. Results, derived from tests of the J85-GE-13 engine with hub-radial, mid-span, and tip-radial profiles, are shown in Figure 3.13 through 3.17 (Reference 8). Correlations similar to those for circumferential distortion can be developed from these data. Since radial distortion effects can be favorable, it may be necessary to apply a methodology which accounts for the fact that ΔPRS changes are not monotonic (Section 2, Figures 2.42 and 2.43).

3.3.3 COMBINED CIRCUMFERENTIAL AND RADIAL DISTORTION

The distortion patterns encountered during normal aircraft operation are a combination of circumferential and radial profiles. It is necessary that all correlation methodologies collapse data of this format. Figures 3.18 and 3.19 present the loss in surge margin demonstrated by the J85-GE-13 engine when combined inlet distortions were imposed on the engine.

The examples point up the fact that acquisition of stability response data can be time-consuming and expensive. To minimize the work involved it is important to identify from inlet tests, the major features of the AIP distortion early in the preliminary design and development phases of a program. Assessment procedures for turbofan engines are complex and involve developing a methodology to account for induced radial-flow and bypass-ratio effects through and at the exit from the fan, and for spool interaction.

Test data may not be available in the conceptual design, preliminary design, and early development phases of a new system. The baseline ΔPRS equation, Figure 2.20, is equally applicable to theoretical and semi-empirical stability assessment methods using the ARP 1420 distortion descriptor elements. Theoretical and semi-empirical methods encompass spool-, stage-, and blade-row models- incorporated into numerical computer simulations of the engine. These tools, together with background experience, provide a basis for stability assessment in early design and development phases of a program. The computer methods are applied in conjunction with steady and transient engine computer decks, (References 9 and 10).

Figures 3.20 and 3.21 show the results of a stability assessment, expressed in terms of an AIP distortion descriptor compared with flight test results. Figure 3.20 refers to fixed-throttle engine operation. Figure 3.21 refers to throttle transient (accel) operation. The examples show that the fixed-throttle assessment correctly predicted the flight stability limit. The throttle transient results serve to illustrate the influence of AIP distortion on acceleration capability. Prior to flight test, such assessments may be used to identify critical inlet/engine compatibility conditions within the flight envelope.

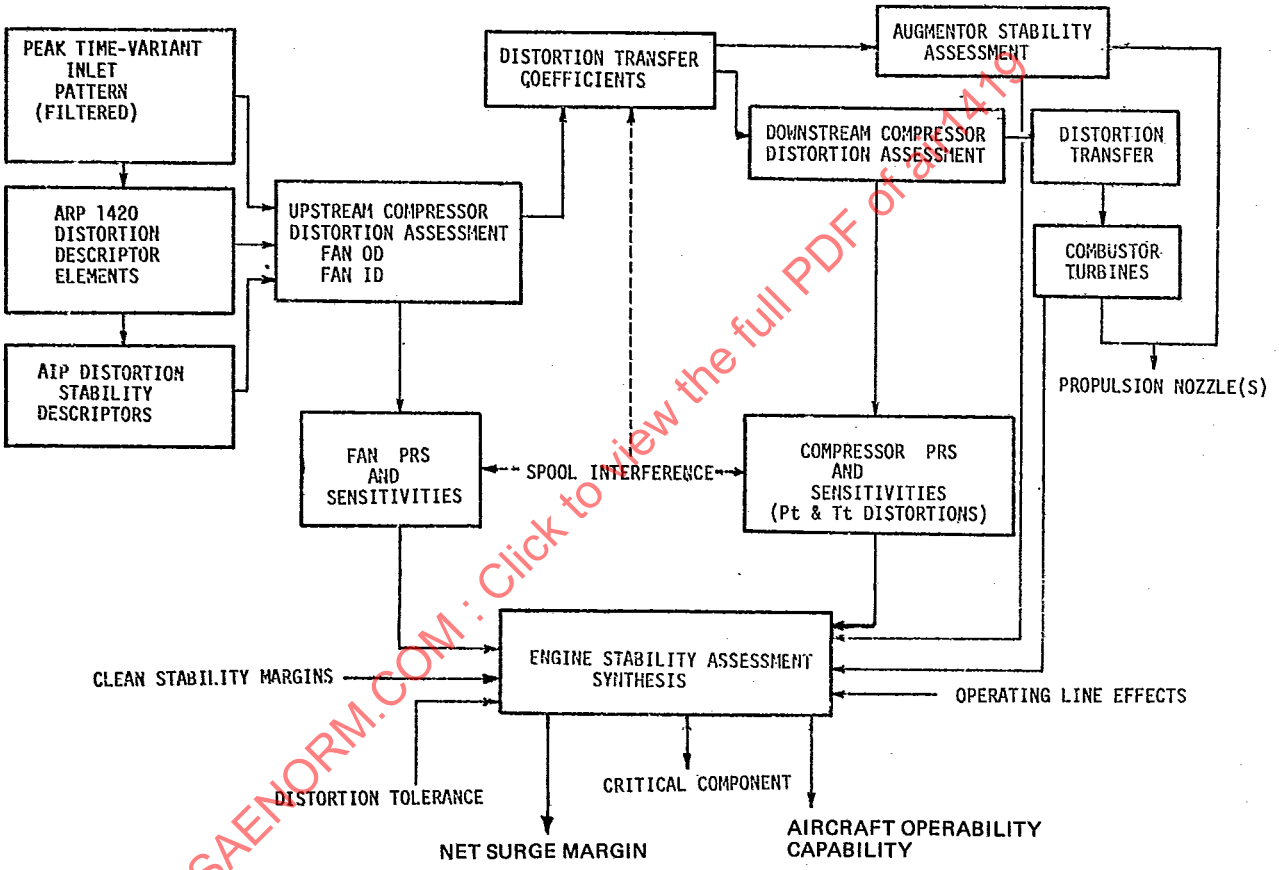

FIGURE 3.4 Distortion Stability Assessment

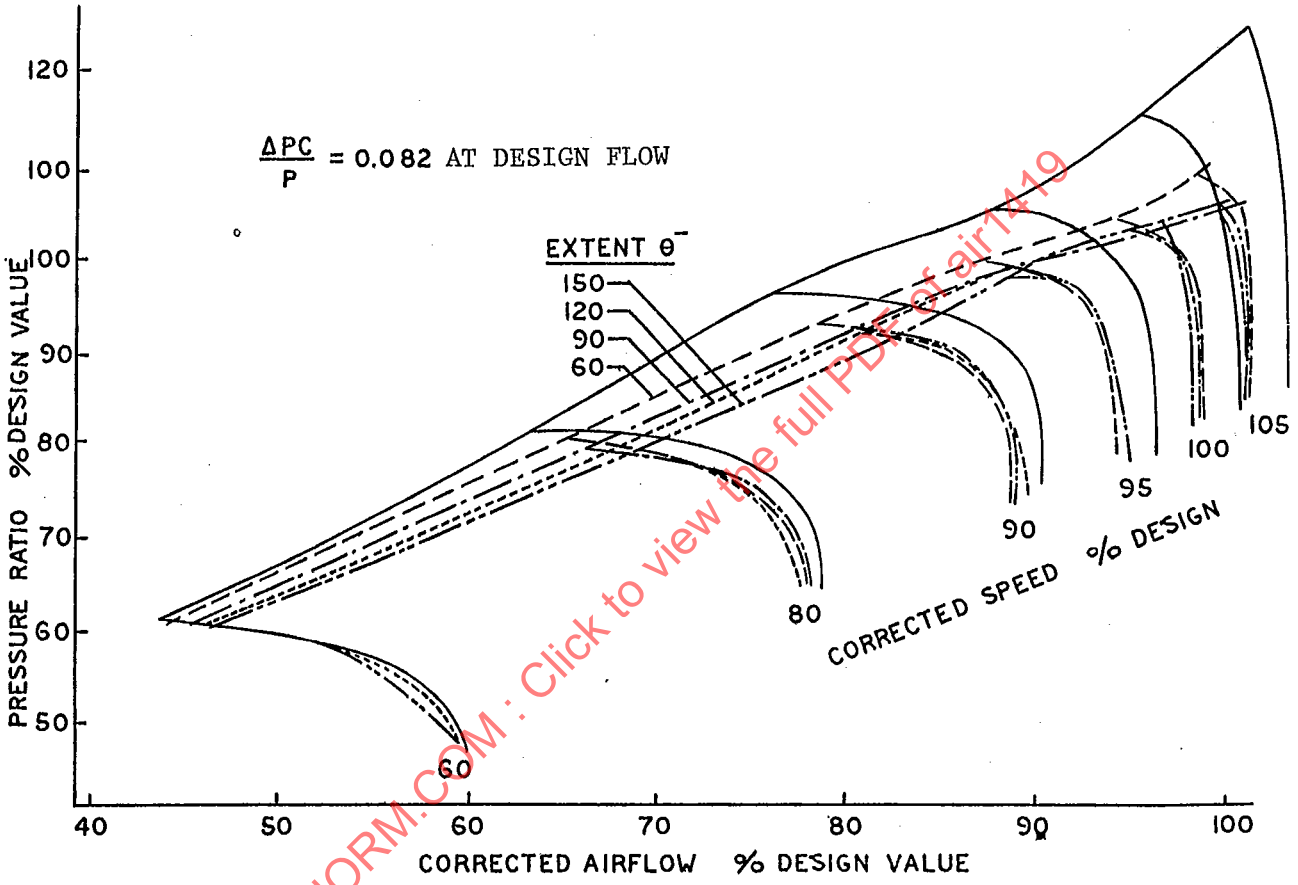

FIGURE 3.5 Example of One-Per-Rev Square Wave Circumferential Total-Pressure Distortion

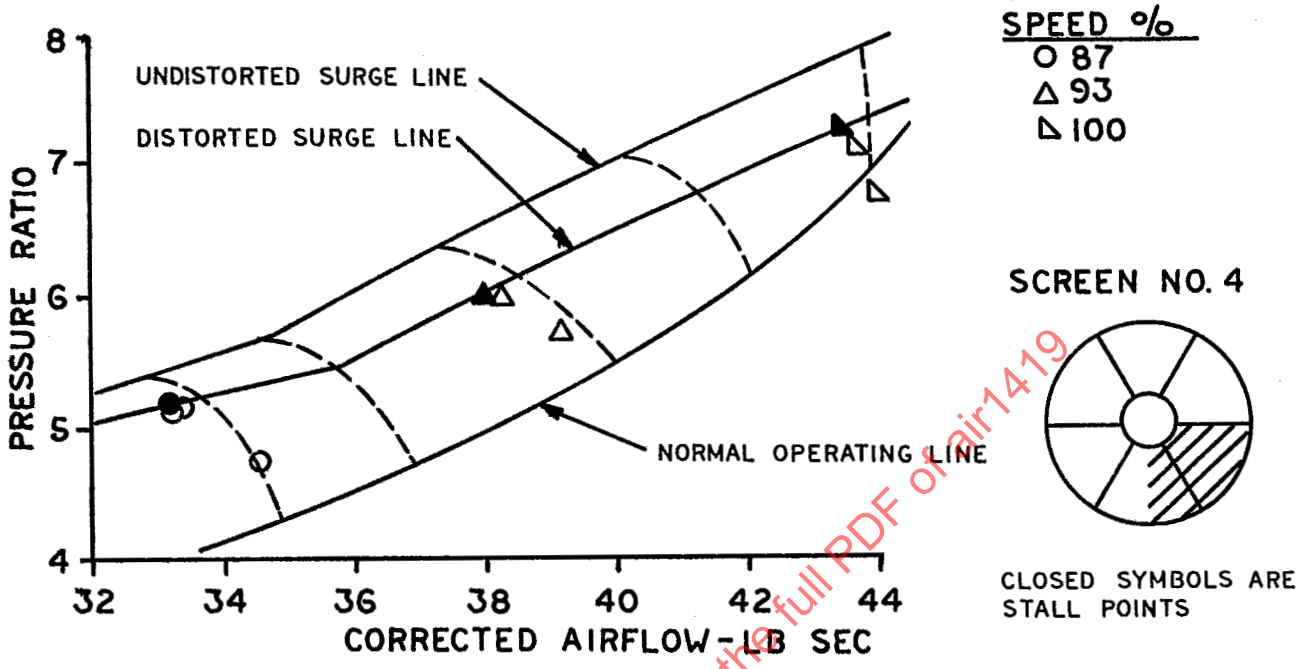

FIGURE 3.6 Example of One-Per-Rev Circumferential Total-Pressure Distortion, 90 Degree Extent

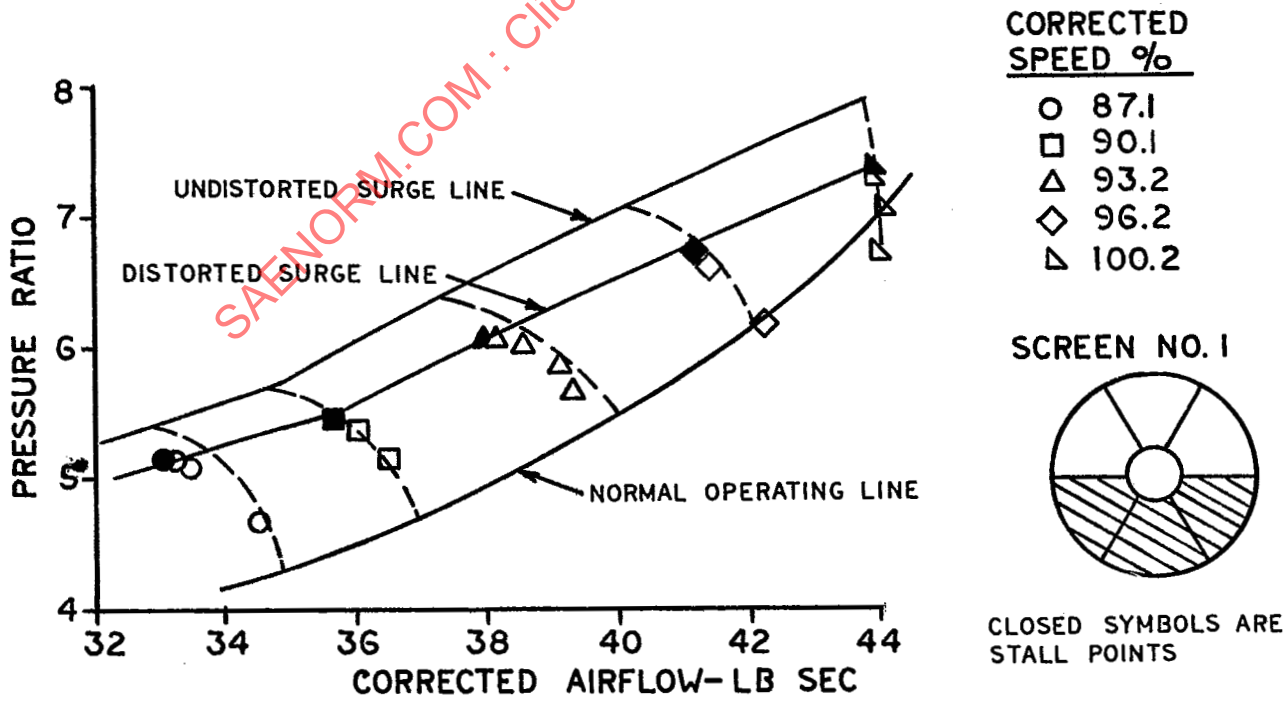

FIGURE 3.7 Example of One-Per-Rev Circumferential Total-Pressure Distortion, 180 Degree Extent

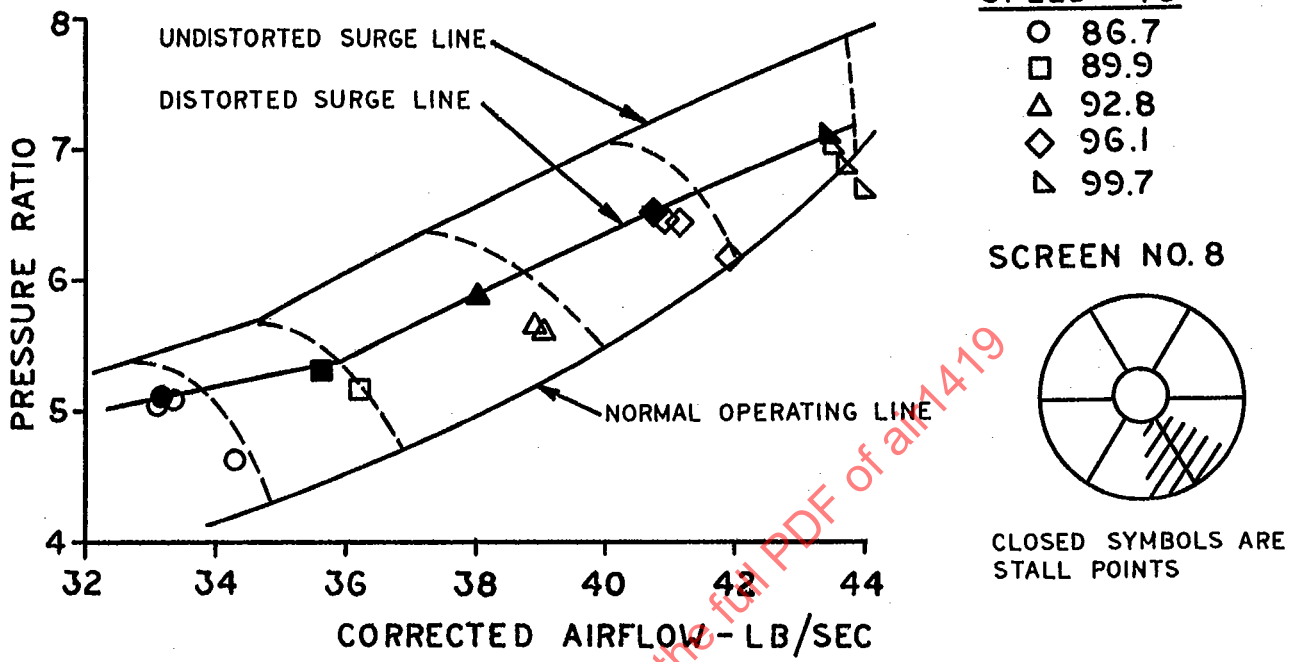

FIGURE 3.8 Example of One-Per-Rev Circumferential Total-Pressure Distortion, 45 Degree Extent

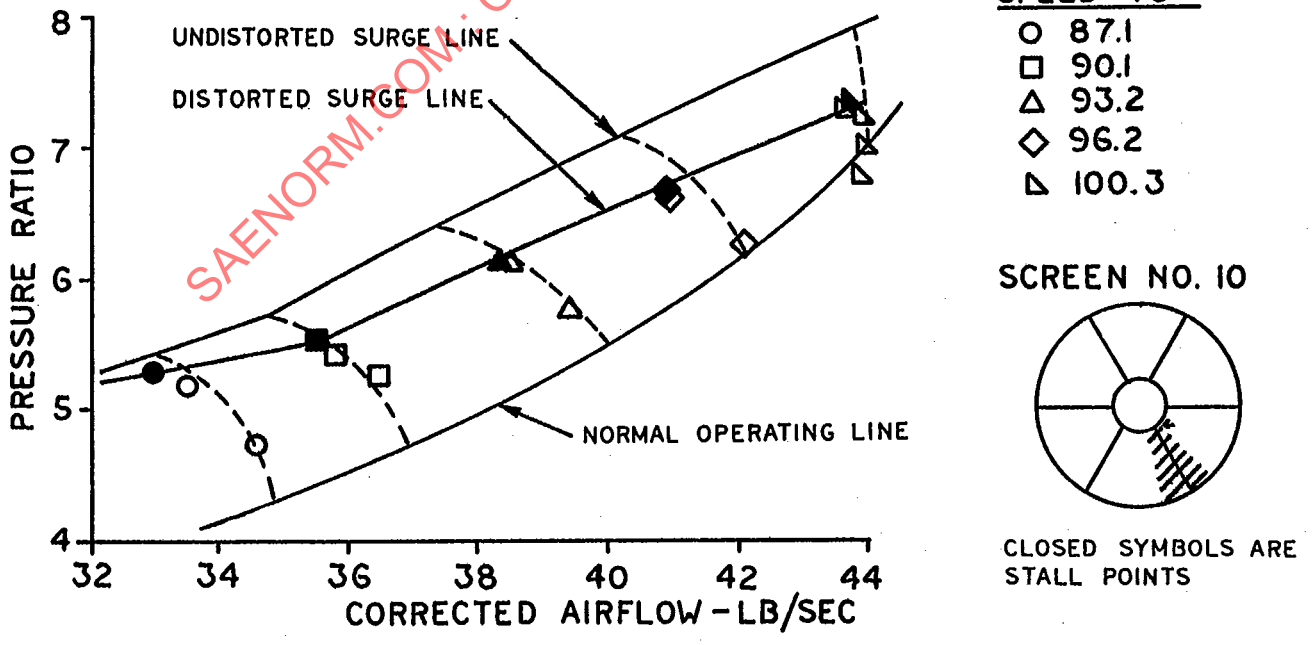

FIGURE 3.9 Example of One-Per-Rev Circumferential Total-Pressure Distortion, 22 Degree Extent

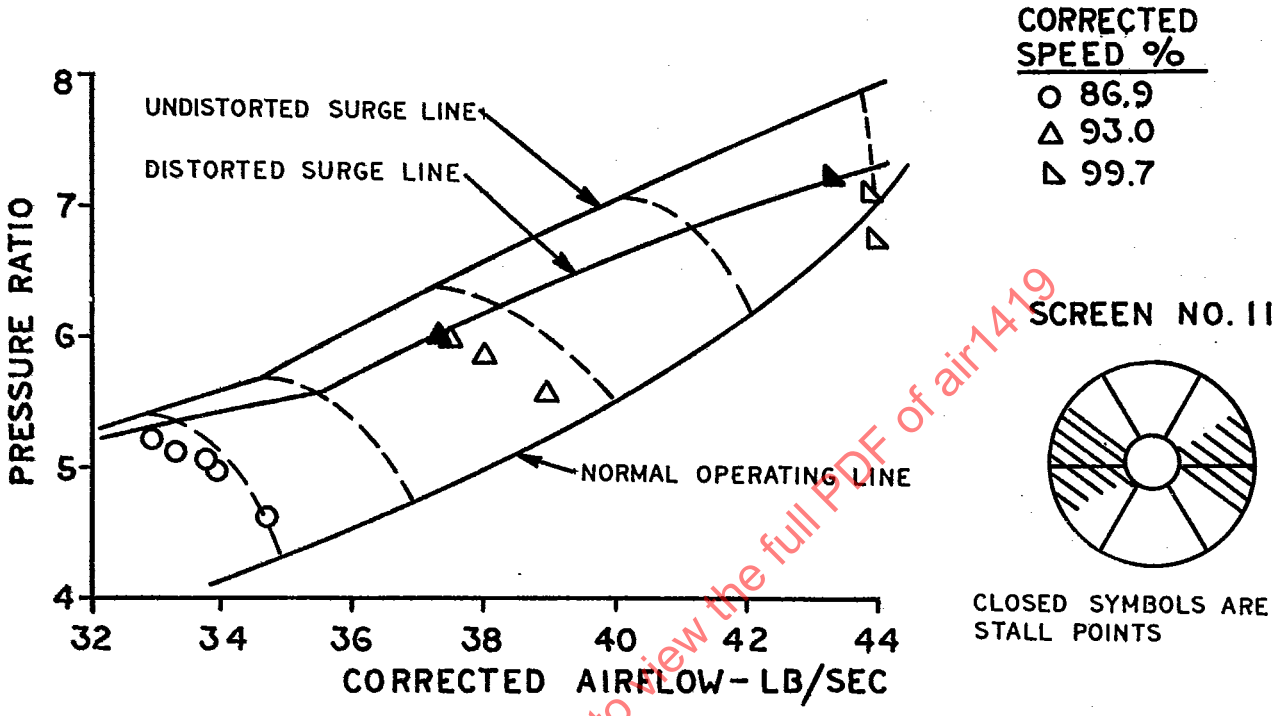

FIGURE 3.10 Example of Two-Per-Rev Circumferential Total-Pressure Distortion

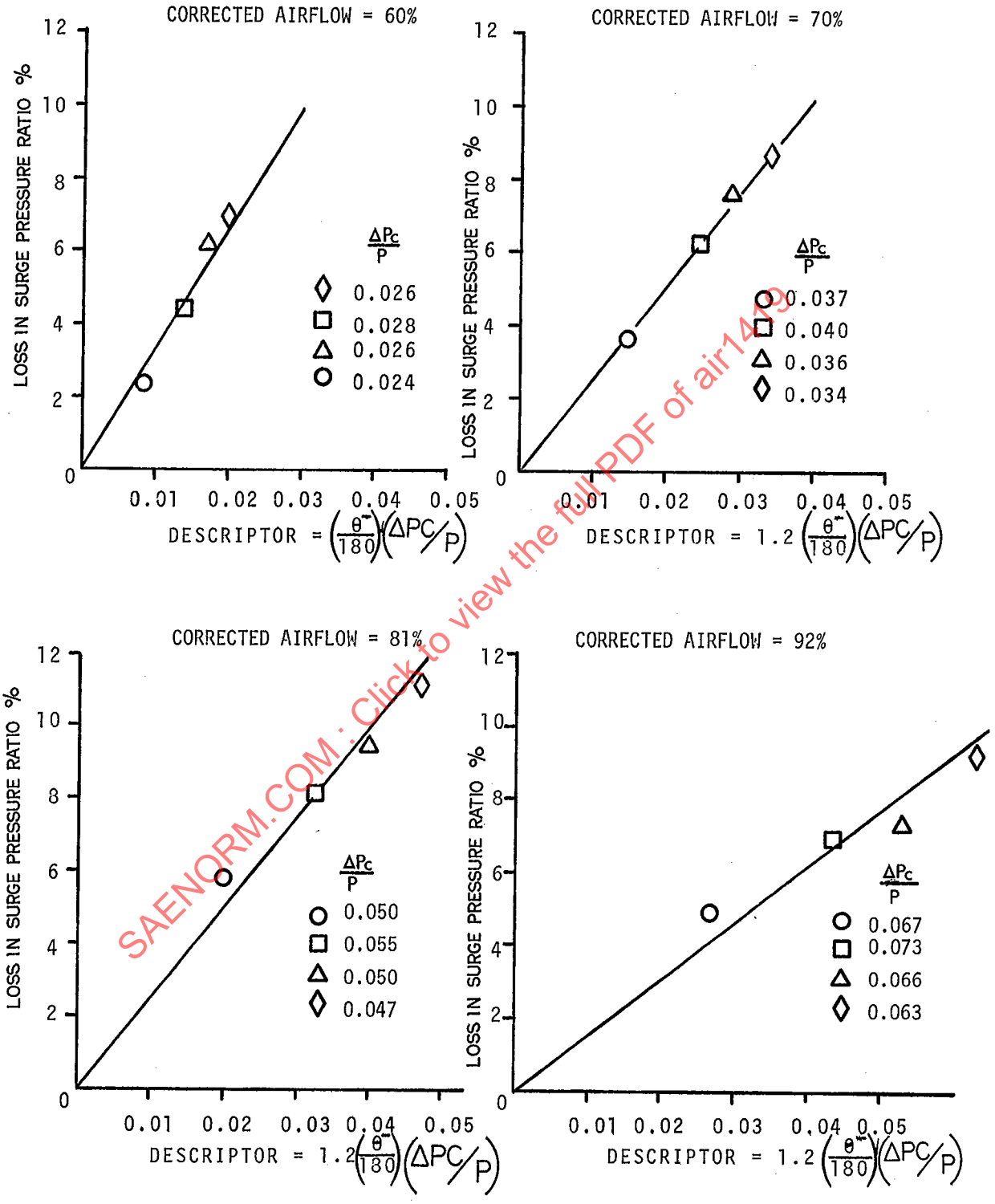

FIGURE 3.11 Compressor Sensitivity to One-Per-Rev Circumferential Total-Pressure Distortion

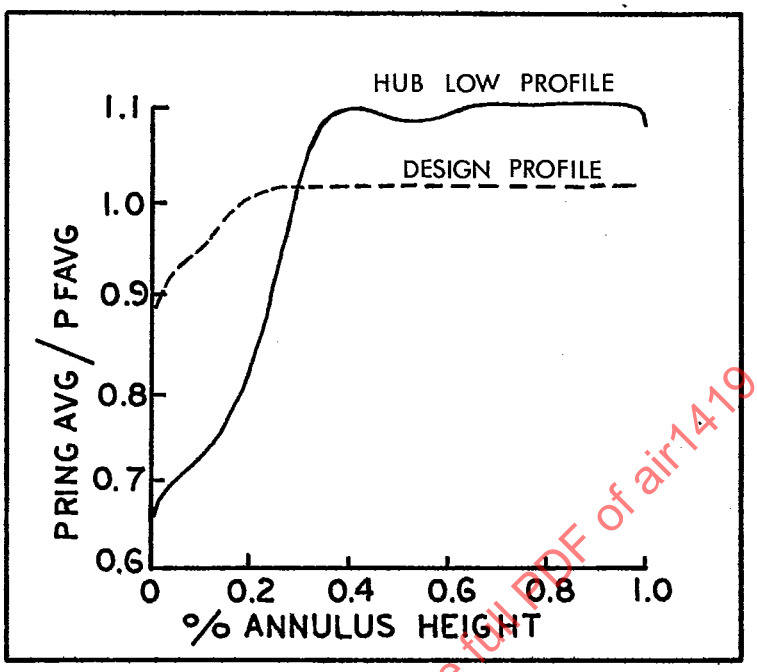

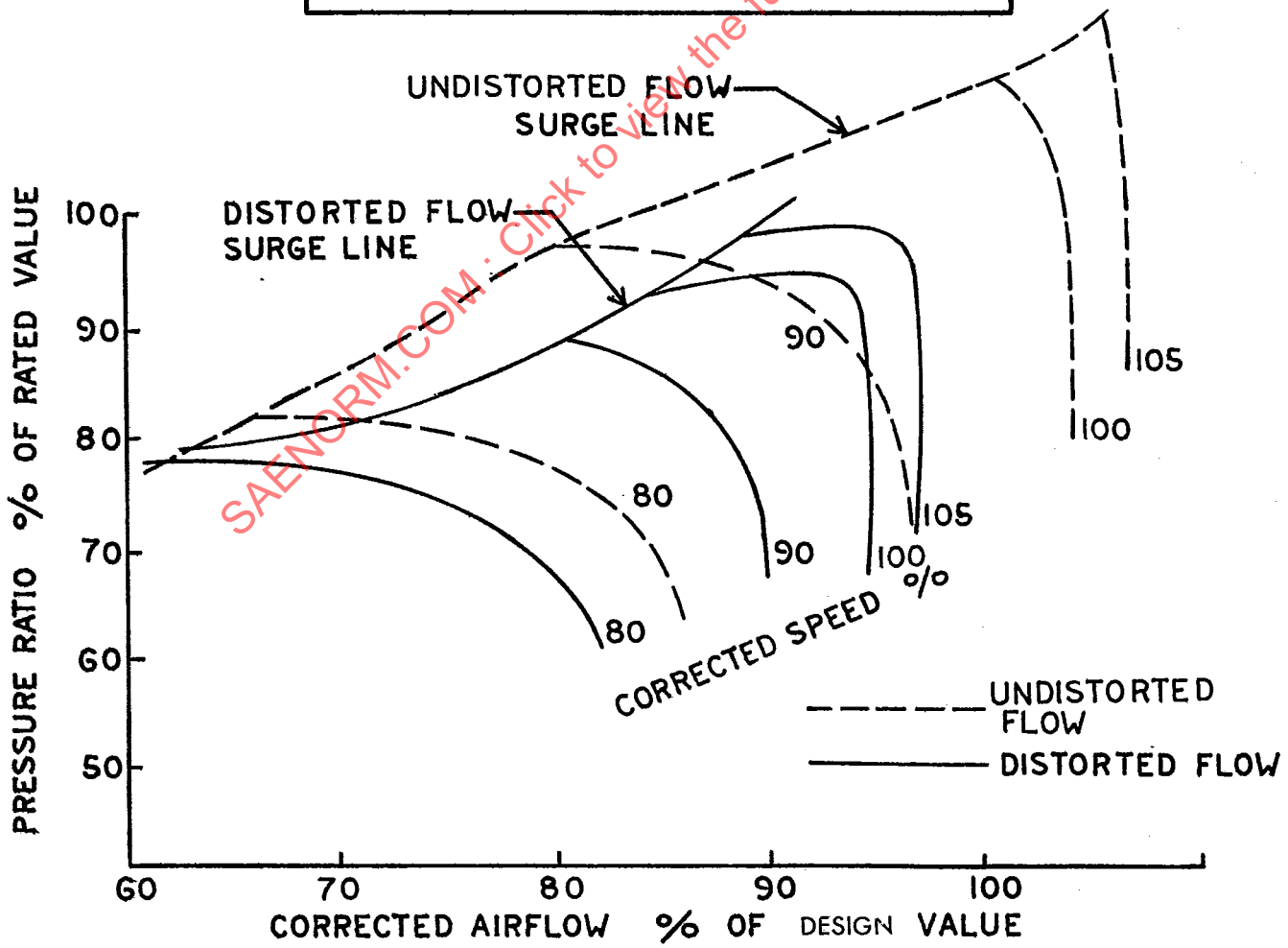

FIGURE 3.12 Example of Hub Radial Total-Pressure Distortion

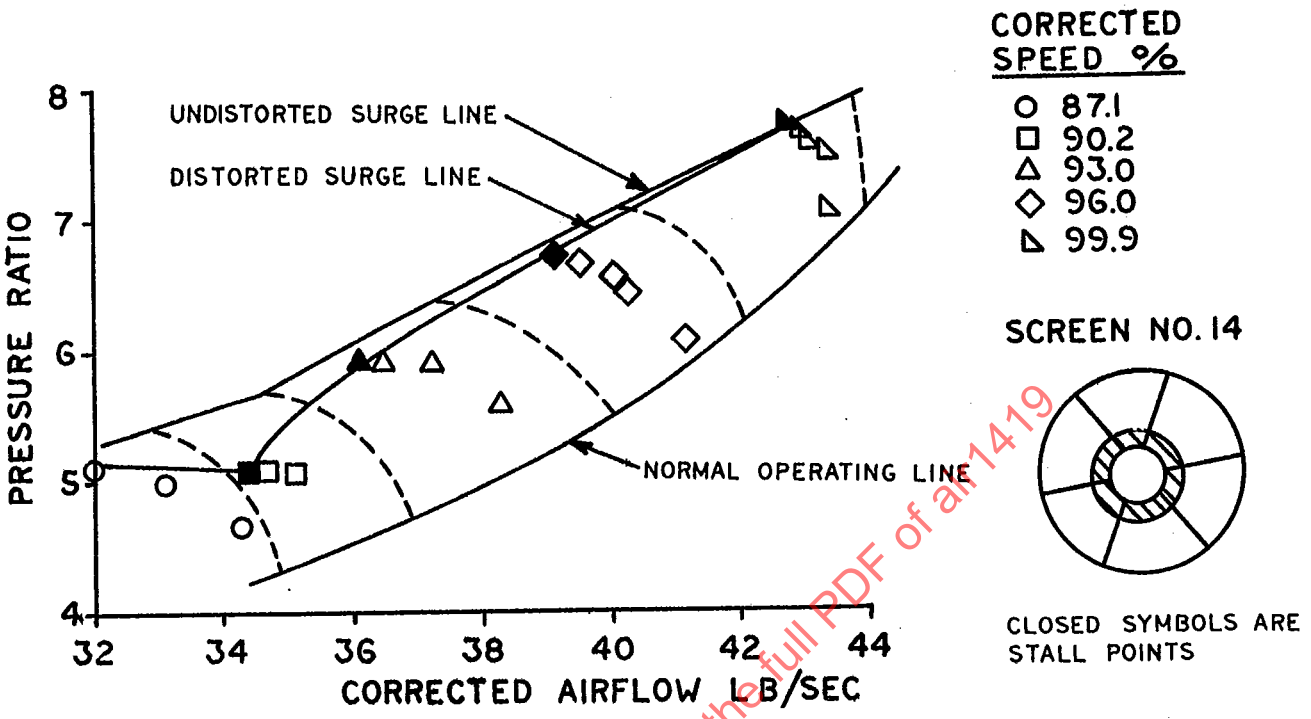

FIGURE 3.13 Example of Hub-Radial Total-Pressure Distortion, Narrow Extent

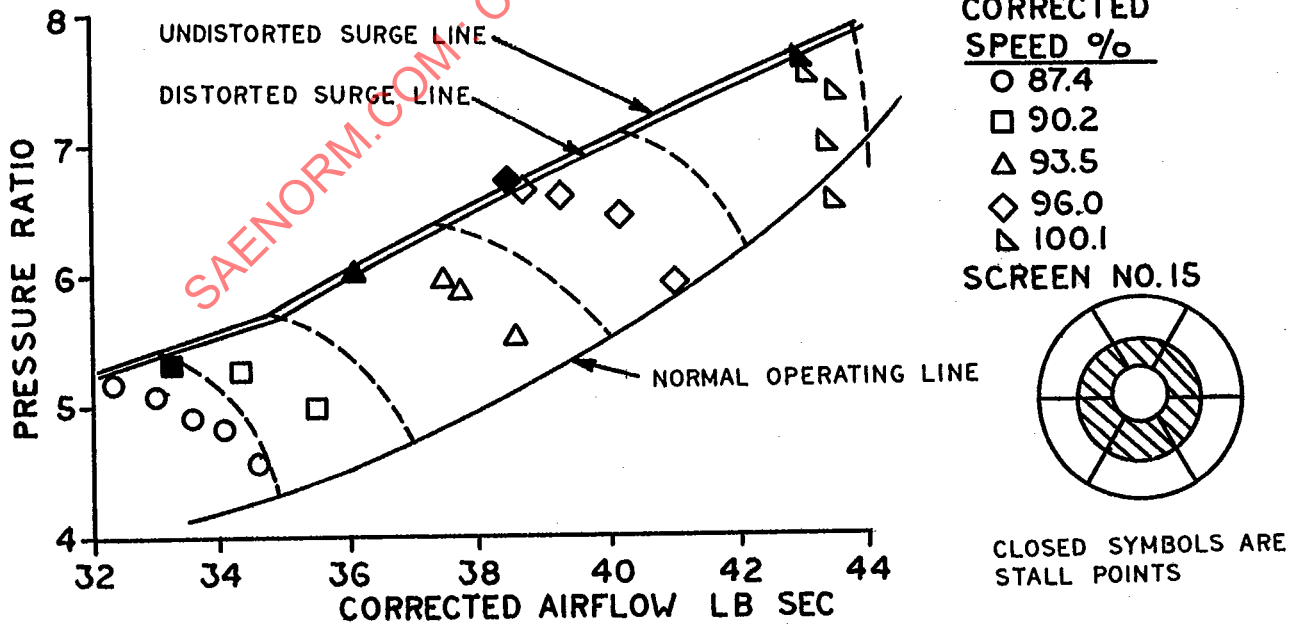

FIGURE 3.14 Example of Hub Radial Total Pressure Distortion, Wide Extent

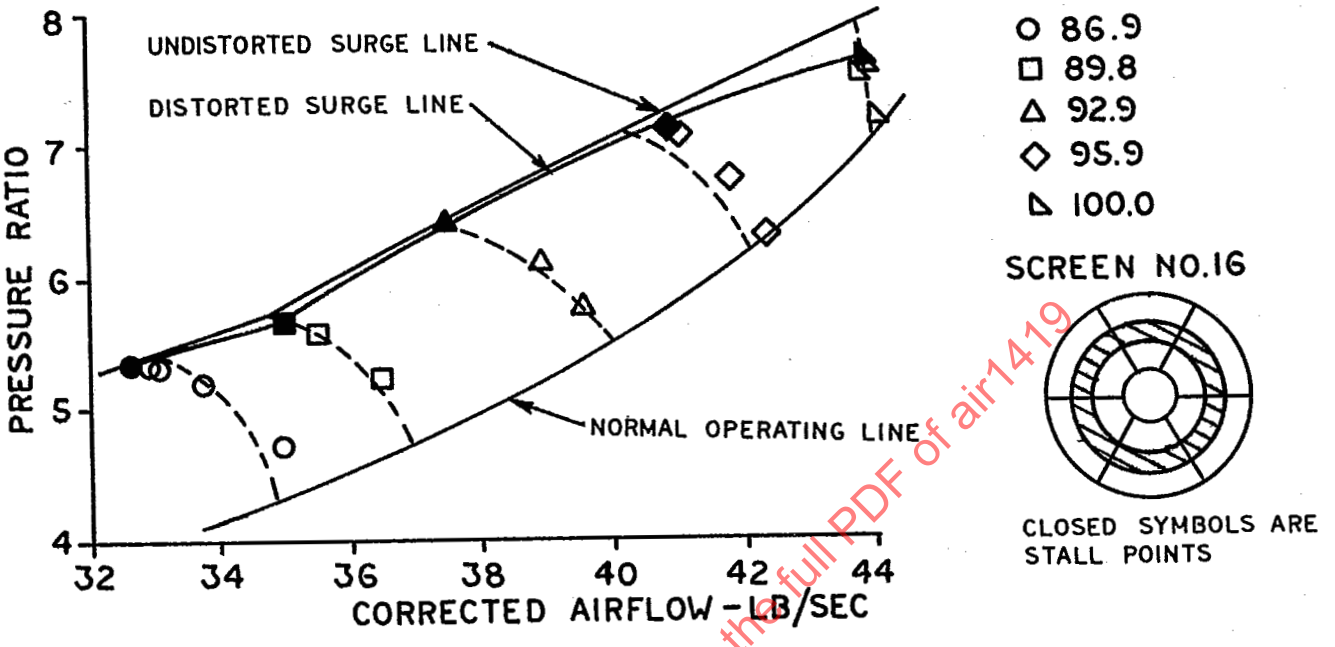

FIGURE 3.15 Example of Mid-Span Radial Total-Pressure Distortion

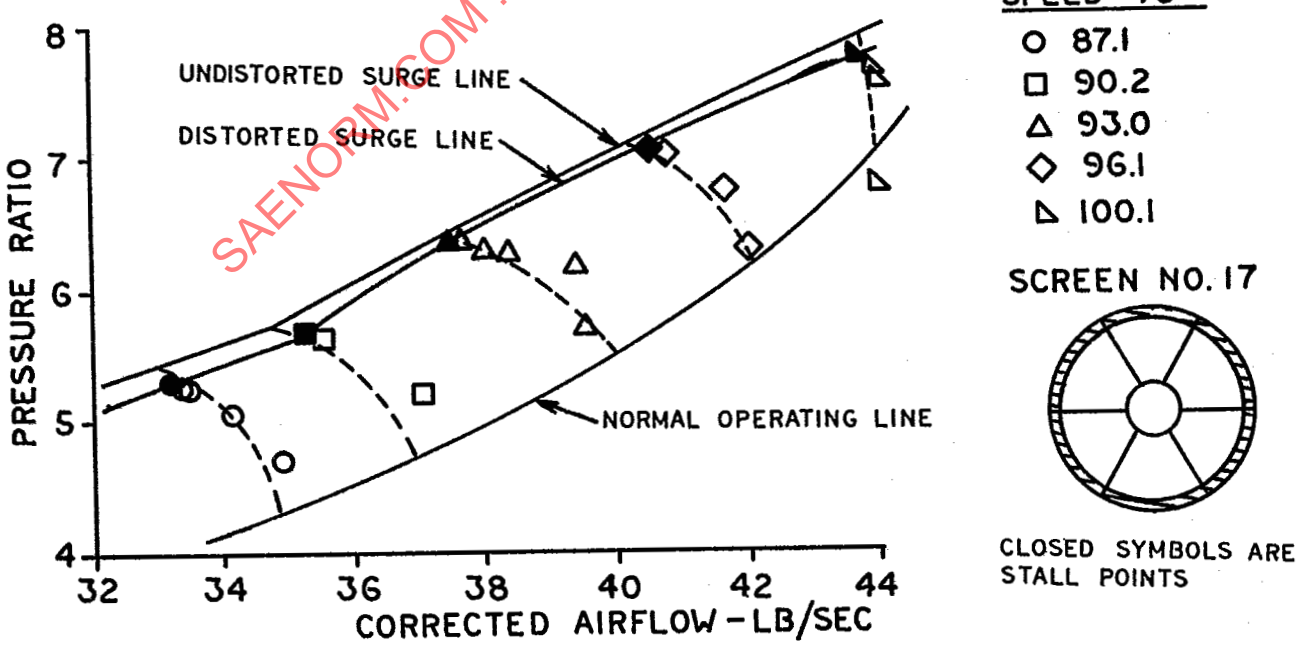

FIGURE 3.16 Example of Tip Radial Total-Pressure Distortion, Narrow Extent

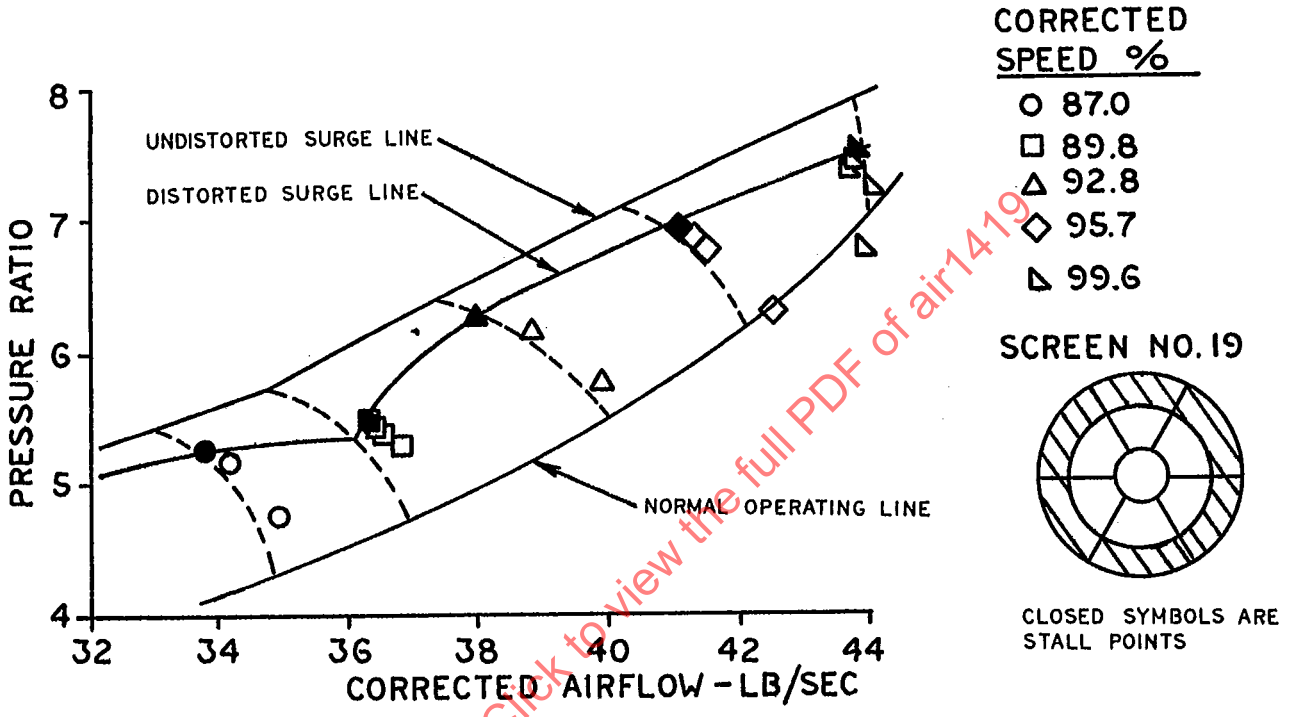

FIGURE 3.17 Example of Tip Radial Total-Pressure Distortion, Wide Extent

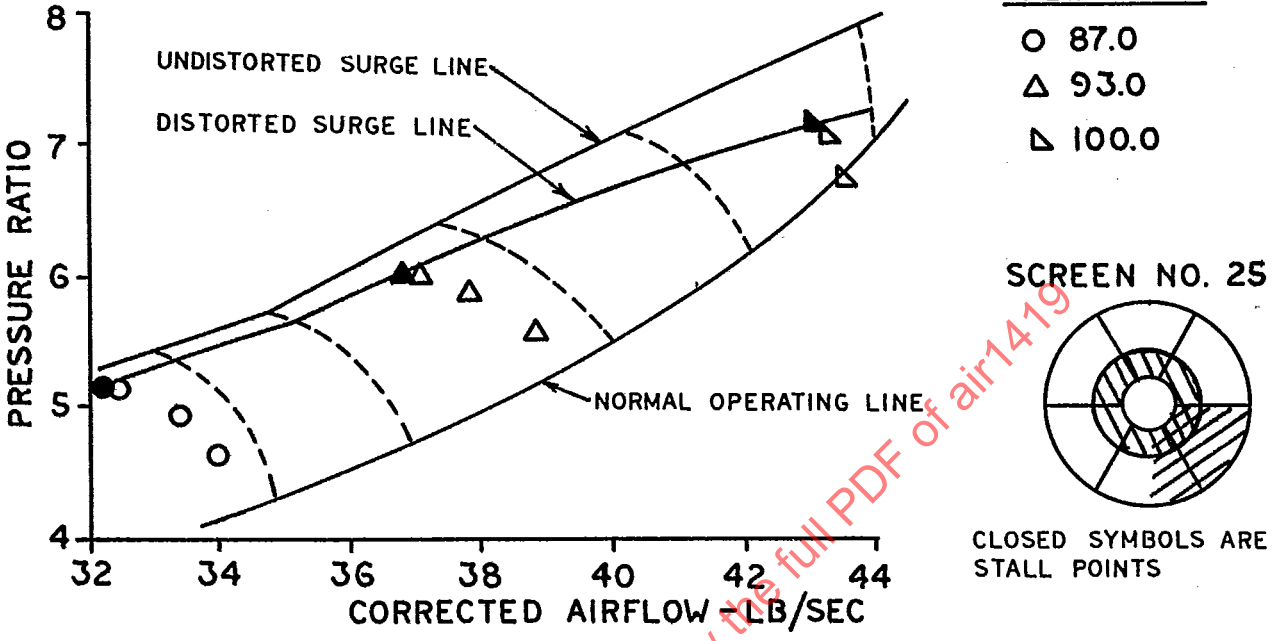

FIGURE 3.18 Example of Combined Hub Radial and Circumferential Total Pressure Distortion

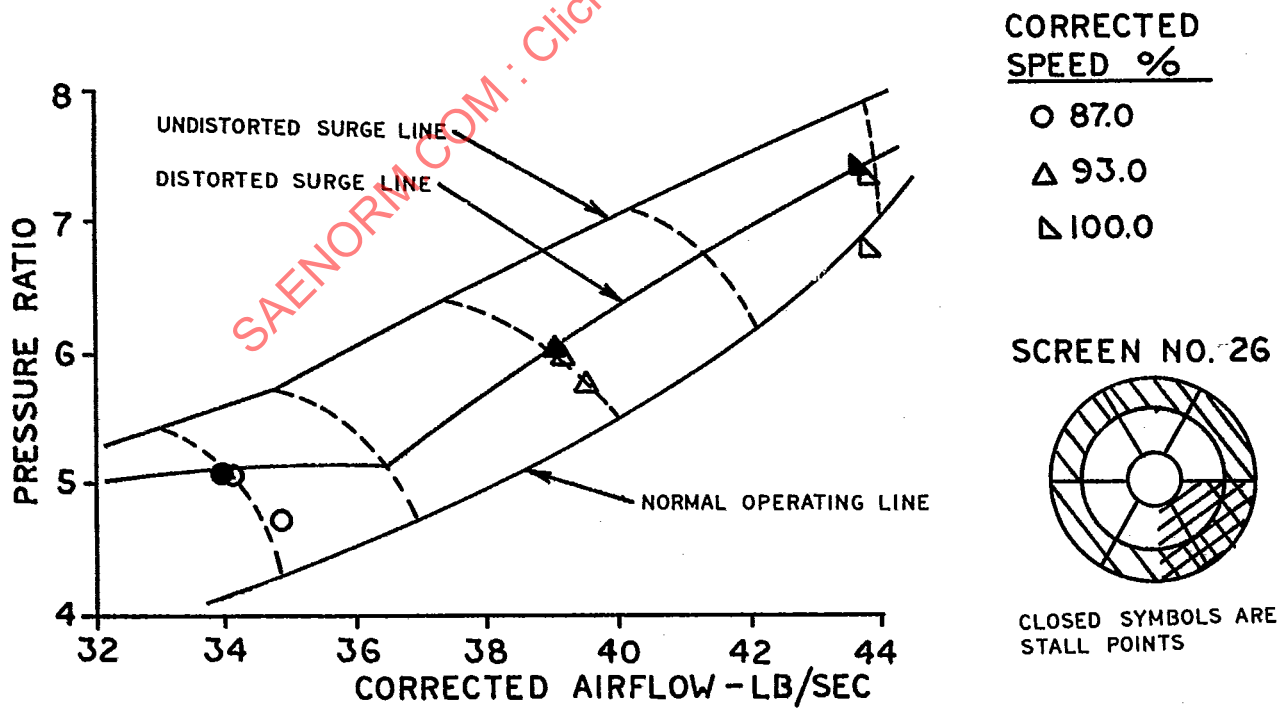

FIGURE 3.19 Example of Combined Tip Radial and Circumferential Total-Pressure Distortion

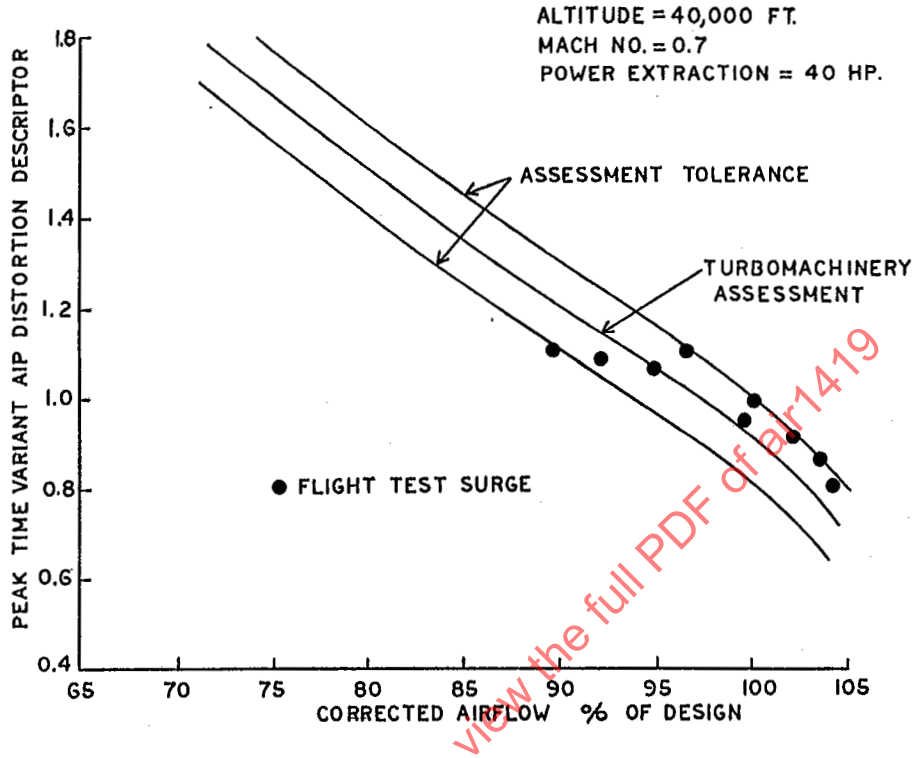

FIGURE 3.20 Comparison of Distortion Stability Assessment with Flight Test Results for Fixed Throttle

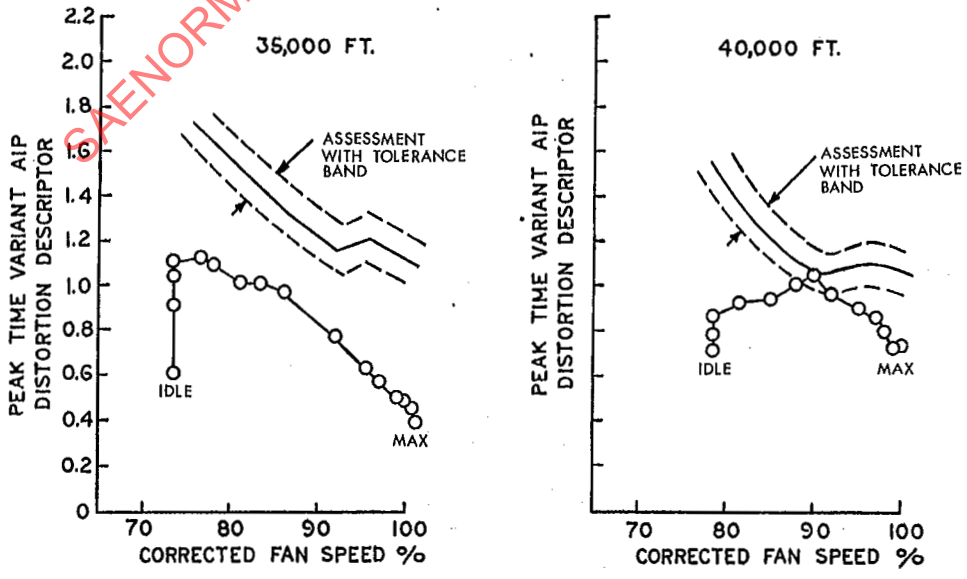

FIGURE 3.21 Comparison of Distortion Stability Assessment With Flight Test Results for Snap-Throttle Transients-No Surges

SECTION 4

PERFORMANCE ASSESSMENT

Propulsion system internal performance is assessed normally by evaluating inlet performance in terms of total-pressure recovery and installed engine performance at the corresponding value of AIP face-average total pressure, PFAV. Engine thrust, fuel consumption, airflow, and accel/decel times at appropriate inlet/engine operating conditions are established by treating the AIP airflow as an equivalent one-dimensional flow. Assessment procedures take into consideration changes in engine and matched engine-component performance resulting from losses of inlet total pressure, and account for control interactions.

In many cases where the AIP airflow pattern is substantially uniform so that spatial total-pressure distortion, PFAV fluctuations, and turbulence levels are low, these assessment procedures provide adequate performance accuracy. The effect of inlet flow distortion is small and well within experimental measurement scatter. Engine and engine component performance tests with simulated distortion are not usually necessary.

When the engine inlet airflow is distorted significantly, assessments of installed engine performance on a face-average total-pressure basis may be insufficient, and a procedure for accounting the effect of spatial total-pressure distortion, and perhaps flow unsteadiness, may be desirable. The assessment procedure adopted for a particular engine installation may, depending on the anticipated severity of the problem, involve synthesizing overall engine performance from estimated or empirical data, using appropriate computer simulations, and from engine tests with simulated inlet distortion. The assessment of the effects of distortion then forms part of an overall assessment of installed engine performance at selected aircraft mission and powerplant operating conditions.

Distortion assessment procedures take different forms according to the type and development status of the propulsion system. They need to be constructed to account for the effects of changes in engine-component performance maps, component matching changes, and changes in control system pressure and temperature input signals (engine control interactions) resulting from modifications to flow profiles at intermediate stations throughout the engine. Results may be expressed directly as installed thrust, airflow, fuel consumption, and other relevant performance parameters for a defined AIP distortion pattern or, explicitly, as changes relative to face-average or equivalent uniform flow performance. It may be desirable for some purposes to widen the scope of the distortion assessment to correlate overall performance changes with relevant AIP distortion elements or combinations of those elements for a range of patterns and levels of distortion.

Practical difficulties arise in synthesizing and measuring performance changes specifically due to distortion. Accuracy problems are experienced since changes are derived from small differences between large estimated or measured flow quantities. These can cause uncertainties in assigning numerical values to threshold levels of distortion below which performance losses can be regarded as negligible, in establishing meaningful numerical performance/distortion sensitivity or trade factors, and in deciding on the extent of testing required to establish valid distortion response data.

4.1 INLET PRESSURE RECOVERY AND DISTORTION

Aspects of inlet performance relevant to engine performance assessments are discussed in terms of inlet type and location, the definition of AIP face-average total pressure, and distortion in the following paragraphs.

4.1.1 INLET TYPE/LOCATION - DISTORTION CHARACTERISTICS

Average total-pressure recovery and distortion characteristics at the AIP differ markedly according to inlet type, location on the airframe, and mode of operation. Inlet designs of conventional powerplants range from relatively simple round-lip, short, straight duct configurations, appropriate to podded subsonic transport aircraft; to complex, sharp-lip, long, curved-duct configurations for highly integrated subsonic and supersonic combat aircraft.

The simple podded inlet designs are very efficient. They provide close to 100 percent recovery and virtually zero total-pressure distortion at most major performance points within the normal aircraft flight envelope. Total-pressure-defect regions are generally of the tip-radial or wall-boundary-layer type and are comparable to those observed in engine component and engine test facilities. Total-pressure distortion problems may need to be addressed at high inlet crossflow conditions to provide for emergencies outside the normal operational envelope.

The more complex inlet designs provide lower inlet recovery as a consequence of larger total-pressure-defect regions at the AIP. Distortion patterns generally contain radial and circumferential elements. Numerical inlet performance characteristics are used together with pattern data to establish the need for and to conduct quantitative assessments of engine performance in distorted flow. Figures 4.1 and 4.2, and 4.3 present data for three inlets. The steady or time-averaged inlet data are expressed in terms of ARP 1420 recommended distortion descriptor elements and area-weighted face-average total pressure.

The figures illustrate several features relevant to the assessment of installed engine performance. The long-duct supersonic inlet in a typical cruise configuration exhibits low radial and circumferential distortion (Figure 4.1). Installed engine performance is predominantly dependent on the face-average total-pressure level. An assessment of performance changes due to distortion is unlikely to be necessary in this case. Figure 4.2 presents low speed data for a different supersonic inlet design. Distortion elements are higher for the

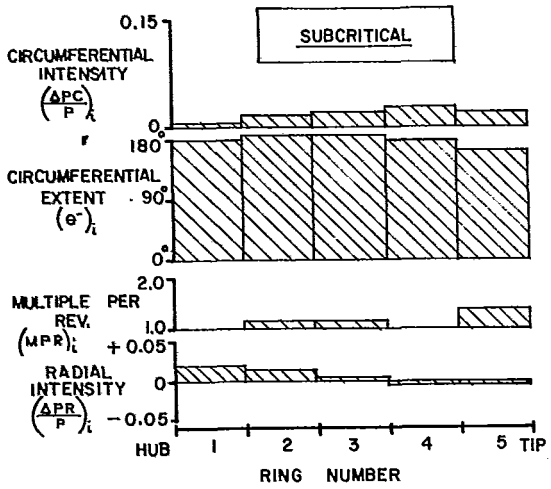

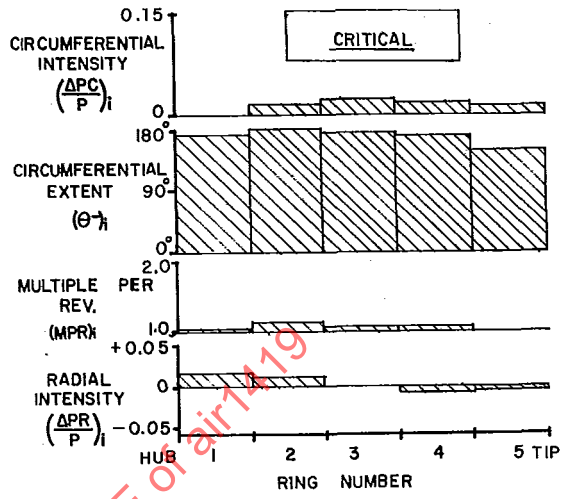

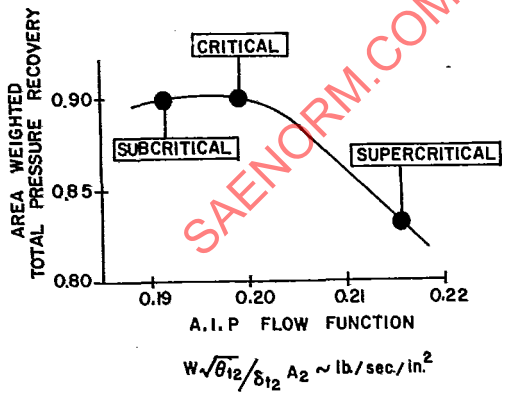

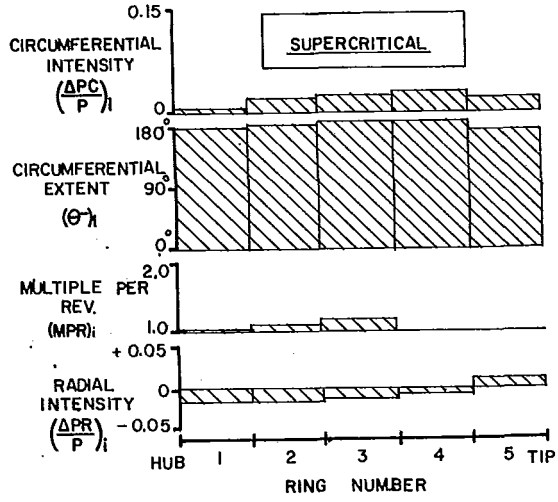

FIGURE 4.1 Supersonic, Two-Dimensional, External-Compression Inlet, Mach 2.0, Cruise Incidence, Fixed Ramps

AIR 1419

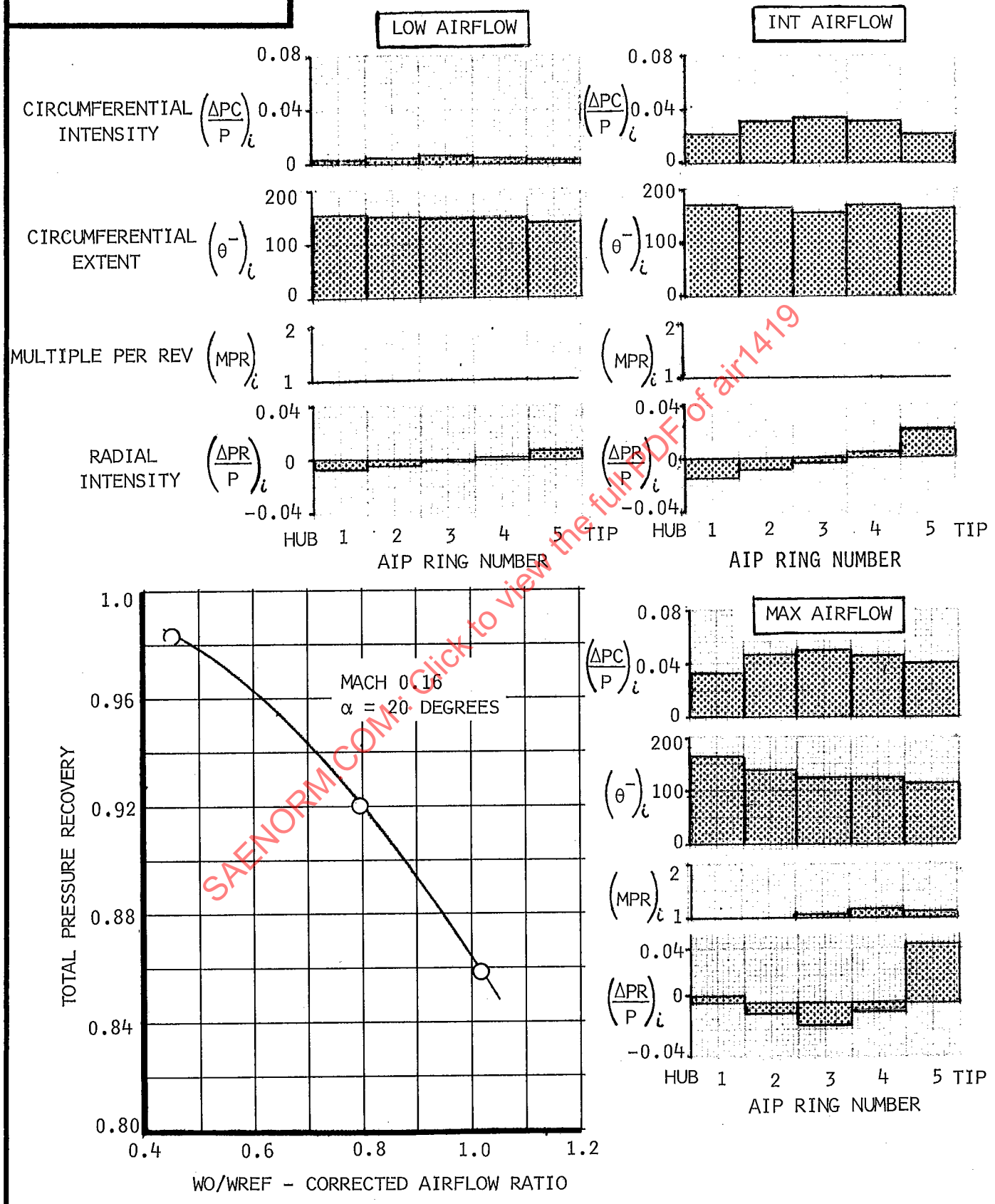

FIGURE 4.2 Supersonic, Two-Dimensional, External-Compression Inlet, Distortion Characteristics During Low-Speed Operation

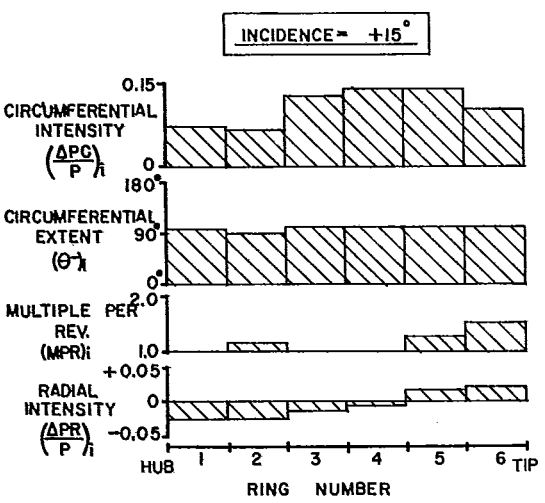

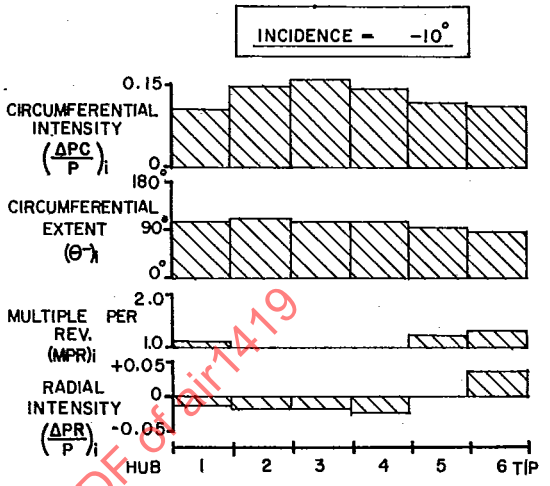

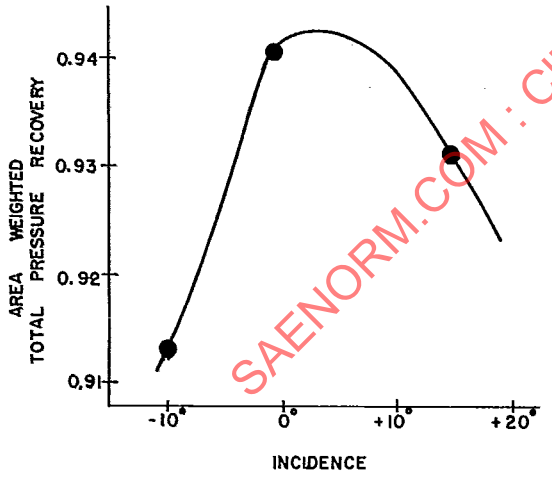

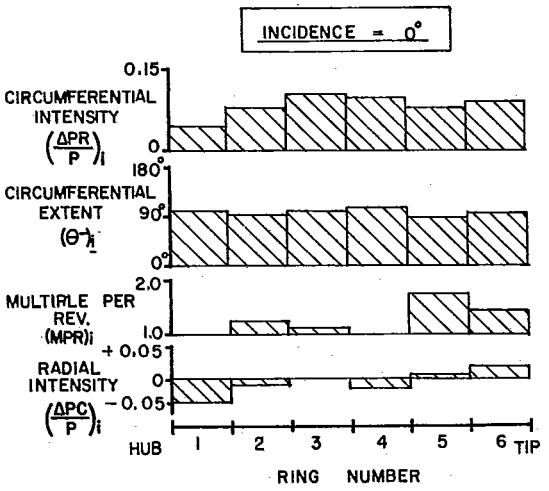

FIGURE 4.3 Short Subsonic Bifurcated Inlet

intermediate and maximum flow conditions. An assessment of performance changes due to distortion is likely to be necessary in this case. The short subsonic bifurcated inlet (Figure 4.3) exhibits peak recovery at cruise incidence, and the circumferential intensity elements are high. Both recovery and distortion deteriorate with incidence. An assessment of performance changes due to distortion may be required in this case also.

4.1.2 FACE-AVERAGE TOTAL PRESSURE

Alternative definitions of face-average total pressure are possible at the AIP in distorted flow conditions. This situation stems from the fundamental fluid mechanical difficulty of constructing a unique one-dimensional or equivalent face-average flow that can simultaneously account for mass flow-, momentum-and energy-flux variations across the AIP. Definitions which are employed include flow-continuity, area-weighted (area-averaged), mass-flow-weighted, momentum-weighted, and entropy-derived face averaging. Differences in the numerical values of the alternate face-average definitions can be on the order of one percent of the face-average total-pressure level, depending on pattern shape.

Area-averaged total pressure is used widely throughout the Aerospace Industry, has considerable technical merit, is simple and easy to apply, and eases inlet and engine data acquisition and processing requirements. Area-averaging greatly facilitates the definition and quantification of distortion at the AIP, and is the recommended basis of ARP 1420 guidelines. Alternative definitions, appropriate to a particular propulsion system development, such as mass-flow weighting for compressor efficiency accounting, can be related to the area-averaged value for defined AIP patterns.

When instrumentation rings are located at centers of equal area:

$$PFAV = \frac{1}{N} \sum_{i=1}^{N} (PAV)_i = \frac{1}{N} \sum_{i=1}^{N} \left[\frac{1}{360} \int_0^{360} P(\theta)_i \, d\theta \right]$$

where, N is the number of instrumentation rings and $(PAV)_i$ are the ring-average total pressures.

The numerical distortion descriptor elements are defined relative to the area-averaged, AIP, mean total-pressure, PFAV. The above definition implies that:

$$\sum_{i=1}^{N} \left(\frac{\Delta PR}{P} \right)_i = 0$$

where $\left(\frac{\Delta PR}{P} \right)_i$ are the radial intensity elements

ARP 1420 guidelines for assessing installed engine performance in distorted flow conditions thus involve accounting for baseline uniform-flow

performance using the area-averaged AIP total-pressure, and performance changes due to distortion relative to this area-averaged datum.

In this context it may be noted that, by virtue of the area weighting involved, PFAV is related to the conservation of momentum flux at the AIP.

4.1.3 INLET DATA ACQUISITION

As time-averaged performance is of prime interest, it is usual to base assessments on steady-state AIP pressure data obtained from a low-response instrumentation array used for model and full-scale inlet tests (Section 6). Early assessments of inlet performance use small-scale inlet data, accounting for Reynolds number effects at defined performance conditions within the operational envelope. For a given scale of inlet model there will be a minimum Reynolds number below which performance data would be unacceptable.

4.2 ENGINE PERFORMANCE DATA

As a preliminary to discussing guidelines to procedures for assessing the effects of distortion on performance, illustrative examples of the effects of distortion on engine and engine compression components are presented to highlight the main technical issues and candidate data needs. The data presented apply to time-averaged or steady-state distortion and performance.

4.2.1 COMPRESSION COMPONENTS RESPONSE TO DISTORTION - EXAMPLES

The upstream, low-pressure compressor or fan is unshielded from, and is most likely to be affected by, the inlet flow distortion. Significant changes in the fan performance map can occur.

Compressor rig tests with screen-simulated total-pressure distortion should include classical (square-wave) patterns and simulated aircraft inlet patterns (Section 5.2). Tests using classical patterns provide information on the types of distortion to which the compressor is most sensitive. Tests are conducted for both stability and performance evaluations and usually include distortions more severe than those corresponding to aircraft mission performance points. The test data provide a basis for deriving compressor numerical performance/distortion sensitivity factors.

Figure 4.4 presents the results obtained from rig tests of a five-stage axial compressor with three classical time-averaged circumferential distortion patterns. The multiple-per-rev elements were unity. At these levels of circumferential distortion, which are not untypical of those encountered in the mixed radial and circumferential patterns of inlets at cruise conditions, flow and efficiency losses were less than one percent and were of the order of the measurement accuracy. Area-averaged compressor performance was not greatly affected.

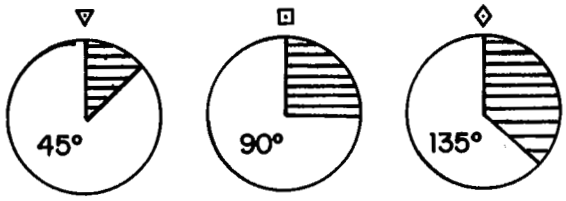

SCREEN	EXTENT ELEMENT (Θ)°	CIRCUMFERENTIAL INTENSITY ELEMENT ΔPC/P (100% FLOW)
▽	45° SCREEN	0·037
⊡	90° SCREEN	0·032
◇	135° SCREEN	0·026

——— CLEAN FLOW

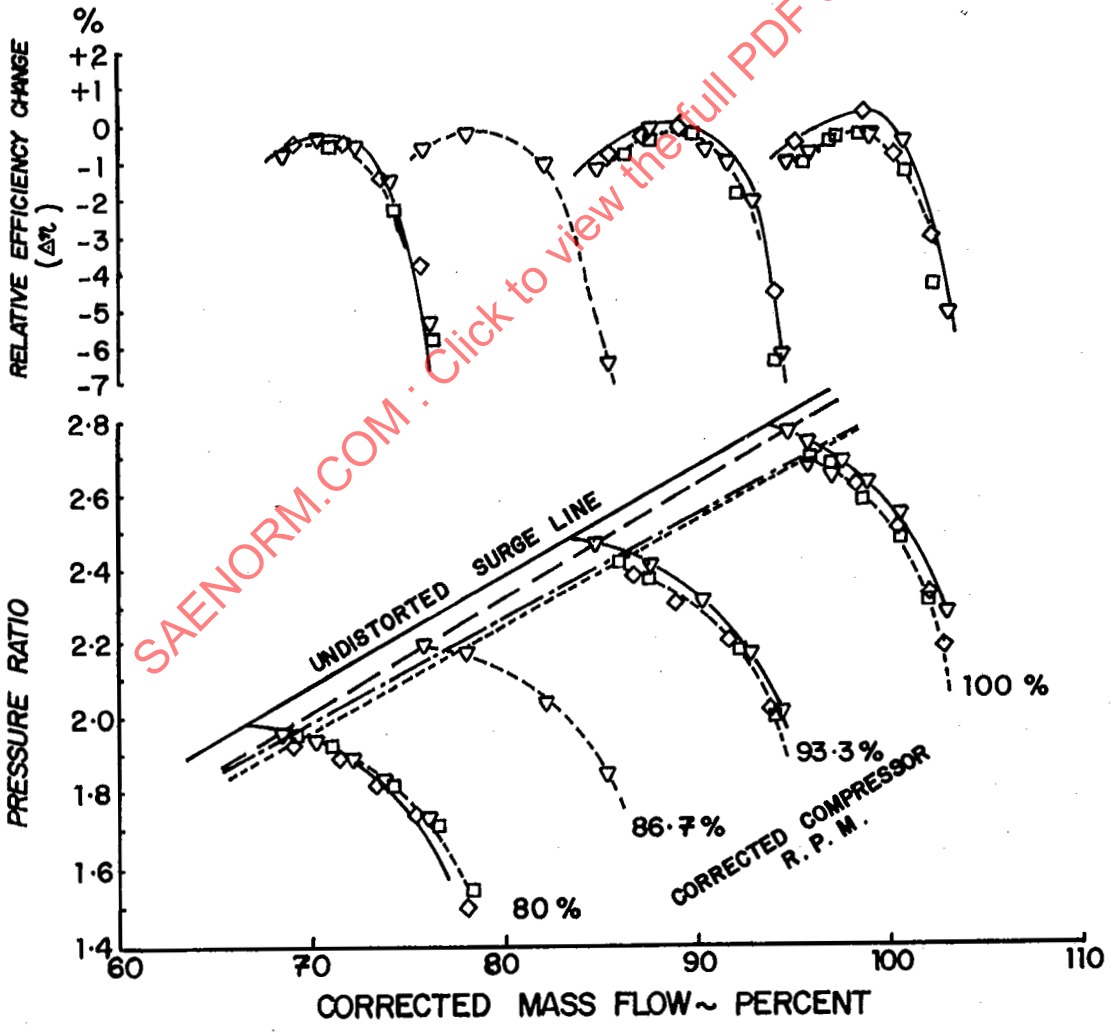

FIGURE 4.4 Effect of Classical Circumferential Inlet Distortion Patterns

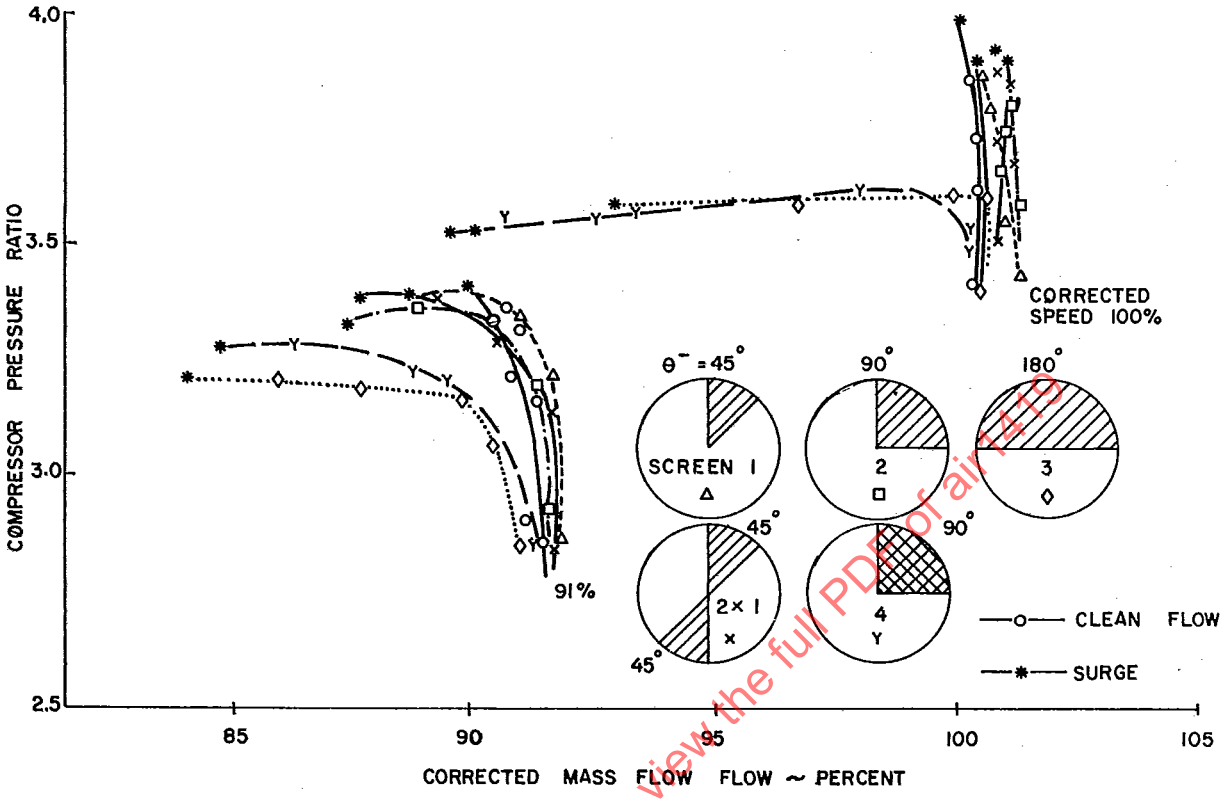

FIGURE 4.5 Rig Compressor Tests - Classical Distortion

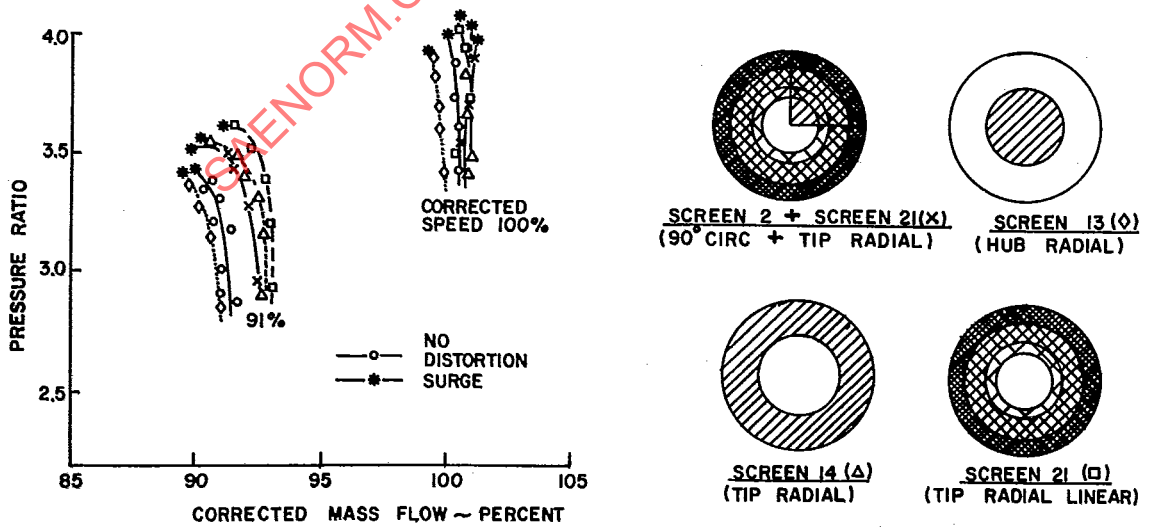

FIGURE 4.6 Rig Compressor Tests - Radial and Mixed Distortion

Figure 4.5 shows the results of a seven-stage axial compressor test with classical circumferential screen patterns (Reference 11). Screen details are presented in Table 4.1.

TABLE 4.1

Classical Circumferential Screens

Screen		Extent ($\theta^{-\circ}_{\#}$)	Intensity ($\Delta PC/P$) (100% Flow)	Multiple-Per-Rev. MPR
Clean Flow	0	-	-	-
1	Δ	45	0.06	1
2	□	90	0.044	1
3	◇	180	0.064	1
4	Y	90	0.07	1
5	X	2x45	0.046	2

In this case the predominant distortion effect for the more severe patterns (screens 3 and 4) was loss of corrected flow, particularly close to surge. Efficiency changes (not shown) also occurred. The data give an indication of the measurement scatter problem for less severe distortions (screens 1, 3, and 2 of No. 1).

Figure 4.6 shows the results of tests of the same seven-stage compressor with hub-radial and tip-radial patterns. Classical, and graded, tip-radial patterns were tested. A mixed classical pattern consisting of the tip-radial and 90 degree circumferential screens was also tested. Screen data are presented in Table 4.2.

TABLE 4.2

Radial And Mixed Screens

Screen		Distortion Type	Radial Intensity $\frac{\Delta PR}{P}$	Radial Extent (Percent)
Clean	0	-	-	-
13	◇	HUB RADIAL (CLASSICAL)	±0.04	50 (Area)
14	△	TIP RADIAL (CLASSICAL)	±0.055	50 (Area)
21	□	TIP RADIAL (LINEAR)	RING 1 2 3 4 5 -0.15 -0.03 +0.02 +0.06 +0.10	100
2+21	X	MIXED	SCREEN 2+21	+100

The dominant effects observed were loss of compressor corrected flow for the hub-radial distortion and a gain in corrected flow for tip-radial distortion when the compressor is unchoked. AIP distortion, tip-radial distortion in this case, does not necessarily produce losses in compressor corrected flow. The increase in corrected flow due to the graded tip-radial distortion, screen 21, was mitigated to some extent by adding the circumferential distortion element, screen 2, which had very little effect on flow when tested alone (Figure 4.5).

The data illustrate several points relevant to the assessment of distortion effects on performance:

- o Testing with classical patterns provides important quantitative insights into compressor performance response.
- o Some distortion elements can have a favorable effect.
- o The interpretation of test data for moderate distortion levels can be occluded by data random error and repeatability scatter.

The combined tip-radial and circumferential distortion pattern (screen 2+21) results imply that upstream compressors should be tested with inlet patterns to determine the performance changes.

Figure 4.7 shows the results of testing on a three-stage turbofan with the inlet pattern illustrated in Figure 4.11. Overall fan performance was affected significantly, corrected flow and efficiency changes being approximately two percent. In this case, additional data relevant to changes in split-flow OD and ID performance characteristics and by-pass ratio may be required for analysis.

The assessment procedures can use compressor test results in the form of modified performance maps for specified distortion patterns, as discrete changes due to those patterns, or as changes correlated with numerical distortion descriptors. An example correlation for a three-stage research compressor tested with a number of classical patterns is shown in Figure 4.8 (Reference 11). Fan corrected flow, pressure ratio, and efficiency changes for nominal matching of the operating line correlated well with radial distortion. Tip-radial distortions were favorable, and hub-radial distortions were unfavorable. Circumferential distortion elements were not dominant in this case. The particular distortion descriptor used for the correlation is defined by a combination of radial distortion elements:

$$\frac{(PAV)_{ID} - (PFAV)}{PFAV} = \frac{1}{N} \sum_{i=1}^{N} \left(\frac{\Delta PR}{P}\right)_i$$

where

$\left(\frac{\Delta PR}{P}\right)_i$ are the radial intensity elements.

and N denotes the number of instrumentation rings describing the ID region of the patterns. (For this example, N = 2, and $(PAV)_{ID}$ equals the average pressure in the ID region.)

If the major effects of distortion are not confined to the upstream compressor, then compression component distortion transfer data - principally total pressure and temperature data - may be required to assess the effect of AIP distortion on downstream components. Pattern and numerical distortion descriptors at low-pressure-compressor exit would be required for this purpose.

4.2.2 ENGINE RESPONSE TO DISTORTION - EXAMPLES

Engine tests with total-pressure distortion play an important part in the assessment of performance changes due to distortion. Figure 4.9 shows the results of tests conducted in a direct-connect altitude test facility on a turbofan engine with inlet distortion simulated by a screen at Mach 0.9, 40,000 ft., standard day conditions. Data are presented in terms of changes in corrected fuel consumption and corrected gross thrust relative to tests with undistorted inlet flow. No significant trends in the corrected gross thrust and fuel flow changes due to distortion were observed in the data range 70 to 100 percent corrected fan speed for this limited sample test case. Airflow changes were on the order of 0.5 percent.

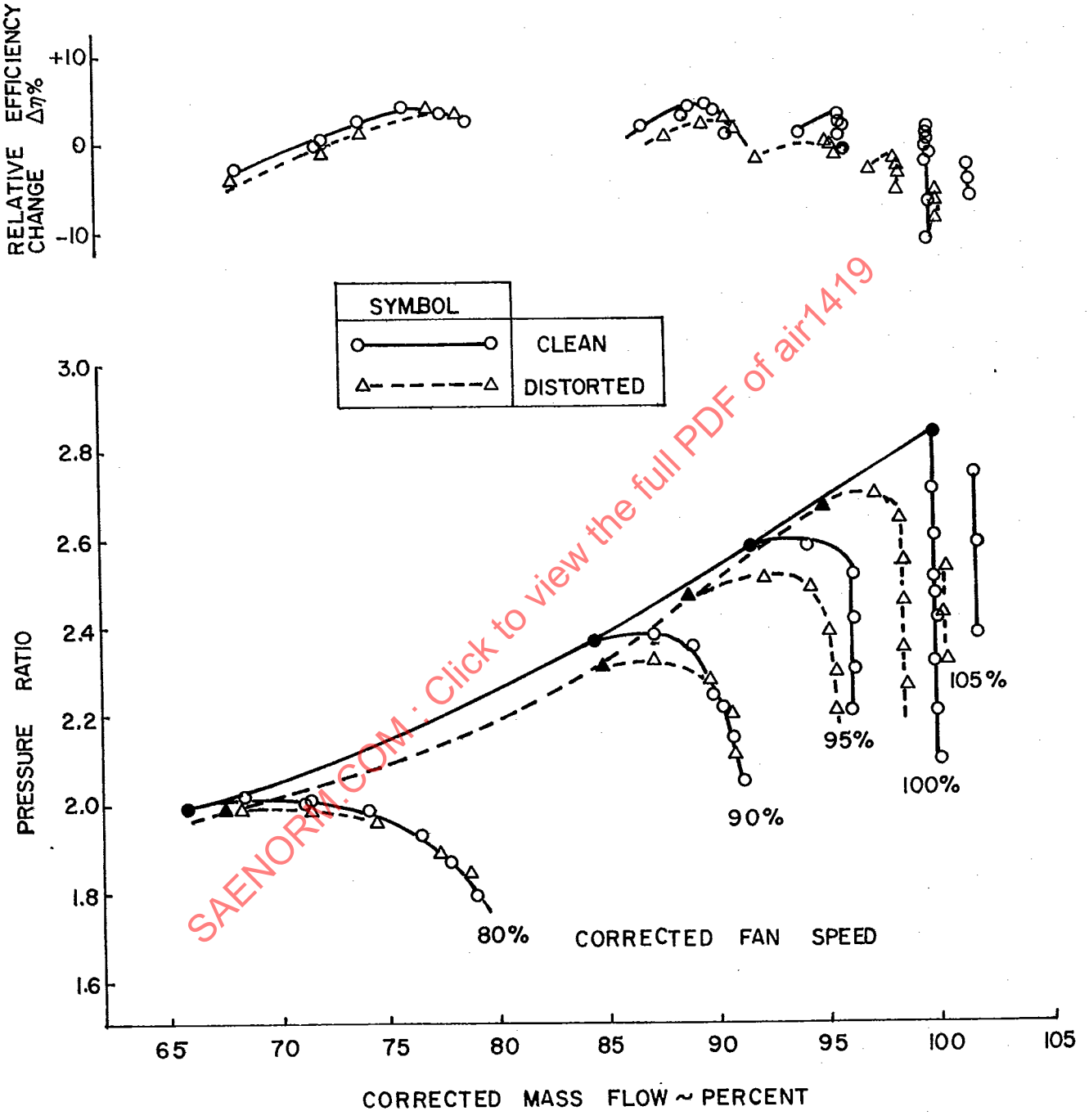

FIGURE 4.7 Rig Compressor Tests - Screen Simulated Distortion

AIR 1419

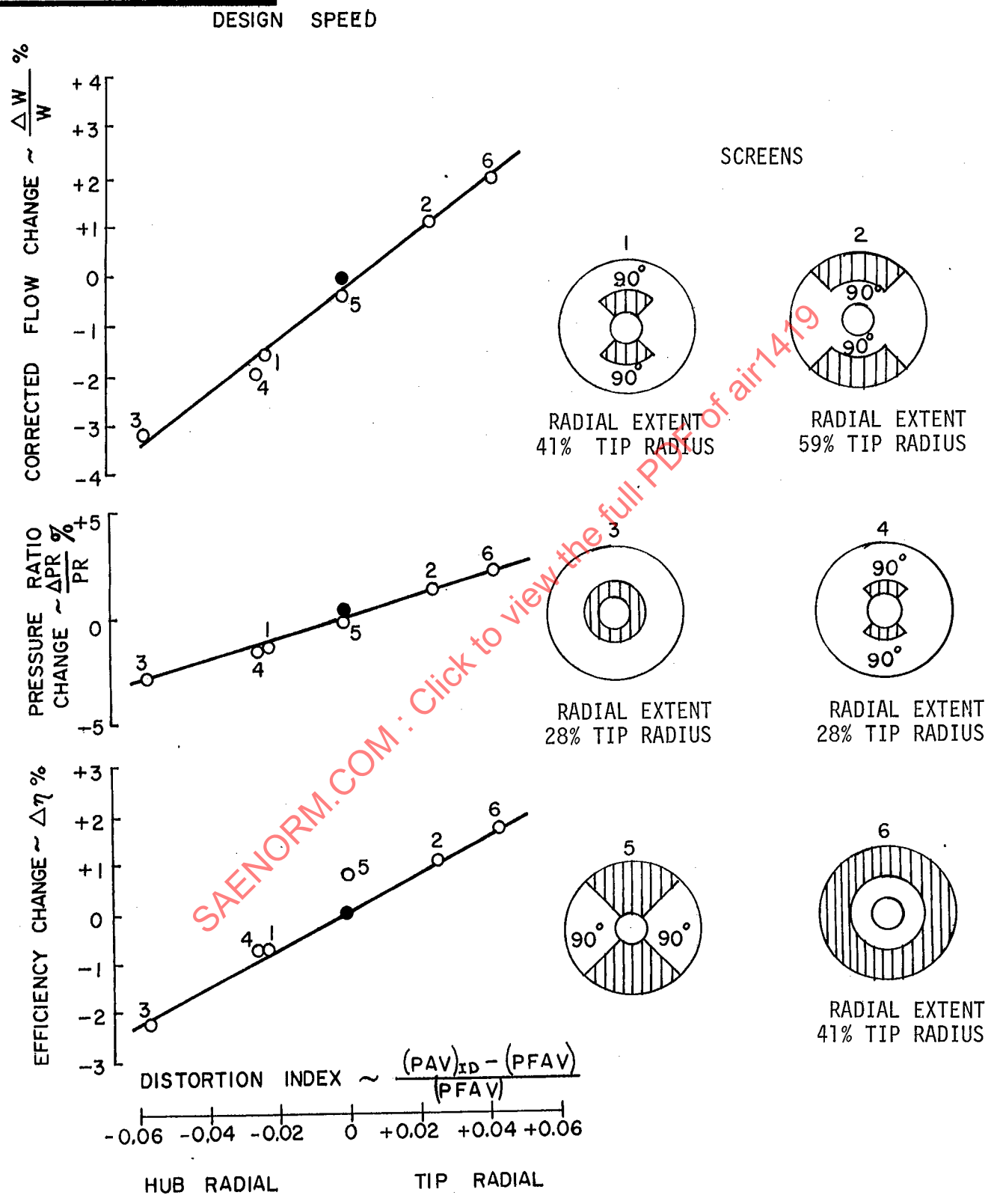

FIGURE 4.8 Distortion Effects on Three-Stage Fan Performance

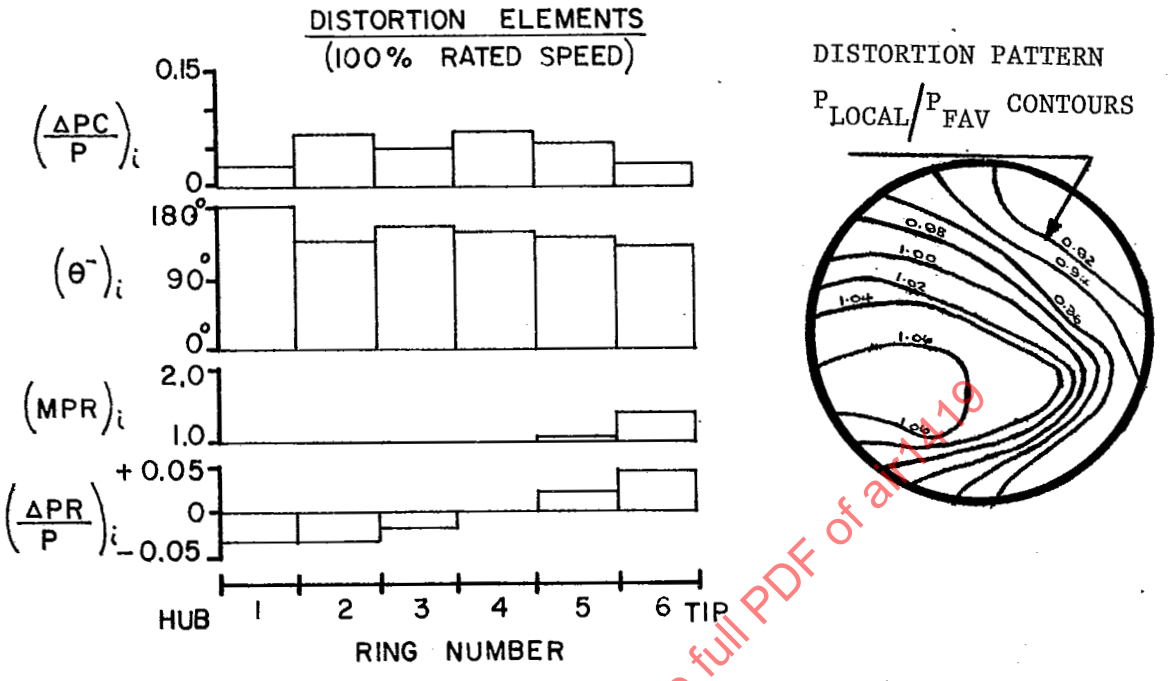

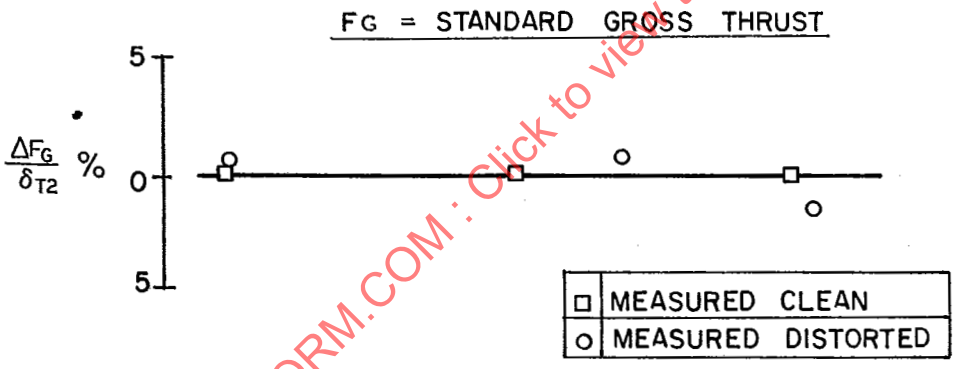

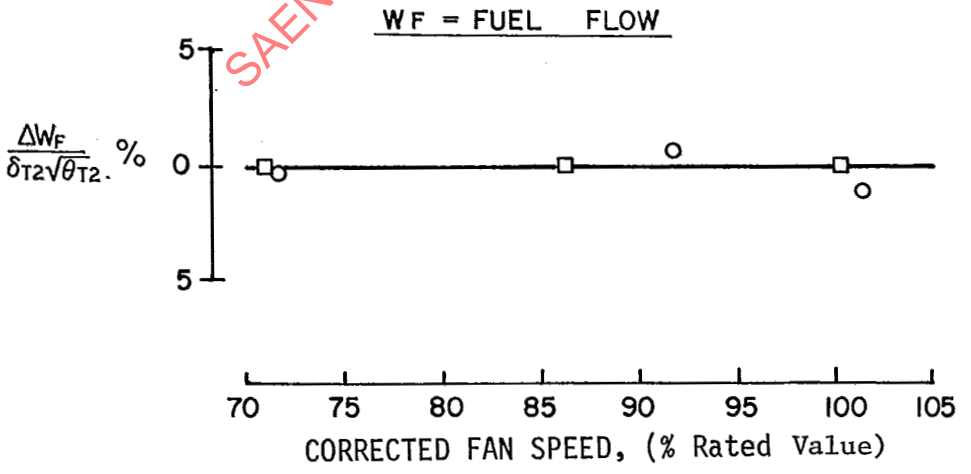

FIGURE 4.9 Turbofan Engine Performance with Inlet Distortion

Engine tests in both undistorted and distorted inlet flow are necessary to establish distortion effects. Individual data points can be misleading. A factor of some importance in the interpretation of the data is that of accounting for screen pressure loss which affects the engine test Mach number/altitude setting for a given nominal flight condition, the power extraction, and the intercomponent match. No corrections for engine final nozzle rematch were necessary in this choked nozzle operating case.

Figure 4.10 shows results obtained from turbofan engine tests conducted on the sea-level test stand with a classical circumferential inlet distortion pattern. Significant changes in corrected gross thrust and specific fuel consumption were caused by the inlet screen. Specific fuel consumption increased by six percent and thrust decreased by two percent relative to undistorted-flow engine performance. These changes were not due solely to the effects of distortion, however, but to the combined effect of distortion and loss of inlet recovery which caused engine component rematching with the unchoked mixed-flow nozzle. Corrections to the measured results for the effect of the screen losses reduced the magnitudes of the performance changes so that they fell within the undistorted-flow engine-performance data scatter. Corrections for average total-pressure loss are necessary in order to isolate the effect of distortion if the screen loss does not correspond to that of the inlet loss. Tests with uniform screens designed to simulate the distortion screen pressure losses may be required to establish the appropriate corrections and validate cycle deck calculations.

4.2.3 CONTROL SYSTEM RESPONSE TO DISTORTION - EXAMPLES

Inlet flow distortion can affect rated performance if the engine control employs discrete or local-flow parameter sensing, e.g., a local exhaust pipe total-temperature signal. In this case very significant changes in performance due to distortion can occur due to flow profile effects within the engine, created as a consequence of AIP distortion transfer. Figure 4.13 shows circumferential total-temperature profiles at HP compressor and LP turbine exits for a turbofan engine operating at constant HP compressor speed behind the screen-simulated distortion shown in Figure 4.12. Significant performance changes would result if the engine were controlled to a fixed temperature limit using a single local sensor. The performance change would depend on the sensor location relative to the distortion pattern. Figure 4.14 shows that this, in fact, occurred. The changes in normalized specific fuel consumption, gross thrust, airflow, LP and HP compressor speeds were very significant. The data, which were derived from sea-level-static tests, are uncorrected for screen loss, which was constant for all screen positions. The data points were obtained by rotating the screen. Figure 4.15 shows results obtained from turbofan engine tests where a fan pressure ratio control was being investigated. Significant changes in fan operating line position were observed for various screen positions.

Compression system designs which incorporate variable geometry, e.g., variable stagger stator blading, may employ local flow sensors to schedule the

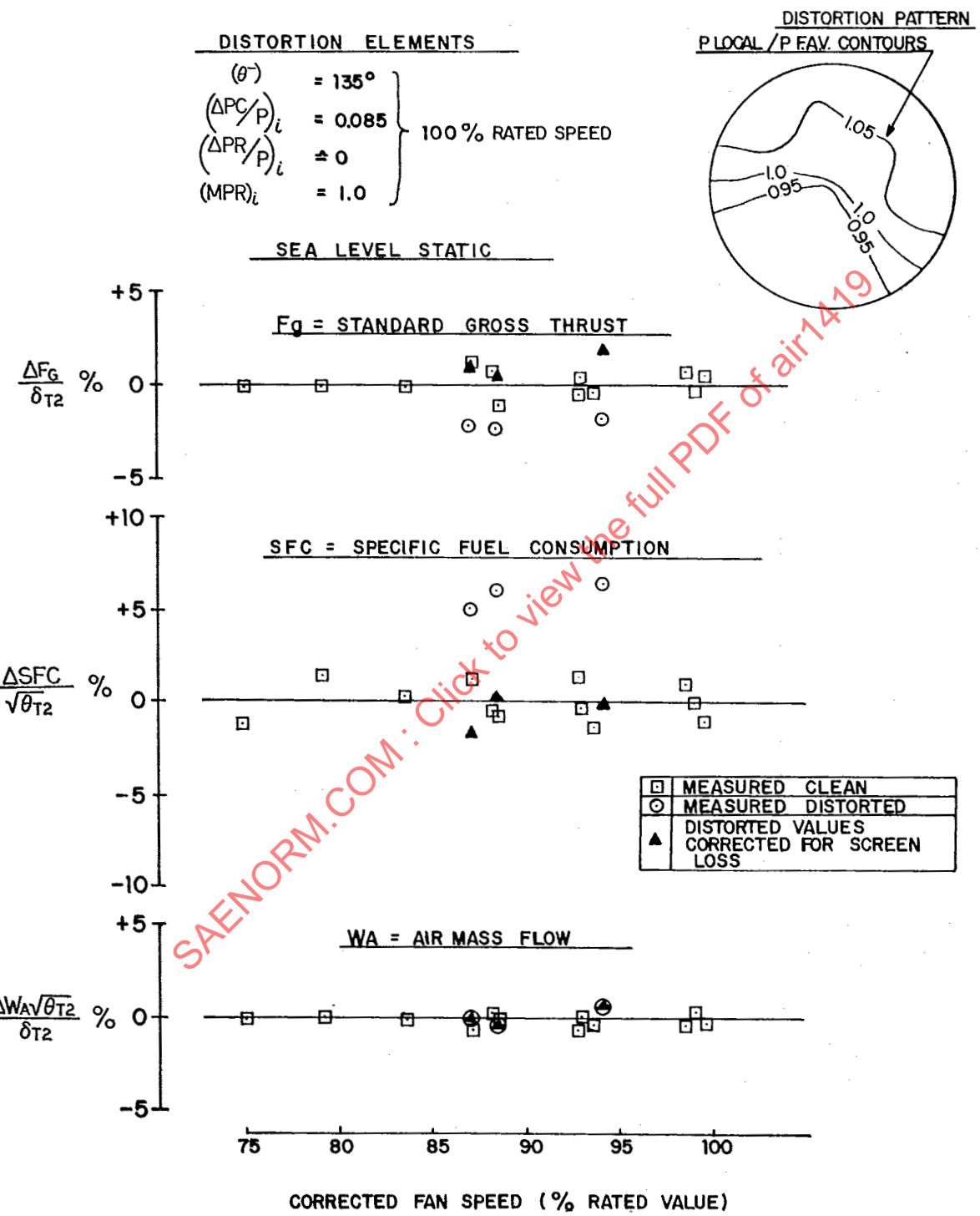

FIGURE 4.10 Turbofan Engine with Classical Circumferential Distortion Pattern

AIR 1419

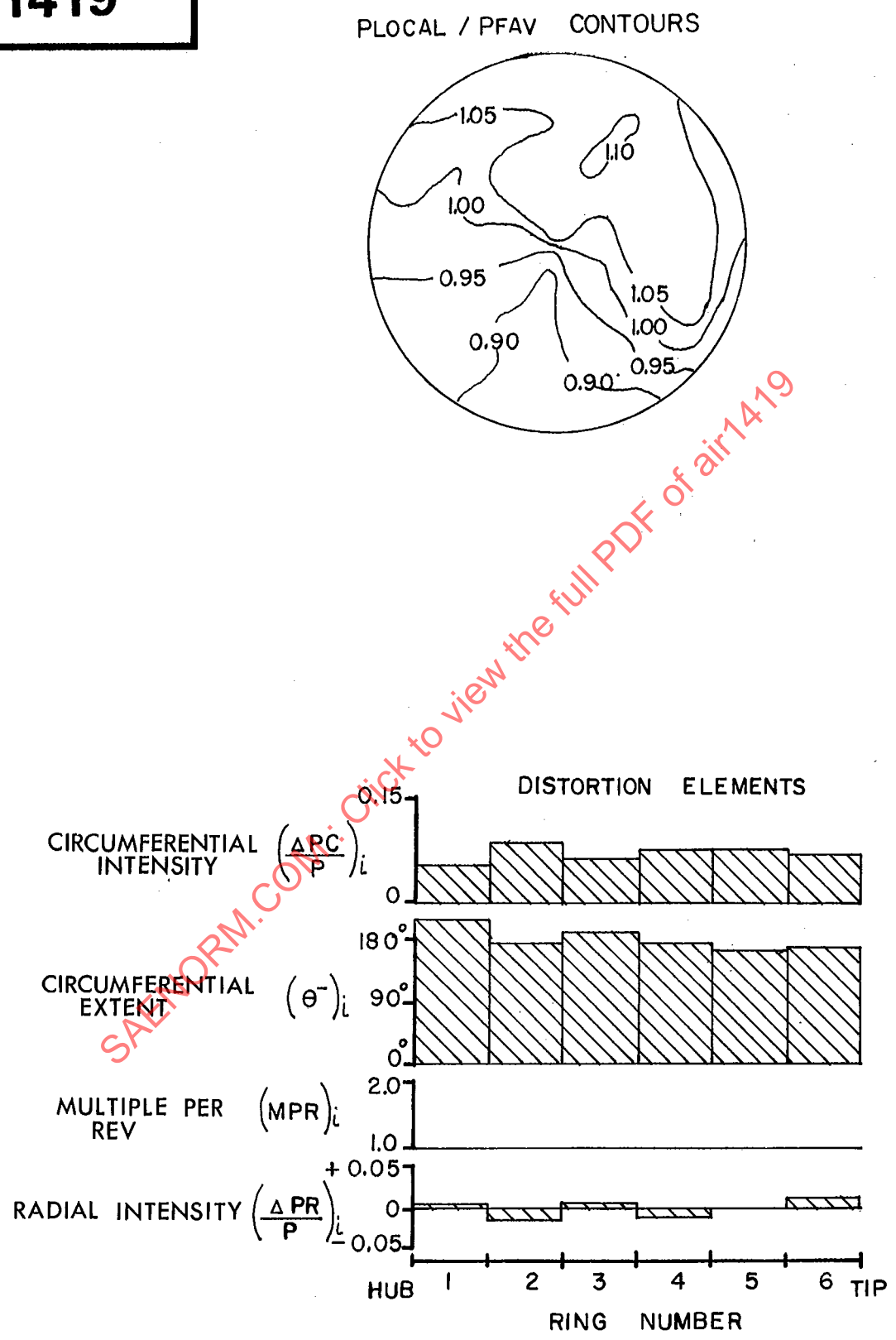

FIGURE 4.11 Simulated Inlet-Distortion Screen

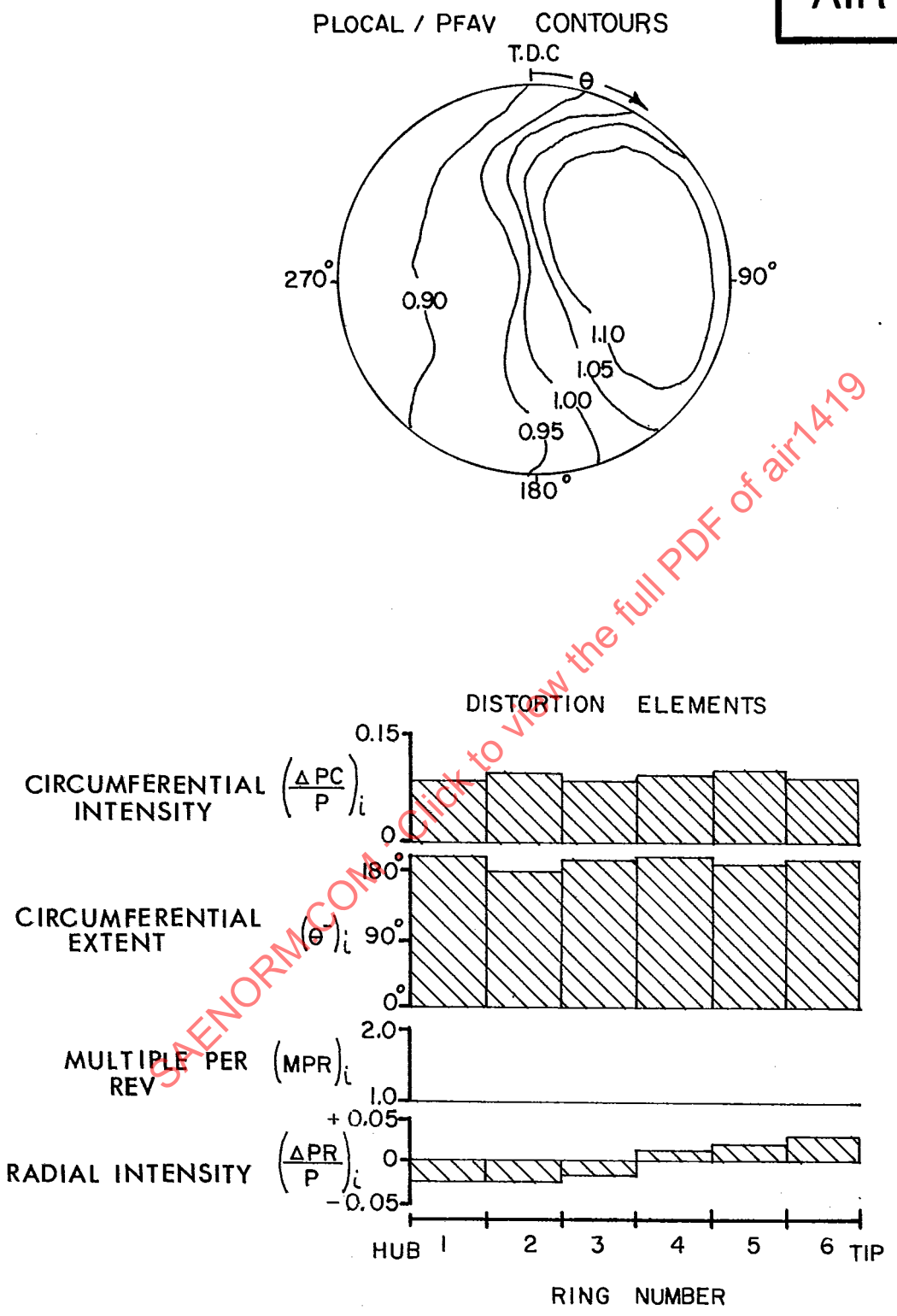

FIGURE 4.12 Simulated Inlet-Distortion Screen

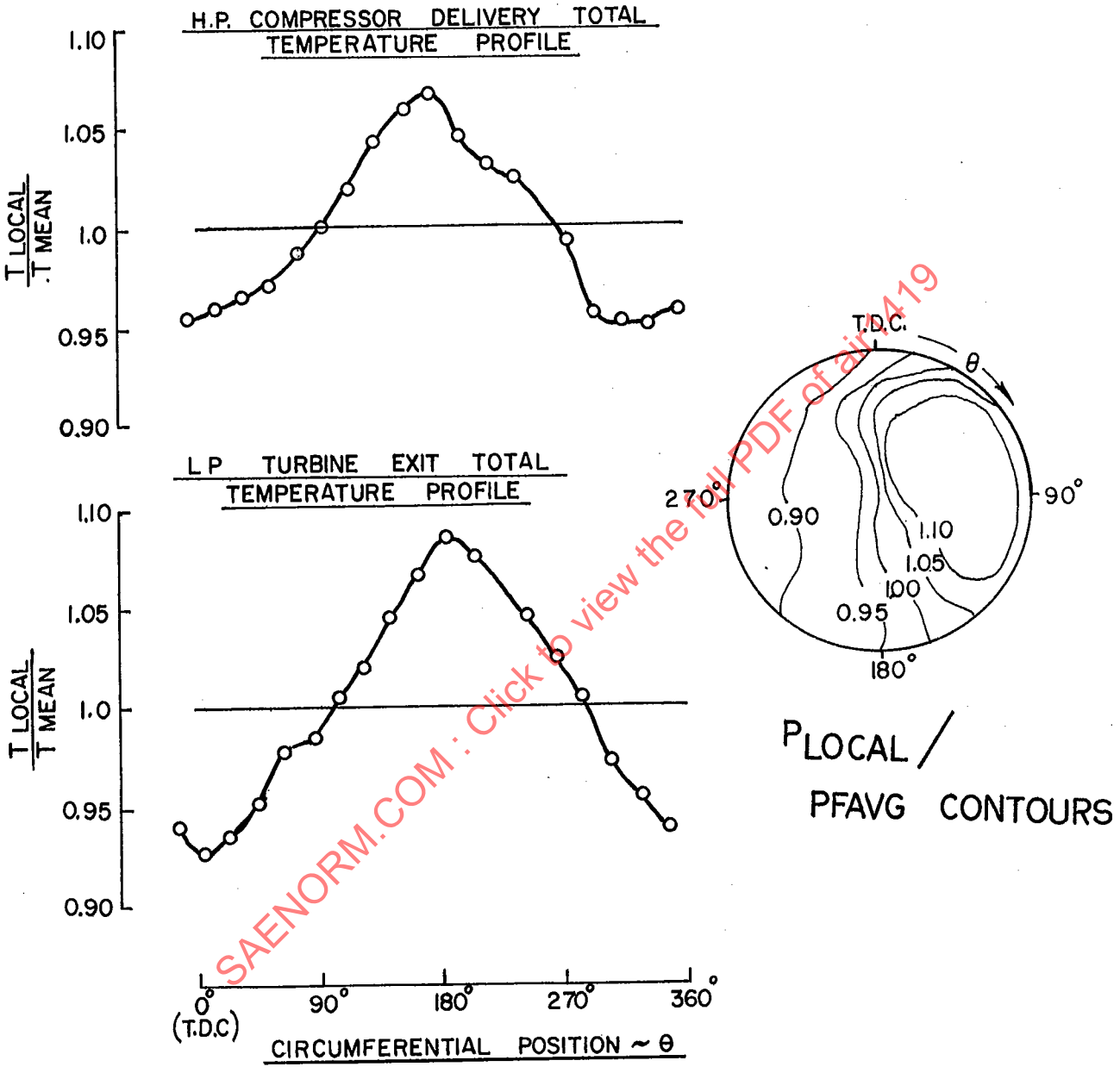

FIGURE 4.13 Turbofan Engine Performance with Distortion

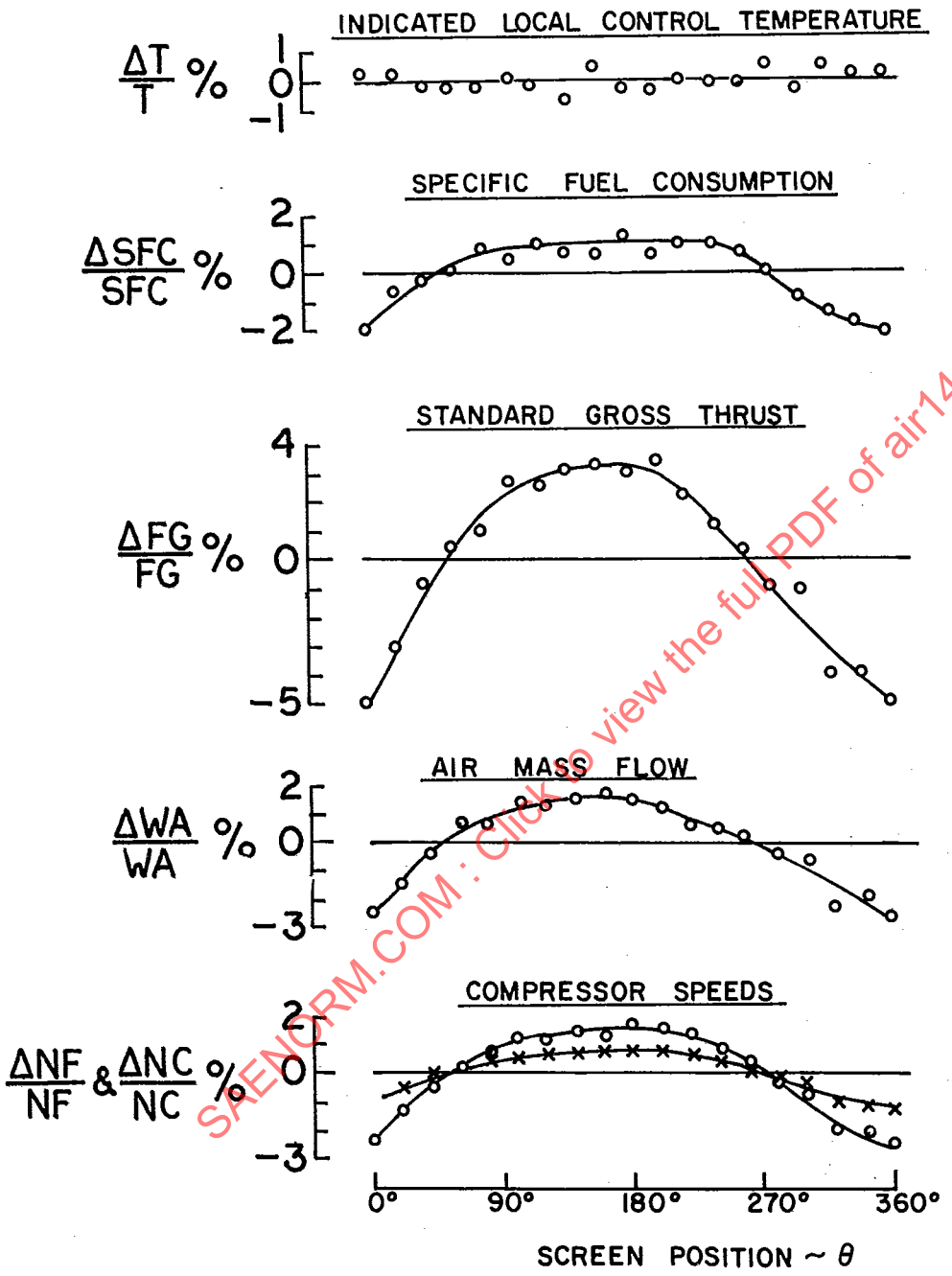

FIGURE 4.14 Turbofan Engine Performance - Screen Position Effect

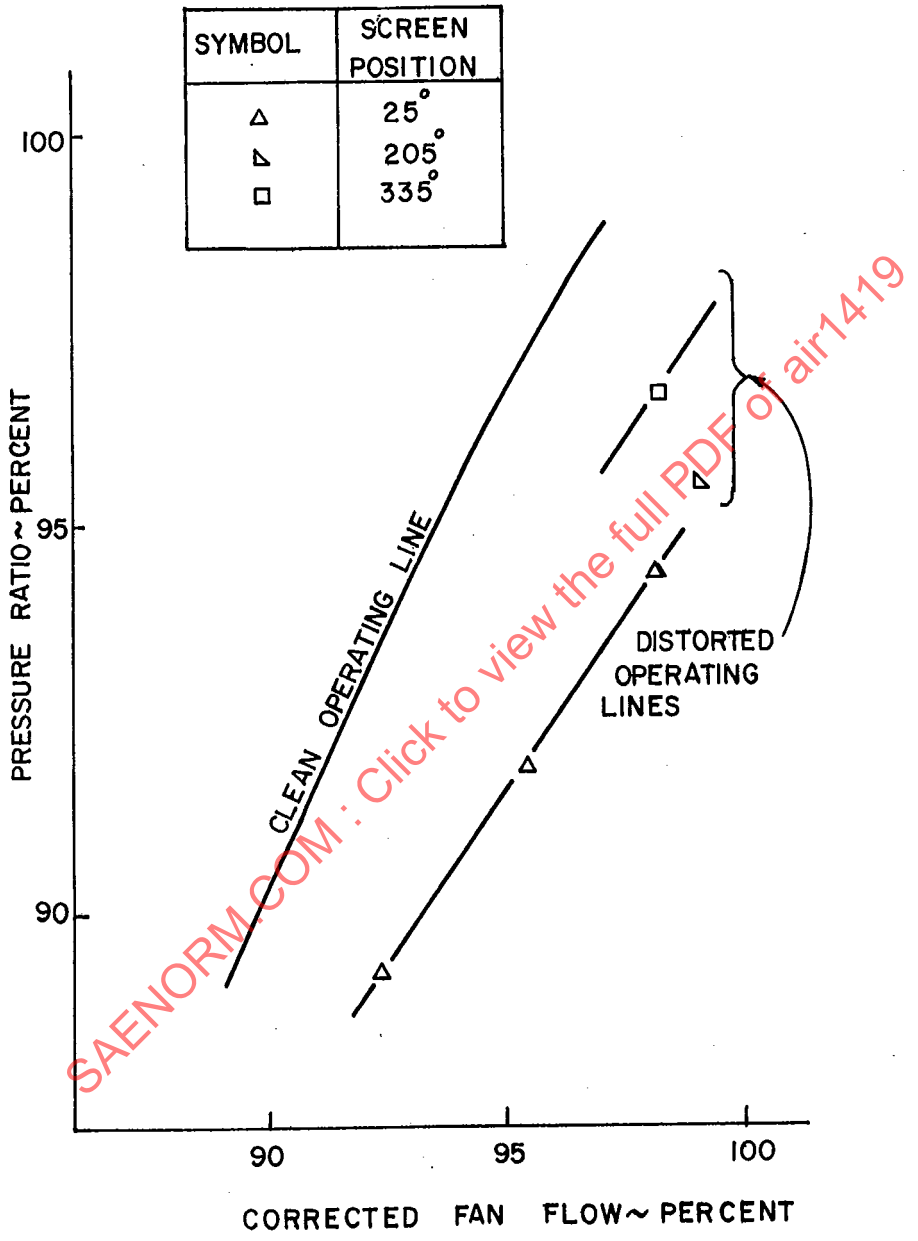

FIGURE 4.15 Effect of Engine Sensor Location

geometry. In such cases, the effect of flow distortion on the schedule and the resultant change in component matching and overall engine performance should be evaluated.

The data illustrate that performance assessment procedures may need to account for circumferential distortion pattern position and that more than one screen position may need to be tested to cover multi-engine (mirror imaged) installations. Engine control mode and sensor selection studies should address the anticipated distortion characteristics. In view of the complexity of the question, engine tests would be necessary to account such effects with confidence.

4.3 ASSESSMENT PROCEDURES

Procedures for assessing the effect of AIP total-pressure distortion on engine performance are part of the procedure for evaluating installed engine performance. A prime concern is to identify the technical need to account distortion effects explicitly. This need should be judged against performance and performance accuracy goals and the anticipated severity of the distortion problem. Each propulsion system should be considered on its own merits.

Assessment procedures for determining installed engine performance fall into two broad categories; Performance Synthesis and Performance Testing. Synthesis and testing activities interact. They are not sequential, and they evolve as updated information becomes available. A logic flow chart for the evaluation of installed engine performance is shown in Figure 4.16.

Performance synthesis activities include:

1) Assessments of baseline undistorted flow or uninstalled performance using estimated or empirical engine component data.

2) Assessments of installed performance based on AIP face-average pressure and engine component data.

3) Assessments of AIP distortion effects using component distortion response data.

Performance testing activities are organized to yield performance data for:

1) The uninstalled engine in undistorted flow. Programs may include sea level test stand and altitude test facility (ATF) testing.

2) The "installed" engine with simulated AIP distortion. Programs may include distortion tests on the sea level test stand and in the ATF with simulation of aircraft services, including bleed and power extraction.

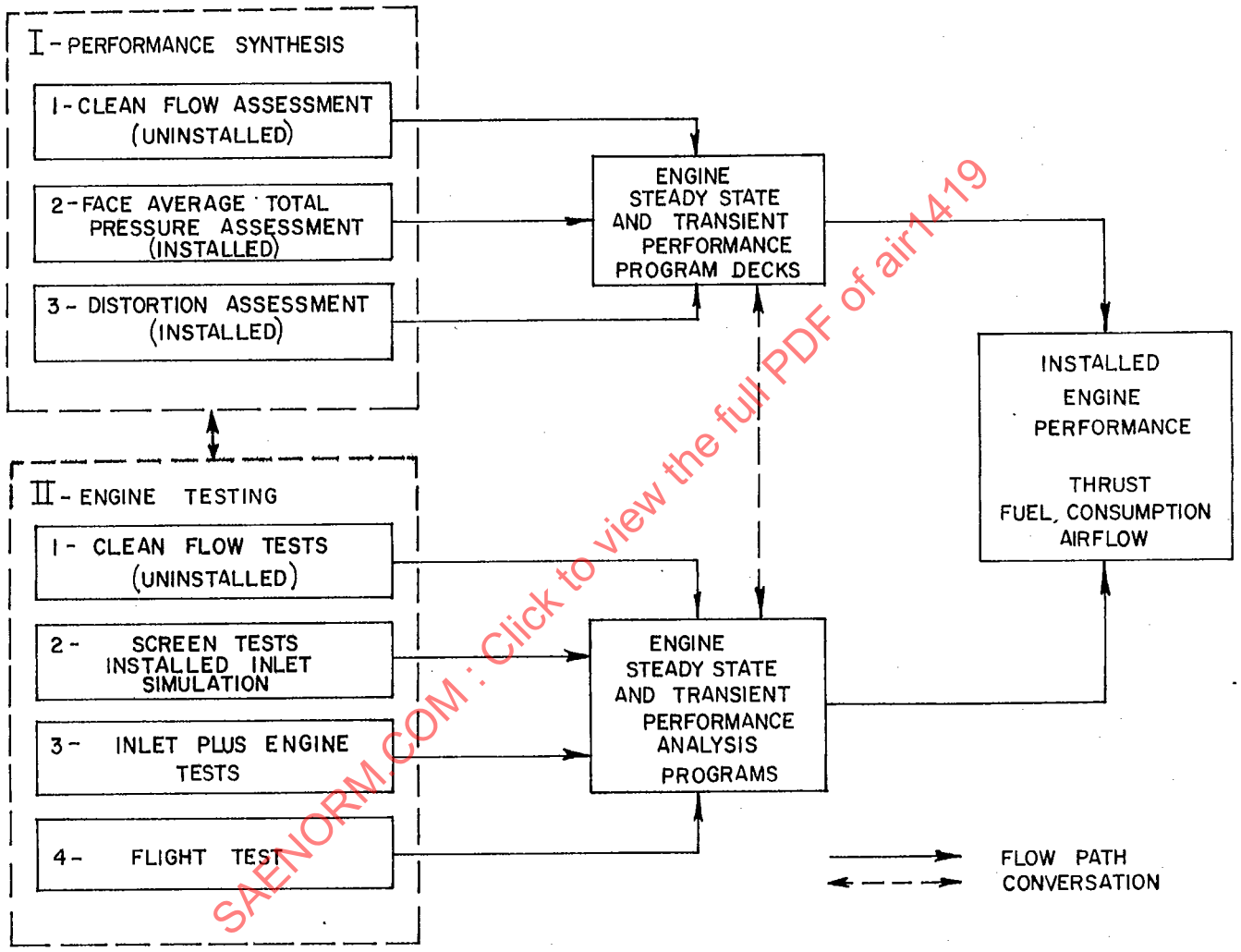

FIGURE 4.16 Installed Engine Performance Assessment Guideline

3) The inlet plus engine. Programs may include sea level test stand and free-jet ATF testing.

4) The installed flight test engine.

Performance assessments are conducted at operational conditions defined in Table 4.3.

TABLE 4.3

Operational Conditions

Aircraft	Inlet	Engine
Temperature	Configuration	Power Level
Altitude	Bleed	Service Bleeds
Flight Speed	Reynolds No./Scale	Power Extraction
Attitude (α, β)	Mass Flow	Afterburner
Thrust (Drag) Level		Thrust Reverse

4.3.1 PERFORMANCE SYNTHESIS

Synthesis methods are organized into steady-state and transient computer programs, or performance and handling decks, which incorporate engine component performance maps, matching and control logic in mathematical models of the engine. Treatments of uninstalled and installed engine performance based on AIP face-average total pressure are well established. For example, steady state and transient performance presentations for digital computational programs are presented in References 9 and 10. Other relevant data are presented in References 12, 13 and 14.

In assessing installed performance on a face-average inlet pressure basis, engine rematching due to changes in inlet pressure level and in non-dimensional engine performance parameters are taken into account. The non-dimensional component performance maps correspond to undistorted AIP flow conditions. This implies that the effects of distortion on the non-dimensional performance maps (in particular, compressor maps) are assumed to be negligible. Rematching effects due to distortion are assumed to be small. Changes in engine internal flow profiles and distortion effects on the control system are assumed not to occur.

Synthesis outputs at matched inlet flow conditions are installed thrust, airflow, fuel consumption, aircraft performance parameters and engine gas generator performance and control parameters.

The extent to which explicit distortion assessment procedures are incorporated into a performance synthesis methodology will depend on the particular propulsion system and initial assessments of the magnitudes of the performance changes likely to be involved. Experience may, for instance, indicate that distortion will not affect installed engine performance significantly and that detailed assessments will not be required. The quality of information on the inlet and engine available during the conceptual studies and preliminary design phases of the power-plant development will be relevant.

4.3.1.1 Inlet Recovery Guidelines

The need to account for distortion is indicated by the level of inlet recovery. A level close to 100 percent indicates a low performance effect, and low levels mean that distortion effects might be significant. This stems from the fact that recovery and distortion levels are often correlated in the inlet data. Loss of recovery may be used in face-average performance synthesis programs to establish performance sensitivity factors - $\Delta(\text{Thrust})/\Delta\text{PFAV}$, $\Delta(\text{Fuel})/\Delta\text{PFAV}$, - at a given operating condition. Losses may be expressed relative to a standard inlet recovery schedule.

A first assessment of the effects of distortion on turbofan engines can be made by representing the AIP distortion as an equivalent OD (by-pass) and ID (core) square-wave, radial, total-pressure distortion. Inlet OD and ID recovery factors may then be defined and input to engine performance decks incorporating split-flow fan characteristics, i.e., separate by-pass and core-flow performance accounting methodology. Estimated distortion patterns and actual inlet patterns, if available, can be used, and parametric studies can be conducted. The OD/ID split line may be taken as the radial stream-tube corresponding to the matched engine by-pass ratio.

$$\left(\frac{A_{core}}{A_{overall}}\right)_{AIP} = \frac{1}{1 + BPR}$$

For an ID (core) region having n instrumentation rings in the ID flow, the average ID total pressure is related to the face-average total pressure by:

$$\frac{(PAV)_{ID}}{PFAV} = \frac{1}{n} \sum_{i=1}^{n} \left[1 - \left(\frac{\Delta PR}{P}\right)_i \right]$$

and for the OD (bypass) region having (N-n) rings in the OD flow, the average OD total-pressure is given by:

$$\frac{(PAV)_{OD}}{PFAV} = \frac{1}{N-n} \sum_{i=n+1}^{N} \left[1 - \left(\frac{\Delta PR}{P}\right)_i\right]$$

where,

$$\frac{n}{N}\ (PAV)_{ID} + \frac{(N-n)}{N}\ (PAV)_{OD} = PFAV$$

and $\left(\frac{\Delta PR}{P}\right)_i$ are the distortion radial intensity elements.

Figure 4.17 illustrates the procedure.

An example performance synthesis output for a separate-flow two-spool turbofan engine operating at sea-level-static, standard day conditions is given in Table 4.4. Thrust data for engine operation either at constant fan speed or constant jet-pipe (LP turbine exit) total temperature are provided for cases where the inlet total-pressure loss is confined either to the bypass or the core flow region of the AIP (square-wave radial pattern). A local pressure loss of ten percent was assumed. The effects on thrust are expressed in terms of thrust loss sensitivity factors and are compared to uniform flow thrust loss factors. Significant differences occur in the engine total thrust sensitivity, depending on the location of the total-pressure- defect region and engine control mode. In this example, hub radial distortion nearly doubled the thrust loss factor in the temperature-control mode. Data on engine internal temperature, pressure, spool speed, flow, bypass ratio, and fuel consumption changes, can also be obtained as outputs.

The example, which can be generalized to cover other distortion cases, illustrates three points of general interest:

- Turbofan performance synthesis programs can provide valuable and timely quantitative indications of the effect of distortion on engine performance for defined AIP patterns - inlet type or parametric patterns - and engine control modes.

- Performance changes can be correlated with numerical distortion descriptors, (Table 4.4 results may be expressed as differences).

- Such correlations are only valid for a specified class of distortion so that care is required when attempting generalized correlations. Different results would be obtained for different ID/OD total pressure distributions.

Appropriate provisions for engine component rematching at specified propulsion system operating conditions should be included in the computational system.

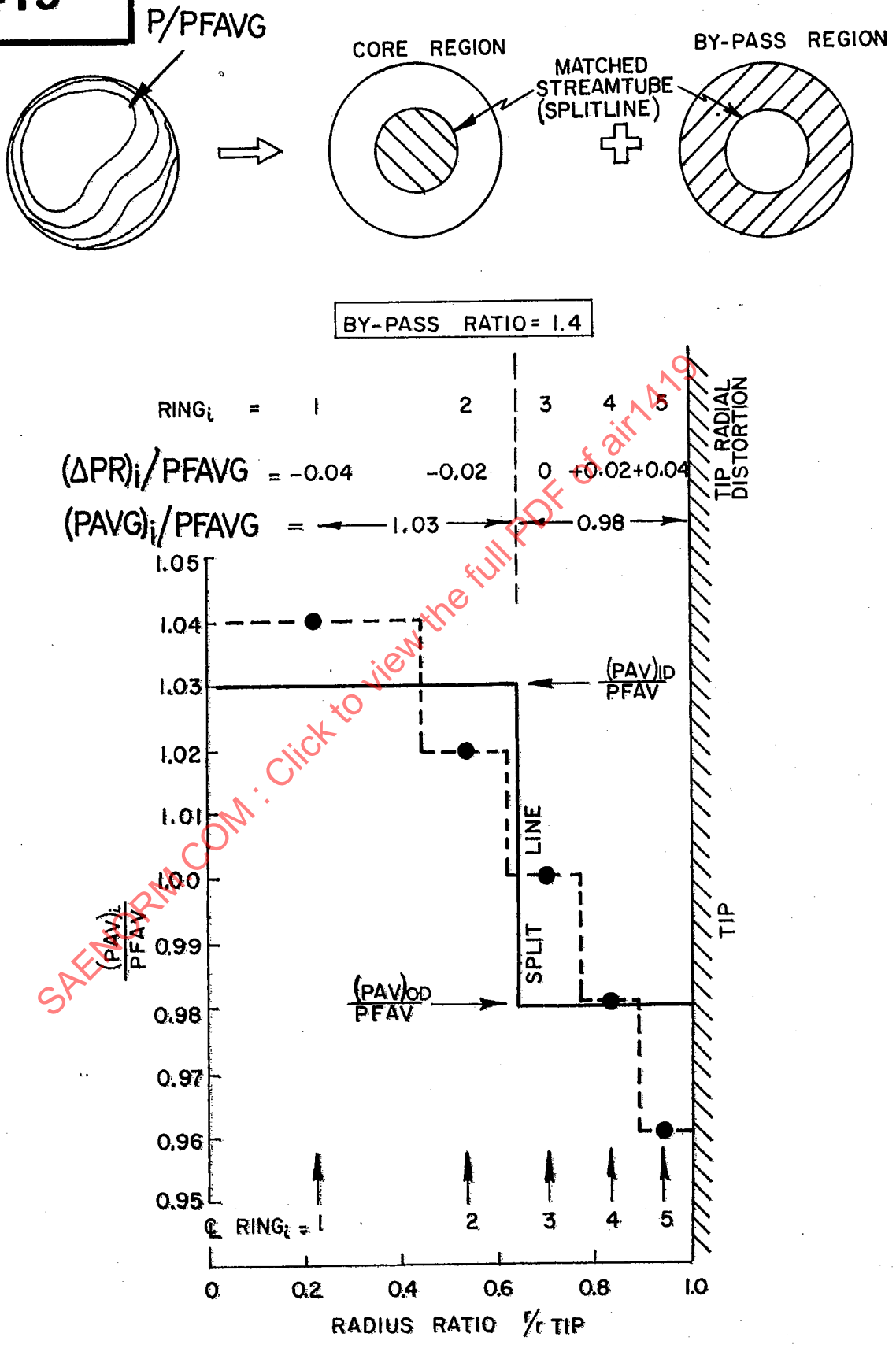

FIGURE 4.17 Split-Flow AIP Distortion Analysis Example

TABLE 4.4

Turbofan Thrust Loss Synthesis

ENGINE CONTROL MODE	CONSTANT FAN SPEED 100%			CONSTANT JET PIPE TEMPERATURE		
INLET RECOVERY LOSS REGION	OVERALL (UNIFORM LOSS) 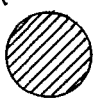	CORE 	BY-PASS 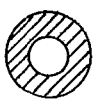	OVERALL (UNIFORM LOSS) 	CORE 	BY-PASS 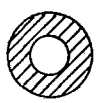
LOCAL RECOVERY LOSS ~ PERCENT	10 (DATUM)	10 (ID) 0 (OD)	0 (ID) 10 (OD)	10 (DATUM)	10 (ID) 0 (OD)	0 (ID) 10 (OD)
DISTORTION $\left\{\frac{PFAV-(PAV)_{ID}}{PFAV}\right\}$	0	+0.0615	-0.0604	0	+0.0615	-0.0593*
$\left\{\frac{PFAV-(PAV)_{OD}}{PFAV}\right\}$	0	-0.0427	+0.0456	0	-0.0427	+0.0466
PFAV RECOVERY LOSS ~ PERCENT	10	4.1	5.7	10	4.1	5.6
THRUST LOSS ~ %	15.8	5.9	9.6	16.4	13.1	3.4
THRUST SENSITIVITY $\left(\frac{\text{THRUST LOSS \%}}{\text{PFAV RECOVERY LOSS \%}}\right)$	1.58 (DATUM)	1.54	1.73	1.64 (DATUM)	3.3	0.62
RADIAL DISTORTION $\frac{(PAV)_{ID}-(PAV)_{OD}}{PFAV}$	0	-0.104	+0.106	0	-0.104	+0.106
THRUST SENSITIVITY CHANGE ~ %	0	-0.04	+0.15	0	+1.66	-1.02

* DIFFERENT BYPASS RATIO FROM CONSTANT SPEED CASE DUE TO ENGINE COMPONENT REMATCH

4.3.1.2 Distortion Data Use

The assessment outlined above accounts for engine component rematching and control interactions but uses undistorted or clean-flow component non-dimensional performance maps and excludes the potential effects of distortion on engine control sensing in the mathematical modelling.

Assessments of the performance effects of AIP distortion can be updated during the development phase when the effects of distortion on engine component performance maps - in particular those of the compression system - are available from component rig and engine tests. Distortion test results then can be used in higher order mathematical models appropriate to the powerplant under development.

Numerical assessment programs using empirical distortion data should provide for the following inputs:

- o Numerical AIP distortion descriptor elements.
- o Performance-related AIP distortion parameters. (These combined descriptor elements are not necessarily the same as those for stability assessments.)
- o Performance changes within compressor, main combustion, turbine, afterburner, and nozzles components.
- o Control system effects.

A logic flow chart illustrating alternate procedures for synthesizing engine performance changes due to distortion is shown in Figure 4.18. Main points are:

- o Distorted compressor performance maps, available from compressor rig tests with a given AIP distortion pattern, can be directly input to the steady state computer programs (Reference 9), as an alternative to the undistorted flow map, to enable matched thrust, fuel consumption, airflow and other engine performance variables to be determined. The impact of distortion can be established by comparing face-average assessment outputs. This procedure is an important turbofan assessment option where ID/OD rematching is important. Split-flow fan performance characteristics are required in this case.

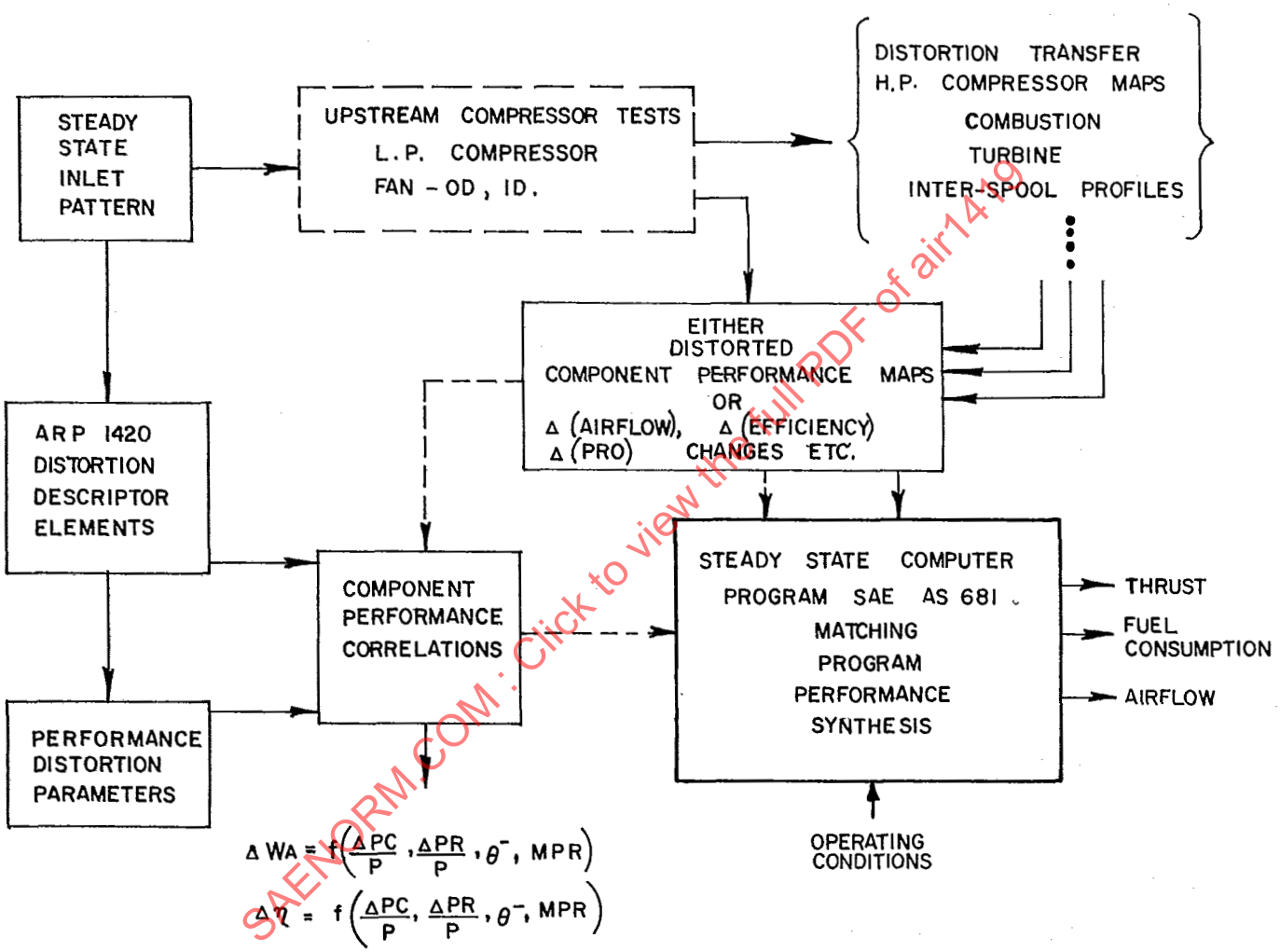

FIGURE 4.18 Steady-State Performance Assessment with Inlet Distortion

- Compressor distortion-response data for a given AIP pattern can be expressed incrementally as changes in corrected airflow, $\Delta(W\sqrt{\theta_t}/\delta_t)$, and efficiency, $\Delta\eta$, for specified compressor operating conditions. The increments may be functions of several relevant compressor flow variables, for example, N_c and PR (Figure 4.6). Separate terms for ID and OD flows may be necessary for assessing turbofans. The component performance increments may be used as input data to the engine matching program to provide absolute or normalized engine performance with inlet distortion.

- Compressor flow and efficiency increments may be correlated with the distortion descriptors at specified compressor operating conditions provided a suitable background of component testing has been conducted. Correlated changes may be input to the engine matching program. This procedure is straightforward for turbojet engine assessments. However, care is required in turbofan applications to assure correct ID/OD matching. Distortion transfer data applied to downstream components provide similar input data to the engine matching program, which may need to provide for estimating the effects of flow profile changes on engine control functions.

A flexible approach to the organization of performance synthesis procedures should be adopted whenever possible in order to facilitate program options.

4.3.2 PERFORMANCE TESTING

Engine and engine component tests with distortion provide data essential for the assessment and validation of distortion effects on installed engine performance. Component and engine test data acquisition should be regarded as complementary processes. Test planning and implementation guidelines are presented in Section 5 together with a discussion of state-of-the-art test techniques available.

General points relevant to data acquisition for performance assessments are:

- Engine tests provide data for installed components and extend rig experience to include the effects of component interactions (rig-engine interference terms).

- Engine tests provide development data on flow profile/control system sensor interactions for appropriate patterns and pattern positions, which may affect control system design.

- Measurement repeatability and accuracy in rig-component and engine tests are primary considerations as the quantification of performance changes due to distortion essentially involves measuring small differences between large quantities. The validity of performance loss/distortion data correlations and the amount of testing required to establish meaningful performance changes rest heavily on the measurement technology employed. Assessments should be accompanied by uncertainty analyses.

- AIP distortion patterns tested for performance should correspond to inlet patterns representative of prime mission performance points.

- The need for tests at distortion levels high enough to produce measureable performance changes should be considered.

- The effects of screen loss on engine rematching, in particular for unchoked nozzle operation, need to be isolated if distortion-induced performance changes are to be accounted for explicitly. This may require uniform screen testing through the requisite test flow range.

- Adjustments to nominal test conditions (for example, screen inlet pressure levels) may be required to account for screen losses over the test flow range and provide controlled performance assessment data.

Assessment data acquired from inlet-plus engine-ground facility tests, flying test beds, and flight development prototype aircraft are included implicitly in measurements made with gas path instrumentation. The quality of flight test performance assessment data will depend on the extent to which instrument calibrations include the effects of AIP distortion. The increased trend towards the use of on-board diagnostic and monitoring data systems provides means for acquiring engine performance in service operation.

4.4 TIME-VARIANT DISTORTION

Current methods of accounting for the effects of AIP total-pressure distortion on steady-state engine performance use time-averaged data from low-response instrumentation at the AIP. Available information is insufficient to define the effect of time-variant AIP total pressure distortion and PFAV fluctuations on steady-state engine installed thrust, fuel consumption, and airflow. At typical mission performance points, AIP distortion data indicate that turbulence levels are low and the performance effect minimal.

Data available from compression component rig tests indicate that the time-averaged performance may be affected by time-dependent flow (References 15 and 16). Random AIP flow fluctuations may cause losses of corrected flow in the order of 1 percent $\pm$ 0.5 percent RMS total-pressure amplitude. (filter range 0 to 1500 Hz). The test results indicate that compressor performance responds to a wider turbulence frequency range than compressor stability.

SECTION 5

DISTORTION TESTING

Tests provide the technical data base for the development and verification of the stability and performance assessments discussed in Sections 3 and 4. The validity of the assessments depends on the quality of the data bank generated during the test effort. A program, with techniques defined in terms of the instrumentation, data management, equipment, procedures, and analysis and communication of results, should be established by all involved parties to assure maximum utilization of the data.

The primary objectives of distortion tests are to define the flow distortion characteristics of the inlet and to quantitatively determine the effects of distortion on the stability and performance of the engine. The scope of the test effort must be tailored to the specific needs of the propulsion system. The extent and type of the tests must be balanced with regard for system requirements, program milestones, program risk assessments, program schedules, and cost constraints. Tests may be required on inlet and aircraft components, engine and engine components, and the propulsion system. Information acquired from these tests decreases the risk of incompatibility between the inlet and engine as propulsion system development progresses (Figure 5.1).

5.1 INLET AND AIRCRAFT COMPONENT TESTS

The purpose of the inlet system is to supply the desired quantity and quality of air to the engine throughout the flight envelope while minimizing aircraft drag items chargeable to the propulsion system. A well-constructed inlet development program is necessary to identify appropriate performance, weight and cost trades. The tests required depend on the degree of complexity and risk associated with individual designs. Highly integrated systems, involving significant advances in the state-of-the-art, may require tests that extend over a period of years. With a concomitant engine development program, time phasing and appropriate information exchanges become critical to the development of an optimal system. In less complex programs, or where a higher degree of technical risk is acceptable, limited tests over a relatively short time period may be adequate.

A checklist, identifying test objectives during various stages of the inlet development program, is given in Table 5.1. Appropriate wind tunnel models, test facilities, major independent test variables and data requirements are summarized. Tests are grouped in three major categories: 1) inlet development tests, 2) inlet verification tests, and 3) full-scale, inlet-engine compatibility tests. Individual aircraft development programs may require the use of various combinations of these tests.

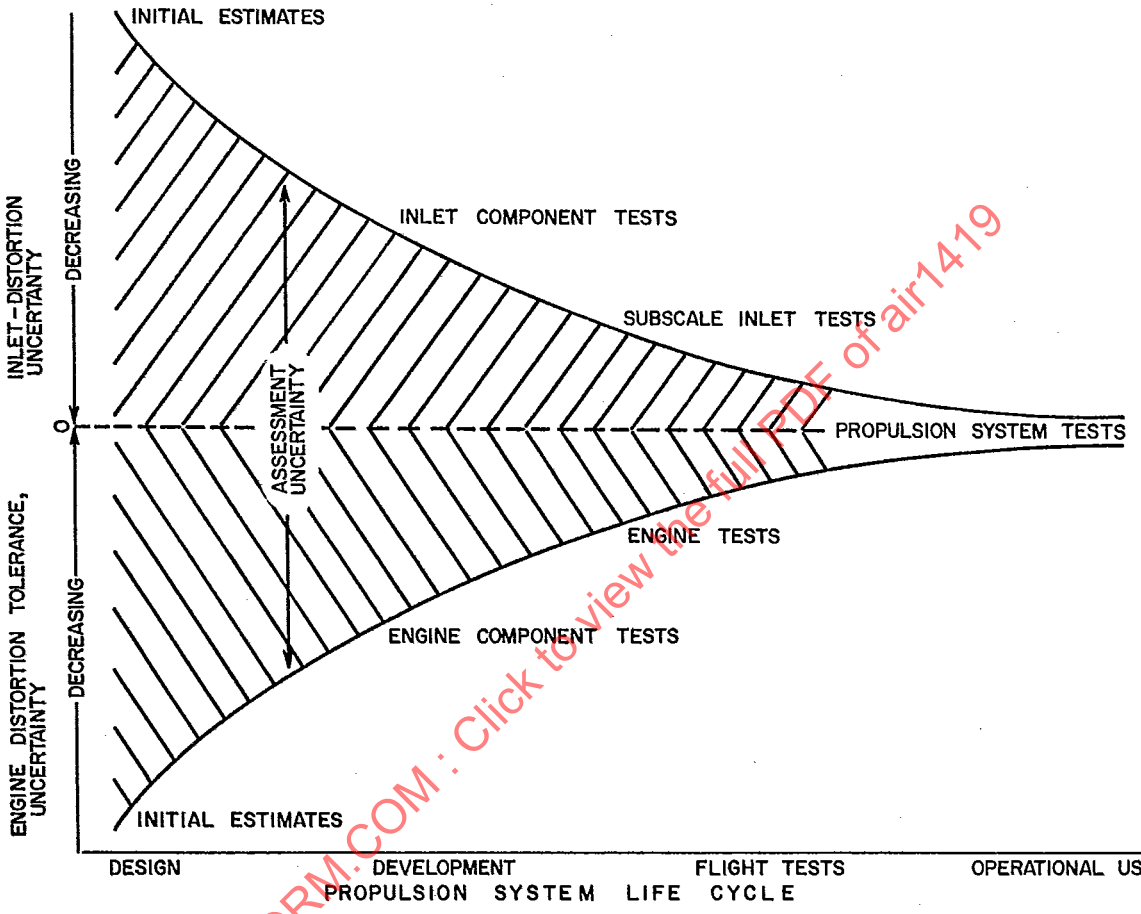

FIGURE 5.1 Distortion Assessment Uncertainty During Propulsion System Life Cycle

Inlet/aircraft models of differing scales, tested in a number of facilities are used to acquire inlet data. Model scale, Reynolds number, and facility type can all introduce uncertainities in the data. Tests with short subsonic inlets have indicated that the distortion in flight may be significantly different from the distortion measured in scale model tests due to the effect of engine pumping, Reynolds number, and other wind-tunnel-to-flight differences. Reference 17 shows that engine pumping substantially reduces distortion following separation at high angle of attack. It appears that these effects are most significant in close-coupled installations such as those utilized in commercial aircraft. Programs on conventional supersonic inlets indicate that, with sufficient attention to detail, good correlation can be obtained between subscale and full-scale model tests for selected inlet configurations (References 18, 19 and 20). The data of Reference 18 show that Reynolds number effects on inlet distortion due to model scale and/or tunnel conditions, were negligible at static and subsonic conditions. Full-scale model data at Mach 2.2 and high Reynolds number showed higher total-pressure recovery and slightly lower distortion compared to results with sub-scale models. Comparable results were obtained in both blowdown and continuous wind tunnel facilities. Similar results are reported in Reference 19.

Flight test and wind tunnel results are compared in Reference 20. Distortion patterns recorded during flight tests were found to be similar to wind tunnel results obtained during static, subsonic and supersonic operation. Flight data resulted generally in slightly higher total-pressure recovery and slightly lower total-pressure distortion than recorded during comparable wind tunnel conditions. These differences were smaller than the differences recorded among different aircraft at comparable operating conditions. Results, comparing data from full-scale inlet/engine tests with data from "cold pipe" (no engine present) tests, indicated that the effects on total-pressure recovery and distortion were negligible. The latter result is attributed to good simulation of the acoustic impedence of the engine achieved by locating the choking station (used for airflow control) close to the AIP.

5.1.1 INLET DEVELOPMENT TESTS

Small-scale inlet test results are used to define the inlet/forebody configuration. Tests to evaluate the inlet in terms of the flow quality at the AIP are described in Paragraph 5.1.1.1. Tests to evaluate inlet drag, to identify appropriate trades, and to optimize performance are described in Paragraph 5.1.1.2

5.1.1.1 INTERNAL PERFORMANCE

Internal performance, (defined by total-pressure recovery and distortion at the AIP, airflow, and the inlet operating stability limits), is obtained from 1) isolated-inlet tests, 2) subsonic-supersonic inlet/forebody tests, and 3) low speed inlet/forebody tests. These tests are described separately in Table 5.1. However, no single test accomplishes all the stated objectives. In practice, the design process is iterative and requires more than one wind tunnel entry. Each test generates data that are used to modify the configuration for the next test.

TABLE 5.1

Inlet And Aircraft Component Tests

Model/Facility/Test Variables	Data	Objectives
Inlet Development Tests		
A. Isolated Inlet Model		
1. Inlet Alone (Scale > 0.1) 2. Blowdown Wind Tunnel 3. Mach, Inlet MFR, Geometry	Steady-State AIP Pressures Limited Turbulence Engine Airflow	Inlet sizing Internal Diffuser Lines Cowl/Sideplate arrangements Initial BLC Configurations Bypass/Auxiliary Inlet Configurations Inlet Stability Characteristics Buzz Frequencies/Amplitude Ramp Configurations Inlet Shielding Devices for Radar Cross Section (RCS)
B. Subsonic-Supersonic Inlet/Forebody Model		
1. Inlet/Forebody with Fwd A/C Control Surfaces/Wing Stub (Scale > 0.1) 2. Blowdown Wind Tunnel 3. Mach, α, β, Inlet MFR Bleed Airflow, ECS Airflow, Geometry	Steady-State AIP Pressures High-Response AIP Pressures Engine, Bleed, ECS Airflows Static-Pressure Distribution	Initial Subsonic/Supersonic Inlet Performance and Distortion Characteristics Boundary Layer Gutter Development Inlet Flow Field Inlet to Inlet Independence Inlet Control Sensor Locations Inlet Control Schedules Maneuver Envelopes Bleed, Separation, Exit Configurations A/C Control Surface Vortex Ingestion Bypass Configurations ECS Scoop Configurations Inlet Shielding Devices for RCS Inlet Stability Limits External Stores Inlet/Engine Airflow Matching
C. Low-Speed Inlet/Forebody Model		
1. Same Model as B1 Above 2. Low Speed, Continuous Wind Tunnel 3. Mach, α, β, Inlet MFR, Geometry	Steady-State AIP Pressures High-Response AIP Pressures Engine Airflow Static Pressure Distribution	Initial Static/Take-off (Mach < 0.2) Performance, Distortion Characteristics Auxiliary Inlet Arrangements Ground Plane Effects Crosswinds Nose Gear Wake Ingestion Wing Slat Effects Off-Scheduled Ramp Geometry High α/β Operation to Support A/C Stall Investigations
D. Drag Models		
1. Complete Aircraft Model with Appropriate Portions of Inlet on Force Balance (Scale < 0.1) 2. Continuous and/or Blowdown Wind Tunnel 3. Mach, α, β, Geometry	Inlet Drag Components External Static Pressures	Drag data to support inlet configuration trades and to estimate installed performance.
Inlet Verification Tests		
1. Inlet/Forebody with Fwd A/C Control (Scale ≈ 0.2) 2. Continuous Wind Tunnel 3. Mach, α, β, Inlet MFR Bleed Airflow, ECS Airflow, Geometry	Steady-State AIP Pressures High-Response AIP Pressures Engine, Bleed, ECS Airflows Static Pressure Distribution	Critical High-Response Distortion Patterns and Levels Reduced Bleed Requirements Inlet Performance Over Flight and Maneuver Envelopes Wake/Vortex Ingestion Envelopes Duct Loads - Hammershock Weapon Bay Doors - Spoilers External Stores Refined Control Schedules External PODS, Scoops Inlet Shielding Devices for RCS Refined Inlet Control Sensor Locations Bypass Door Operation
Inlet/Engine Compatibility		
1. Full-Scale Inlet Model and Prototype Inlet Control, Prototype Engine and Control Tests Consists of 3 Phases: a. Inlet Alone b. Inlet Plus Inlet Control (No Engine Present) c. Inlet Plus Inlet Control (Engine Present)	Steady-State AIP Pressures High-Response AIP Inlet/Engine Airflows	Inlet/Engine Compatibility Demonstration Inlet Control Operation
2. Continuous Wind Tunnel 3. Mach, Limited α, Inlet MFR, Geometry, Distortion	Inlet Static Pressures Full Engine Instrumentation	Inlet Control Response Rates Engine Control Sensitivity to A/C Distortion Inlet Stability Limits Engine Throttle Transients Hammershock Loads Vortex Ingestion Engine Distortion Tolerance Flight Test Instrumentation Checkout

Tests are conducted with small-scale models to permit the use of less expensive test facilities. To a great extent, model size is determined by wind tunnel capability, but the model should be at least 1/10 scale to achieve accurate geometric similarity. Typically, the allowable projected frontal area of models required to simulate the downstream aerodynamic environment should be approximately one percent of the cross-sectional area of the test section. The allowable model size for tests in which only the inlet conditions need be simulated can be approximately 15 percent of the cross-sectional area of the test section.

Initial inlet tests may be performed with an isolated inlet model in a facility that permits frequent access to the model. Geometry, flight Mach number and engine airflow are duplicated. The tests provide the initial configuration evaluation and performance estimates. Alternate geometries (ramp, sideplate, diffuser, internal line, cowl lip) are evaluated. Limited dynamic instrumentation is used to identify potential distortion problems. The tests provide sufficient data to permit detailed configuration development.

An example of an isolated-inlet test facility is shown in Figure 5.2. The subsonic diffuser model was built to evaluate the internal performance of various inlet duct configurations. Total pressure recovery, steady-state distortion, and RMS pressure levels were measured by a 40-probe rake mounted at the simulated engine face station. Internal components could be changed easily to evaluate different diffusers. Other low-cost techniques are also available for investigating subsonic diffusers. One method, employing an altitude chamber as a vacuum source, is described in Reference 21.

Inlet/forebody models, tested at low speed, subsonic and supersonic conditions, are configured with a forebody, a wing stub, any forward control surfaces, and other aircraft features which affect the flow forward of the inlet. Flow-field tests are performed to measure the local Mach number and the flow direction of the air entering the inlet. For some tests, the inlet is replaced by a rake of flow-field probes and is tested over the Mach number and attitude range. Flow-field data are used to optimize inlet placement and orientation. More than one series of inlet/forebody tests may be necessary to acquire the internal performance data. Tests are conducted over the full range of flight conditions from static operation to high Mach number. A full complement of low- and high-response AIP instrumentation is employed to obtain distortion data. All parts of the aircraft that affect the inlet internal operation are duplicated.

As an example, a 0.10-scale B-1 model with a single nacelle dual-inlet design mounted to a complete fuselage forebody with stubwings, is shown in Figure 5.3. A weapons bay just forward of the nacelle is simulated. This model was used to determine the effects of weapons bay doors and external stores on inlet performance. Acoustical measurements inside the bay cavity and on the doors were obtained. Tests were conducted to define inlet performance in detail, identify the effects of the aircraft and adjacent inlets, define the inlet control requirements, and provide data to refine the initial design.

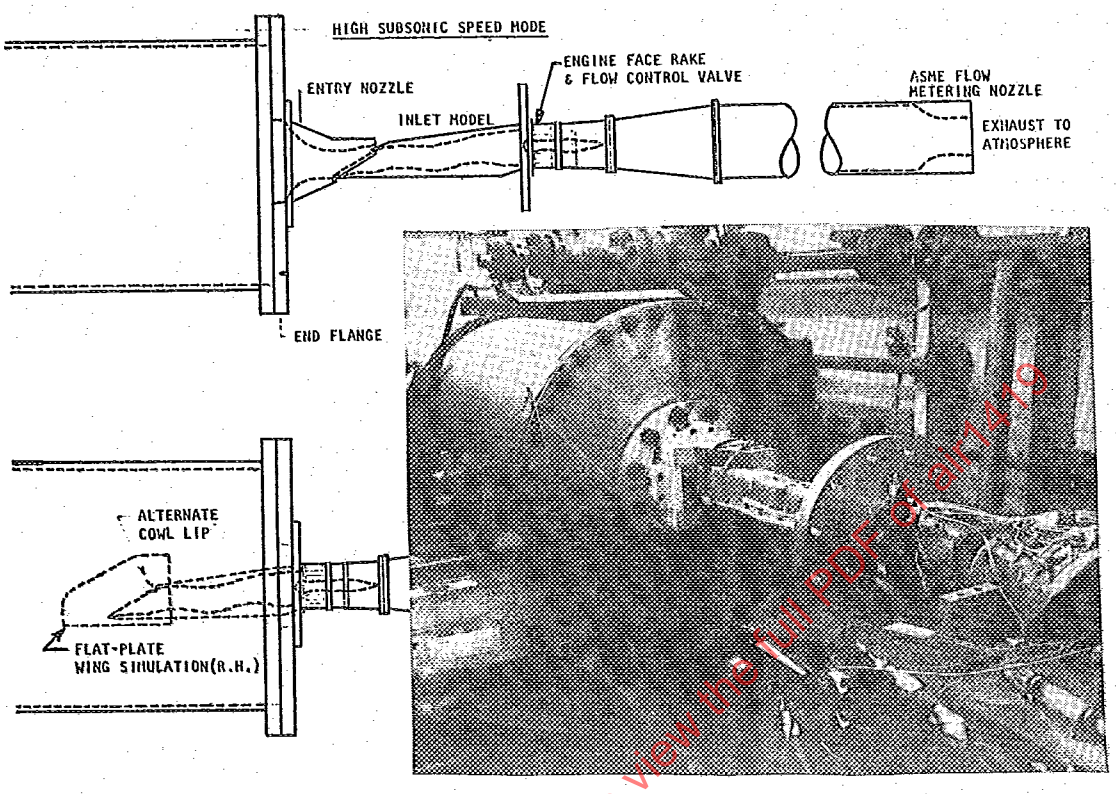

FIGURE 5.2 Subsonic Diffuser Model for Investigating Internal Performance

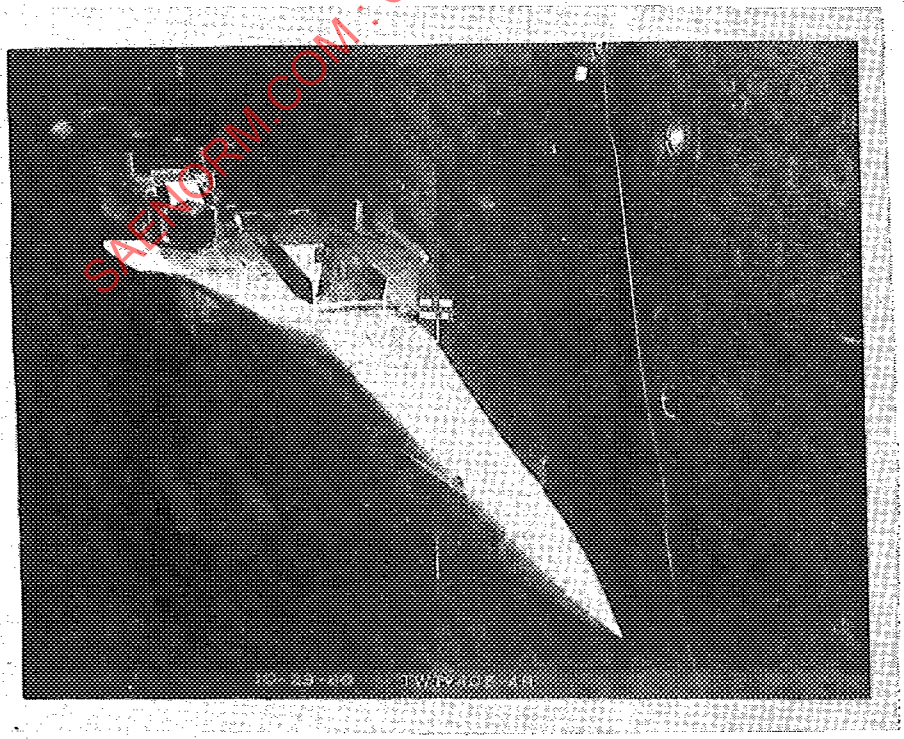

FIGURE 5.3 Inlet/Forebody Wind Tunnel Model

Diagnostic testing in a low-speed (Mach 0.2) wind tunnel can also be of value for screening configuration changes. Use of the low-speed tunnel permits the use of a large-scale model in a continuous flow environment. Flow visualization tests of the diffuser can be conducted. In addition, AIP steady-state instrumentation can be used as an evaluation tool. These tests permit assessment of inlet changes in the presence of a flow field and are relatively inexpensive.

5.1.1.2 External Performance

The tests described above define and quantify the factors which affect internal performance. Concurrently, tests should be conducted to evaluate external performance which includes all drag items chargeable to the inlet (inlet spillage drag, bypass drag, bleed drag, and any interference effects of the inlet flow on aircraft drag). Because testing requires a complete aircraft model and the external flow field is important, the model is generally smaller than the internal performance model. It is designed with several internal balances and extensive static pressure instrumentation to evaluate the drag associated with the inlet. These tests provide drag data to evaluate configuration changes resulting from the internal performance tests as well as providing data for overall aircraft performance assessments.

As an example, a 0.07 scale B-1 inlet drag model is shown in Figure 5.4. This model represents the left-hand dual inlet nacelle mounted to the fuselage forebody. Fuselage structural mode control vanes, stub wings, and the opposite-side flow-through nacelle are simulated. Model drag is measured by an internal force balance supporting the metric system. The model provides incremental inlet drag data for installed engine performance calculations.

5.1.2 INLET VERIFICATION TESTS

This test phase provides the final subscale evaluation of inlet internal performance. Model size is usually 20 percent scale or larger to assure that all forebody and other parts of the airframe which may influence the inlet flow field are represented. The overall purpose of verification tests is to define the inlet performance characteristics throughout the required Mach number, angle-of-attack, sideslip, and corrected airflow ranges. Items that affect the inlet are optimized. The model should fully represent each configuration item that has a potential influence on inlet operation. This requires that all scoops, vents, exits, and protuberances be simulated. As an example an F-18 model, constructed for this type of testing, is shown in Figure 5.5.

Auxiliary air induction systems, environmental control system inlets, radar cooling circuit scoops, and gun bay purge devices, are evaluated during the tests. Flow and recovery characteristics are established as functions of speed and angle of attack. The effects of wake and shock ingestion from adjacent structures are evaluated. Typical items include flight-test or production noseboom and nozzle, auxiliary tanks and pods. An evaluation of aircraft protuberances should be made. Items include angle-of-attack vanes, total-pressure and total-temperature probes, and antennae.

Alternative inlet control-sensor locations are investigated during the tests. Several options can be evaluated simultaneously to establish locations that best provide the desired signals. Boundary-layer-bleed systems should be refined to minimize inlet drag. The inlet bypass system is optimized to minimize bypass drag for non-maneuvering conditions, while maintaining optimal inlet operation during maneuvers or at high speed. Calibrated mass flow measurements are required. Inlet operation in buzz is investigated. Distortion, in-phase pressure oscillation amplitudes, and frequency content at the AIP are used to evaluate engine response. Static pressure loads are obtained to determine structural design criteria for the inlet.

Instrumentation for the inlet verification test phase is comprehensive. Low- and high-response static-pressure taps are located in the bleed and bypass systems, and in the diffuser. The AIP is fully instrumented with both low- and high-response total-pressure probes. Static pressure taps at the AIP can provide further useful information. High-response instrumentation may be required in auxiliary air induction systems to determine if pressure oscillations occur.

Digitized peak time-variant distortion data will provide patterns for stability evaluation by the engine manufacturer. Distortion trends with Mach number, angle of attack, angle of sideslip, and mass flow are established. Inlet recovery, stable-airflow-range, and steady-state distortion data, are obtained for use by the engine manufacturer to determine whether engine performance is affected.

Results of verification tests are used to establish the final design of the inlet, including control schedules, bleed and bypass requirements, and external flow field effects. Definitive flow distortion and recovery levels are obtained for the final design.

5.2 ENGINE AND ENGINE COMPONENT TESTS

Engine and engine component tests are required to develop and verify the initial (design phase) assessments of the effects of inlet distortion on engine performance and stability. The tests that may be required are based on three engine-inlet AIP flow conditions: uniform, steady flow (Section 5.2.1); steady-state distorted flow (Section 5.2.2); and time-variant distorted flow (Section 5.2.3).

Candidate engine and engine component tests are shown in Table 5.2. The primary objective and data requirements for each type of test are outlined. Since inlet flow distortion may affect the basic aerodynamics of a number of engine components, interactions between those components, and the engine control system, testing of the engine components, (primarily the compression system components), and the engine is usually required.

Direct-connect test facilities provide controlled inlet flow conditions to the engine and are generally used for developing and verifying compressor and engine stability and performance. It is neither technically nor economically feasible to obtain sufficient data for in-depth assessments from free-jet or flight tests of the propulsion system.

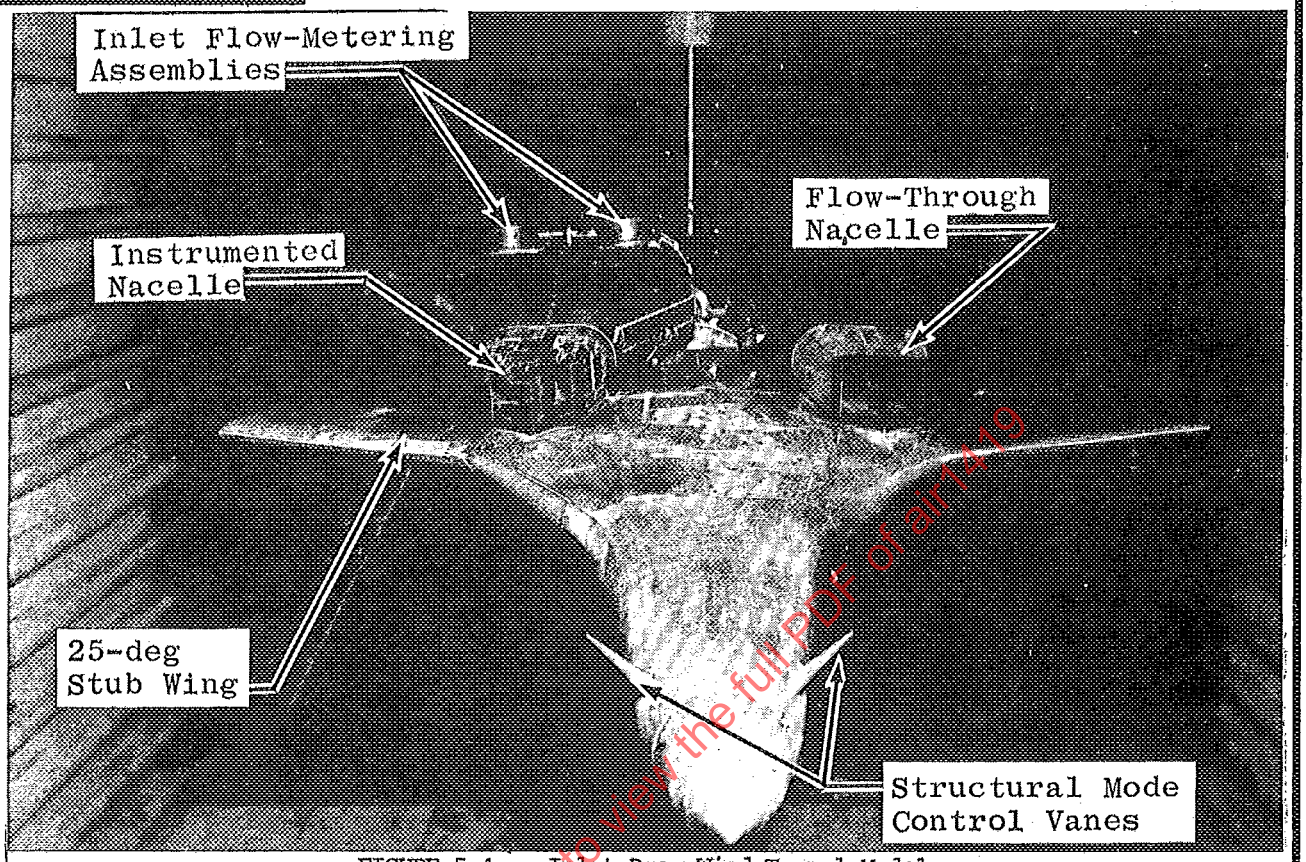

FIGURE 5.4 Inlet Drag Wind Tunnel Model

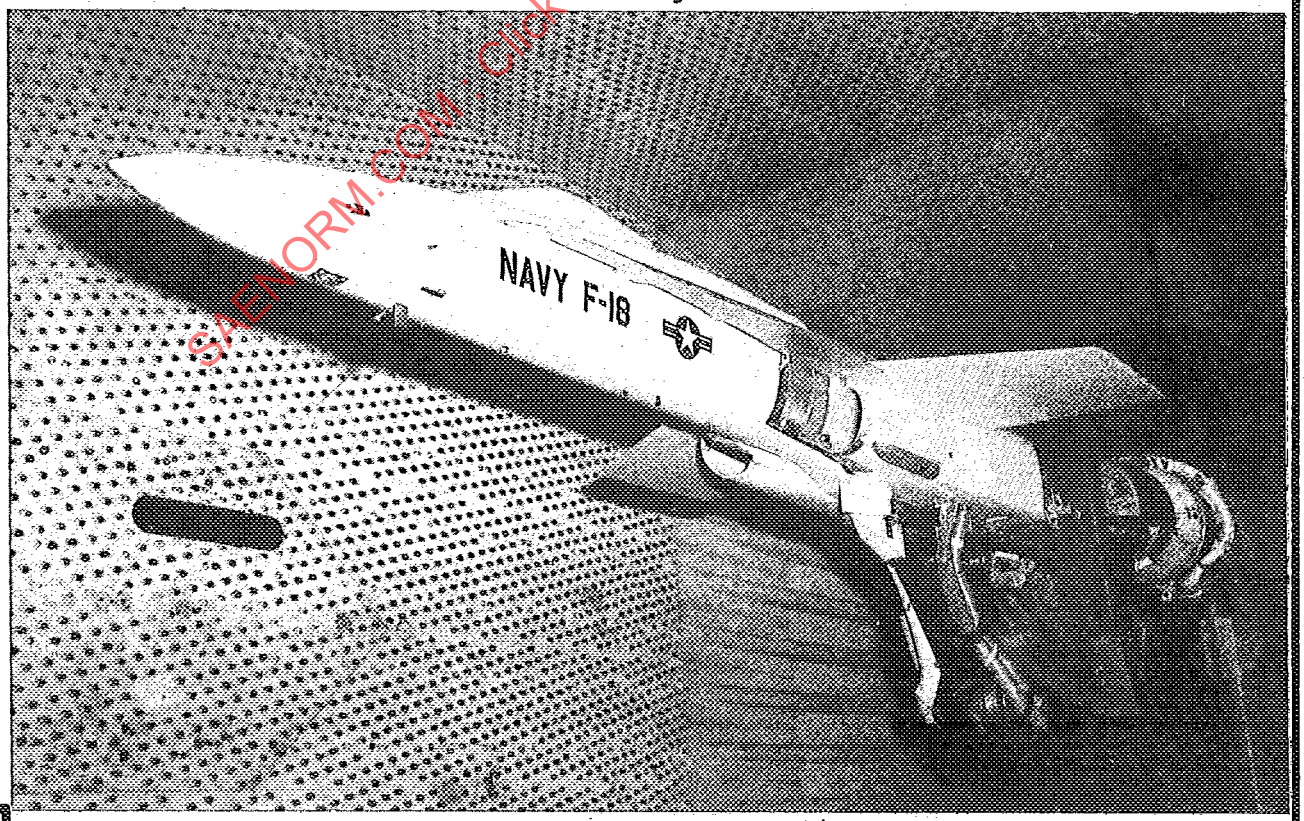

FIGURE 5.5. 1/5 Scale F-18 Model Used for Inlet Verification Tests

TABLE 5.2

Engine Component And Engine Tests

OBJECTIVES	TESTS	DATA
Develop Flow Stability Define Descriptor Define Control Sensor Locations Evaluate Off Schedule Geometry Evaluate Bleed Effects Evaluate Reynolds Number Effects	Compressor Rig/Diffuser Test with Classical and Flight Patterns	Surge Pressure Ratio Airflow Efficiency Exit Profiles Distortion Sensitivities Control Tolerance Distortion Transfer
Define Spool Interactions	Dual Spool or Engine Tests with Distortion Burner Rig Tests with Distortion	Spool Supercharging Bypass Ratio Shifts Speed Mismatch Surge Pressure Ratio Airflow Efficiency Exit Profiles Distortion Transfer Distortion Sensitivities
Evaluate Compressor-Burner Interactions Define Control Sensor Locations	Burner Rig Tests with Distortion	Burner Pressure Loss Exit Temperature Profiles Exit Pattern Factor Rich/Lean Fuel/Air Limits
Define Augmentor Stability Define Control Sensor Locations	Augmentor Rig Tests	Exit Total Pressure and Temperature Pressure Transients Rumble and Screech Light and Blowout
Define Control System Destabilizing Effects	Engine Tests with PLA Transients and Flight Trajectory Transients Fuel System Stability Checks	Linkage Rates Travel Limits & Lags Compressor Operating Lines Fuel Pressure Pulsations Control Tolerance
Define Engine Stability and Performance	Engine Tests with Classical Patterns and Flight Patterns Installation Effects at Critical Flight Conditions	Stability Limits Airflow(s) Efficiency(s) Distortion Transfer Speed(s) Thrust SFC
Define Response to Time-Variant Distortion	Engine Tests with Time-Variant Distortion	Stability Limit Critical Compressor Airflow
Define Response to Special User Requirements	Engine Tests with Water Ingestion Steam Ingestion Hot Gas Ingestion	Stable Operating Range

Inlet flow distortion may significantly affect engine mechanical integrity and life. Experience indicates that distortion may increase the risk of exceeding turbine nozzle and blade temperature limits, promote forced compressor rotor vibration and coupled blade-disk-mode excitation, may increase stator stress loads, and affect compressor flutter onset limits (References 22 through 25). During engine tests with inlet distortion it is necessary to assure that engine component stress and temperature limits are not exceeded. The aeromechanical limits of the engine components, such as the compressor operating limits shown in Figure 5.6 (Reference 25), must be considered in test program planning.

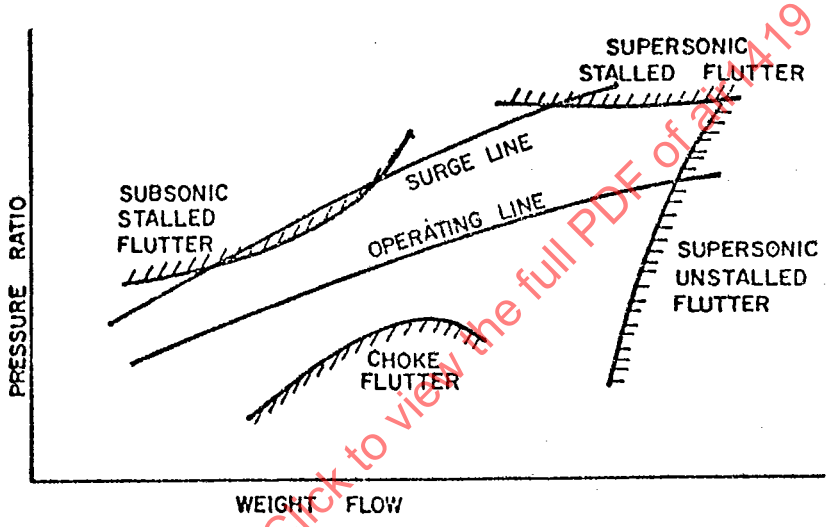

FIGURE 5.6 Compressor Map Showing Boundaries of Four Types of Flutter

5.2.1 UNIFORM STEADY-STATE INLET FLOW

Testing with uniform, steady, inlet flow establishes the baseline performance and stability of the engine and engine components. Uniform steady-state inlet flow conditions are defined as those conditions having low steady-state and time-variant total-pressure and total-temperature distortion. Studies (Reference 26) have defined uniform steady-state flow quality goals as:

$$\frac{P_{MAX} - P_{MIN}}{PAVG} < 0.01$$

$$\left(\frac{\Delta P}{P}\right)_{RMS} < 0.01 \text{ in the frequency range 0-1000 Hz.}$$

$$\frac{T_{max} - T_{min}}{TAVG} < 0.005$$

$$\left(\frac{\Delta T}{T}\right)_{RMS} < 0.005 \text{ in the frequency range 0-1000 Hz.}$$

Compressor rig tests usually take place early in an engine development program and precede engine tests. They provide a flexible means for evaluating the effects of distortion over a range of throttle conditions using comprehensive instrumentation.

An example of a typical single-spool, single-discharge compressor rig is shown in Figure 5.7. The facility includes a large intake plenum, an inlet bellmouth, and a low-volume, quick-opening throttle valve. The first two items provide high quality airflow at the compressor face and the third allows rapid surge recovery. The rig tests define the performance of the test compressor from open throttle settings to the surge throttle setting at each of several constant rotational speeds. The test results are presented as a compressor map defining performance in terms of flow pressure ratio, efficiency, and stability limit. If the test compressor is an integral unit of a multiple-compressor-compression system, such as a dual-spool engine, then aerodynamic coupling effects between the spools (spool interference) may need to be accounted in the test set-up and procedures.

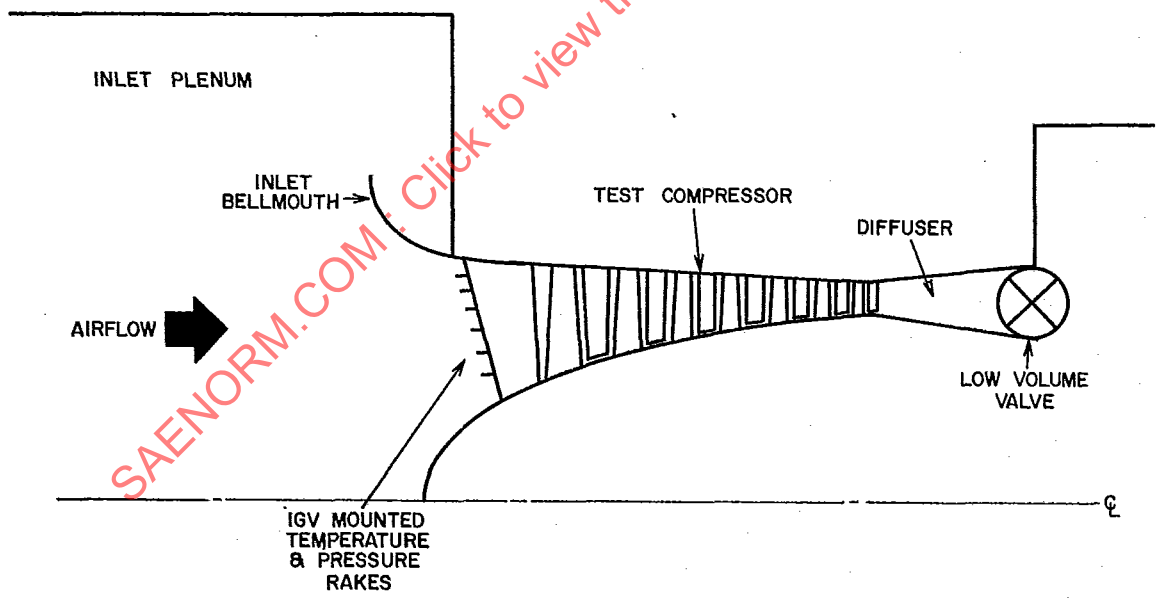

FIGURE 5.7 Single-Spool Compressor Facility

Figure 5.8 is a schematic of a dual-spool rig used to characterize the stability of a fan/low-pressure unit and its corresponding high-pressure compressor. Dual-discharge rigs are necessary for testing fan/low-pressure units, with close attention paid to simulating the expected discharge flow schedules. Variances in these schedules can cause significant changes in unit

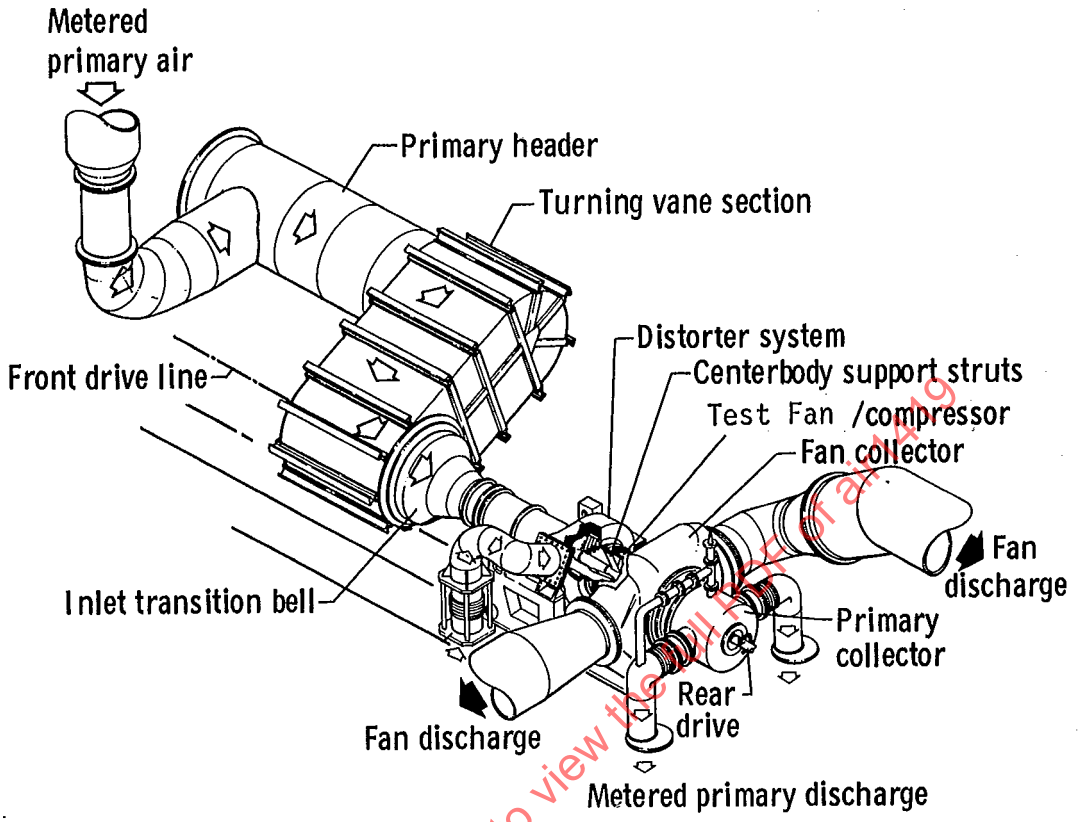

FIGURE 5.8 Dual-Exhaust, Dual-Spool Compressor Facility

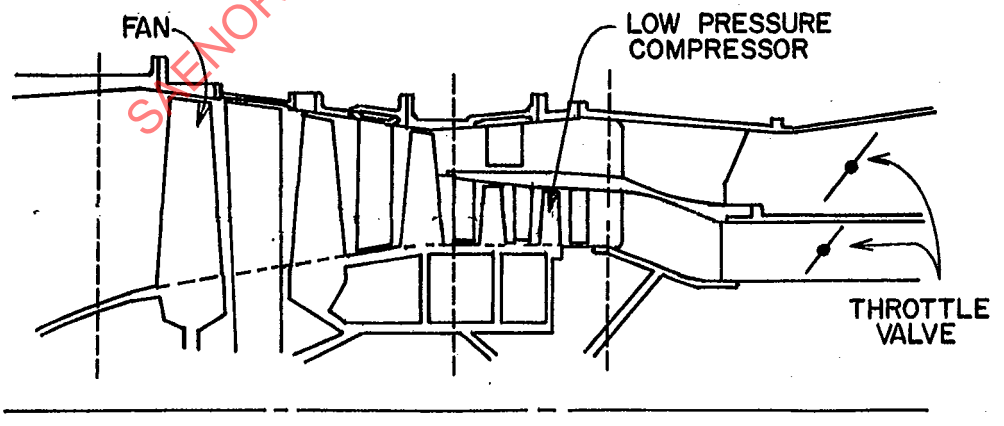

FIGURE 5.9 Dual-Discharge Compressor Flowpath

performance and stability characteristics. Figure 5.9 is a schematic of the test section of a typical dual-discharge rig designed to independently vary fan and low-pressure-compressor discharge-flow schedules.

Engine tests define overall performance and stability, verify the results of component tests (e.g. compressor rig tests), and ascertain the effects of component interactions on engine system stability and performance. Tests are conducted to assess the effects of the engine operating environment, and the effects of the engine operating condition. Environmental considerations include the effects of flight Mach number, altitude, Reynolds number, nonstandard day conditions, external engine thermal environment, and flight transients where performance or stability characteristics vary prior to the achievement of engine thermal equilibrium. Typically, the engine operating characteristics are established with and without engine airbleed and power extraction, with control system variations representative of control tolerances, and in steady-state and transient nonaugmented and augmented control modes.

Direct-connect sea-level and altitude test facilities can be used for engine baseline testing. A typical direct-connect engine test installation in an altitude test facility is illustrated in Figure 5.10. The salient features of the installation are a critical-flow airflow-measuring venturi, a large inlet plenum, and a bellmouth at the engine inlet duct to provide uniform steady flow to the engine. Flow straighteners are fitted in the inlet plenum to assure that the flow is uniform.

5.2.2 STEADY-STATE TOTAL-PRESSURE DISTORTION

Tests with steady-state inlet total-pressure distortion define the effects of classical and composite distortion patterns on engine and engine component performance and stability. Testing with classical patterns establishes the basic sensitivity characteristics of the engine. Testing with composite patterns establishes performance changes and the loss in stability attributable to flight-type inlet-distortion patterns. Composite patterns are based on inlet test results at selected operating conditions. The established practice in industry is to simulate peak time-variant distortion patterns with steady state-patterns, thus avoiding the need for extensive compression system development testing with high-response instrumentation and data-acquisition systems. Compressor and engine testing with steady-state total-pressure distortion can be accomplished in the direct-connect installations described for testing with uniform inlet flow conditions using steady-state distortion generators located approximately one engine diameter forward of the compressor inlet.

Distortion levels up to 30 percent $(P_{avg} - P_{min}) / Pavg$ generally are sufficient for most steady-state distortion testing needs. The time-variant component, $\Delta P_{rms}/P_{avg}$ (0-1000 Hz), should be less than one percent and total-temperature distortion, $(T_{max} - T_{min}) / T_{avg}$, should not exceed one-half percent.

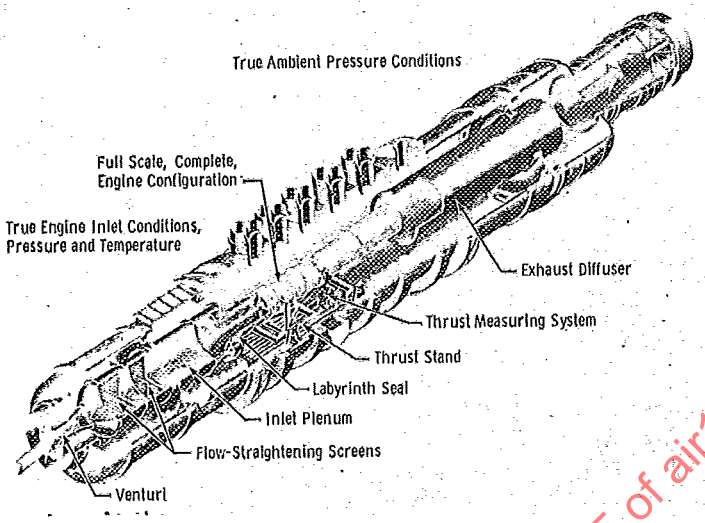

FIGURE 5.10 Typical Direct-Connect Engine Test Installation for Baseline Stability and Performance Testing

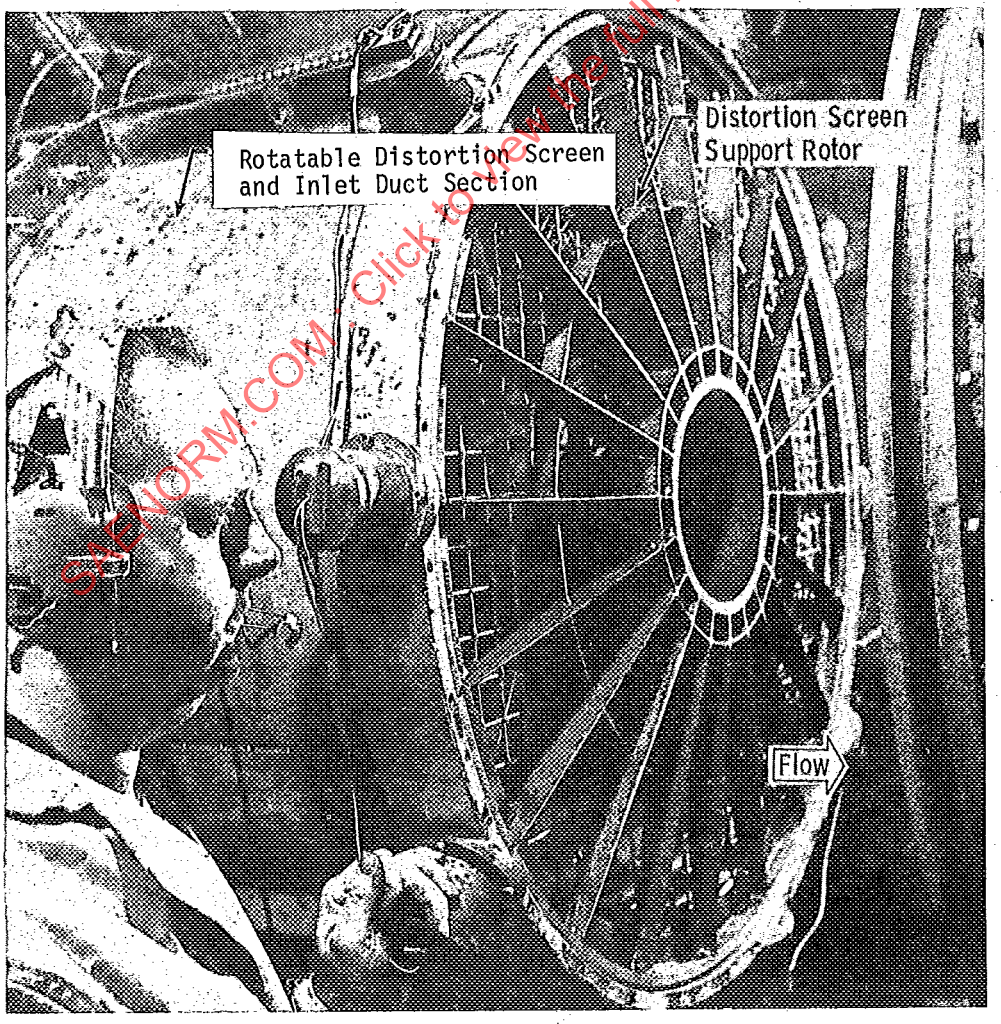

FIGURE 5.11 Rotatable Distortion Screen Assembly

5.2.2.1 Screens

Wire-mesh screens are used to generate steady-state total-pressure distortion at the compressor and engine inlet. Screen systems have several significant advantages. They are relatively simple to fabricate and use. Once calibrated, screen systems may be used with limited AIP instrumentation in different facilities having identical engine inlet configurations. Rotatable distortion screen assemblies may be used to obtain detailed distortion data from a minimum number of installed sensors (AIP and engine internal sensors) at a stabilized engine/environmental test condition and to assess engine control system interactions at a constant engine power lever position. An example of a rotatable distortion screen assembly used for engine testing is illustrated in Figure 5.11 (Reference 27).

Screen design techniques have been developed to aid in the development of screens to provide defined total-pressure distortion patterns (Reference 28). Selected inlet distortion patterns usually can be established to required accuracies to within two to four screen tailoring test iterations. Screens have undesirable operating chracteristics in that their pressure losses are dependent on the screen porosity (blockage) and approach velocities, so that the simulation of a number of inlet distortion patterns requires a screen change with a consequent loss of test time.

5.2.2.2 Air Jet Distortion Generators

An airjet system can be used as an alternative steady-state distortion generator. Airjet-distortion generators use a counterflow (to the primary engine inlet airstream) air jet system in which the jet flow momentum cancels part of the primary compressor inlet airstream momentum with an accompanying total-pressure loss. The flow distortion pattern is varied by remotely controlling the jet flow rate and distribution.

A typical airjet distortion generator (Figure 5.12) is reported in Reference 29. The system includes a secondary (airjet) air temperature conditioning system (to match the temperature of the primary engine airstream), an airjet nozzle array (56 equally spaced flow nozzles), and a computerized airjet nozzle flow control system to provide "dial-a-pattern" capability. Defined parametric or flight-related patterns can be established within approximately 90 seconds during testing to approximately the same accuracy limits obtainable with a screen distortion generator (two percent rms error on a probe-by-probe basis). The airjet system provides a capability for producing variable-amplitude and variable-pattern steady-state distortion at a fixed engine operating condition or a constant distortion level and pattern over a range of engine airflow without hardware changes.

The airjet distortion generator requires the use of a full AIP steady-state total-pressure probe array and a secondary air supply system. The time-variant distortion levels obtained with the airjet system may be higher than comparable levels obtained with screen systems, necessitating the use of high-frequency-response inlet instrumentation (Reference 29). Similar airjet distortion generators are reported in References 30 and 31.

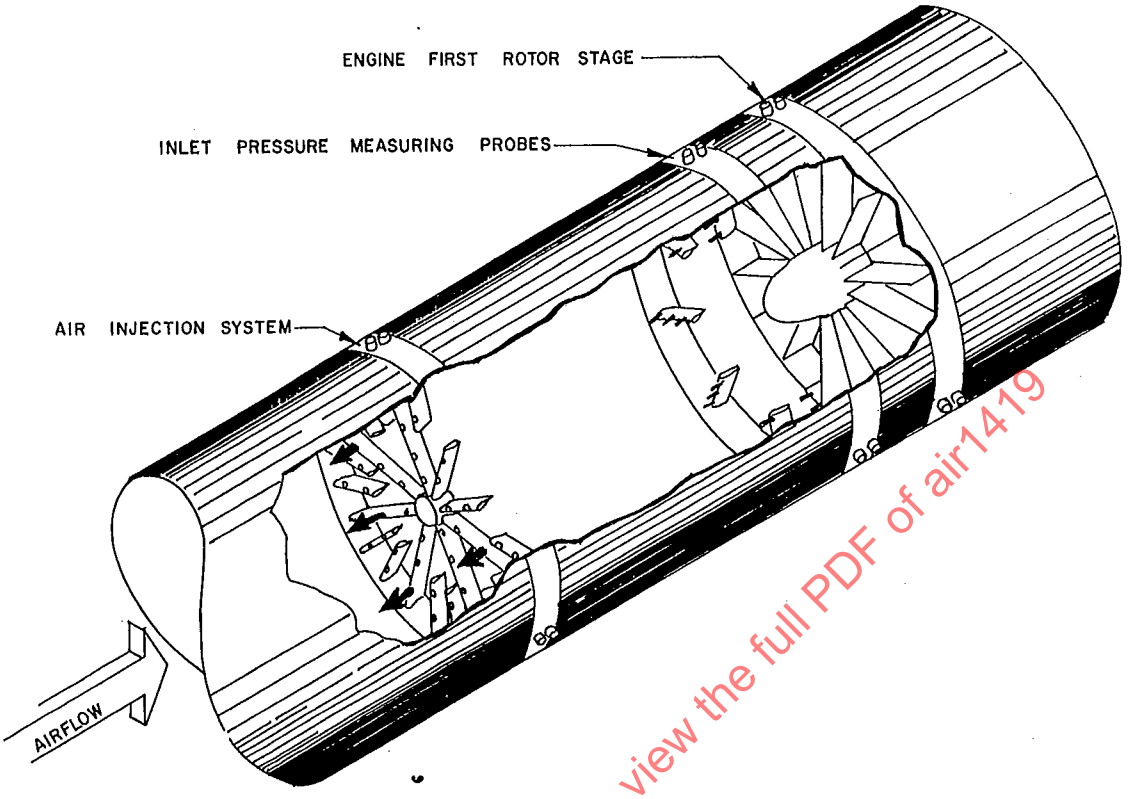

FIGURE 5.12 Schematic of Airjet Distortion Generator

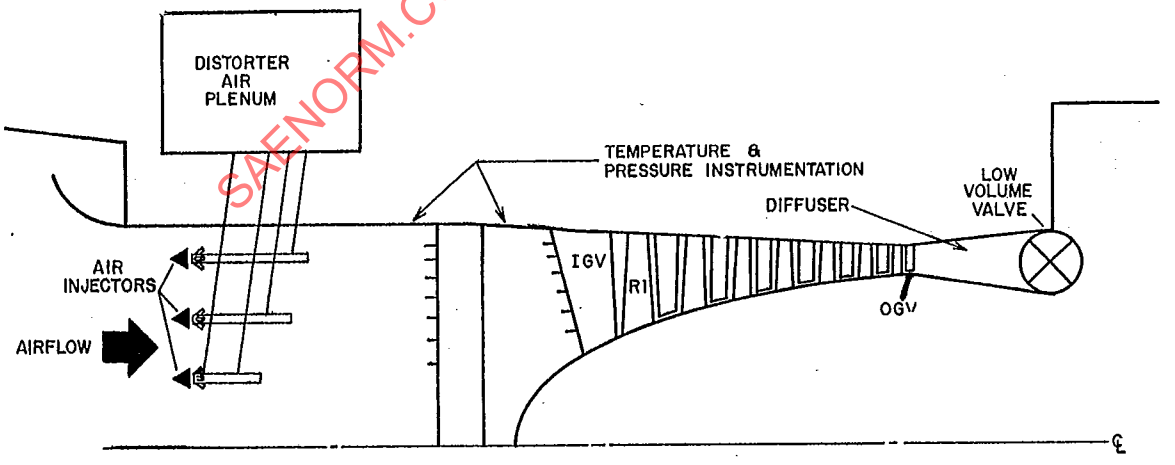

FIGURE 5.13 Compressor Rig Test With Airjet Distortion Generator Installed

5.2.2.3 Compressor Tests

Initial assessments of compression system sensitivity to inlet distortion usually are made by compressor rig testing. A typical test sequence starts with a baseline test conducted with a "clean inlet" configuration, as discussed in Paragraph 5.2.1. The test facility is then modified to include distortion-producing devices, and distorted-flow compressor maps are produced for each distortion pattern.

Total-pressure distortion at the inlet of a multi-component system is converted to combined pressure and temperature distortion at the inlets of down-stream compression-system components. It may be desirable, therefore, to test HP compressors with both pressure and temperature distortion patterns. Figure 5.13 is a schematic of an airjet distortion system which accomplishes this objective by injecting high-temperature, high-pressure air at appropriate angles to the inlet flow. The injection angle determines the degree of pressure distortion included in the pattern. Another system for producing temperature and pressure distortions involves the use of hydrogen burners in combination with screens (Figure 5.14).

The compressor rig test results are analyzed to assess compressor sensitivity to each inlet distortion pattern. The typical test sequence involves testing with classical patterns such as "pure" 180 degree-circumferential, tip-radial, and hub-radial patterns and then proceeding to more complex patterns such as graded-radial patterns, combined radial and circumferential patterns, and two per rev patterns. The classical pattern test data serve to define basic compressor distortion sensitivities and offset coefficients, while the complex pattern data allow generalized sensitivities to be derived.

Testing on a compressor rig imposes constraints which may affect the applicability of the rig test results to a complete engine. Insofar as practical, the compressor rig should include a simulation of downstream components if these are anticipated to affect the distortion sensitivity of the compressor. Aeromechanical constraints may prohibit testing with high levels of distortion, and rig drive-power limitations may preclude testing above design speed.

5.2.2.4 Engine Tests

Engine tests are conducted to establish the overall effects of AIP total-pressure distortion on engine performance and stability, verify installed compressor sensitivity coefficients and distortion transfer characteristics, and confirm initial distortion assessments. Tests at selected environmental operating conditions are performed over a range of fixed-throttle settings and PLA transients (accel/decel rates) with representative customer bleeds and power extractions. Diagnostic tests with the normal control functions muted can be carried out, and classical or parametric patterns can be tested to determine the distortion sensitivity characteristics of multi-spool compression systems using heavily-instrumented engines. For qualification or certification testing, test matrix requirements are generally limited to specified engine and environmental "rating" conditions using flight-type distortion patterns.

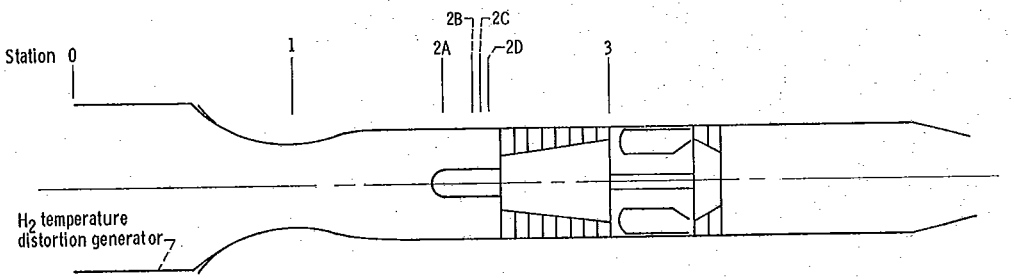

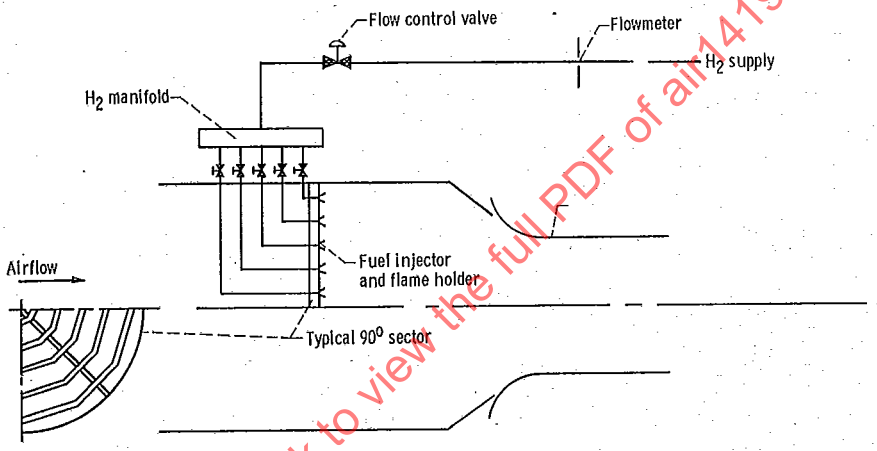

(a) Schematic of installation.

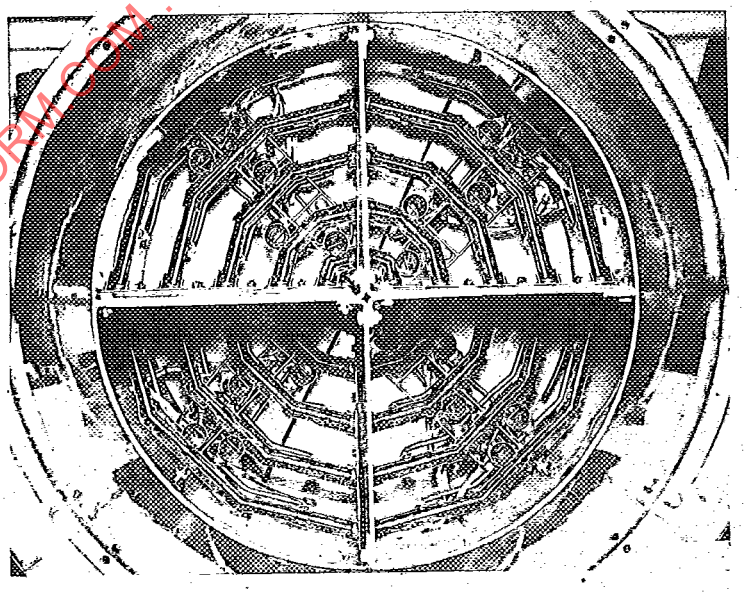

(b) Photograph looking upstream.

FIGURE 5.14 Test Configuration for Temperature Distortion Testing

Engine tests with steady-state inlet-flow distortion are performed in the test installations used for baseline clean-flow engine performance and stability test assessments, modified to include a selected steady-state distortion generator. An engine inlet-airflow metering system, such as a critical-flow venturi, forward of the inlet plenum provides accurate engine airflow measurements while testing with the steady-state distortion generator. Engine-installed compressor loading test techniques to assess installed compressor stability limits may be employed (Paragraph 5.4).

5.2.3 TIME-VARIANT TOTAL-PRESSURE DISTORTION

Tests with time-variant inlet total-pressure distortion may be required to assess the effect of random- and discrete-frequency pressure fluctuations on compression-system stability and performance. Time-variant distortion analysis techniques are similar to steady-state techniques, except that the inlet data are filtered via analog and/or digital data processing systems to match the compression system dynamic response characteristics. The objective of the tests is to correlate surge or stall events with the maximum time-variant distortion level producing the instability. A "low-pass" filter with a cutoff frequency of 1/2 to 1 times the compressor rotor speed is sufficient to assess the response of most current engines (Reference 32).

5.2.3.1 Random Frequency Generators

An example of a random frequency generator installation is shown in Figure 5.15. A critical-flow convergent-divergent nozzle with a variable-position centerbody is used to generate turbulent flow by interaction of a shock wave and a boundary layer in the same manner as turbulent flow is generated in an aircraft inlet. A turbulence attenuation screen located downstream of the venturi may be used to modify the characteristics of the turbulent flow system. The centerbody may be offset to obtain asymmetric distortion patterns. The random frequency generator (RFG) should simulate the length/volume characteristics of the aircraft inlet duct from the inlet throat to the compressor face.

Random frequency generators may be designed to simulate specific inlet configurations. The two-dimensional random frequency generator, reported in Reference 6 (Figure 5.16), is designed to produce distortion patterns which are similar in shape, level and dynamic content to those obtained from two-dimensional inlet models. Testing an engine with the generator provides a means for evaluating pressure distortion sensitivity and transfer characteristics as well as engine/control performance in a realistic environment prior to inlet/engine and flight testing. The random frequency generator consists of a duct 39.85 inches square and 18.5 feet long. The upper and lower duct walls each consist of three articulated ramps that may be positioned remotely using screw jacks. Changing the flow channel geometry by positioning these ramps induces distortion via boundary layer separation and shock/boundary layer interaction. Distortion level and extent is controlled by the particular geometry of the ramp positions and airflow. The turbulence level and ratio of unsteady to steady-state distortion is controlled by a full-span monoporosity screen located just behind the aft ramp. The distortion levels produced by the RFG are, in general, controllable and repeatable.

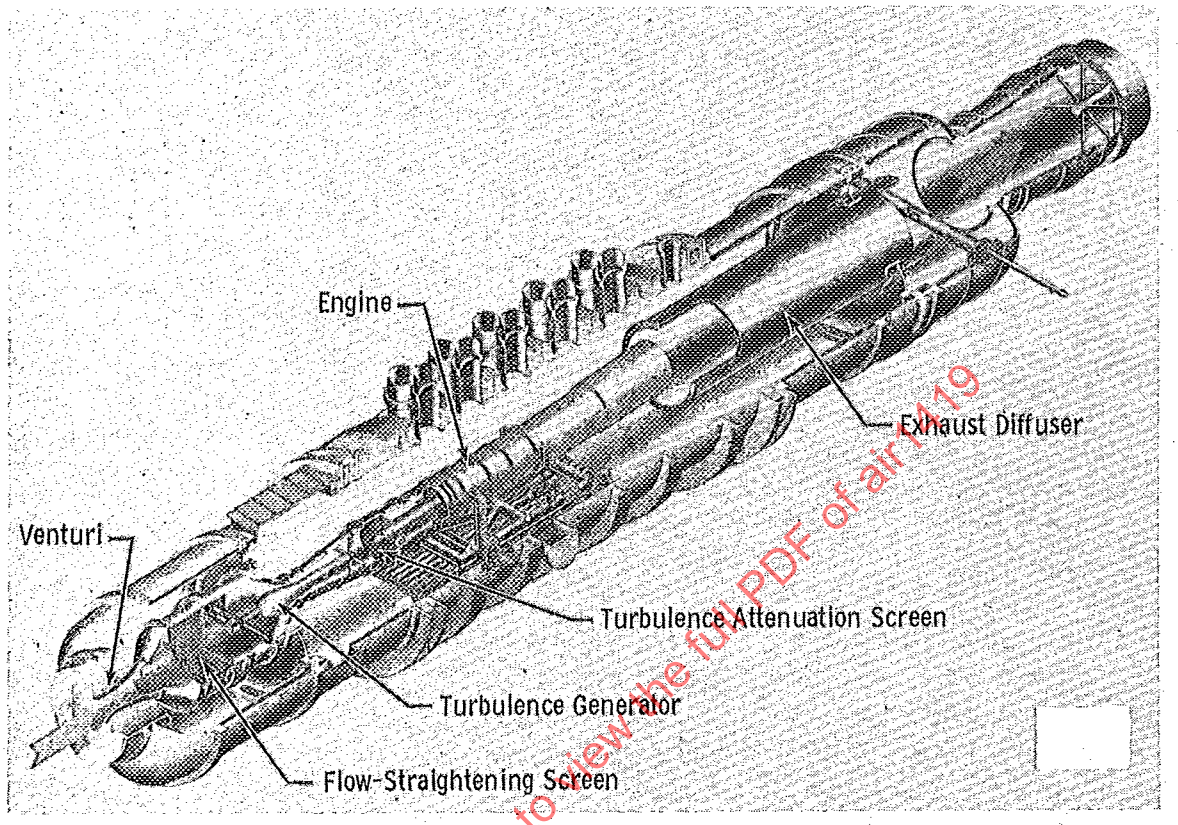

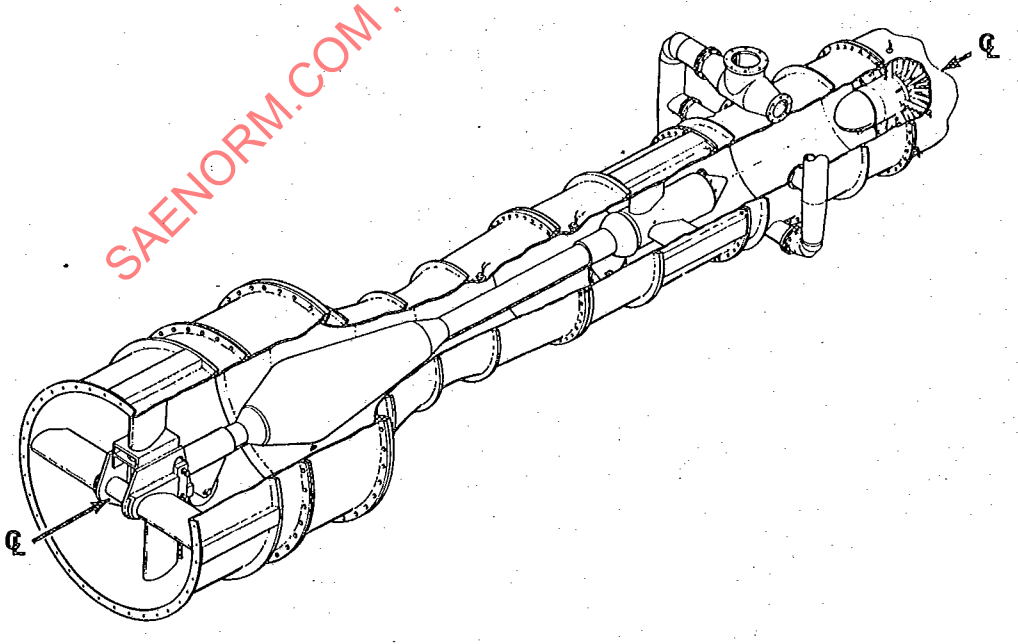

FIGURE 5.15 Typical Random Frequency Generator Test Installation for Engine Stability Assessment

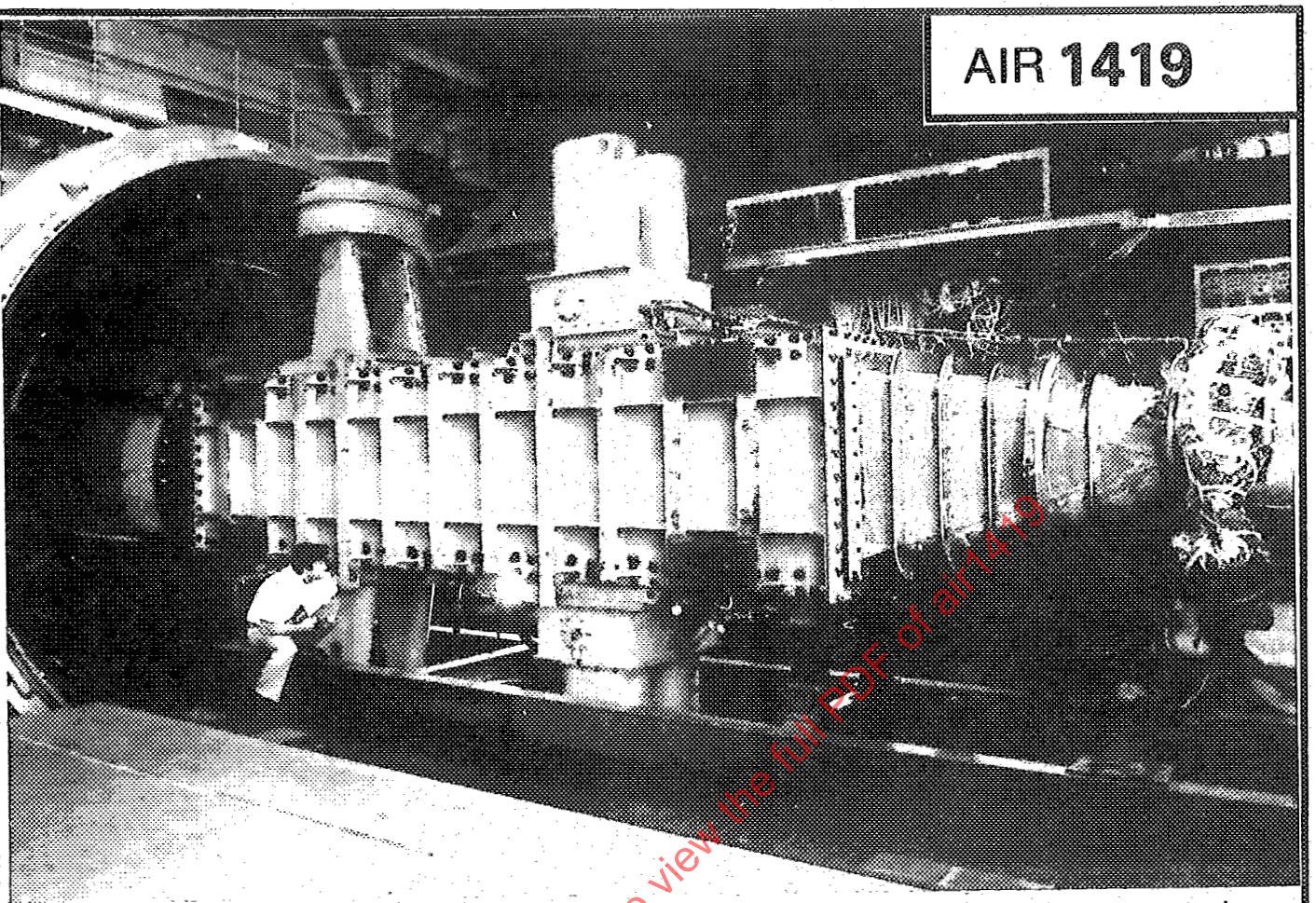

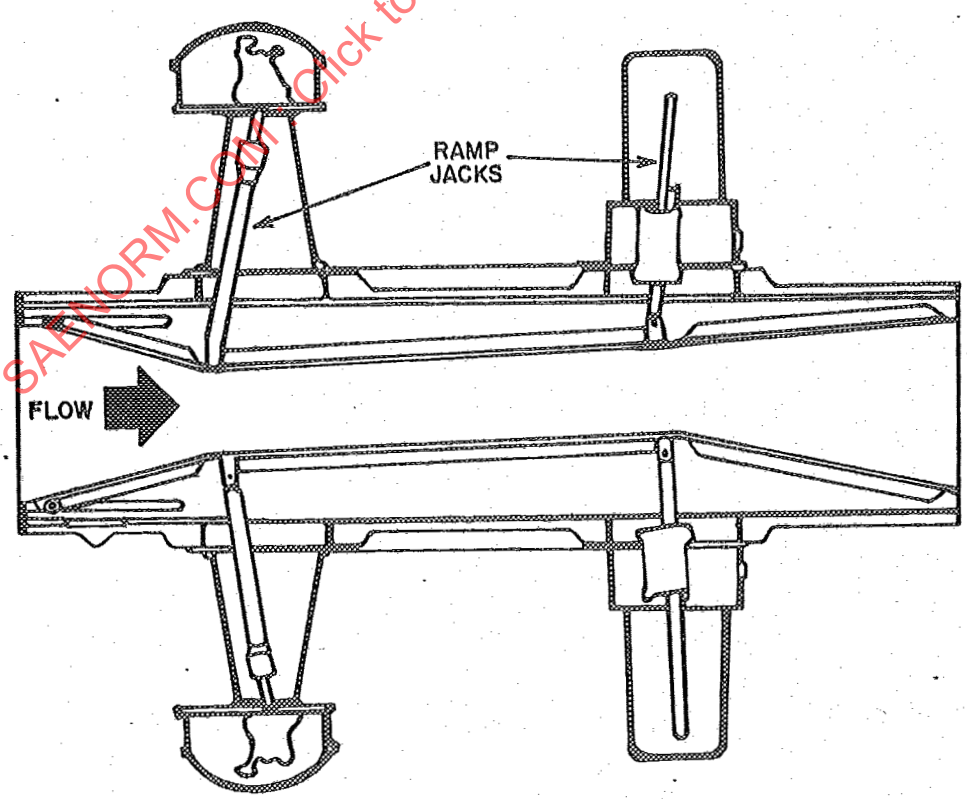

FIGURE 5.16 Random Frequency Generator Designed to Simulate Flow Conditions of Two-Dimensional Inlet Configuration

Typical RFG test results are shown in Figure 5.17. The data were acquired with an analog recording system and were digitized for off-line analysis. The data were filtered to a time constant nearly equal to one engine revolution. The curves show (a) one second of data with an engine stall near 0.80 seconds and (b) calculated distortion parameters and face-average pressure in an expanded region from 0.75 seconds to 0.85 seconds.

Another method for generating AIP time-variant distortion involves the use of a perforated plate simulator designed to reproduce the AIP steady-state total-pressure distortion pattern and the statistical characteristics of the inlet flow. An arrangement of slots or holes in the plate can be adjusted to reproduce steady-state and local RMS, pressure contours, amplitude probability density, and spectral density characteristics (Reference 33). High-response AIP instrumentation is required to develop the simulator.

5.2.3.2 Discrete Frequency Generators

Discrete-frequency pressure fluctuations occur in an aircraft inlet duct due to turbulence and as a result of inlet instability, such as buzz, or as a result of duct resonances. The propagation characteristics, the surge, and the performance effects of the planar inlet pressure fluctuations may be determined using discrete-frequency generators. They are effective tools for evaluating time-variant analytical models which describe the dynamic behavior of compressors.

Several types of discrete frequency generators have been developed. The air jet distortion generator designs reported in References 30 and 31 have discrete frequency pressure pulse capabilities. A rotor/stator flow blockage design is reported in Reference 34. The generator consists of a rotor installed between matched stator assemblies. The output frequency of the generator is controlled remotely by varying the speed of the rotor. The amplitude of the pressure fluctuations can be varied by changing the solidity (blockage) of the rotor/stator assemblies. A similar design concept, the Planar-Pressure-Pulse-Generator (P^3G) is reported in Reference 16. The P^3G is a choked-flow device which uses a single-stage rotor and stator combination to sinusoidally modulate the minimum area. The frequency of the planar waves is governed by the rotor-to-stator spacing (Figure 5.18). An advantage of this device is its ability to produce planar waves with peak-to-peak amplitudes of 10 to 30 percent of the mean total pressure over a frequency range from 420 to 800 Hz.

5.3 PROPULSION SYSTEM TESTS

Testing of the integrated inlet/engine system prior to installation in the flight test aircraft provides the first verification of installed performance and inlet/engine compatibility. Tests on a representative system may be carried out on a sea-level-static test stand, in an altitude-propulsion wind tunnel or a flying test bed, depending on installation and program requirements. Flight testing demonstrates and verifies the performance and compatibility of the propulsion system over flight/maneuver envelopes of the flight test aircraft.

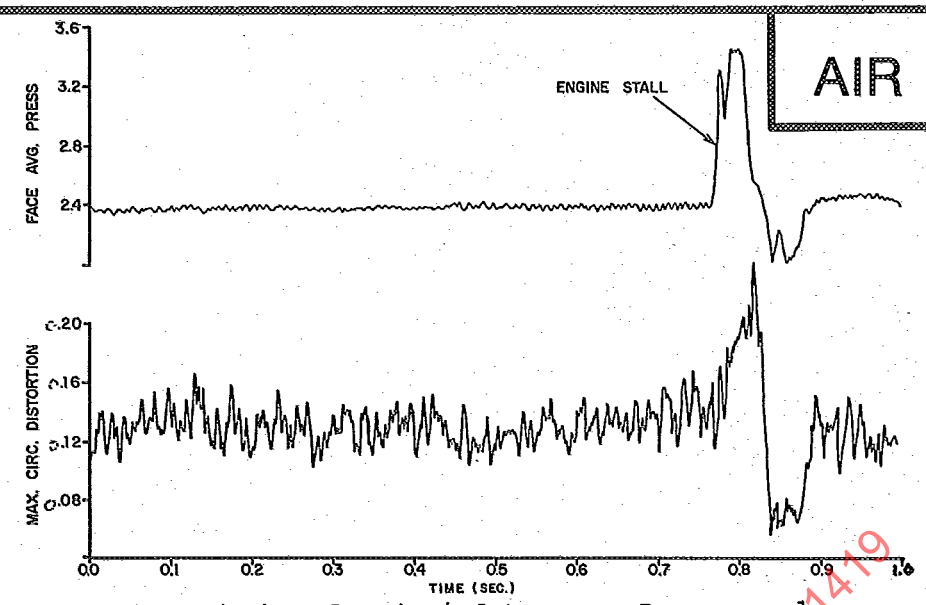

(a) Variation of Engine/Inlet Average Pressure and Circumferential Distortion at Onset of Stall

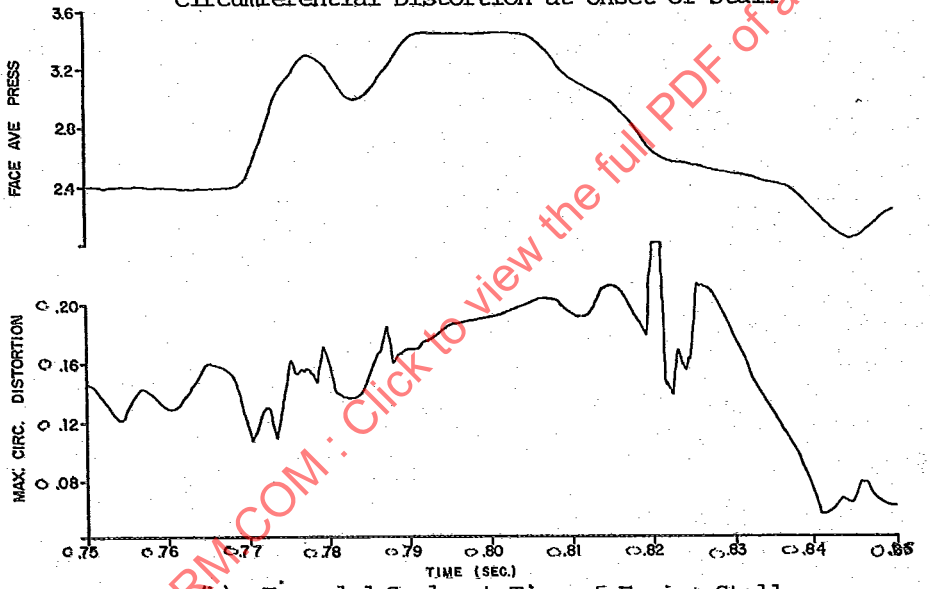

(b) Expanded Scale at Time of Engine Stall

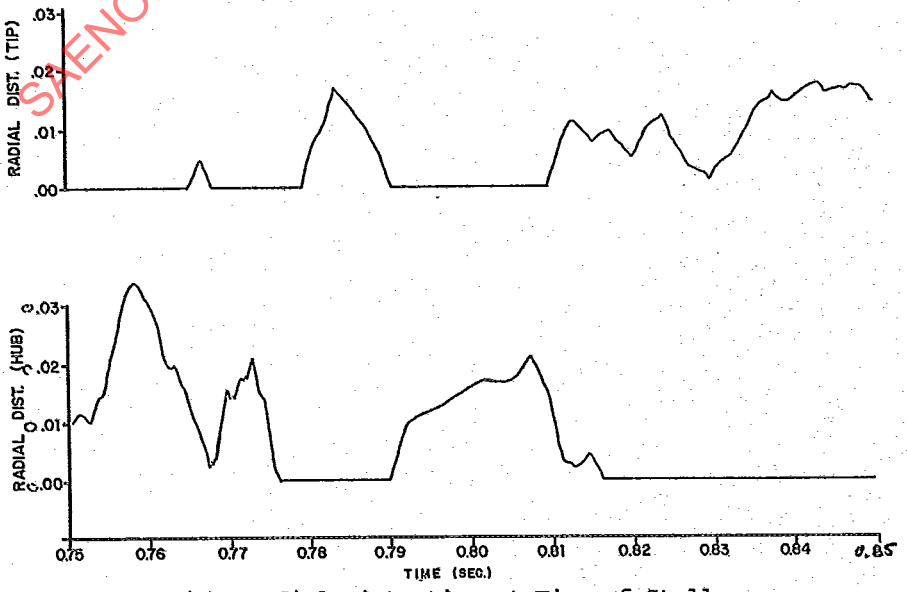

(c) Radial Distortion at Time of Stall

FIGURE 5.17 Typical Engine Test Results Obtained with a Random Frequency Generator

AIR 1419

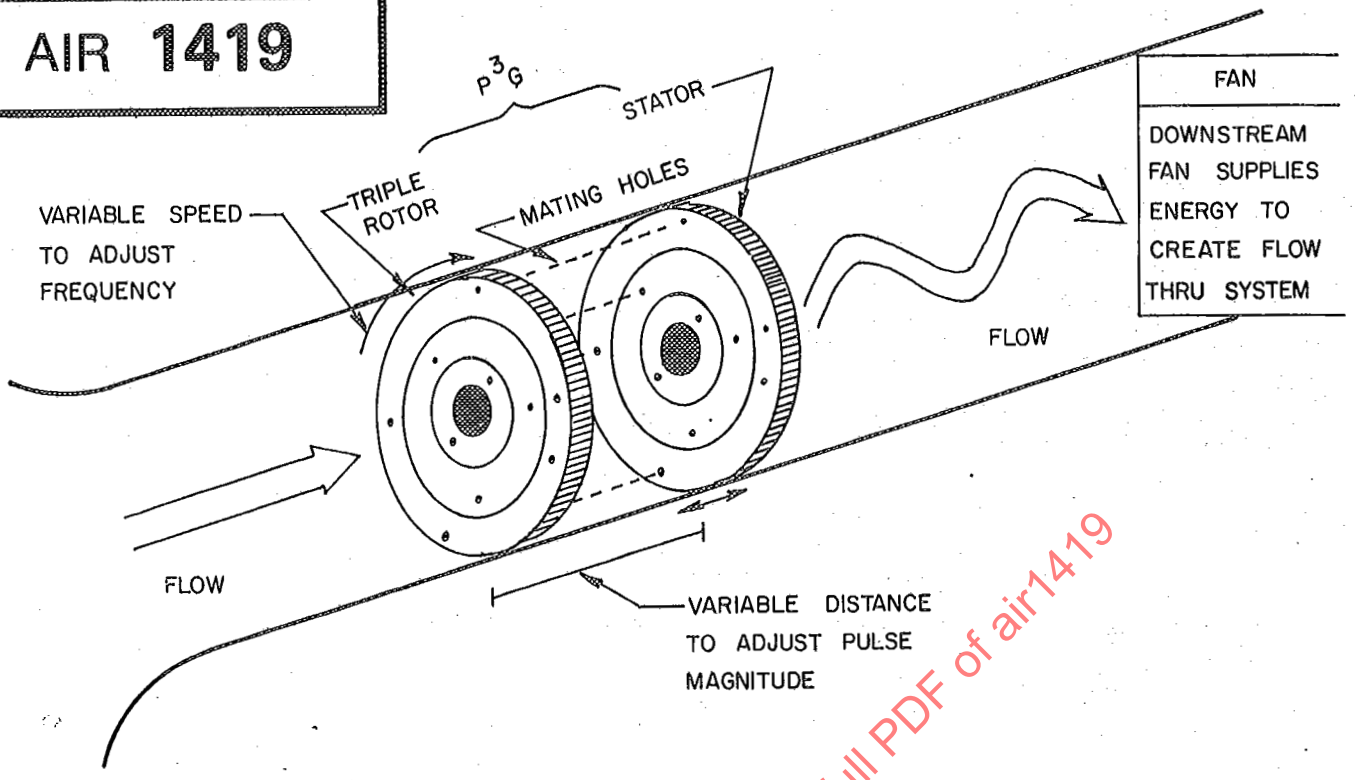

FIGURE 5.18 Schematic of Planar Pressure Pulse Generator

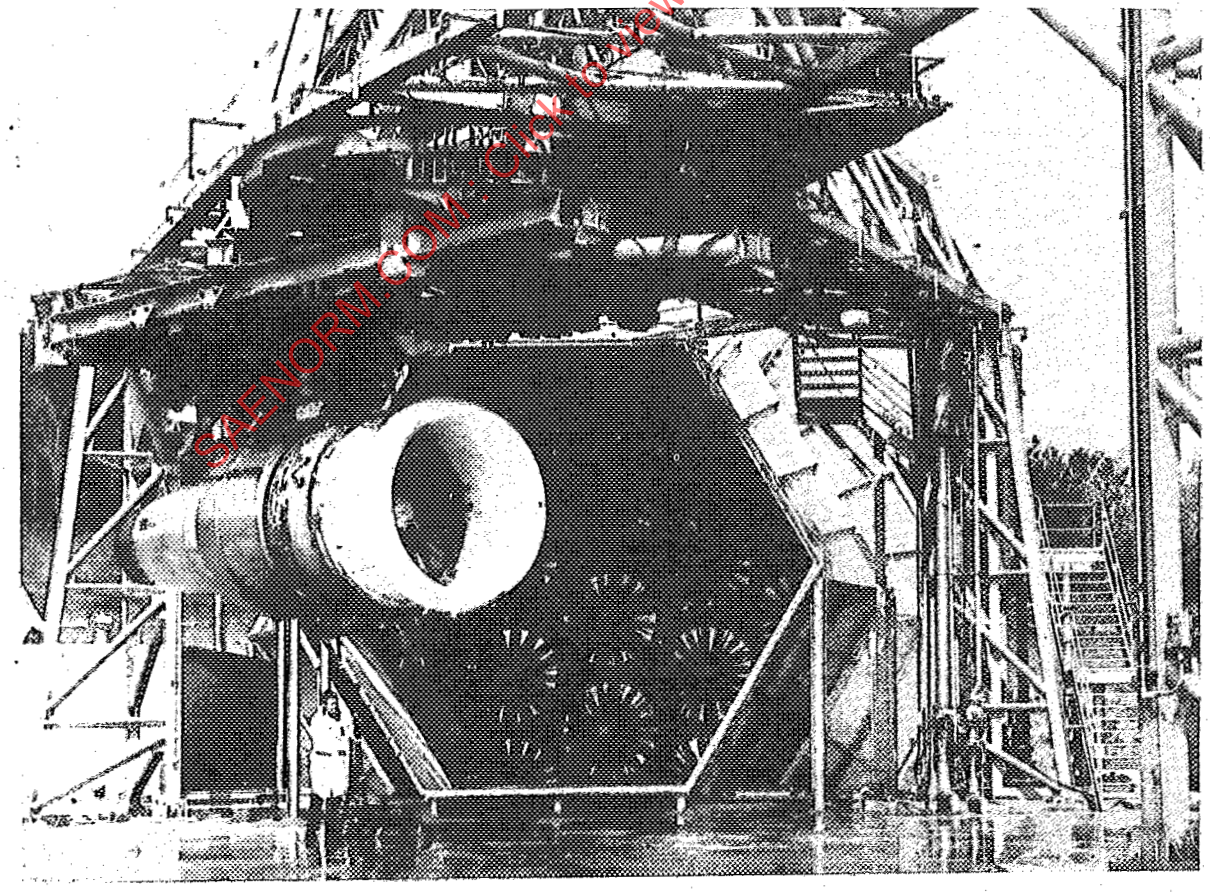

FIGURE 5.19 Peebles Crosswind Facility

The types of test, primary test objectives, and basic data requirements which may be needed for system development are shown in Table 5.3. Primary considerations for the selection of the desired test techniques for specific programs include: (1) test model availability and cost, (2) test condition/ matrix requirements, (3) data and instrumentation system considerations, and (4) test facility requirements/limitations.

5.3.1 STATIC TESTS

Static tests of the inlet/engine system can provide an early indication of inlet/engine operation at take-off. Test configurations represent the aircraft as closely as possible and include simulation of the ground plane, adjacent aircraft structure or adjacent engine, as appropriate. Tests enable the effects of the external environment on the flow quality at the AIP to be established at static or near-static conditions.

The General Electric Peebles Cross-Wind Facility (Figure 5.19) was designed for testing large turbofan engines and determining the effects of winds ranging from quartering tailwinds to headwinds. The facility is composed of 13 individually controlled fans capable of creating uniform-velocity flows ranging from 15 to 78 knots, and has a capability for ground plane simulation and ground vortex suppression.

5.3.2 WIND TUNNEL TESTS

In aircraft programs involving significant advances in the state-of-the-art, inlet/engine tests in a wind tunnel can prove to be a cost-effective way of demonstrating inlet/engine compatibility prior to the start of flight testing.

Inlet tests with a cold pipe installation (no engine present) can be conducted to determine the full-scale inlet characteristics over a wide range of inlet mass flow ratios. These tests provide airflow calibrations for subsequent use in tests with the engine. Although complete aircraft maneuvers envelopes cannot be explored, tests with off-scheduled inlet geometry can be conducted to simulate distortion characteristics observed during previous sub-scale tests throughout the maneuver envelope. The effects of known external disturbances (external weapons, control vanes, weapon bay doors and others) can be simulated. If variable geometry inlets are employed, programs usually include a second, cold-pipe phase consisting of development tests of the inlet and inlet control system. Use of the actual aircraft control system, if timing permits, can be an effective means of system checkout and of minimizing the flight test development program, particularly for supersonic aircraft. The third test phase includes all three elements: inlet, inlet control system, and engine including the engine control system. Emphasis is placed on demonstrating inlet/engine compatibility over a complete range of equilibrium operating conditions and engine throttle transients at critical flight conditions. Techniques for intentionally stalling the engine to determine structural loads and to verify the system stability limits can be employed. Engine distortion limits can be explored by off-scheduling inlet geometry to generate high distortion levels. The use of

TABLE 5.3

Propulsion System Tests

Objective	Tests	Data
System Performance and Stability Verification at Sea-Level-Static	Static Tests with Simulated Ground Plane and Forebody	Stability and Performance Time-Variant Distortions Inlet Recovery Surge Pressure Ratio Cross Wind Effects Distortion Transfer Power Transients
Pre-Flight Performance and Stability Verification at Altitude	Altitude Test Cell/Propulsion Wind Tunnel Tests With Simulated Flight Envelope	Time-Variant Distortion Reynolds Number Effects Inlet Recovery Stability and Performance Inlet Stability Range (Buzz-Unstart-Supercritical) Failure Modes Transients Control Interactions Distortion Transfer
In-Flight Performance and Stability Verification over Flight and Maneuver Envelopes	Ground and Flight Test Development in Aircraft	Stability and Performance Inlet Distortion at Critical Flight Conditions Additional Pattern Data Bank Aircraft Dynamics Weapon Firing Reingestion Behavioral Statistics Control Interactions

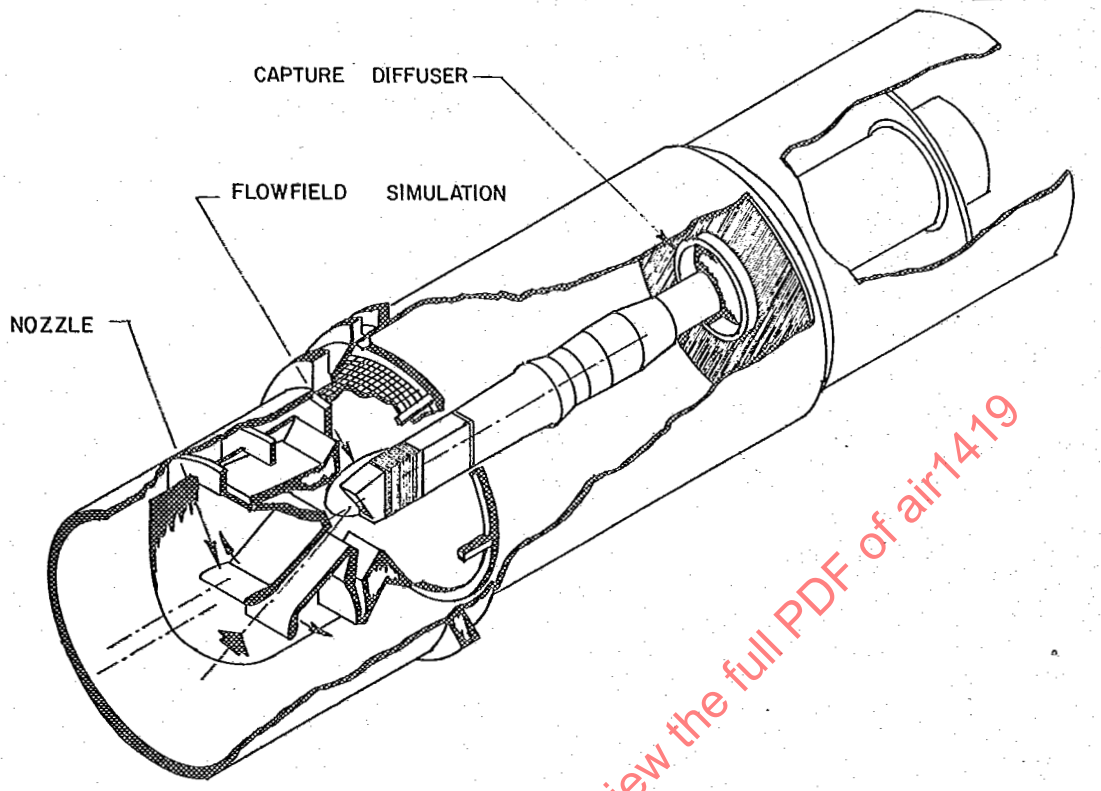

FIGURE 5.20 Free-jet Propulsion-System Test Installation Schematic

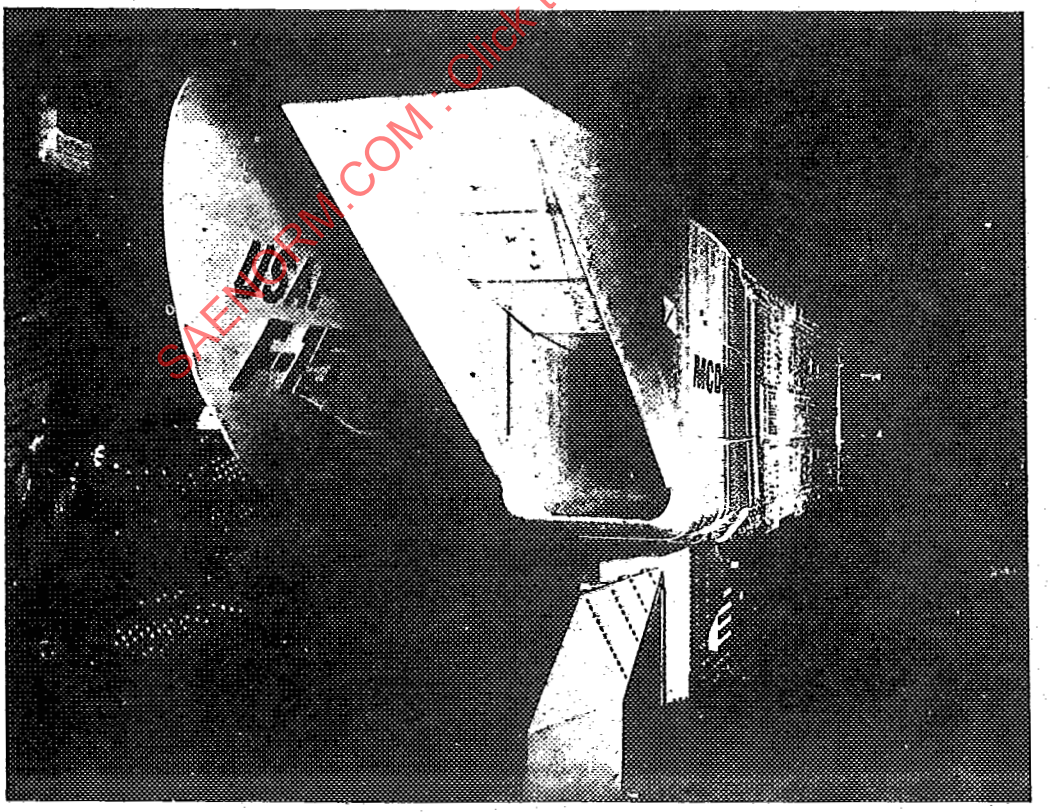

FIGURE 5.21 Propulsion-System Test Installation in Propulsion Wind Tunnel

flight test instrumentation and data reduction procedures during these tests can be an effective means of reducing the required effort during the flight test program. A successful program requires a high degree of coordination among the parties involved.

A schematic of a typical free-jet engine test facility is presented in Figure 5.20. The test facility is configured to duplicate the inlet environmental operating conditions at selected points in the flight and maneuver envelopes for defined propulsion system operating conditions. A propulsion wind tunnel test installation is shown in Figure 5.21.

Model size requirements have a significant effect on the selection of desired propulsion system test techniques. The historical growth in engine airflow requirements has led to increased test facility airflow requirements. Semifree jet (inlet simulator) techniques can be used where test facility limitations exist. Semifree jet tests may be used to produce inlet/engine interface flow conditions to a high degree of fidelity over the operating range of the propulsion system. An example of an inlet design simulating an aircraft inlet system downstream of the initial compression shocks of an external compression inlet is reported in Reference 35. Figure 5.22 illustrates the basic concepts of the simulator.

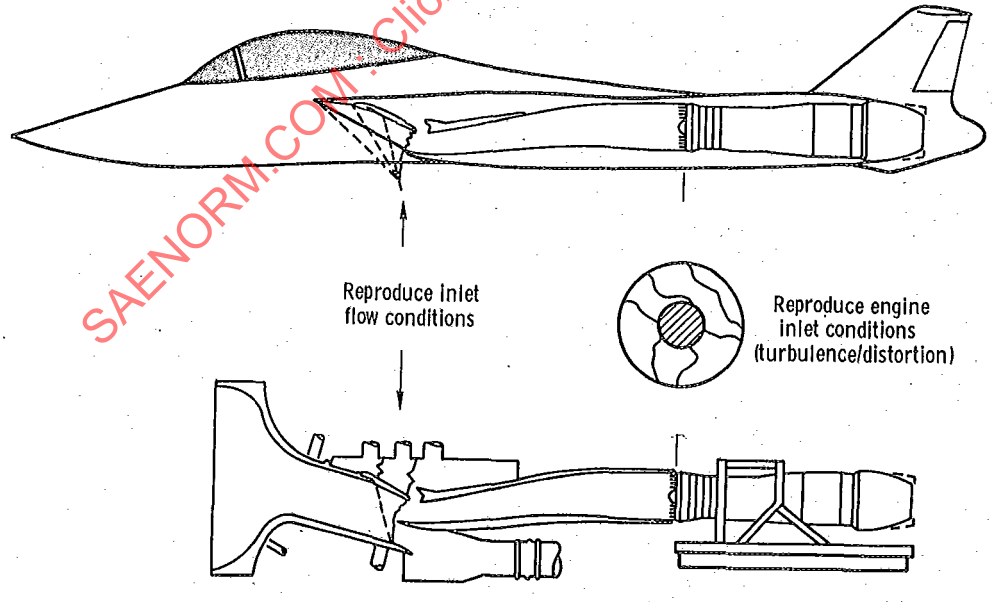

FIGURE 5.22 Schematic of Inlet Simulator

5.3.3 FLIGHT TESTS

Flight tests are oriented to demonstrate propulsion system operational goals and to provide verification of system performance, stability, and mechanical integrity over the aircraft flight and maneuver envelopes. Since installed surge margin is usually not measured in flight, propulsion system stability is demonstrated by operating to the aircraft-engine-surge-free limits. Flight tests will gradually expand the envelope from low speed to supersonic conditions and from nominal to extreme altitudes and attitudes. Table 5.4 lists typical conditions which are tested.

Both steady-state and high-response instrumentation may be used at the AIP. In addition, the engine(s) can be instrumented to permit measurement of internal engine performance and in-flight thrust. Flight testing provides the opportunity to verify performance and distortion levels predicted from wind tunnel data. Sufficient instrumentation should be provided to identify any propulsion problems encountered during the flight test program.

The comprehensive wind tunnel testing described in Section 5.1 and Paragraphs 5.3.1 and 5.3.2 will have provided the data to identify and correct any major system deficiencies prior to flight test. It is possible, however, that problems may be encountered during the early part of the flight test program due to ground facility constraints. Wind tunnel size limitations prevent complete duplication of the aircraft and may limit incidence and sideslip to less than the aircraft limits, and rapid changes in aircraft attitude or in-flight condition cannot be simulated properly. Significant areas need to be explored during the flight test program, particularly with respect to flight dynamics. The flight test program provides the opportunity to evaluate refinements to the propulsion system design in terms of their effects on aircraft performance and inlet/engine compatibility. For example, inlet geometry may have a significant impact on aircraft trim drag. Minor changes to inlet geometry schedules may improve performance with essentially no adverse effect on distortion. The flight test program should be structured to explore those areas where interaction between the propulsion system and the aircraft may not have been fully tested during wind tunnel tests.

Correlation of flight test and wind tunnel data provides a data bank for evaluating future modifications to the system and for the development of new aircraft. References 19 and 20 are examples of correlations between scale model and flight data.

5.4 STABILITY ASSESSMENT VERIFICATION

Test verification of the validity of stability assessments is based on a building block concept. The quantitative evaluation of all destabilizing factors cannot be assessed during a single engine or engine component test. Consequently, stability assessments at program milestones are based on the test data available at that time. Hence, test programs must be carefully controlled to maximize the applicability of test results. Stability assessments are based on experimental audits at defined propulsion system operating conditions.

TABLE 5.4

Flight Test Conditions

GROUND OPERATION
- Fod Screens
- Static Taxi Operations
- Crosswinds
- Runway Conditions

LOW SPEED OPERATION
- Rotation Takeoff
- Approach Landing
- Crosswinds
- Auxiliary Inlet Transients
- A/C Stall Characteristics
- Thrust Reverser

AIRCRAFT TRANSIENT OPERATION
- Accelerations
- Decelerations
- Automatic/Manual Inlet Controls
- Emergency Procedures

SUBSONIC PERFORMANCE
- Throttle and Augmentor Transients
- A/C Maneuvers
- A/C Control Surface Effects
- Weapon Bay Door Operation
- Weapon Release
- External Stores

SUPERSONIC PERFORMANCE
- Inlet Control - Automatic/Manual
- Throttle and Augmentor Transients
- A/C Maneuvers
- Emergency Procedures
- A/C Control Surface Effects
- External Stores

Surge margin destabilizing factors for a typical turbine engine compressor are shown in Figure 5.23 (Section 3). Normally, qualification/certification test engines are not subjected to intentional surge because of the hazard of structural damage and delays in engine qualification/certification testing. Consequently, the compressor surge line and engine stability margin requirements must be determined during component and engine development test programs conducted with qualification/certification components. Verification of the operating line excursions caused by control requirements and distortion effects may be obtained during the qualification/certification test. Engine operation in the region above the maximum predicted operating line but below the anticipated surge line(s) should be accomplished whenever practical.

A test assessment methodology intended to demonstrate remaining margin, is illustrated in Figure 5.24. In the example shown, an equivalent maximum operating line is established to account for the estimated internal effects (engine quality and deterioration) margin allocations of the stability assessment. By using the equivalent maximum operating line, a portion of the remaining margin (estimated net margin available to assure stable operation) can be demonstrated during engine testing (Figure 5.25) without subjecting the engine to surge.

Several installed compressor loading techniques are available for this purpose. These techniques can be divided into two general classifications, transient and steady-state loading methods. The most extensively used transient technique is the fuel step method which is based on the use of a controlled transient fuel step to increase the compressor ratio above the normal transient or equilibrium operating line. The technique usually requires only minor test equipment modifications, but does require transient measurements. Steady-state loading techniques include flow-blockage methods such as "inflow bleed" or mechanical blockage systems (Figure 5.26). Use of either system is straightforward with single fixed-geometry rotor configurations. By simultaneous use of both systems, selected rotor speed ratios can be controlled during loading of dual rotor configurations, as illustrated in Figure 5.27 (Reference 36).

Defined engine and environmental boundary conditions are necessary for engine stability tests. Typical criteria are listed in Figure 5.28. The inlet/engine interface criteria are based on a projected flight condition (mission requirement) and are specified using a point-by-point distortion pattern definition. Other environmental criteria which require definition are the projected aircraft service requirements such as compressor bleed and power extraction. Engine operating conditions are defined in terms of corrected rotor speed, corrected rotor speed ratio, engine service bleeds, and control mode operation. The operating condition matrix should be organized on a building block concept. Baseline data are established first; then the various destabilizing factors (Reynolds number, inlet distortion, control mode, and aircraft service requirements) are evaluated.

5.5 PERFORMANCE ASSESSMENT VERIFICATION

Test verification of performance assessments may be required to validate the effects of inlet flow distortion on engine thrust, fuel consumption and airflow.

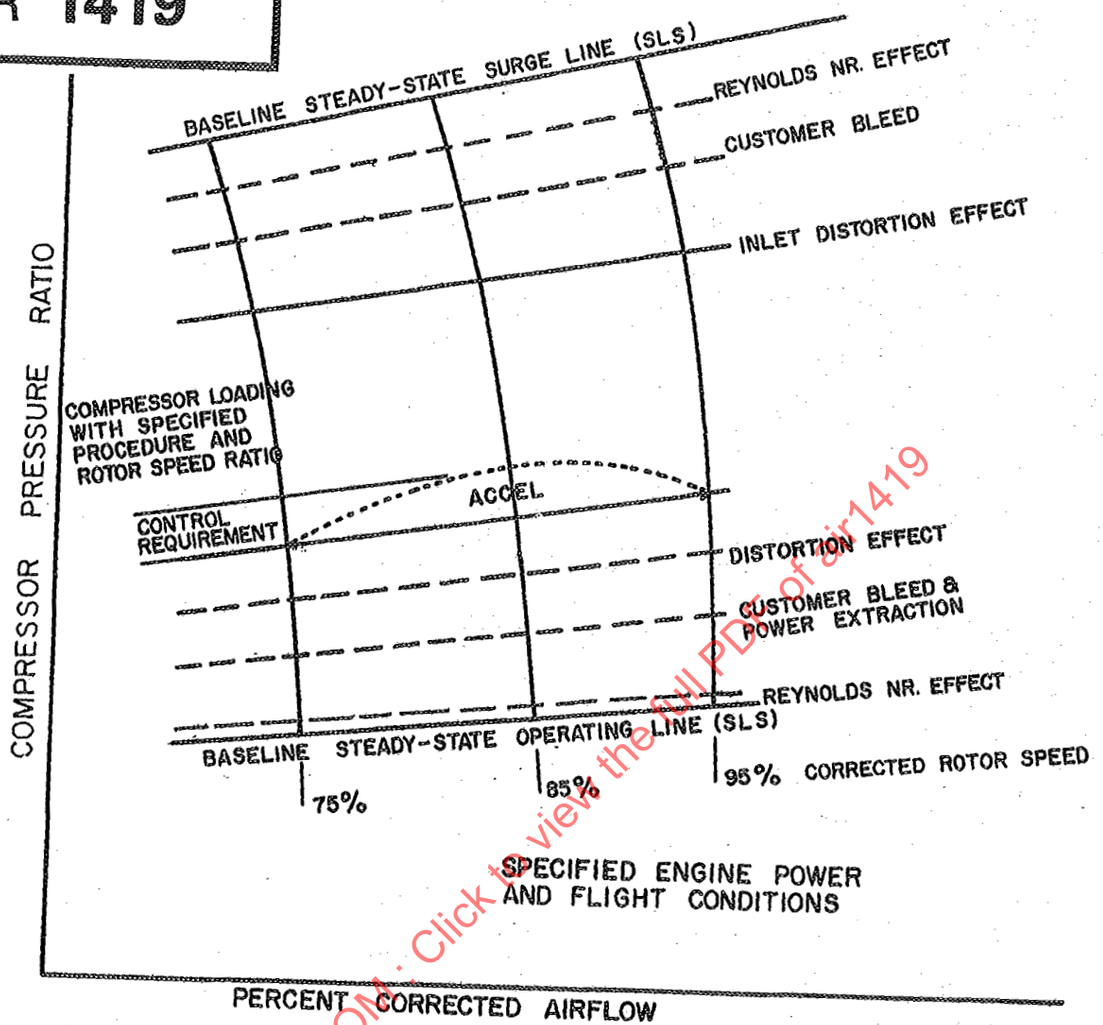

FIGURE 5.23 Typical Test Data Base/Test Matrix Requirements for Stability Assessment Verification

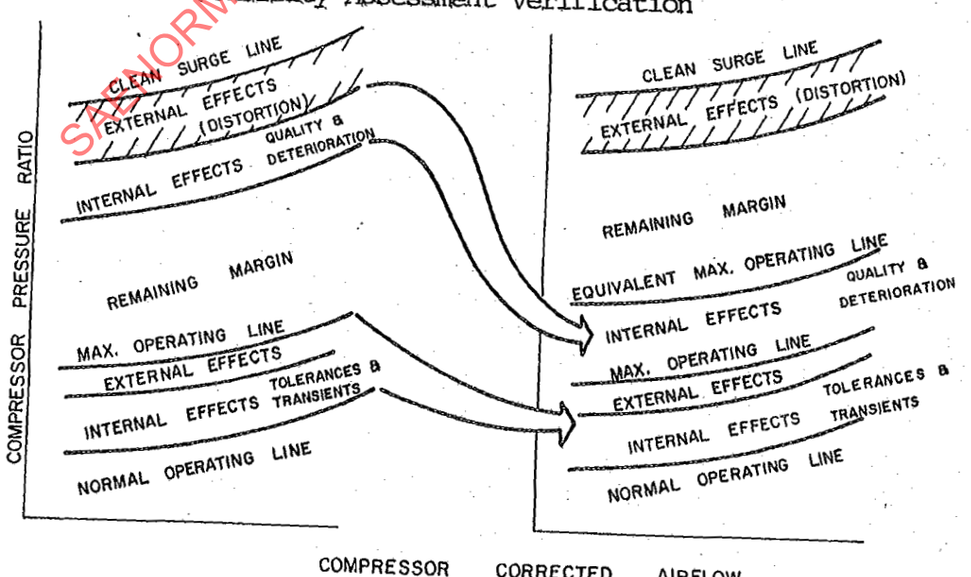

FIGURE 5.24 Stability Assessment Test Verification Methodology

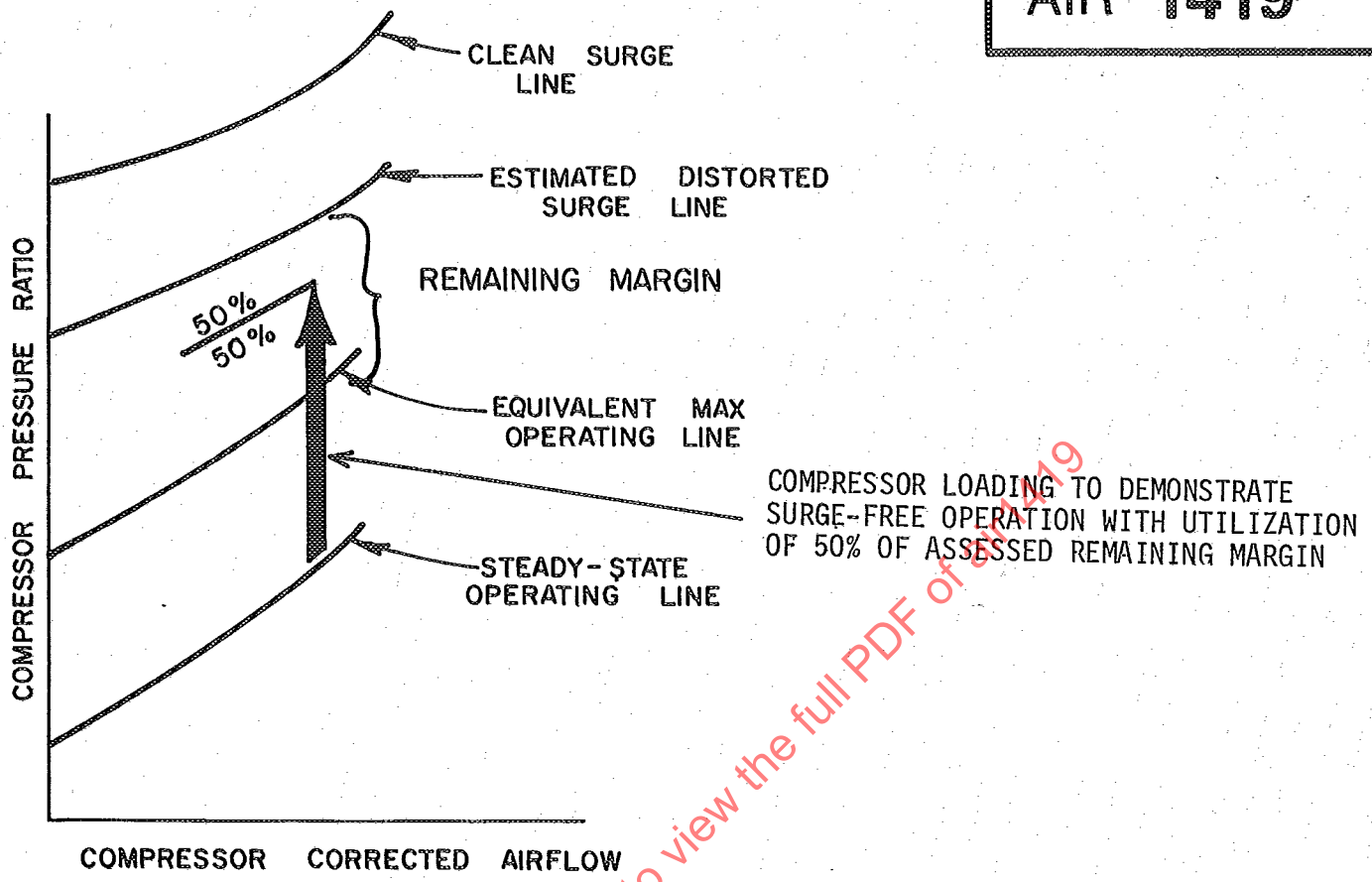

FIGURE 5.25 Test Procedure to Demonstrate Available Margin

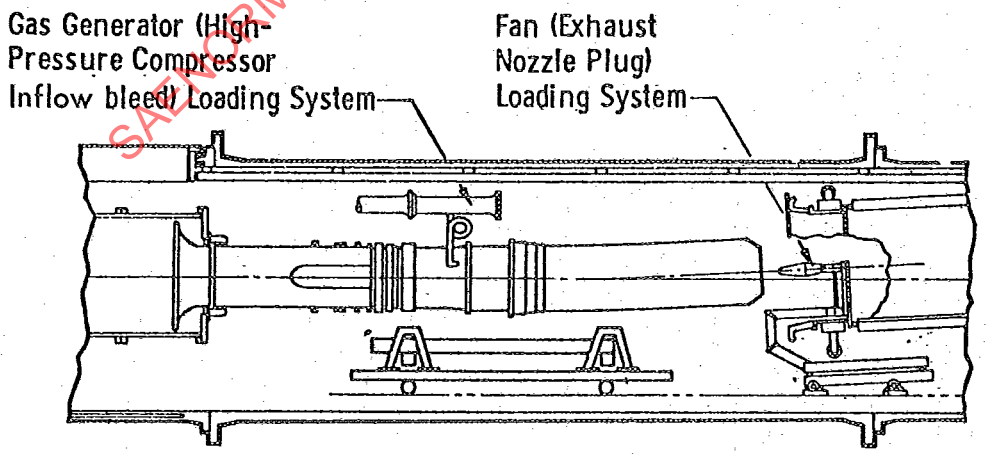

FIGURE 5.26 Schematic of Test Hardware for Simultaneous Loading of Fan and Gas Generator Hardware

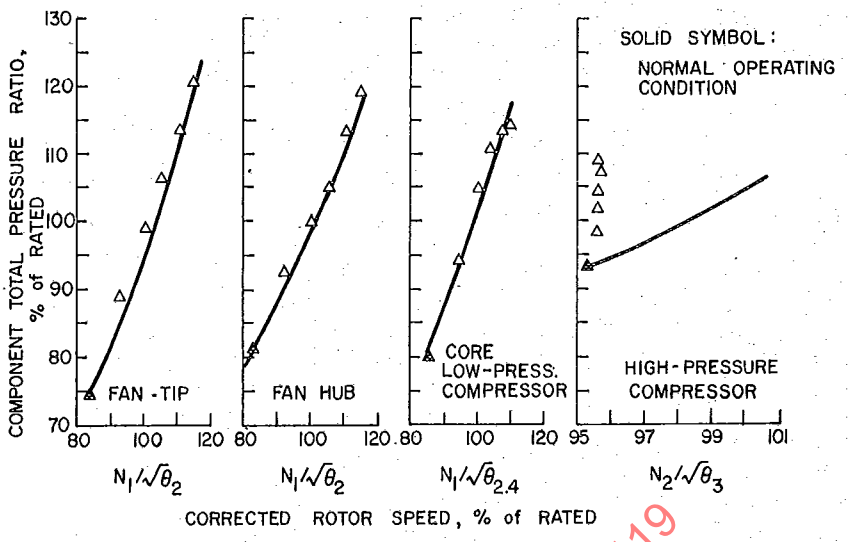

(a) High Pressure Compressor Inbleed Loading with Corrected Rotor Speed, $N/\sqrt{\theta}$=95.6 Percent

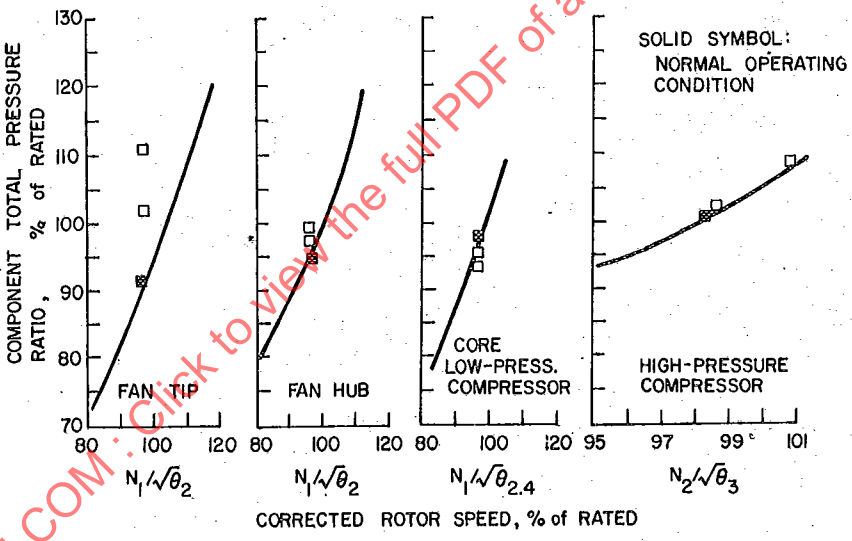

(b) Fan Loading with Corrected Low-Pressure Compressor Rotor Speed, $N/\sqrt{\theta}$=96 Percent

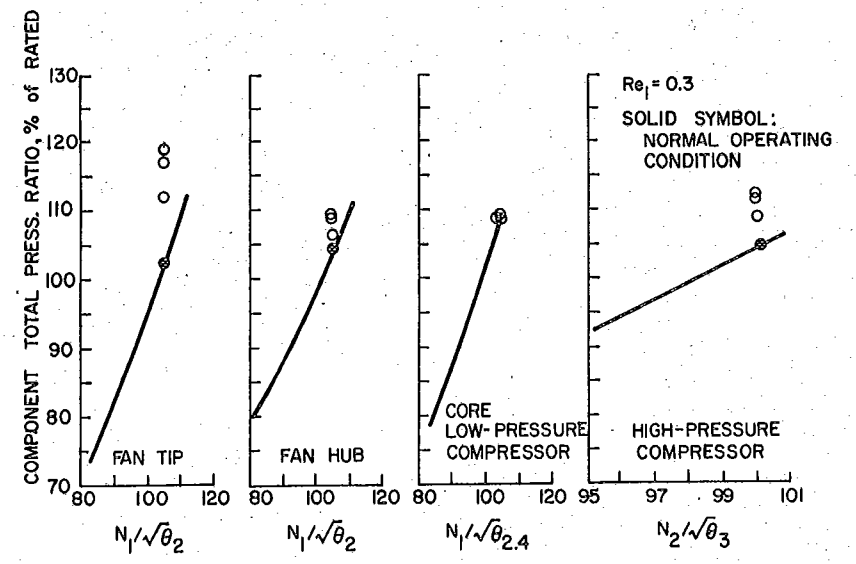

(c) Simultaneous Loading of Fan and Compressor

FIGURE 5.27 Compressor Operating Characteristics During Compressor Loading Operations

INLET-ENGINE INTERFACE CONDITIONS

INLET	ENGINE
Corrected Airflow	Corrected Airflow
Altitude	Altitude
Mach Number	Total Pressure
Ram Recovery	Total Temperature
Angle of Attack	Distortion Pattern (Point-by-Point Definition)
Angle of Yaw	

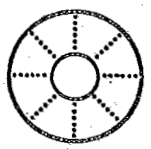

Instrumentation Definition

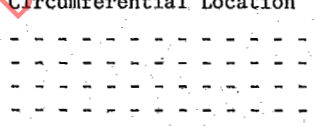

Installation Interface Conditions (Aircraft Service Requirements)
- Customer Bleed
- Power Extraction

Engine Operating Conditions
- Corrected Rotor Speed
- Corrected Rotor Speed Ratio
- Engine Service Bleeds (Intercompressor, Anti-Ice)
- Control Function - Steady-State (SS), Transient
- Control Operating Mode - Afterburning, Nonafterburning

FIGURE 5.28 Engine and Environmental Condition Criteria for Test Verification of Stability Assessments

The most significant engine test objective is, in many cases, the evaluation of engine/control system interactions and engine-rotor-speed rematch characteristics with inlet flow distortion. For example, maximum-power engine performance may be control-limited at different engine operating conditions with or without inlet distortion; or engine performance, at a selected thrust level may vary due to rotor speed rematch. (Section 4.0)

Performance tests are conducted on defined engine and environmental boundary conditions, as discussed for stability assessments (Figure 5.28). The effects of inlet distortion may be assessed directly in terms of installed thrust, airflow, and fuel consumption for a defined AIP distortion pattern or, in terms of thrust, airflow, and fuel consumption changes relative to uniform inlet flow performance for the defined pattern. Because the impact of inlet flow distortion may be small relative to experimental measurement uncertainties, it may be desirable to conduct tests in a back-to-back mode (with and without a defined inlet distortion pattern) to minimize the effect of measurement bias errors. Back-to-back testing with and without inlet distortion screens may not always be practical in direct-connect test installations because test operations must be interrupted to manually install the inlet distortion screen. For specific applications, specialized test configurations may be used to provide an "on-line" inlet distortion screen change capability. A screen changer assembly successfully used for small engine testing is illustrated in Figure 5.29. The operating time required to change screens is on the order of one-half second. Engine power is reduced during the screen change transition period to reduce the possiblities of engine operational instabilities during the screen change transient.

The air jet distortion generator is also a potential tool for back-to-back testing with and without inlet flow distortion. Transitions from uniform inlet flow conditions to defined inlet flow distortion patterns may be accomplished in time periods on the order of 90 seconds with the engine operating at a fixed power level.

Two basic engine thrust measurement techniques are used for engine performance assessments in ground test facilities. Both can be employed for distortion tests and are comparable in terms of measurement uncertainty with uniform (undistorted) flow engine tests. Use of both techniques simultaneously provides maximum understanding and the best assessment of engine thrust. The external force balance method (Figure 5.30a) requires assessment of the flowstream force at the inlet of the thrust-stand-mounted engine inlet duct. The measurement uncertainty of the stream force is higher in a non-uniform flow field and may significantly affect thrust measurement uncertainties during testing with inlet flow distortion. The internal force balance method (Figure 5.30b) is an alternative way of testing to assess the effects of inlet distortion on engine thrust performance. Engine fuel flow and engine exhaust ambient pressure measurement uncertainties usually are not impacted by inlet flow distortion so that conventional measurement techniques may be used to assess engine performance with and without inlet flow distortion.

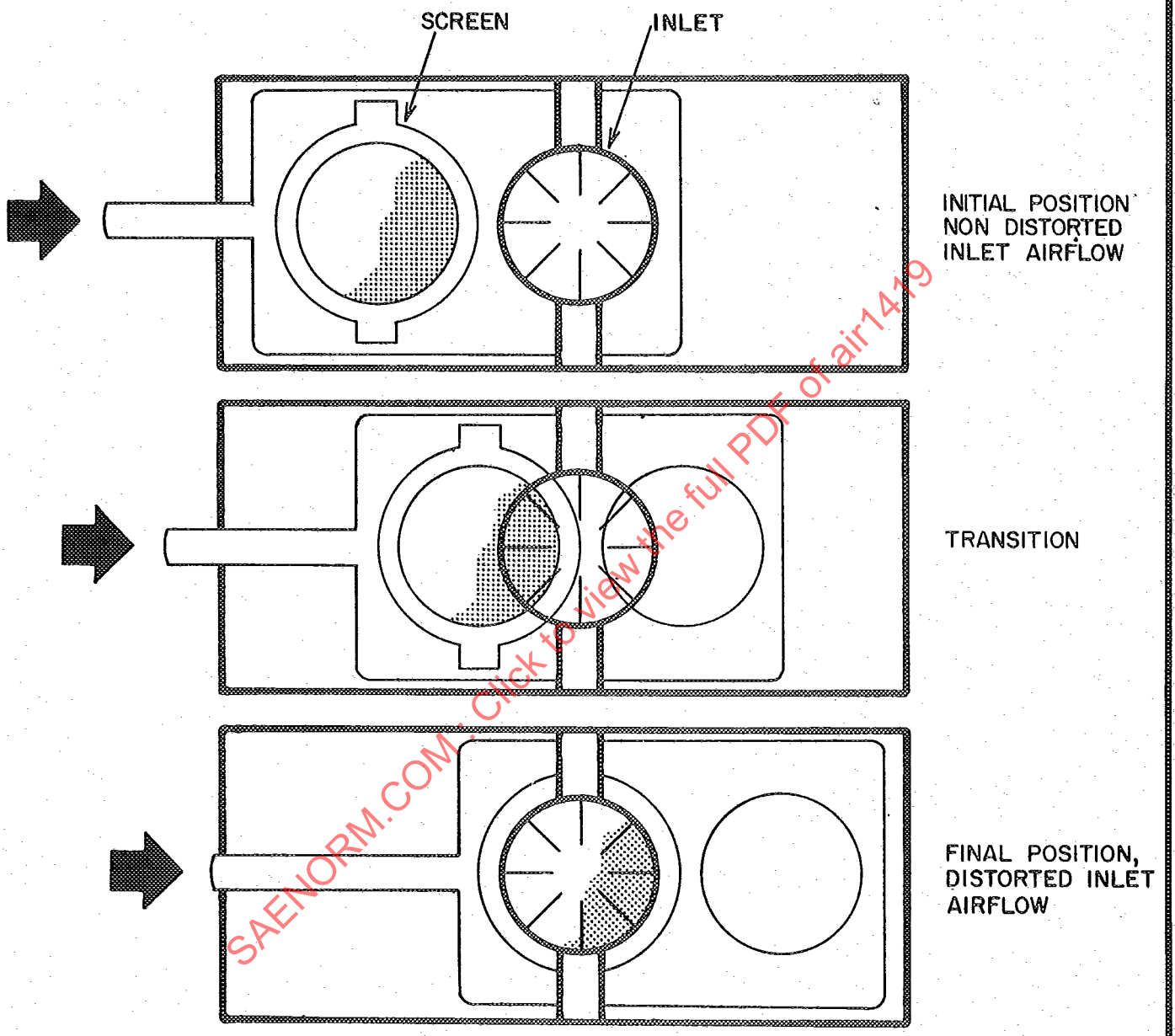

FIGURE 5.29 Screen Changer Assembly

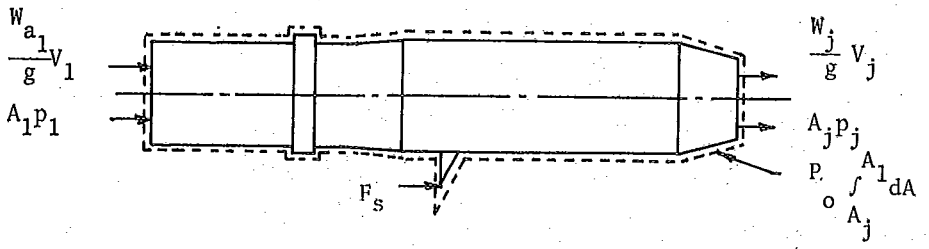

Momentum In = +
Forces to Right = +

$$\Sigma F_x = C$$

$$\frac{W_{a_1}}{g} V_1 + A_1 p_1 + F_s - P_o \int_{A_j}^{A_1} d A - \frac{W_j}{g} V_j - A_j p_j = 0$$

$$\frac{W_j}{g} = V_j + A_j (p_j - p_o) = \frac{W_{a_1}}{g} V_1 + A_1 (p_1 - p_o) + F_s$$

$$F_{j_s} = \frac{W_j}{g} V_j + A_j (p_j - p_o)$$

$$F_{j_s} = \frac{W_{a_1}}{g} V_1 + A_1 (p_1 - p_o) + F_s$$

(a) External Force Balance System

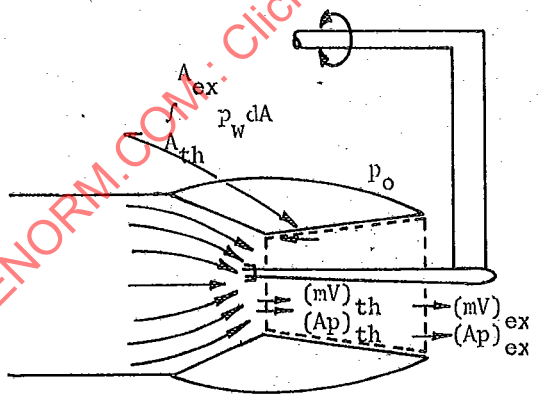

$$\Sigma F_x = 0$$

$$\Sigma F_x = \int_0^{A_{th}} \frac{(Mv)_{th}}{A} dA + \int_0^{A_{th}} p_{th}\, dA - \int_{A_{th}}^{A_{ex}} p_w dA - \int_0^{A_{ex}} \frac{(mV)_{ex}}{A} dA - \int_0^{A_{ex}} p_{ex} dA$$

$$F_j = \int_0^{A_{ex}} \frac{(mV)_{ex}}{A} dA + \int_0^{A_{ex}} p_{ex}\, dA - A_{ex} p_o$$

$$F_j = \int_0^{A_{th}} \frac{(mV)_{th}}{A} dA + \int_0^{A_{th}} p_{th}\, dA + \int_0^{A_{ex}} p_w dA - A_{ex} p_o$$

(b) Internal Force Momentum Balance

FIGURE 5.30 Engine Thrust Measurement Techniques in Ground Test Facilities

SECTION 6

INTERFACE INSTRUMENTATION AND DATA MANAGEMENT

Instrumentation, data acquisition systems, data editing, and data reduction techniques necessary to acquire total-pressure distortion and performance test data are described. Since not all aircraft systems will have the same requirements, examples of recent, past systems are presented to serve as a guide. Formats found useful in establishing valid interpretations of test results and transmittal of those results among concerned agencies also are presented.

6.1 INLET/ENGINE AERODYNAMIC INTERFACE PLANE

The inlet/engine aerodynamic interface plane (AIP) is the instrumentation station used to define total-pressure recovery and distortion interfaces between the inlet and engine. As described below, the selection and configuration of the AIP are dependent upon the nature of the program and the specific design of the inlet and engine. The AIP definition, as stated in ARP 1420, must be agreed upon by all involved parties and remain invariant throughout the test program.

6.1.1 AIP LOCATION

The location of the AIP is a function of the details of engine and inlet design for a particular installation. The guidelines presented in ARP 1420 are listed in Table 6.1. In general these guidelines suggest that the AIP be located within a few inches of the compressor face. This will permit location of the rake downstream of takeoff or bypass doors and other inlet variable geometry. In some cases it may be feasible to locate the instrumentation in the fan inlet guide vane (IGV) leading edge to minimize the effect of rakes upstream of the IGV's on the engine. In other cases it may be difficult to locate a rake close to the engine face. One example is an engine without IGV's and a rotating bullet nose. In such a case, it may be more reasonable to locate the rake forward of the bullet nose providing the inlet is sufficiently long. During engine distortion tests with installations where the AIP is located appreciably forward of the first blade row, the inlet diffuser lines between the AIP station and the first blade row should be duplicated. Photographs of AIP instrumentation locations in several recent flight test aircraft are shown in Figures 6.1 through 6.3. Each installation has advantages and disadvantages that must be weighed against program objectives.

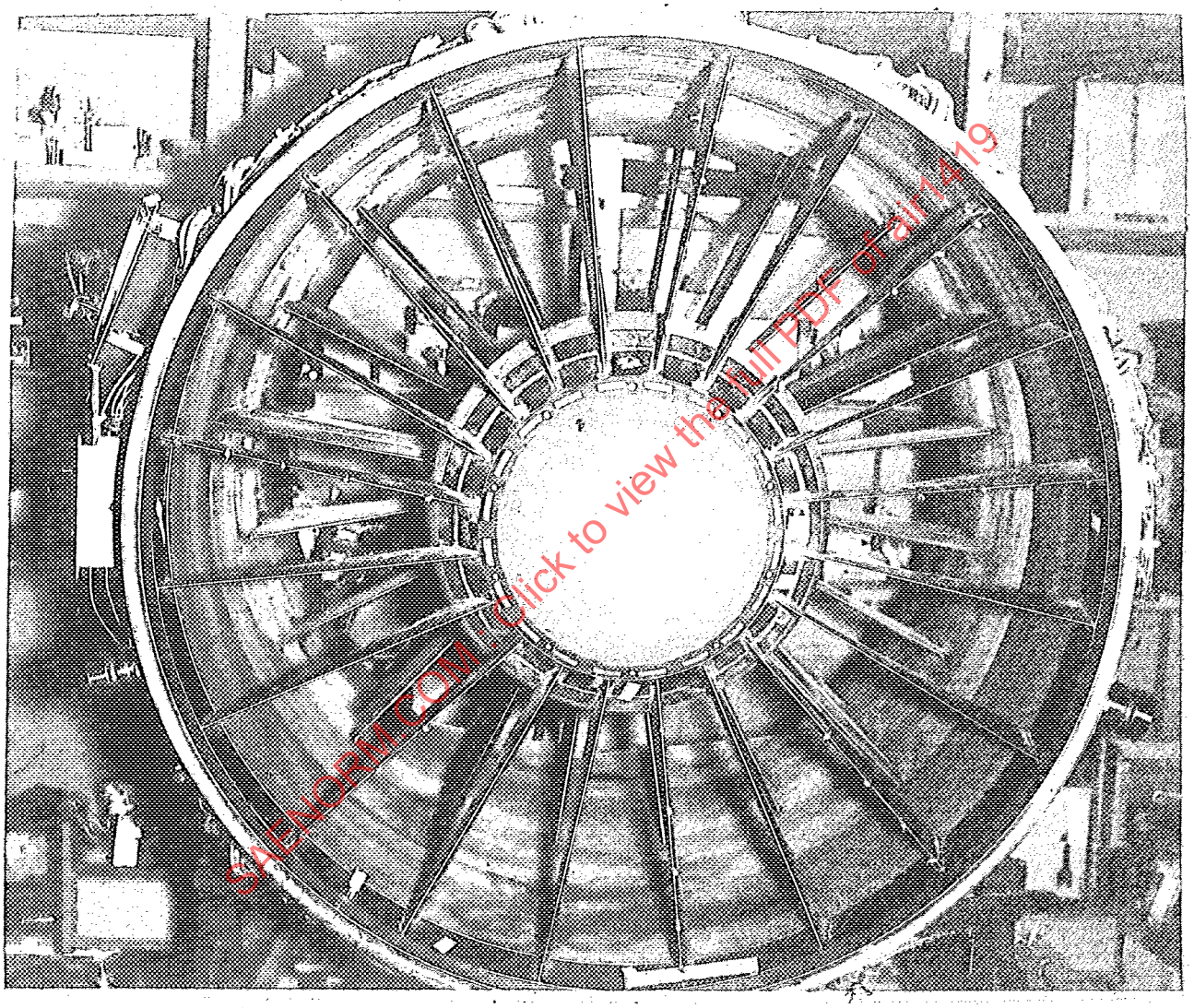

FIGURE 6.1 AIP Instrumentation Integral with IGVs

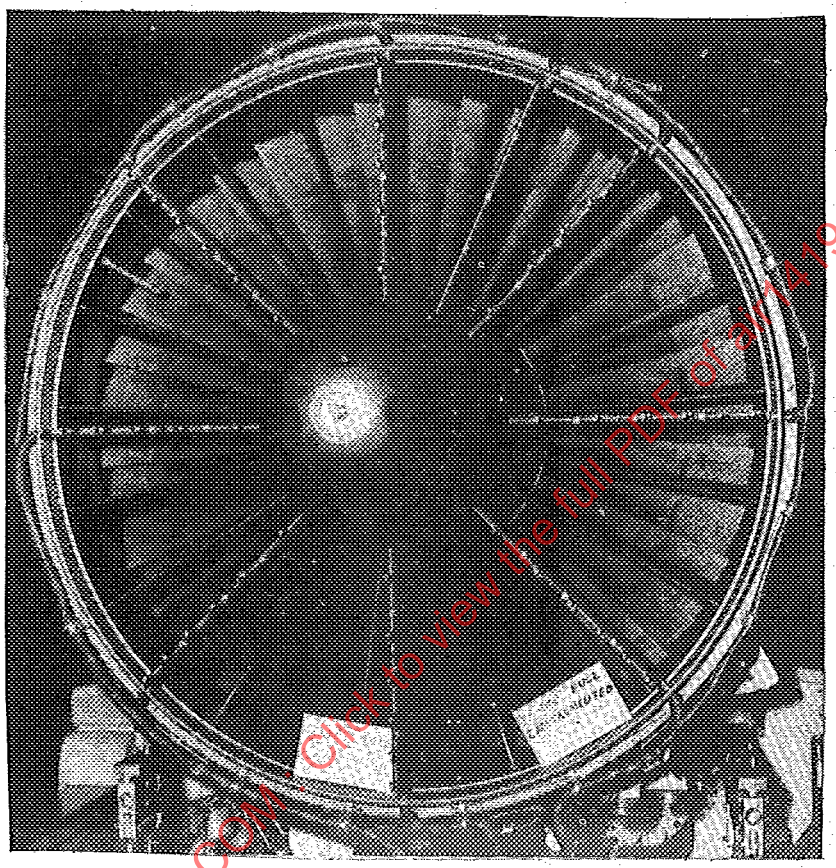

FIGURE 6.2 AIP Instrumentation Mounted on Aircraft Rakes Just Forward of IGV Leading Edge

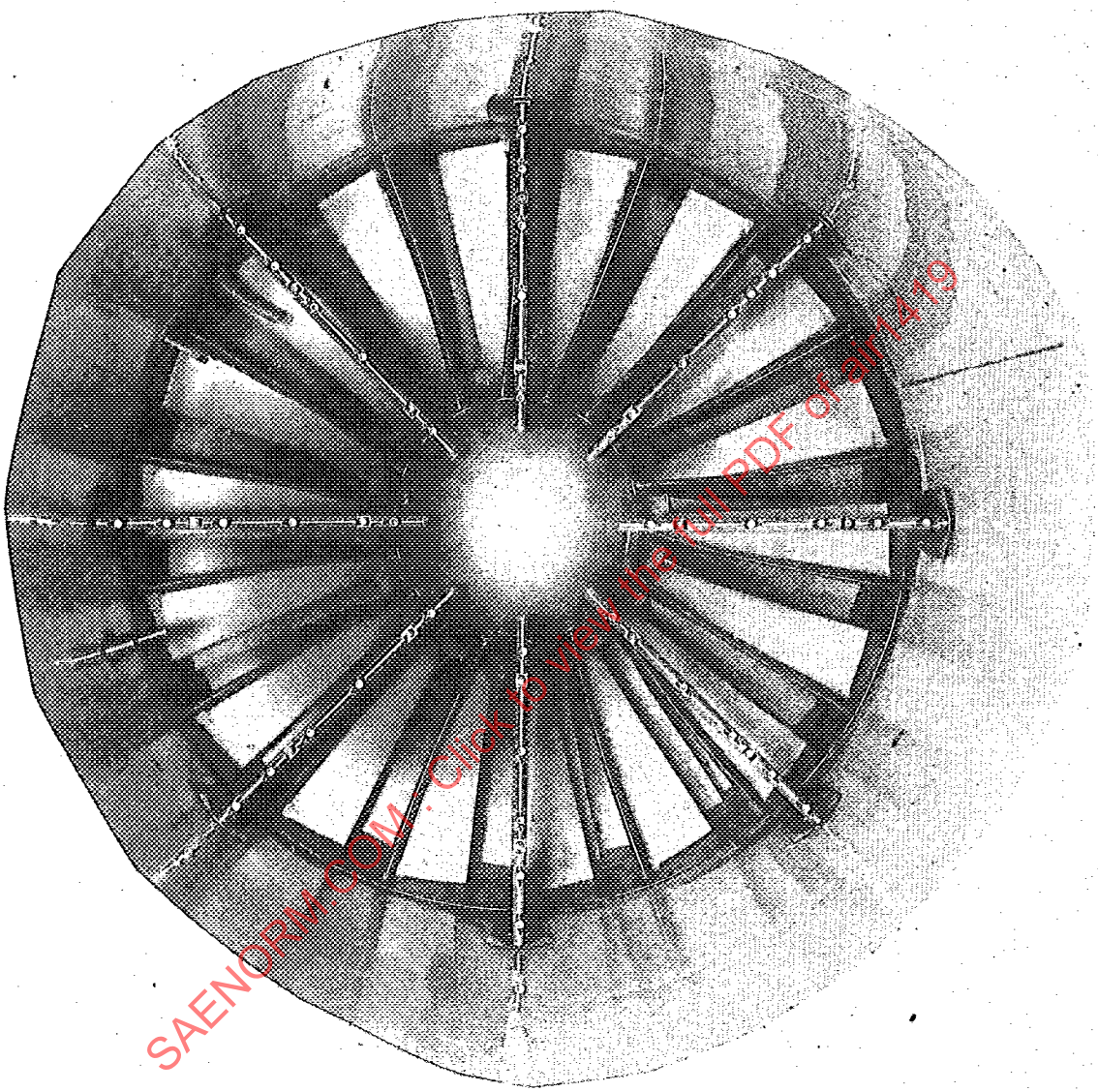

FIGURE 6.3 AIP Instrumentation Mounted on Aircraft Rakes Installed Upstream of the Bullet Nose

TABLE 6.1

ARP 1420 Guidelines For Location Of The AIP

1. The AIP should be located in a circular or annular section of the inlet duct.

2. The AIP should be located as close as practical to the engine-face plane. The engine-face plane is defined by the leading edge of the most upstream engine strut, vane, or blade row.

3. The AIP should be located so that all engine airflow, and only the engine airflow, passes through it. The distance between the inlet auxiliary air systems and the AIP should be such that the effect of the auxiliary air systems on distortion is included in the measurements at the AIP.

4. The AIP location should be such that engine performance and stability are not measureably changed by interface instrumentation.

6.1.2 PROBE LOCATION

Selection of the number and location of probes at the AIP is a compromise between accuracy of the pattern measurement and problems associated with data acquisition system complexity and rake-induced flow blockage. Studies have been conducted (e.g., References 37 and 38) in which specific patterns were evaluated using different rake arrangements. The general conclusion is that, for a typical pattern, a 40-probe (8 rakes of 5 probes each) arrangement like the one shown in Figure 6.4 is the minimum density of instrumentation required for reasonably accurate measurements. As an example, Figure 6.5 shows a pattern evaluated in the Reference 37 study. The pattern is highly distorted circumferentially, with relatively low radial distortion. Several probe/rake configurations were used in the study. Each probe-rake configuration was rotated through 360 degrees in 20 degree increments and pressure readings were taken at each probe position for each incremental rotation. Circumferential and radial distortion factors, K_θ and KRAD, were computed from each set of data. The results are plotted in Figure 6.5 where ΔK_θ is the maximum K_θ minus the minimum K_θ realized for a given probe-rake combination. At least eight rakes are required to define the circumferential distortion. The large percentage errors in radial index are primarily due to the low levels of radial distortion.

For a particular installation, the type of pattern anticipated may influence the rake selection. For example, an inlet with a strong radial distortion may require more than five probes per rake. A bifurcated inlet may require that special attention be given to the circumferential location of the rakes in relation to the trailing edge of the bifurcation.

Generally, the probes should be of such design that both the steady-state and dynamic components of total pressure can be recovered (see Paragraph 6.2.1). This can be accomplished with various combinations of rake-mounted transducers,

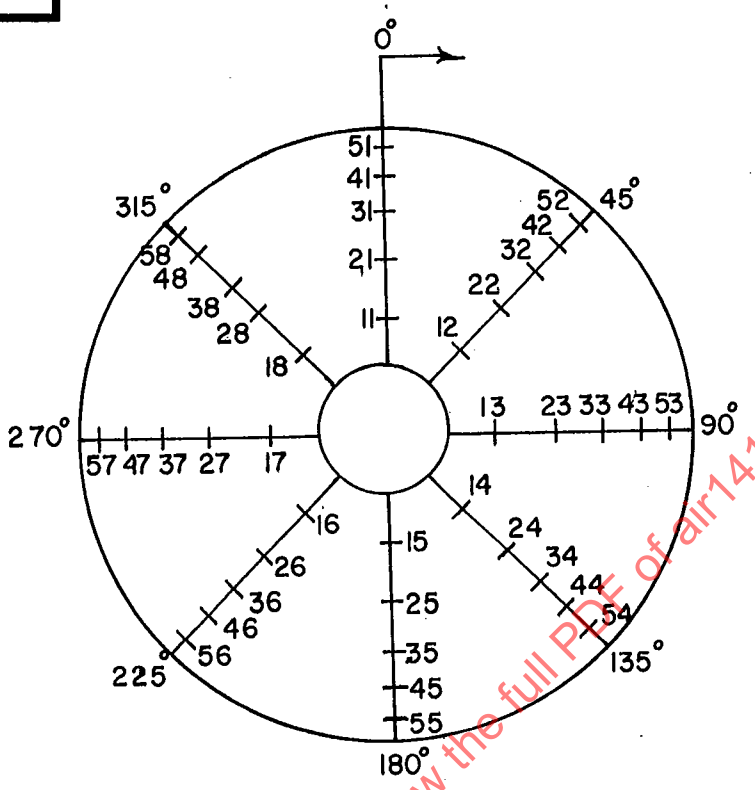

PROBE ORIENTATION –
VIEW LOOKING FORWARD

Nomenclature per ARP 246B

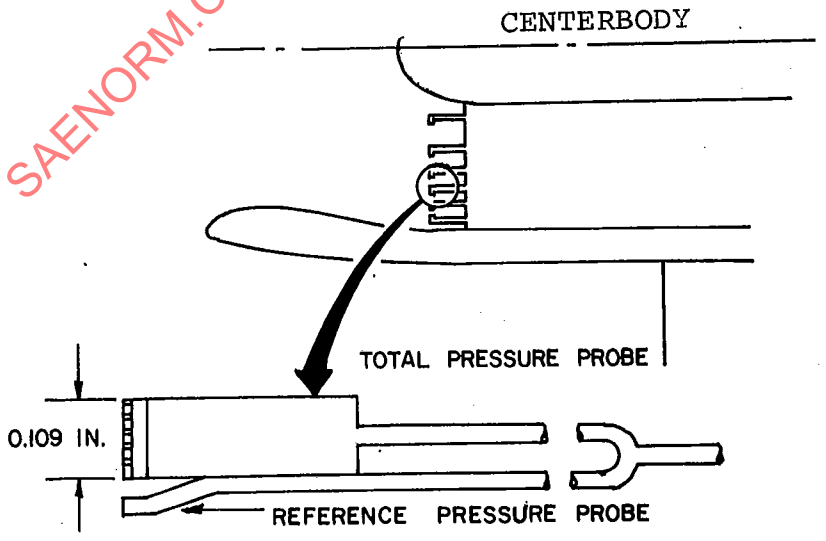

FIGURE 6.4 Typical 40-Probe/Rake Arrangement

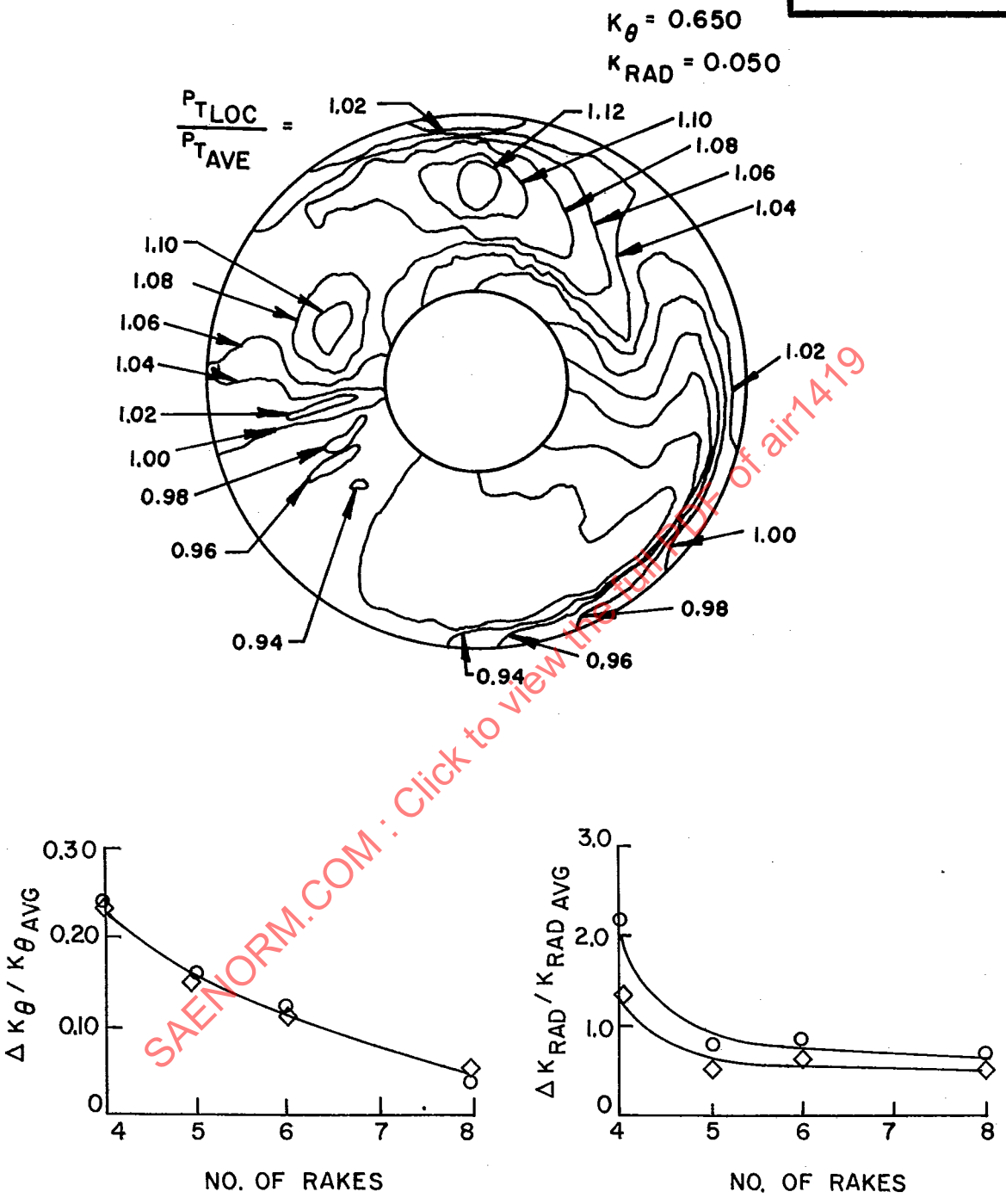

FIGURE 6.5 Distortion Factor Dependence on Probe/Rake Configuration

close-coupled transducers and signal conditioning equipment. Paragraph 6.3.2 discusses several approaches, and Reference 39 reviews current technology in probe design and placement.

Considerable research effort has been expended to investigate accuracies to which instantaneous distortion parameters can be defined with various rake and probe configurations. Reference 38 concludes that reasonably accurate values of engine face distortion parameters can be obtained with fewer than 40 total pressure probes, particularly when sufficient knowledge exists to select a proper data fill procedure. Using this approach, the optimum probe location for any given number of probes is dependent on the particular distortion pattern and the descriptor to be used.

6.1.3 APPLICATIONS

The preceding paragraphs have described the general requirements for probe location and arrangement. Examples presented below illustrate a variety of probe locations and arrangements employed in recent aircraft programs.

Large subsonic transports are not usually subjected to high angle-of-attack conditions. This point when combined with the small range of aircraft speed, usually permits an inlet to be designed with a minimum of engineering resources. Important exceptions include initial climbout and crosswind operation. For example, scale model testing of the Boeing 747 inlet indicated that the total-pressure defect was restricted to the fan tip. As a result of these data and the constraint imposed by a rotating bullet nose on the engine, flight tests were conducted using partial span rakes cantilevered from the inlet wall. These rakes extended well into the high-pressure region of the inlet.

The full span, high-response rake, shown in Figure 6.6, was used by Pratt and Whitney in a JT9D/747-100 nacelle flown on a B-52 test aircraft evaluating thrust reverser induced stalls, Reference 40. The rake has a bearing-supported ring at the hub to accommodate the rotating hub. This type of installation is useful in exploring reverser or crosswind related patterns which may be substantially different from flight patterns.

A 40-probe matrix was used throughout the B-1 development program. The program included 0.10, 0.20 and full-scale inlet tests as well as flight tests. Small differences in angular location were necessary among these models due to the evolving nature and availability of particular IGV locations. Probes were integral with the leading edge of the IGV's, and attempts were made to align the probes with the flow streamlines. Both steady-state and high-frequency total-pressure signals were generated from single transducers at each location.

On fighter aircraft programs, AIP instrumentation is also used to define both total- pressure recovery and appropriate distortion descriptors. Inlet geometry can be variable, and the aircraft is frequently required to perform highly dynamic maneuvers. The Integrated Propulsion Control System (IPCS) Program (Reference 41) employed the 40-probe matrix shown in Figure 6.4 to evaluate inlet

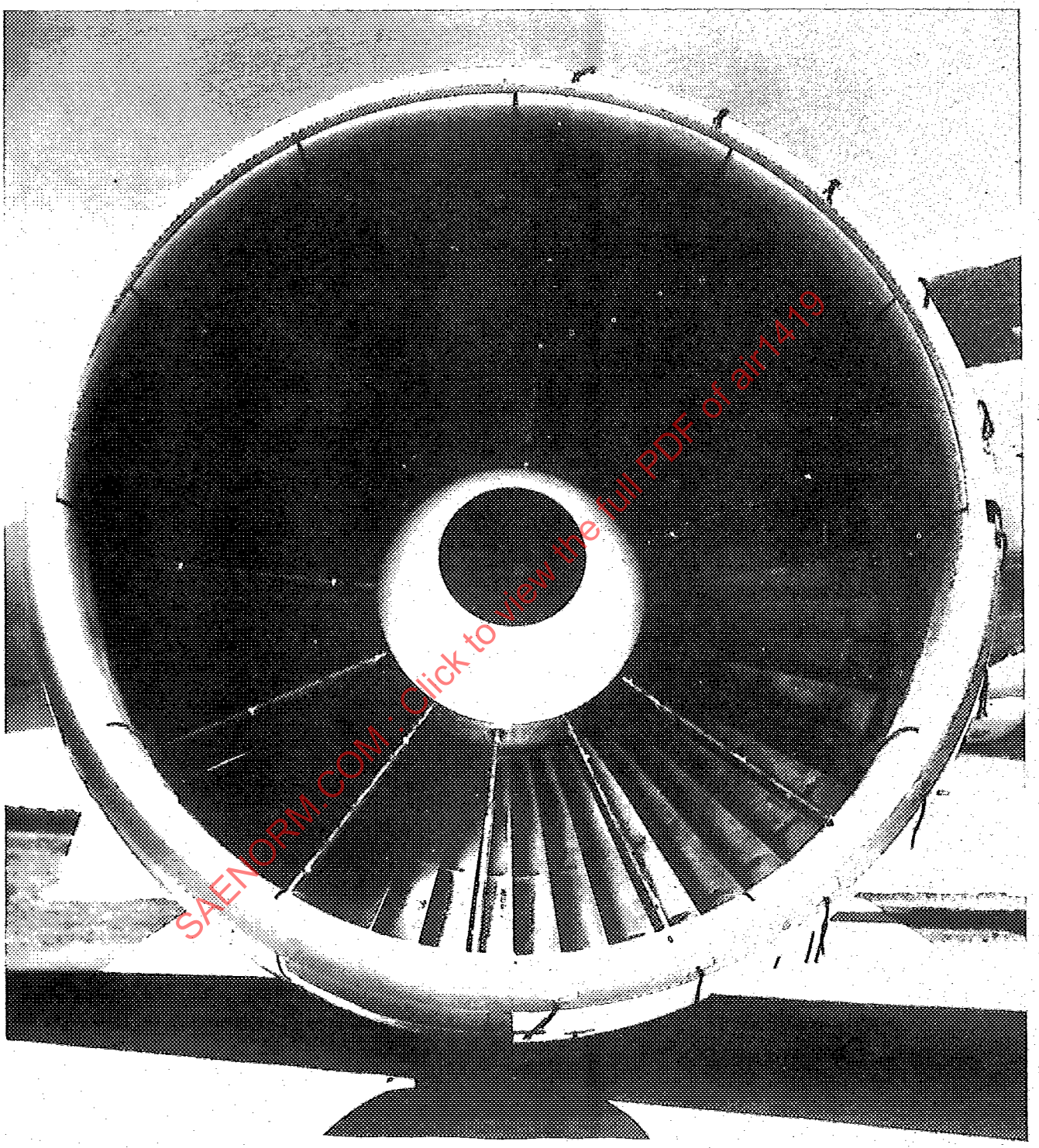

FIGURE 6.6 Full Span Non-IGV Engine Inlet Rakes

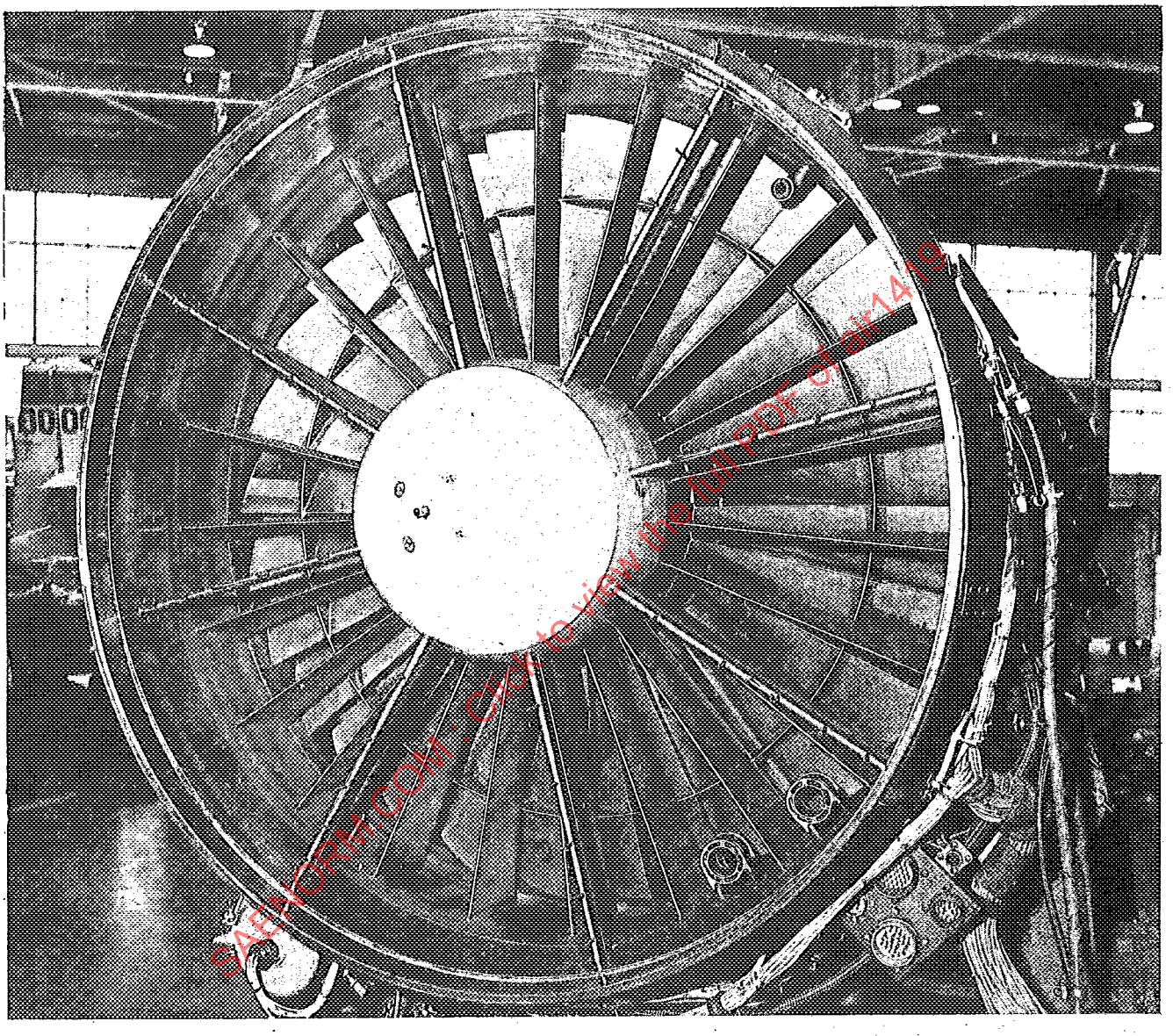

FIGURE 6.7 Compressor Face Rake

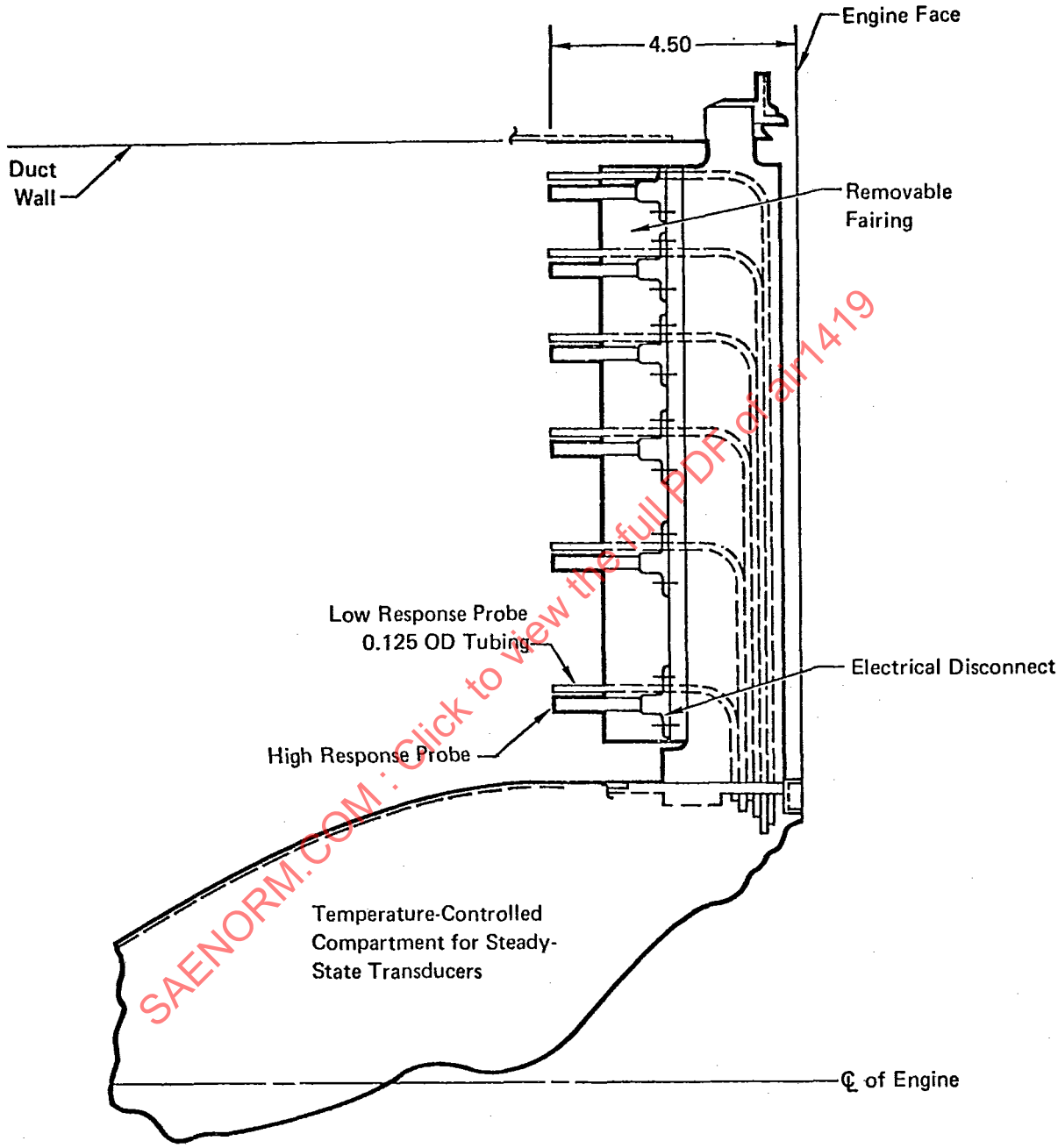

FIGURE 6.8 F-15 Rake Configuration

performance and distortion using an F-111 aircraft. The AIP was located approximately four inches upstream of the leading edge of the inlet guide vanes. A photograph of the AIP rake is shown in Figure 6.7, and the design is discussed in Paragraph 6.3.2.

The F-15 program employed a 48 probe arrangement on subscale and full-scale wind tunnel test programs as well as during the flight test program. The double probe configuration used for full-scale tests is shown in Figure 6.8. Dynamic transducers were installed in the airframe assembly in a manner that permitted replacement without engine removal. Pressure was sensed 4.5 inches upstream of the leading edge of the IGV's. Steady-state pressures were sensed at the same inlet station with the transducers installed in a controlled environment in the bullet nose.

The HIMAT and F-16 provide two examples of recent programs where no AIP data were recorded during initial flight tests of highly maneuverable aircraft. However, both programs employed engines with well-developed stability characteristics, and the inlets were modeled after proven designs.

Another example, a subscale XFV-12A used a 40-probe matrix in wind tunnel tests to identify inlet-distortion characteristics of a modern V/STOL fighter/attack aircraft.

In summary, AIP instrumentation for each system was judged on its own merit, balancing costs and technical objectives against risks. However, it is evident that whenever relatively new inlet/aircraft concepts are programmed in conjunction with the development of a new engine, inlet/engine compatibility characteristics are of sufficient concern to warrant the use of the 40-probe 8 x 5 total-pressure matrix located as close as possible to the engine inlet. It is this preference that is expressed in ARP 1420.

6.2 TRANSDUCER/PROBE CHARACTERISTICS

A transducer/probe configuration must meet two basic requirements to properly resolve the fluctuations produced by turbulent flow: (1) the transducer must have a nominally flat response to frequencies in excess of the highest frequency of interest, and (2) the probe must be smaller than the characteristic size of the eddy producing the highest frequency of interest. Both of these requirements are discussed in Reference 42 and are summarized in the following paragraphs.

6.2.1 FREQUENCY RESPONSE

Studies of the effect of time-varying flow on compressors, such as the one described in Reference 7 have shown that distortion at frequencies corresponding to the appropriate design RPM of the critical compression unit has a significant impact on stability. In addition, higher frequency fluctuations, up to 2000 Hz have been shown to affect compressor pumping characteristics (Section 4.4). The frequency response requirement can be met because of recent advances

in transducer technology. A flat transducer response also requires that the natural frequency of the transducer be two to three times higher than the highest frequency of interest to avoid problems in signal amplification. Further, the transducer must be sufficiently close to the measurement location that frequencies of interest are not affected by the installation.

6.2.2 SIZE CRITERIA

Spatial averaging of the total-pressure fluctuations occurs as the eddy characteristic size becomes commensurate with the transducer or probe diameter. The result is that the measured auto-power spectral density at high frequencies is less than the actual auto-power spectral density.

Consider a turbulent flow with convective velocity, U_c. In the free-stream, an eddy would propagate with the flow velocity.

$$U_c = f_u \lambda_u \tag{6.1}$$

where f_u is one frequency component and λ_u is its associated characteristic wave length. Suppose it is desired to resolve an eddy of characteristic wave length λ_u using a transducer of diameter D such that $D \ll \lambda_u$.

The characteristic length of the eddy is $L = 1/2\ \lambda_u$, shown in Figure 6.9. As a rule of thumb, the sensor size should be at most one-tenth the size of the phenomenon under examination. Hence,

$$D = \frac{L}{10} = \frac{\lambda_u}{20} \tag{6.2}$$

Then,

$$f_u = \frac{U_c}{20D} \tag{6.3}$$

where f_u is interpreted to be the highest frequency to which a turbulent flow can be resolved. Two important conclusions can be drawn from the above equation:

1. The upper frequency limit for a given velocity and accuracy of resolution can be increased by using smaller diameter transducers.

2. The upper frequency limit for a transducer of a given size and accuracy of resolution decreases as the velocity decreases.

For a given frequency component, as illustrated in Figure 6.9, as the wave length becomes commensurate with the transducer diameter, both high and low values of the property being measured will be located simultaneously over the transducer surface. The values will tend to average out each other. In essence,

this is the concept of "spatial averaging." Hence, the spatial averaging of turbulence that occurs during any measuring process in a turbulent flow depends upon the interrelationship of flow velocity, highest frequency of interest, and transducer diameter.

Equation 6.3 is derived from theoretical considerations and is intended to provide a quick, order-of-magnitude estimate of the limiting frequency. Experimental data have been evaluated and are presented in Reference 42 for specific probe sizes. Effects of probe diameter on spatial averaging are shown in Figure 6.10. Typical smoothed auto-power spectra, ø, were obtained from the total-pressure fluctuations at a flow velocity of 236 fps. The spatial averaging effect is quite apparent, and as expected, the smallest diameter probe gives the highest auto-spectral values.

Finally, the limiting frequency for which 90 percent or more of the actual total-pressure power spectra is resolved is given in Figure 6.11 as a function of the convective velocity for several commonly used transducer diameters. These data show a limiting frequency approximately three times that given by the equation above. Typically, the convective velocity will be of the order of 200-600 fps. Transducers in the 0.06- to 0.125- inches diameter range are available. As shown in Figure 6.11, it is possible to acquire data over the frequency range of interest for stability evaluation. Scaling criteria, discussed in Paragraph 6.3.3, are also applicable to transducer/probe characteristics.

6.3 DATA ACQUISITION SYSTEM

Foresight in configuring appropriate data acquisition systems can result in large dividends in subsequent data reduction and analysis tasks. Recording techniques are described, and guidelines are provided for system accuracy, frequency response, and data record length.

6.3.1 GENERAL DESCRIPTION

The data acquisition system consists of the hardware required to sense and record the data. The details of the system required will depend on the specific transducer selection. A schematic of a typical system is shown in Figure 6.12. The signal from the high-frequency-response transducer is generally low level (less than 50 mv), and its voltage is proportional to the sensed pressure. That signal, filtered if necessary, is input to a voltage controlled oscillator (VCO). The output of the VCO is a variable-frequency signal with the variation, relative to a nominal center frequency, proportional to the input voltage. The outputs of the VCO's (one per transducer), each having a different center frequency, are added (multiplexed) using a summing amplifier and recorded on one track of a tape recorder. Several tracks are used to provide sufficient recording channels. Time code and a high frequency signal, used to compensate for variation in tape speed, are recorded on additional tracks. Recorders, VCO's, discriminators, and tape speed must be compatible with recovering data to the maximum frequency of interest. If tape recorders of sufficient capacity are

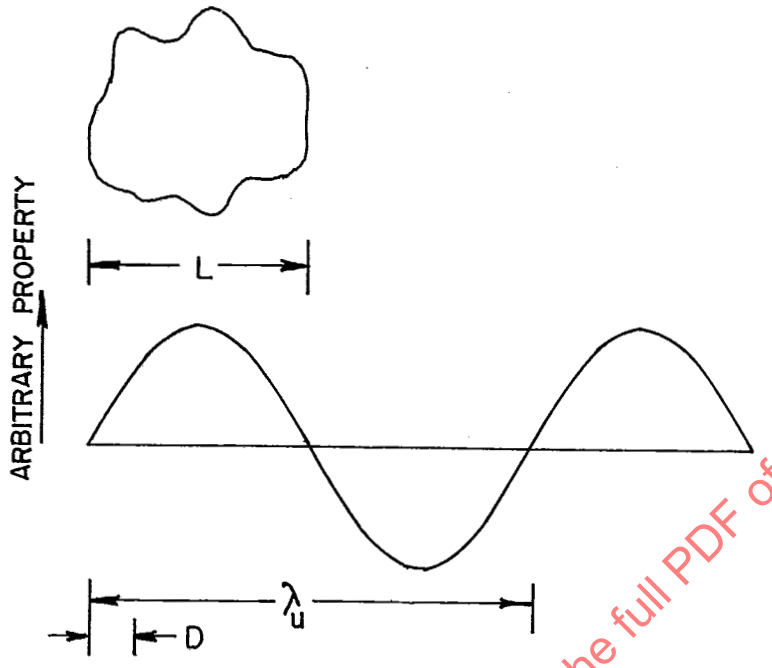

FIGURE 6.9 Sketch Illustrating the Effect of Probe Size

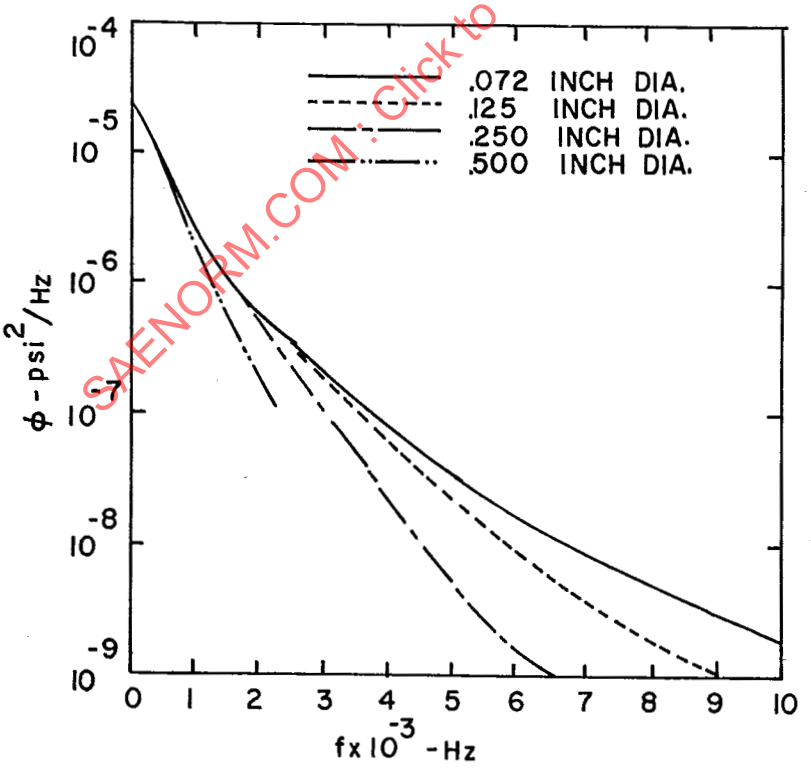

FIGURE 6.10 Effect of Transducer Diameter

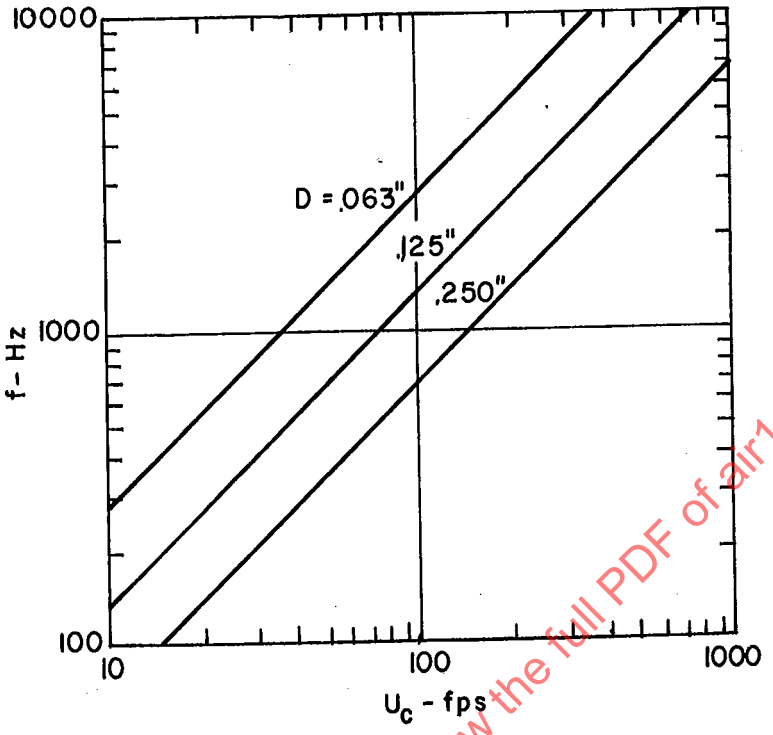

FIGURE 6.11 Frequency Below which at Least 90 Percent of Spectral Function is Sensed

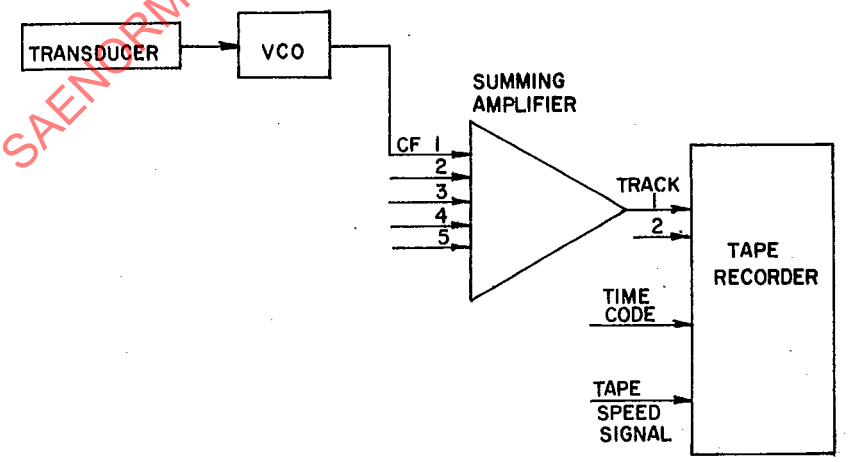

FIGURE 6.12 Typical Data Acquisition System

available, a single track can be used per transducer rather than multiplexing. However, it is generally advantageous to record all related signals on the same recorder.

6.3.2 SYSTEM ACCURACY

A high degree of accuracy in the pressure measurement is necessary in order to quantify the distortion. Small differences between pressures become significant in the distortion descriptors presented in Section 2. The problem is made more difficult by the large range of inlet pressure levels encountered at different flight conditions. For example, pressures as high as 34 psi will be measured at Mach 1.2, sea level, and the pressure will drop to 2.8 psi during operation at Mach 0.9, 50,000 ft. These required pressure ranges make even the measurement of steady-state pressures difficult.

Individual steady-state pressures (signals time-averaged to attenuate frequencies greater than 0.5 Hz) should be recovered with an error not to exceed ± 0.5 percent (± two standard deviations) of the absolute pressure being measured. Individual dynamic absolute pressures (containing data to at least the highest frequency of interest) should be recovered with an error not to exceed ± 2.0 percent (± two standard deviations) of the absolute pressure being measured for stability and ± 5.0 percent (± two standard deviations) for performance. These errors include all errors introduced by the sensing, recording, playback, and processing systems from the point where the pressure signal is being measured to the point where it again appears as an output pressure. Current practice indicates that these accuracy levels are attainable if the data system is carefully developed, with appropriate experience and calibration procedures being employed.

Measurement of dynamic or time-varying pressure is more difficult because transducers with adequate frequency response and sufficiently small size are not sufficiently accurate. It is generally necessary to apply some form of inflight calibration to achieve the accuracy goals stated above, over the whole flight envelope. This is particularly true when the operating temperatures in an exposed inlet rake are considered. The following paragraphs discuss calibration methods that have been used.

The dynamic content of inlet total pressure is small. Turbulence RMS levels of less than three percent are typical. This leads to the idea of separately measuring the high- and low-frequency components of total pressure. Accuracy can then be improved by tailoring transducer and signal conditioning ranges to maximize resolution for each of the individual components. Low frequency response measurements can be made with larger, more accurate transducers. These transducers can be located remotely in environmentally controlled areas to increase accuracy.

Several different approaches have been used. The following paragraphs describe three: (a) the use of a rake which mechanically zeros a high-frequency-response, differential-pressure transducer, (b) post-test correction of average

pressure using accurate steady-state measurements, and (c) analog summing of low- and high-frequency measurements.

In testing an F-111 aircraft, NASA/DFRC used a rake which provided transducer zero shift data by mechanically applying a reference pressure to both sides of the transducer diaphragm (Reference 43). The concept is shown in Figure 6.13. A solenoid-operated pneumatic actuator positioned the center rod in either the "zero" or "data" positions. In the "data" position the transducer was connected to the rake probe. In the "zero" or "null" position the reference pressure was vented to both sides of the diaphragm. This rake was used in a number of flight test programs (e.g., Reference 41) with reference pressure a function of flight condition to minimize the component measured by the high response transducer.

The major advantage of this approach is that only one low-frequency-response transducer is required instead of 40. This reduces data acquisition and maintenance costs. There are, however, two significant disadvantages: (1) it is difficult to prevent leakage in the rake seals, particularly under high temperature flight conditions, and (2) the steady-state measurements are made with the high-frequency response transducers.

A variation of this approach (Figure 6.14) was used during the B-1 flight test program. Instead of venting the reference pressure to both sides of the diaphragm, the sensed pressure was routed to both sides to provide a "zero" measurement. Additionally, the back side of the transducer was routed to a pressure regulated to 5.0 psi above the reference pressure. This required a three-way pneumatic valve for each transducer. Valves were cycled once per minute throughout the flight with the zero and calibrate positions held for two seconds each. In order to maintain signal resolution, provisions were also incorporated to change gains as a function of freestream total-pressure level. Although the data reduction effort becomes a little more involved, considerable success was achieved in measuring both low- (quasi-steady state) and high-frequency total-pressure components with a miniature transducer. (Success in this case means obtaining wind tunnel and flight test results that were consistent with each other.)

A second approach, used in engine/inlet testing at NAPC and AEDC (Reference 44), involved the use of a rake having separate probes for steady-state and high-frequency-response measurements (Figure 6.15). In the postevent data processing, the time average of the high-response data for each probe was corrected to the steady-state value measured at the same time. With this approach, only the dynamic pressure fluctuations were measured with the high-frequency-response transducer. As with the zeroing rake, it requires significant postevent processing. This method also requires the additional steady-state transducers.

A third approach is similar to the second in the use of separate probes for steady-state and dynamic measurements. The difference is that the output of the low-frequency "steady-state" transducer is low-pass filtered and electrically

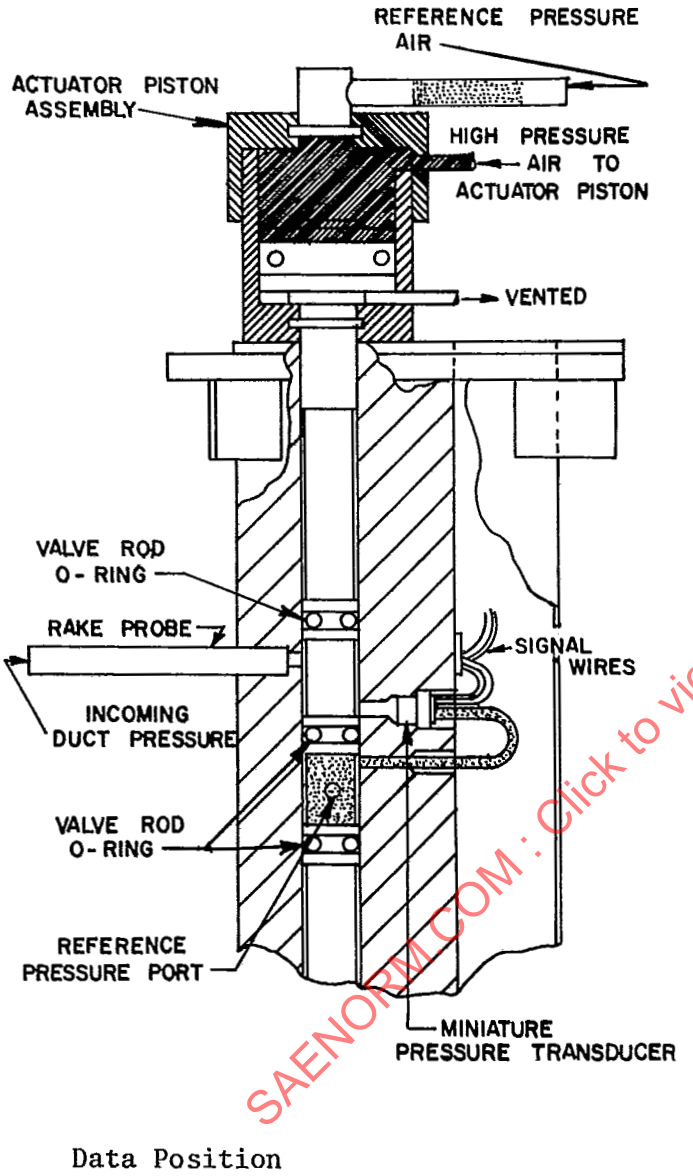

Data Position

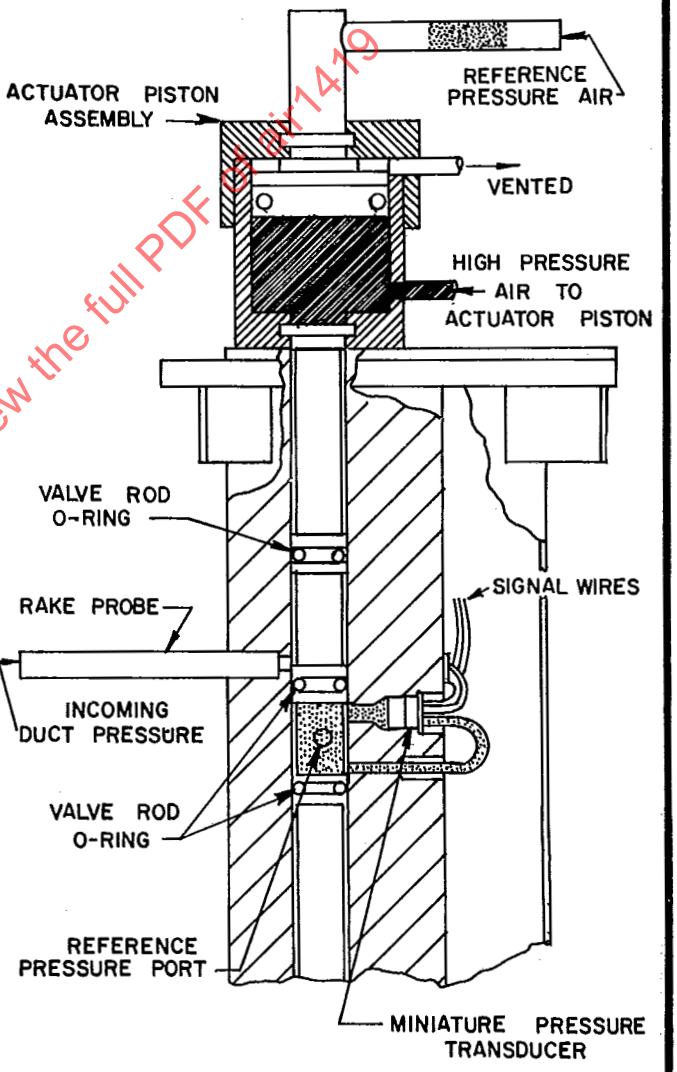

Null Position

FIGURE 6.13 NASA Dryden Flight Research Center Rake

AIR 1419

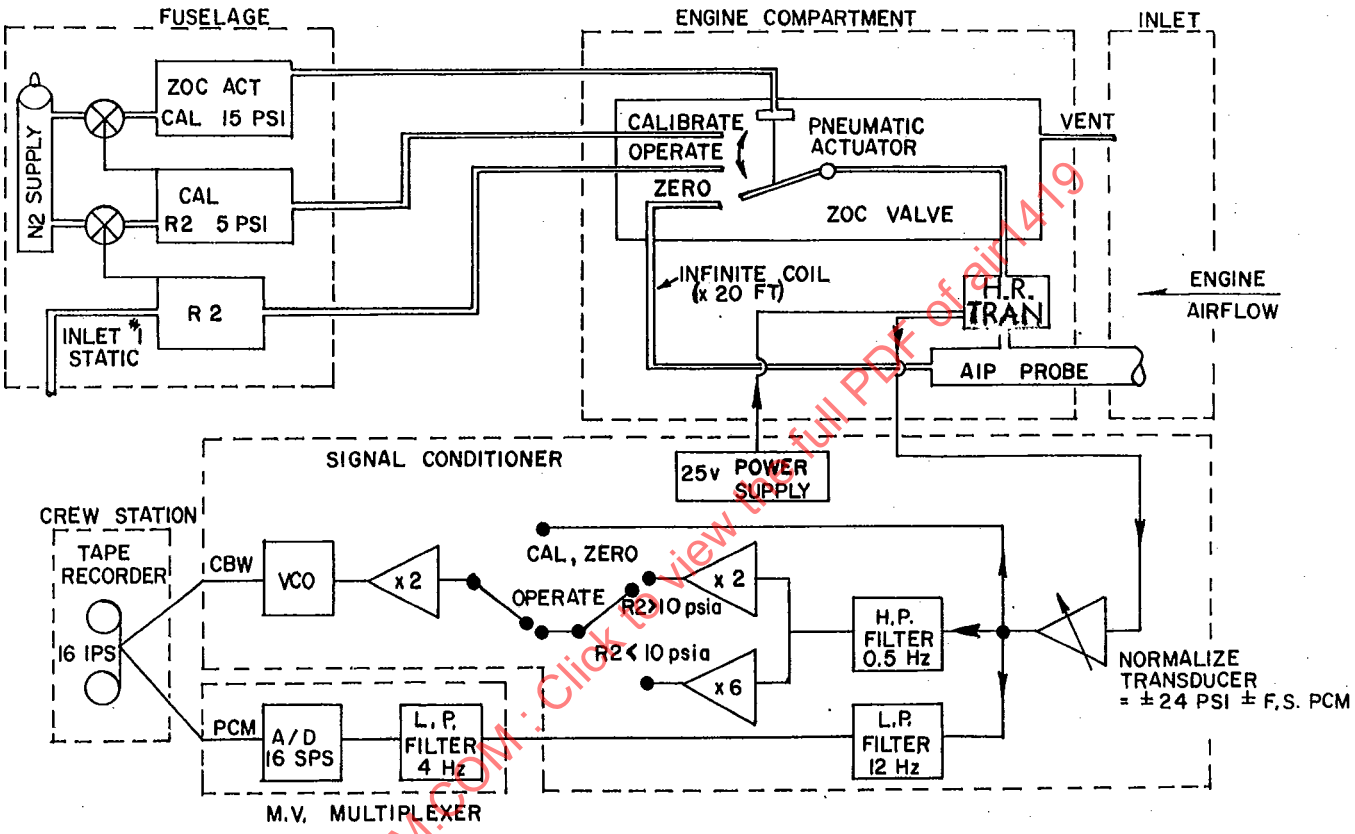

FIGURE 6.14 B-1 Flight Test Data Acquisition System

added to the high-pass filtered output of the high-frequency-response transducer. Figure 6.16 illustrates this process, as used in a Boeing wind tunnel test program. A similar system was used in F-15 flight testing. This approach reduces the data reduction effort and provides an electrical signal with the full frequency content which can be used in subsequent processing. Care must be taken to ensure high accuracy in the filtering and summation circuits to avoid degraded accuracy in the resulting pressures.

The above paragraphs discuss transducer accuracy and techniques for recording steady-state and dynamic data. It is also essential to consider the accuracy of the signal conditioning and recording hardware. A detailed error stackup is useful in evaluating a proposed system. Through such evaluations, sensible decisions can be made on selecting the approach and hardware to be used.

6.3.3 FREQUENCY RESPONSE

The frequency response of the data acquisition system must be sufficient to have negligible effect on the quality of the data over the frequency range of interest. The frequency of interest is difficult to identify and must usually be established empirically by the engine manufacturer. Since requirements must be established early in the program, usually before the actual hardware is available, reliance must be placed on the experience of the participants to select appropriate data acquisition hardware.

A number of studies (Reference 7) have indicated that frequencies of the order of one revolution of the first-stage compression unit are relevant. Generally this is interpreted as the frequency where the signal is attenuated 3 db. It is recommended that signal conditioning units and tape recorders be selected that do not alter frequency content of the pressure signals to at least 1.5 times the maximum frequency of interest.

For scale model tests, the required frequency response scales with Strouhal number, $fL/\sqrt{T}$, where f = frequency, L = representative length, and T = absolute temperature, as shown in Table 6.2. The length is the dominant parameter in the Strouhal number; for typical model testing, the length difference changes the filter cutoff frequency by a factor of 6 to 10, while the temperature difference changes the filter frequency by a factor of 0.8 to 1.13. Because the temperature effects on the filter cutoff frequency are relatively small, and because the value of maximum time variant distortion is insensitive to small changes in filter cutoff frequency, the temperature difference between model test and full scale operating conditions is usually ignored. Current practice is to select a filter cutoff frequency for model test analysis that is inversely proportional to the model scale. This simplified frequency scaling procedure reduces the time and cost of model test analysis and produces good correlation between model and flight data.

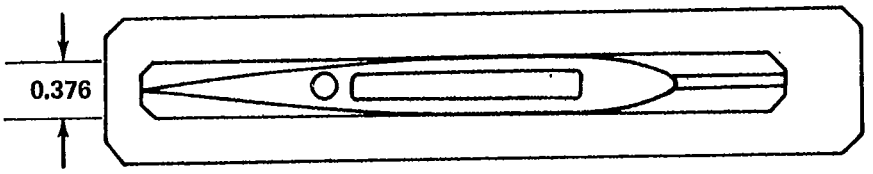

NOTE: ALL DIMENSIONS IN INCHES

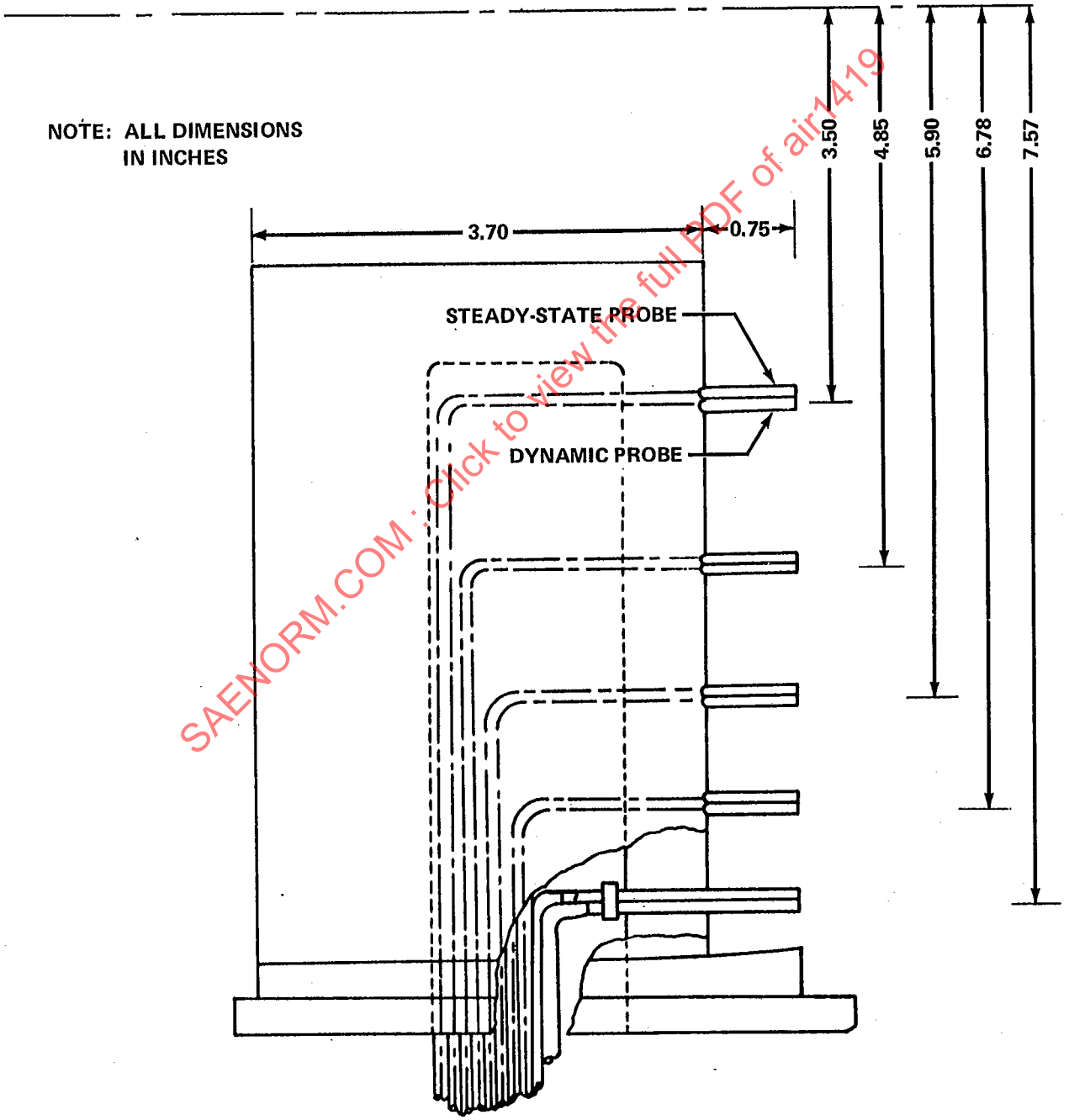

FIGURE 6.15 Double Probe Rake Configuration

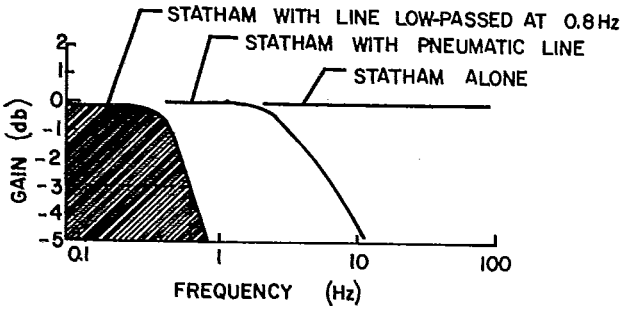

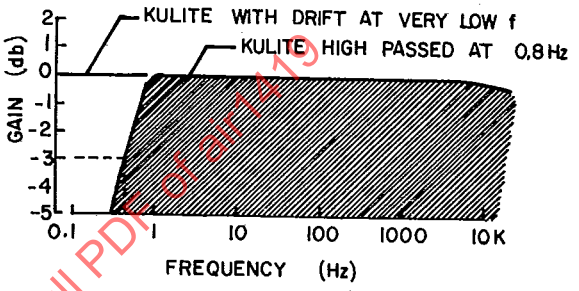

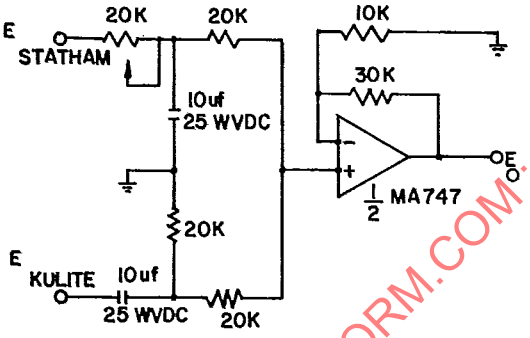

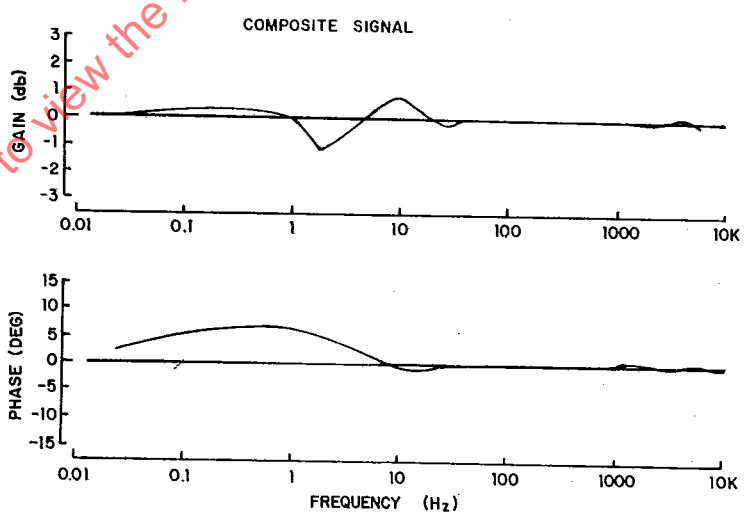

FIGURE 6.16 Development of Composite Signal from Staham and Kulite Signals

TABLE 6.2

Data Scaling Guidelines.
Strouhal Number Constant
(Same Reynolds Number And Mach Number)

. Frequency (Strouhal Number)	$\left(\frac{fL}{\sqrt{T}}\right)_{\text{full scale}} = \left(\frac{fL}{\sqrt{T}}\right)_{\text{model scale}}$
. Record length and time delay	$\left(\frac{\tau T}{L}\right)_{\text{full scale}} = \left(\frac{\tau\sqrt{T}}{L}\right)_{\text{model scale}}$
. Power spectra	$\left(\frac{\phi(f)\sqrt{T}}{p^2 L}\right)_{\text{full scale}} = \left(\frac{\phi(f)\sqrt{T}}{p^2 L}\right)_{\text{model scale}}$
. RMS values	$\left(\frac{\Delta PRMS}{\bar{p}}\right)_{\text{full scale}} = \left(\frac{\Delta PRMS}{\bar{p}}\right)_{\text{model scale}}$
. Covariances	$\left(\frac{C(\tau)}{p^2}\right)_{\text{full scale}} = \left(\frac{C(\tau)}{p^2}\right)_{\text{model scale}}$

6.3.4 RECORD LENGTH

One consideration in the selection of data-record time length is a requirement to acquire statistically stationary data. Stationarity requires the average pressure computed over a small time segment to be the same as the average pressure computed over any other time segment. This is essential to produce repeatable dynamic distortion data. Another consideration is the requirement to record sufficient data to obtain reasonable assurance of encountering maximum distortion levels. Chances of encountering a higher value increase with record length. Experience has shown that maximum values occurring within 30 to 60 seconds are satisfactory for full-scale conditions. Although frequency of interest increases, required record lengths decrease as model scale decreases. Time-variant data should be recorded continuously during inlet/engine/aircraft transients of interest.

6.3.5 RECORDING SYSTEMS

The recording system consists of the VCO's, summing amplifiers, and a tape recorder as shown in Figure 6.12. The performance of these components is extremely important to overall system accuracy. Another consideration is the selection of the FM center frequencies and bandwidths for recording the data. There would appear to be significant advantages to be gained through the use of standardized frequencies. This would simplify the general use of test data by more than one company or agency. Unfortunately, data recording systems are expensive and a range of frequencies is in current use. It would not be reasonable to replace existing systems simply to change to standard frequencies.

Table 6.3 outlines suggested frequencies for new systems. Higher frequencies are required for scale model tests due to the higher frequency-response requirements. The frequencies suggested do not entirely conform to the IRIG standards. However, several industry and government test facilities have modern systems built around these frequencies. Thus, it would appear that progress in achieving consistent frequencies would be made by adoption of the non-IRIG frequencies.

TABLE 6.3

Recording Frequencies

Full Scale and Flight Test			
IRIG B		IRIG C	
Center Frequency	32KHz + N(16KHz)	Center Frequency	32KHz + N(32KHz)
Bandwidth	±4KHz	Bandwidth	±8KHz
Scale Model and Full Scale Ground Engine Testing			
Center Frequency	100 KHz + N(60KHz)		
Bandwidth	±16KHz		

where N is an integer which increases by 1 for each successive center frequency.

For any system it is recommended that IRIG A time code be used. It is also recommended that a high-frequency sine-wave signal be recorded for tape speed compensation.

6.4 DATA EDITING

Data editing consists of three distinct tasks. One is time editing - the essential function of reducing the potentially infinite set of possible data points to a manageable number. Another is the identification of spurious signals. These can be either continuously bad signals, generated from faulty transducers or signal conditioning, or intermittently bad transducers generating occasional spikes in the data. Both types can cause problems in subsequent data reduction effort. Having identified the spurious signals, the remaining task is to decide what to do about them. Several techniques are described with emphasis on those applicable to the AIP instrumentation matrix.

6.4.1 TIME SEGMENT IDENTIFICATION

Enormous quantities of data are recorded during a normal test program. Selection of appropriate time segments for analysis is the key to a successful test program. Appropriate techniques frequently depend on the characteristics of the data acquisition system. Scanivalve systems are frequently used during tests

to acquire steady-state data, and dynamic data are not necessarily recorded concurrently. In blow-down tunnels, each blow may provide a series of individual data points, and care must be exercised to select time periods only where stable flow conditions have been established. With flight test data, the problems are further compounded due to variations in aircraft attitude, variable geometry, and atmospheric conditions. On-line calibration procedures also add complications.

In almost all cases, time history plots of selected parameters provide initial insight for identifying appropriate time segments for analysis. Time histories can be either digital or analog plots and serve not only as roadmaps for actual test conditions, but also provide visibility on the quality of the data and the value of additional analysis. By including the recorded time code signal on the strip charts and selecting appropriate paper speeds (time scale), time segments of interest, during both steady state and transient test conditions, can be identified precisely.

Additional time-editing is required during tests where the objective is to identify AIP dynamic distortion characteristics representing a particular configuration and operating condition. The 30-60 seconds of run time recommended for full-scale tests can result in more than 60,000 distinct distortion patterns. Clearly, additional techniques must be established, and agreed to by the concerned parties, to reduce this volume of data to levels that are manageable and cost-effective.

Experience has shown that for large test programs, analog distortion analyzers provide one of the more successful techniques for editing compressor-face distortion data. In this technique, an analog computer is wired to compute relevant distortion discriptors. One advantage of analog computers is that computations are done in real time, and thus are useful online as well as offline. Visibility of test results is greatly enhanced when the computer is used as an online device, but the validity of the results is strongly dependent on the ability of the operator to identify spurious signals and take corrective action.

Another advantage of analog distortion analyzers is that continuous traces of distortion components and indexes can be recorded on the same analog tape used to record the individual AIP signals. Strip charts of these signals can be helpful in identifying appropriate time segments. Peak detection circuits can also be used to flag maximum distortion levels on the analog tape and/or trigger analog-to-digital converters to digitize the individual signals at the moment of peak detection.

All of these techniques have been employed on recent programs. During the F-18 program, McDonnell-Douglas used an analog device to compute distortion levels and flag maximum values. Post-test processing consisted of digitizing AIP dynamic data only during short time periods spanning the maxima. A photograph of the analyzer and schematic flow diagrams are shown in Figures 6.17 through 6.19. Rockwell used a hybrid computer during B-1 inlet tests, not only to compute distortion indexes in real time, but also to digitize individual AIP pressures at peak distortion levels. The resulting online displays of

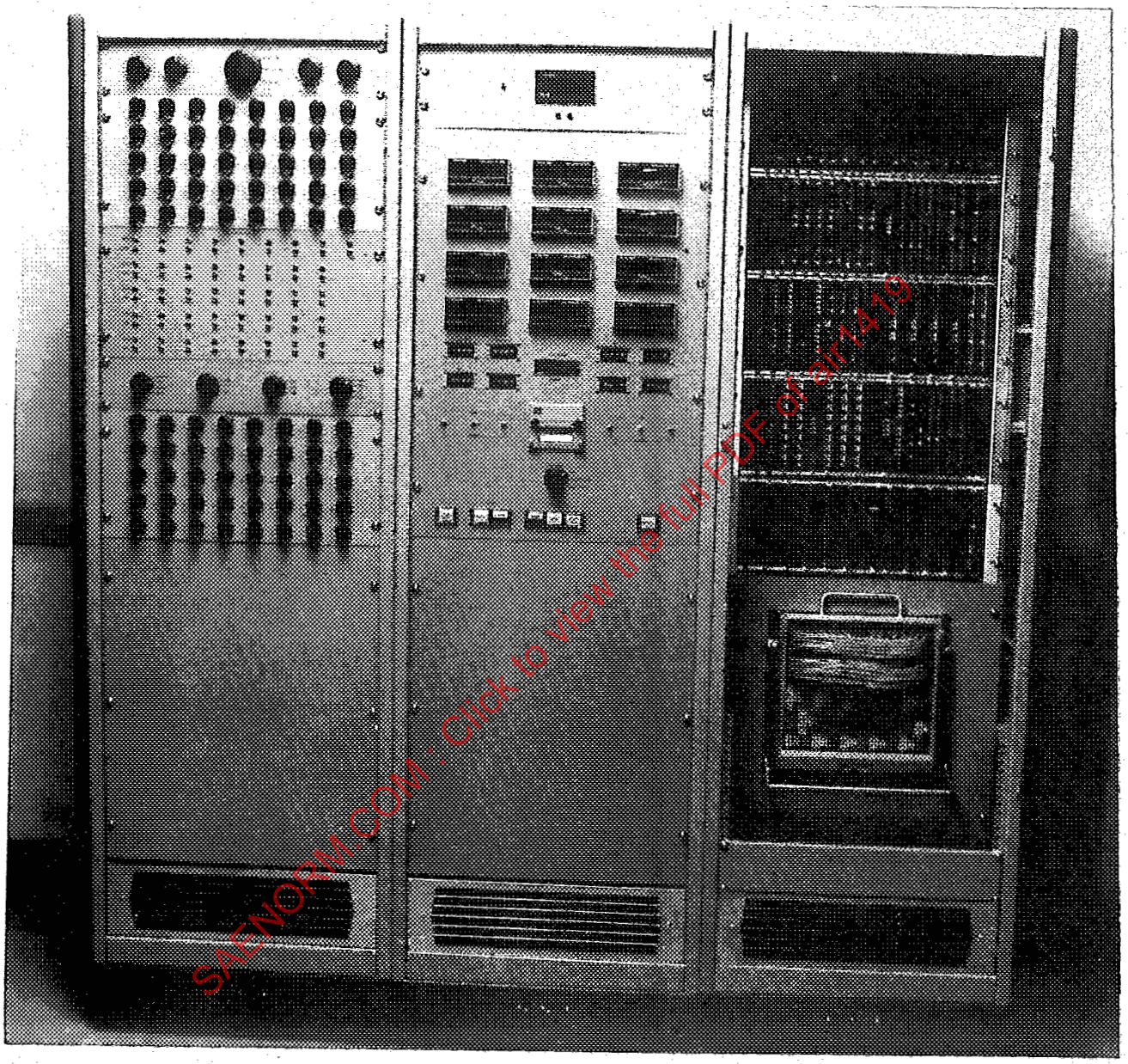

FIGURE 6.17 F-18 Analog Distortion Analyzer

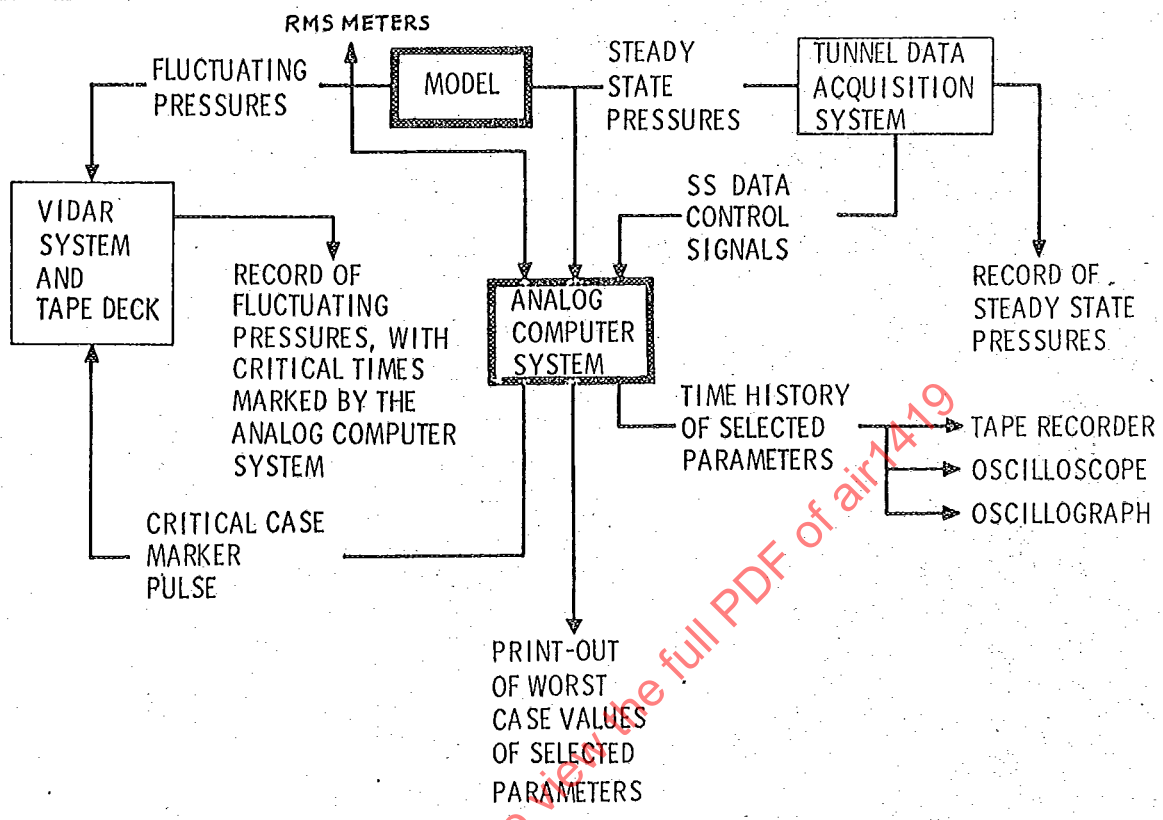

FIGURE 6.18 Analog Data Editing

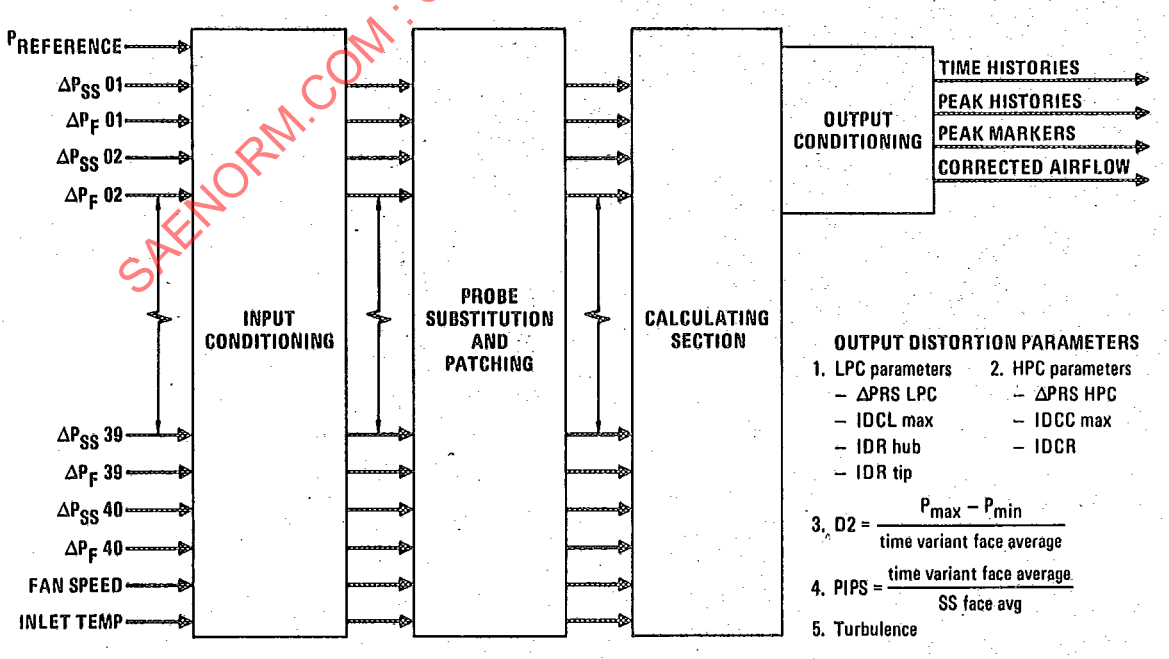

FIGURE 6.19 F-18 Analog Distortion Computer Block Diagram

individual total pressures were useful in redirecting the test and almost completely eliminated the need for post-test processing. A photograph of the analyzer and a schematic flow diagram are shown in Figures 6.20 and 6.21, respectively. An onboard distortion computer was also used during an integrated propulsion control system program (Reference 41). The analog computer outputs were recorded on FM tape and used for editing. The computed distortion was also output to a cockpit display which the pilots used to manually adjust inlet geometry.

The advent of relatively inexpensive, fast, digital computers is rapidly opening the possibility of performing these functions digitally. Regardless of the computation scheme, time-editing is essential to reduce the volume of data.

6.4.2 IDENTIFICATION OF SPURIOUS SIGNALS

A number of different techniques need to be used to identify data channels which have failed. Prior to the start of a test shift or flight, ambient readings can be compared. Any channels that appear questionable can be pressure checked. Periodically, all channels should be calibrated end to end. In wind tunnels or test cells, the pump down period provides another opportunity to calibrate and check for bad channels.

If the data are telemetered during tests in wind tunnels, test cells, or flight, oscilloscopes or strip charts can be used to compare the level of dynamic activity to identify bad channels. The same technique can be applied for post-test processing. This approach is probably the most effective method for identifying bad channels, particularly those that fail for only a portion of the test period.

During the digital processing, each value can be checked against upper and lower limits. These limits can be either absolute (i.e., the range of the transducer) or related to flight conditions or the AIP average pressure. Another technique for identifying bad channels during digital processing is to establish limits for the variation from channel to adjacent channel and regard too large a change as an indication of bad data. Care must be taken in the use of these techniques or valid data may be disregarded because it does not conform to preconceived notions.

One particularly effective technique for editing AIP total pressures is illustrated in Figure 6.22. Data were obtained from flight tests of an aircraft where an 8 x 5 rake/probe matrix was employed. Data from individual probes were normalized to free-stream total pressure and plotted by rake and probe number for a number of distinct data points. In this particular example, sideslip angle is the independent variable. Static pressures measured at the AIP also are shown. Editing can be performed quickly and accurately since experience has shown that the rake data produce consistent patterns. Pressure ratios exceeding unity or falling below measured static levels can be readily identified and examined more closely with regard to variations in the independent parameter. Although the example shown was based on steady-state data, experience has shown the procedure works equally as well with dynamic data.